Lehigh University

Contributions of Floor Systems to Earthquake
Resistance of Building Structural Frames

SEISMIC RESISTANCE CHARACTERISTICS OF REINFORCED CONCRETE BEAM-SUPPORTED FLOOR SLABS IN BUILDING STRUCTURES

by

Masayoshi Nakashima
Ti Huang
Le-Wu Lu

Fritz Engineering Laboratory

Report No. 422.9

Contribution of Floor Systems to Earthquake
Resistance of Building Structural Frames

SEISMIC RESISTANCE CHARACTERISTICS

OF REINFORCED CONCRETE BEAM-SUPPORTED

FLOOR SLABS IN BUILDING STRUCTURES

by

Masayoshi Nakashima

Ti Huang

Le-Wu Lu

Department of Civil Engineering

Fritz Engineering Laboratory
Lehigh University
Bethlehem, Pennsylvania

April 1981

Fritz Engineering Laboratory Report No. 422.9
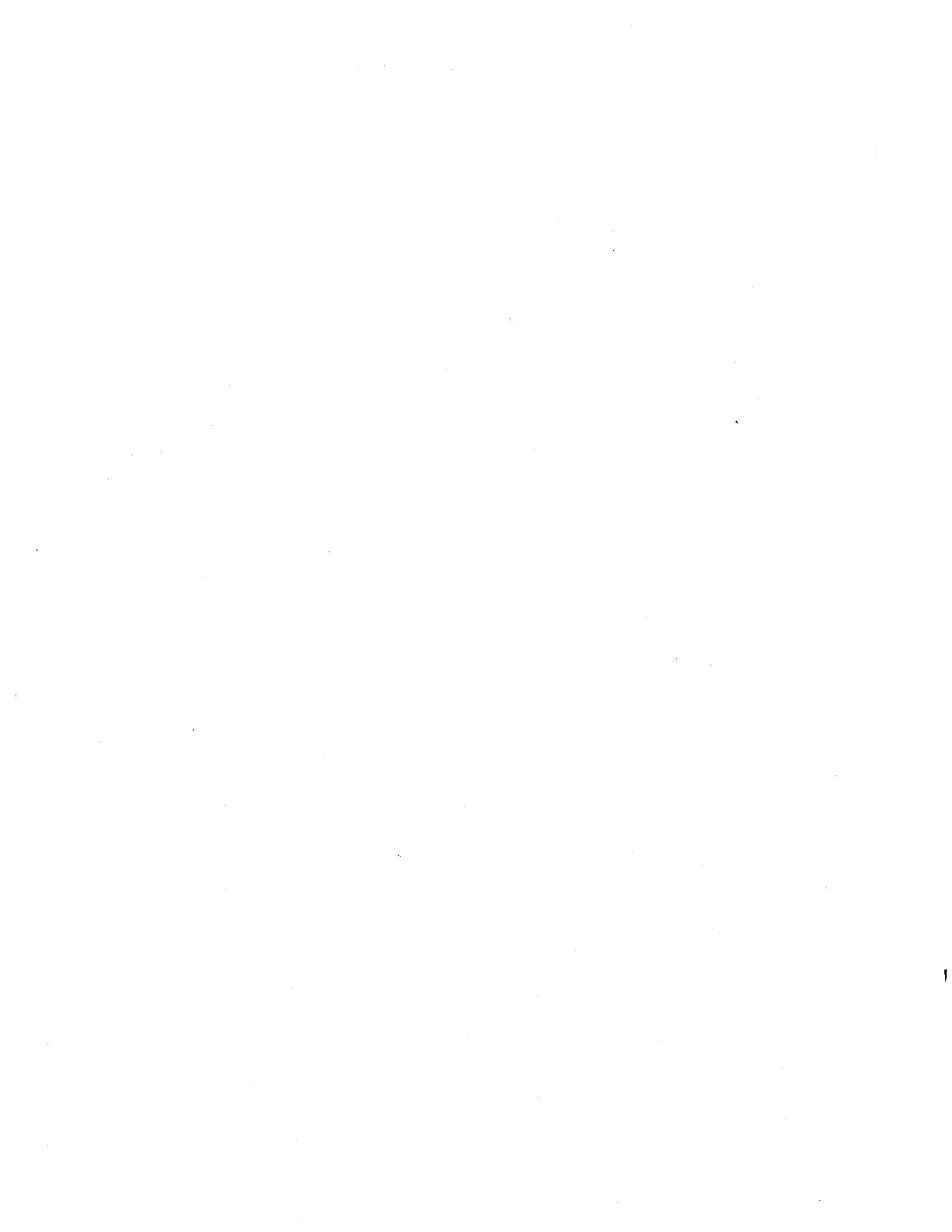
Masayoshi Nakashima, Ti Huang, and Le-Wu Lu.

This study investigates the in-plane seismic characteristics
of reinforced concrete floor slabs which function as
diaphragms placed between lateral load resisting systems.
The paper focuses on the floor slab system with edge beams,
refeered to as the beam-supported floor system. The
investigation consists of four phases: (1) experimental
study, (2) analytical study, (3) parametric study, and (4)
dynamic response analysis.

ACKNOWLEDGMENT

TABLE OF CONTENTS

TABLE OF CONTENTS (Cont.)

ix

LIST OF TABLES

LIST OF FIGURES

LIST OF FIGURES (Cont.)

LIST OF FIGURES (Cont.)

ABSTRACT

This study investigates the in-plane seismic charac-
teristics of reinforced concrete floor slabs which function as
diaphragms placed between lateral load resisting systems. The
paper focuses on the floor slab system with edge beams, referred
to as the beam-supported floor system. The investigation consists
of four phases: (1) experimental study, (2) analytical study,
(3) parametric study, and (4) dynamic response analysis.

In the experimental study, scaled models (a scale ratio
of 1 : 4.5) representing a portion of the floor system in a
building structure were tested under various loading and support
conditions. The experimental findings indicate that the develop-
ment of a crack extending along the boundary between the column
and middle strips controls the ultimate in-plane strength of the
test panels, while the opening and closing of the crack primarily
controls the behavior of the panels in post-ultimate load regions.
It was found that cyclic loading or the application of the ver-
tical load can reduce the ultimate in-plane strength by as much
as 20 to 25 percent.

A non-linear finite element model was developed for the
purpose of the analytical study. The model successfully predicts
the ultimate strength of the test slab panels subjected to mono-
tonic in-plane loading and duplicates the experimental load-
deflection curves. The model also reproduces the unloading

stiffness of the test slab panels.

The effects of geometry, reinforcement, loading, and support conditions on the in-plane characteristics of floor slabs were investigated in the parametric study. General and practical procedures were developed to evaluate the in-plane strength and stiffness of floor slabs. The in-plane flexural strength of floor slabs can be computed by treating them as deep beams considering both flexural and shear deformations. A reduction factor is incorporated into the deep beam calculation in order to represent the stiffness degradation in the post-elastic range.

In the dynamic response analysis, a seven story and six bay symmetrical building model was selected in order to examine the influence of in-plane characteristics of floor slabs on the building response. Compared with the analysis based on the usual rigid slab assumption, the incorporation of elastic in-plane deformation of the floor slabs resulted in a 300 percent increase in the base shear applied to flexible vertical members. The base shear resisted by the flexible vertical members was increased further by 100 percent when the non-linear behavior of floor slabs and vertical members were considered.

I. INTRODUCTION

1.1 General

The dynamic response of structures to strong motion earthquakes and earthquake resistant building designs have been the subjects for a great deal of recent research. According to D'Alembert's principle, the dynamic effect of a structure can be represented in terms of time-dependent inertial forces. Once these equivalent inertial forces have been determined, the analysis and design can be performed by the conventional procedure for static loads. However, the fact that the effective external forces are controlled totally by the earthquake itself complicates the earthquake resistant building design. Since the earthquake disturbance has a displacement-oriented nature, the effective forces are dependent upon the stiffness of the structural elements. As a result, a stiffer structure will be subjected to higher earthquake loads. Structural safety is not automatically improved by arbitrarily increasing the member sizes.

Recent development of high speed digital computers has facilitated the understanding of dynamic behavior of structures during an earthquake. Much progress has already been made in both the dynamic analysis and the earthquake resisting design. Nevertheless, prediction of the inelastic response of structures to strong earthquake motions having a wide range of frequencies

and amplitudes is still difficult because the post-elastic behavior of the structures is greatly influenced by the interaction of individual elements such as beams, columns, and shearwalls. In order to perform a true dynamic analysis, analysts first must know the characteristics of each structural element under all possible loadings. Once all the information with respect to the behavior of structural elements is known, it is possible to carry out a dynamic analysis by assembling these elements. These two steps in analytic process are interrelated obviously. For example, it is possible to model a structure more realistically when more information regarding the behavior of some structural elements is known. A refined dynamic analysis, in turn, can give more accurate evaluation of the forces applied to the individual structural elements.

While the above discussion is valid for any kind of construction material, particular care should be paid to the reinforced concrete structure. Concrete has certain intrinsic advantages over other construction material; it is highly versatile, durable and fire-resistant. Its high density and low ductility, on the other hand, bring about undesirable effects when used in regions susceptible to severe earthquakes. This disadvantage, however, does not necessarily mean that the reinforced concrete should not be used in seismic regions. Properly designed structures will perform well regardless of the material used.

Nevertheless, it should be emphasized that reinforced concrete
is less tolerant of the improper design.

Much work has been performed to determine the behavior
of reinforced concrete structural elements subjected to earth-
quake loading, particularly for the major lateral load resisting
elements such as columns, beams,and shearwalls. Great improve-
ment in the earthquake resisting design has been achieved in
recent years from these studies. On the other hand, earthquake
behavior of floor slab systems has not yet been given very much
attention. Consequently, it is difficult to adequately include
the characteristics of floor slabs in the analysis of buildings
subjected to earthquake loading. Although the floor slab may not
be as critical as columns or shearwalls in providing earthquake
resistance, its contribution cannot be ignored.

The main purpose of this study is to investigate the
effect of the behavior of floor slabs on the earthquake resistance
of reinforced concrete building structures. Also it is intended to
provide suggestions and recommendations about the design of floor
slabs or other structural elements.

1.2 Statement of Problem

The primary function of floor slabs in a building
structure is to carry vertical loads by their out-of-plane bending
action and transmit these loads to the supporting elements such

as columns and walls. Most of the current design provisions for
floor slabs deal with this particular function. [1.1, 1.3, 1.4, 1.7, 1.16, 1.17, 1.22, 1.26, 1.30, 1.32, 1.35, 1.36, 1.41, 1.42, 1.43] Recently, however, structural engineers have recognized that the floor slab also performs as an important function when buildings are subjected to lateral force. [1.19, 1.20]

In many buildings, columns and floor slabs form space frames, and lateral loads are resisted by the flexural action of the frames. In this type of structure, floor slabs serve as horizontal moment resisting members in the frames. This function of the floor slabs is frequently called Frame Action. [1.5, 1.10, 1.11, 1.18, 1.21, 1.25, 1.28] In the current ACI Building Code, the Equivalent Frame Method described in Chapter 13 uses this concept and treats the floor slabs as horizontal flexural members in the frames. The Equivalent Frame Method, however, was developed originally for the design under vertical loads. Consequently, the detailed method described in ACI Building Code, including the empirical distribution coefficients, most probably does not apply to lateral load analysis. The important characteristics of the Frame Action are as follows:

(1) The stiffness of the floor slab as a out-of-plane flexural member directly influences the lateral story stiffness of a frame; therefore, appropriate evaluation for the slab stiffness is critical. [1.5, 1.11, 1.28]

(2) It is a common practice to design a space frame as an assembly of two-dimensional frames. In this situation, floor slabs and beams running perpendicular to the plane being analyzed provide torsional restraint. Proper evaluation of the torsional stiffnesses of these elements is also important.[1.11, 1.28]

(3) Transfer of moment and shear at slab-column junctions becomes a critical factor for safety. A junction must possess the required deformability to guarantee sufficient energy absorption capacity of the total frame. A premature punching failure or a slip of reinforcing bars should be avoided.[1.18, 1.21, 1.25]

Yet another important function of floor slabs in a building subjected to lateral force is the Diaphragm Action.[1.19, 1.20] This action is dependent on in-plane characteristics of the floor slabs, while the out-of-plane flexural characteristics control the Frame Action. When a building is subjected to an earthquake, the inertial forces are transmitted transversely through floor slabs to vertical lateral load resisting elements. In this function, the floor slabs act as diaphragms between lateral load resisting systems. The distribution of lateral load to the lateral load resisting systems depends upon the stiffness character-

istics of both the diaphragms and the vertical elements.[1.29]

In the current design practice, floor slabs are often assumed to be perfectly rigid in their own planes. Under this assumption, lateral loads are distributed into lateral load resisting elements in proportion to their lateral story stiffnesses. Although the assumption is employed widely, experience and research have shown that the maximum lateral forces on some components may be underestimated significantly.[1.29] These underestimates frequently occur in frame-wall structures.[1.13, 1.34, 1.38] These structures are favored because high story stiffness can be expected for stiff walls even though the increase of stiffness and mass causes higher lateral force to be applied to the walls. Arbitrary allocating frames and walls in these structures, however, causes significant floor slab deformation, which, in turn, results in a change in the distirubtion of lateral forces.

In lower stories, generally speaking, the assumption that floor slabs are perfectly rigid in their own planes leads to underestimates of the force carried by frames and overestimates of the force distributed to walls. Evaluation of the forces assigned to the frames and walls is reversed when upper stories are analyzed. It has been shown that the story stiffness of walls decreases in higher stories, while the story stiffness of frames remains relatively constant.[1.13]

An entirely reversed assumption that the in-plane floor

slab rigidity equals zero is usually adopted for low rise build-
ings with no more than two or three stories.[1.34]   The degree
of discrepancy created by these assumptions is affected by the
ratio of the story stiffness of vertical lateral load resisting
elements to the true in-plane stiffness of floor slabs. Whenever
in-plane stiffness of the slab is comparable to the stiffness of
vertical elements, to assign extreme values such as infinite or
zero for the in-plane stiffness of the floor slabs is undesirable.
[1.37]   Buildings having slender cross sections possess the same
potential problem.[1.15, 1.23, 1.24]   In these buildings, the
floor slabs function as slender beams, and, as a result, the
deformation by flexure becomes appreciable.

The above discussion is based on the assumption that the
floor slab behaves elastically. There is no guarantee, however,
that the floor slab maintains its elastic properties under all
earthquake conditions. Shear force applied to a slab increases,
as the difference between the story stiffness of two adjacent
vertical lateral load resisting elements becomes greater. A high
shear force may cause cracks in the slab and change its in-plane
stiffness, which, in turn, will cause a change in the proportion
of the lateral force distributed to each vertical element. It
is quite possible that stiffness degradation and/or decrease of
strength would occur during severe repeated or reversed loading
cycles. Lateral force applied to each vertical member, then, will

be continuously changing due to the continuous degradation of the in-plane slab stiffness. Such a change in force is dangerous for some elements, but safe for others.

The in-plane strength of the floor slab may be as important as its stiffness.[1.2, 1.6, 1.12] In some types of structures such as staggered wall-beam systems, the shear strength of the floor slabs is critical. Because these floor slabs carry lateral forces transmitted by shearwalls, they must possess enough in-plane shear strength to resist the total lateral load. In this regard, special attention should be paid to floor slab-wall junctions because gravity loads may have created high negative moments and high shears, before any lateral force is applied.

1.3 Objectives and Scope

Among various functions of the floor slab, the diaphragm action has received relatively little attention; consequently, floor slab designs frequently are oversimplified. Many of these simplifications result from a lack of vital information. Research, then, should aim at defining the effectiveness of the floor systems as load-transmitting diaphragms between vertical and lateral load resisting elements.

It is proposed to investigate the in-plane characteristics of reinforced concrete floor slabs under various loading and supporting conditions and to provide meaningful information for the design of the floor slabs as well as of other structural elements. This study is concentrated on the floor slab system with edge beams, referred to as the beam-supported slab (slab-on-beam) system.

The planed study presented here consists of five stages, each in a separate chapter. The five stages are: 1) the literature survey, 2) the experimental work, 3) the analytical study, 4) the parametric study, and 5) the dynamic analysis of structures including the floor slab in-plane characteristics. In Chapter II, a comprehensive survey is given to previous research work regarding the diaphragm action of floor slabs. Findings about the diaphragm action, present status of diaphragm designs, research procedure, specific research topics, and areas of needed research are discussed in detail. Chapter III describes the experimental work. A portion of the floor system in a medium to high rise building structure is modelled and tested under various loading and boundary conditions. The results of these experiments provide basic information about the in-plane characteristics of the floor slabs. Critical parameters controlling the in-plane behavior of the floor slabs are selected carefully, and the effects of these parameters on the in-plane characteristics are examined. The test results also provide a basis of comparison for the analytical model developed in Chapter IV. Chapter IV describes an analytical

-11-

model developed for investigating the in-plane characteristics of the floor slabs. The finite element method is used for the modelling. The accuracy of this model is checked by comparing the results derived from this model to the test results described in Chapter III and other existing theories. In Chapter V, the test results are again examined, with specific emphasis on three most crucial in-plane characteristics of the floor slabs: strength, stiffness, and ductility. The analytical model described in Chapter IV is utilized to provide additional data about the effects of the various parameters on these characteristics. The variables included in this parametric study are: the loading condition, the boundary condition, the relative beam size, the amount of reinforcing steel, and the aspect ratio of the floor slab. Based on the findings of the parametric study, suggestions and recommendations for the designs of the floor slabs as diaphragms are provided at the end of this chapter. In Chapter VI, a relatively simple building model representing a commonly used reinforced concrete building is analyzed for its dynamic response under a typical earthquake loading. The in-plane characteristics of the floor slabs defined in Chapter V are incorporated into this dynamic analysis. The intensity of moment and shear applied to the floor slabs during the earthquake motion is examined. The effect of the floor slab in-plane stiffness on the total lateral force and on the lateral load distribution to vertical elements are studied carefully. This study also provides

-12-

information for examining the appropriateness of the rigid

floor assumption.

II. SURVEY OF PREVIOUS WORK

2.1   The Effect of Floor Slab Stiffness on Lateral Load Distribution

Floor slabs are important elements for three-dimensional structural analysis for horizontal loads since they interconnect lateral load resisting components and control the distribution of the total lateral load to these components. In order to determine the loads supported by each vertical component, the in-plane stiffness of the floor slabs must be evaluated properly.

The assumption that the floor slab is infinitely rigid in its own plane has frequently been adopted in structural analyses. This assumption reduces the number of unknown displacements significantly and, consequently, reduces the effort for computation. Various kinds of three-dimensional structural analyses were carried out based on this assumption. Clough et al.[2.12] developed a computer program to analyze three-dimensional buildings subjected to static lateral loads. Floor slabs were allowed two degrees of freedom: two translation components in their own planes. Therefore, all vertical components underwent identical displacements at a given story level. On the other hand, torsional deformation about a vertical axis is significant for structures with irregular plans and those subjected to asymmetrical lateral loadings. Stamoto and

Stafford-Smith[2.39], Neville[2.31], and Macleod et al.[2.26]
conducted static analyses of wall-frame structures having asym-
metrical plans. In the formulation of the governing equations,
the displacements of walls and columns at each floor level were
expressed by two translations and one rotation of the rigid
floor slab. Gluck[2.21] analyzed coupled wall structures accord-
ing to the same procedure. The application of this procedure
was extended further to solve many other problems. Nair[2.30]
investigated the stability of three dimensional wall-frame
structures. He represented the whole structure as a beam-column
and treated the overall stability as lateral torsional buckling
of the beam-column. Heidebrecht and Swift,[2.23] Taranath and
Stafford-Smith,[2.40] and Taranath[1.38] examined the effect of
vertical forces applied to shear walls due to torsion. They
treated the whole structure as a cantilever beam with a cross
section composed of walls. The axial forces carried by the walls
then were evaluated by considering the bending and warping stresses
of this cantilever beam. Shepherd and Donald[2.37] and Gibson
et al.[2.20] examined the frequencies and mode shapes of asym-
metrical wall-frame buildings. Douglas and Trabert[2.15] studied
the response of an approximately symmetrical twenty two story
building under the ground motion caused by blast. A non-linear
analysis of asymmetrical buildings was made by Wynhoven and

Adams.[2.47] They investigated the reduction of torsional stiffness
of the structure caused by the yielding of columns and the accom-
panying change in the total torsional force. In all these studies,
the floor slabs were considered rigid, with three degrees of free-
dom at each floor level.

The in-plane bending of floor slabs is appreciable when
structures having slender cross sections are subjected to lateral
forces. The bending effect is significant particularly if the
lateral stiffnesses of the vertical components differ greatly.
Goldberg and Herness [1.15] investigated the frequencies and mode
shapes of a twenty-story symmetrical building. The building with
twelve bays was composed of frames at the inner bents and walls
at the ends. The characteristics of the floor slabs in their in-
plane directions were represented by beams in which both flexural
and shear deformations were taken into account. The mode shapes
showed significant bowing of the floor slabs. Goldberg and
Herness also reported an appreciable difference between the forces
applied to frames and the forces applied to walls. Majid and
Onen [2.27] performed elasto-plastic analysis of wall-frame build-
ings. In their analysis, the floor slabs were incorporated into
the overall structures as elastic deep beams. Plastic hinges were
inserted wherever the bending moments in the vertical frames

reached the yield values at the location, and the ultimate resistance of buildings was determined by a step-by-step method. Joh and Ohno[1.24] studied the dynamic response of wall-frame structures with slender cross sections and treated the floor slabs as deep beams, using the same procedure as Majid and Onen. The parameters they studied were: the shape of slab panels, and the relative stiffness between walls and frames. Joh and Ohno showed that those parameters affected the distribution of lateral forces and also reported that large differences in lateral stiffness of neighboring vertical components caused large shear forces in the floor slabs. Kostem and Heckman[2.49, 2.50] studied the elastic stiffness and vibrational characteristics of building structures with U-shaped concrete shear cores, reporting the significant influence of in-plane floor slab deformations on the lateral deflections and natural frequencies of the structures.

While the above studies including the flexibility of floor slabs showed the significant effects of the floor slab in-plane stiffness on the response of structures, several other studies had resulted in opposite conclusions. Shepherd and Donald[2.36] investigated the frequencies and mode shapes of three bay frame structures, in which the stiffness of columns was four times larger in the outer bents. The floor slabs were treated as deep beams. These researchers concluded that the in-plane stiffness of the floor slabs did not affect significantly the forces distributed to vertical components although the mode shapes evidently

-17-

showed bowing of the floor slabs. Richter et al. [2.34] and

Rutenberg et al. [2.35] also performed static structural analysis

by replacing the floor slabs with deep beams. They supported

the conclusions of Shepherd and Donald that altering the floor

slabs' in-plane stiffness did not cause significant change in

the distribution of forces transmitted to the vertical

components.

All of the studies discussed above treated the floor

slabs as either rigid or linearly elastic elements. Very few

studies considered potential inelastic behavior of floor slabs

in structural analysis. Ramakrishnan [1.34] tested scale models

of wall-slab structures and examined the forces distributed

to the walls. He pointed out the significant influence of the

walls arranged perpendicular to the load on the stiffness of the

lateral load resisting elements. These walls functioned as

flanges for some vertical elements and greatly increased stiffness.

Adham and Ewing [2.2] analyzed the dynamic response of one-story

two-bay masonry structures under earthquake ground motion. The

wood roof diaphragms interconnecting the masonry walls were

assumed to behave non-linearly, and a time-history analysis was

executed. Because of the non-linear behavior of the diaphragms,

low amplitude test results cannot be extrapolated for the

prediction of the response of these structures under severe

loadings. The also found that softer wood diaphragms would

attenuate the input earthquake accelerations and result in lower

shear forces.

Fintel[2.16, 2.17] and Mee et al.[2.29] studied the

staggered wall system, where floor slabs are part of the lateral

load resisting systems. Their studies, however, focused on the

evaluation of the lateral stiffness of the walls rather than the

load resisted by the floor slabs. They discussed the contribution

of the floor slabs as flanges on the wall stiffness. Their studies

did not refer to either in-plane stiffness or strength of the

floor slabs.

Many computer programs for the analysis of three dimen-

sional structures under static or dynamic loadings have been

developed during the last decade. Wilson and Dovey[2.46] have

developed an elastic finite element program TABS in which floor

slabs are assumed to be perfectly rigid. This program has the

capacity of solving both static and dynamic problems. Guendelman-

Israel and Powell[2.22] have developed a non-linear finite element

program by combining two previously developed programs: TABS and

DRAIN-2D, which was developed by Kanaan and Powell[2.25] to solve

static and dynamic problems of non-linear two-dimensional

structures. This combined program, DRAIN-TABS, is capable of

including non-linearities of structural components except floor

slabs. The floor slab is assumed to be perfectly rigid as in

the program TABS. Cheng and Kitipitayangkul[2.11] have made

another computer program for inelastic analysis of reinforced

concrete steel buildings subjected to three-dimensional ground

motions. All structural components except the floor slabs are

allowed non-linear characteristics. The floor slabs are assumed

to be linearly elastic. Since this program takes geometrical

non-linearity into account, stability effects as well as effects

of material non-linearities can be solved.

2.2 In-plane Characteristics of Floor Slabs

Few studies have been published concerning the in-plane

characteristics of reinforced concrete floor slabs. As a result,

there exists little information to aid the design of these floor

slabs in their function as diaphragm. Cervenka and Gerstle[2.10]

tested two-span continuous reinforced concrete slabs under in-plane

loads and examined their strength and stiffness. The tests

however, were utilized only to verify the accuracy of their finite

element model. Consequently, no design suggestion was made.

Floor slabs as diaphragms are viewed frequently as horizontally oriented shearwalls. This assumption is reasonable because both floor slabs and shearwalls have similar dimensions, and both are subjected to in-plane loads. Shearwalls often have boundary frames. These boundary frames are analogous to the edge beams integral with the floor slabs since both function to confine the flat plate element. Nevertheless, the shearwall and the floor slab are quite different in many respects. Reinforcing bars in shearwalls usually are placed symmetrically about the middle plane of the shearwalls. On the other hand, the arrangement of reinforcing bars in floor slabs is distinctively unsymmetrical; many reinforcing bars in floor slabs are cut off according to the requirement on design flexural moments, while the bars in shearwalls extend from one edge of the walls to the other. Vertical loads applied to structures are resisted differently by shearwalls and floor slabs. These vertical loads cause in-plane compression in shearwalls, while floor slabs must resist these loads by bending. The floor slabs subjected to combined vertical and lateral loads, therefore, are truly three-dimensional, while the shearwalls can still be analyzed as plane stress problems. Boundary frames attached to shearwalls are usually arranged symmetrically about the middle planes of the walls, while integrated beams in floor systems are attached to the lower side of the floor slabs. These restraining

members also differ in size. They are usually much larger in shearwalls than in floor slabs.

Despite these differences, the two structural elements still show very similar behavior, particularly in their function as diaphragm. Consequently, analysis and design of floor slabs as diaphragms frequently make use of experimental findings, theoretical analyses, and design procedures originally developed for shearwalls. Benjamin and Williams[2.7] conducted a comprehensive research of one-story shearwalls subjected to static loadings. They made experimental investigation of the effects of various parameters on the ultimate strength of the shearwalls. The variables chosen in their study were: the aspect ratio, the relative size of boundary members, the amount of reinforcing steel in the shearwalls or the boundary members, and any additional reinforcement arranged diagonally in the shearwalls. Tomii and Osaki[2.41] and Tsuboi et al.[2.44] also studied the behavior of low-rise shearwalls (with height-to-length ratio less than 1.0) surrounded by reinforced concrete or steel frames. They pointed out that the boundary frames improved significantly the ductility as well as the strength of the shearwalls. Barda[2.6] also investigated low-rise shearwalls. He reported on the significant effect of the vertical reinforcement on the shear strength of the shearwalls.

Cardenas and Magura[2.8] presented the results of a laboratory investigation on the strength of shearwalls for high-rise buildings. They chose as variables the amount and distribution of vertical reinforcement and the moment-to-shear ratio. Their test results indicated that the strength of high-rise shearwalls was generally controlled by flexure. They also showed that the flexural strength of these walls could be calculated by using the same assumption used for reinforced concrete beams. Fiorato et al.[2.19] investigated the behavior of high-rise shearwalls with the emphasis on examining the performance of confinement reinforcement in vertical boundary columns and anchorage of horizontal wall reinforcement when the walls were subjected to severe cyclic loadings. The behavior of shearwalls under cyclic loadings also was investigated by Oesterle et al.;[2.32] Alexander et al.;[2.3] and Shiga et al.[2.38] The items studied by these researchers included: stiffness in post-elastic regions, ductility, energy absorption capacity, and stiffness degradation due to cyclic loadings.

While the achievement of the above cited studies has been based mainly on experimental studies, there have also been several theoretical investigations. Tomii and Tokuhiro[2.42] proposed an analytical method to solve the problems of isolated shearwalls surrounded by boundary frames. They used the Airy stress function

to solve the governing elastic equations and offered elastic solutions for several types of loadings. The finite element method has been used in many theoretical studies. Yuzugullu and Schnobrich[2.48] developed a finite element model to simulate the behavior of shearwalls with boundary frames under static loadings. Darwin[2.14] presented a new finite element model and developed load-deformation curves of shearwalls under cyclic loadings. A more detailed discussion of the use of the finite element method in two dimensional plane stress problems will be given in Chapter IV.

2.3 Current Design Procedures

As pointed out in preceding sections, the distribution of lateral forces to vertical lateral load resisting components must be carefully evaluated to enable a proper design. The Uniform Building Code[2.24] stipulates that the total lateral force should be distributed in proportion to the stiffness of vertical components. This procedure is based upon the rigid slab assumption, which, as already discussed, may not be adequate for some types of structures. In order to compensate this deficiency, the Code also stipulates that frames in wall-frame structures should be capable of resisting at least twenty five percent of the total lateral force. On the other hand, the

Applied Technology Council (ATC)$^{(2.4)}$ allows for the flexibility

of the floor slabs by recommending that:

> "The design lateral forces should be based on
> an analysis which explicitly considers diaphragm
> deformations and satisfied equilibrium and com-
> patibility requirements."

Alternately, the ATC suggested that design could also be based

upon the envelope of the two solutions: first by assuming the

diaphragms to be infinitely rigid, then very flexible. It also

suggests that where the horizontal diaphragm is not continuous,

the story shear can be distributed to the vertical components

based on their tributary areas and torsional moments can be

ignored. The ATC also discusses the design forces for

diaphragms:

> "The seismic forces to be resisted by diaphragms
> area a minimum force equal to 0.5 A_v times the
> weight of the diaphragm and other elements of
> the building attached thereto plus the portion
> of V_x required to be transferred to the compo-
> nents of the vertical seismic resisting system
> because of offsets or changes in stiffness of
> the vertical components above and below the
> diaphragms."
>
> A_v: The seismic coefficient representing the
> Effective Peak Velocity-Related Acceleration
>
> V_x: The seismic shear force at any level

Codes and regulations stipulate that the distribution

of the lateral force be determined based on the lateral stiffness

of vertical elements. Evaluation of the lateral stiffness of vertical elements like frames and walls, however, is a cumbersome task. Muto[1.29] has developed a simple method to compute the stiffness of frames and walls. The story stiffness of frames is calculated by assigning inflection points in beams and columns. The wall stiffness, on the other hand, is computed by treating the wall as a deep beam which includes flexural and shear deformations and base rotation.

Once the forces on floor slabs are determined, designers can design these floor slabs according to available codes or spedifications. The ACI Code[1.1] does not have specific provisions for the design of floor slabs as diaphragms. Consequently, designers frequently employ the design procedures developed for shearwalls. Cardenas and Magura[2.8] and Fintel[2.18] offered design methods to determine the flexural capacity of slender shearwalls. The shear capacity of shearwalls has been the subject of research for many years. Cardenas et al.[2.9] and ACI-ASCE Committee 426[2.1] have given comprehensive reviews of previous studies and summaries of various design procedures for shearwalls subjected to shear forces. Tomii[2.43] gave a review of Japanese practices of shear wall designs.

When inelastic behavior of structures under severe lateral loadings is considered, the ductility of the structural components should be evaluated appropriately. The ductility of reinforced concrete components, however, is very difficult to define on account of many complicated phenomena, such as the cracking of concrete, the yielding or slipping of reinforcing bars, or the crushing of concrete. Mattock[2.28], Corley[2.13], and Backmann[2.5] offered empirical formulas to predict the ductility for flexural beams. Uzumeri and Paulay[2.45] later extended Mattock's and Corley's works and proposed design procedures for the ductility of shearwalls. The proposed procedures deal with only slender shearwalls whose performance is controlled basically by flexure and consequently do not accurately evaluate the ductility of stocky shearwalls. Stocky shearwalls, in which shear behavior dominates, are known to have rather limited ductility.[2.6, 2.7]

2.3 Summary

As described in Section 2.1, studies including the diaphragm action of floor slabs have reached different conclusions as to the effect of the floor slabs on the lateral load distribution to vertical elements. One of the primary reasons of the inconsistent results can be the lack of decisive information about the in-plane characteristics of the floor slabs. According to Sections 2.2 and 2.3, little research has contributed to the

understanding of the in-plane behavior of floor slabs, and, practically speaking, there is no design provision for the diaphragm design of floor slabs. The appropriateness of using the design provisions developed for shearwalls to design diaphragms has not yet been verified. Furthermore, procedures to determine the design forces controlling the in-plane behavior of floor slabs have not been established, either.

The following chapters will provide data needed to discuss these unclarified problems and propose practical procedures of the diaphragm design.

III. EXPERIMENTAL STUDY

3.1 General

This chapter describes the experimental study. Scaled models representing floor slab panels in medium to high rise building structures were tested under various loading and support conditions. The results of these experiments provide general information about the in-plane characteristics of the floor slabs. Critical parameters controlling the in-plane behavior of the floor slabs are varied carefully, and the effects of these parameters on the in-plane characteristics are examined.

3.2 Design of Test Structures

3.2.1 Prototype Floor System and Scaled Model

The prototype floor slab for test specimens was taken from a rectangular multi-story, multi-bay reinforced concrete building, in which earthquake resistance was provided by shearwalls located in selected bents. Seismic forces at various floor levels were transmitted to the walls by the diaphragm action of the floor slabs. Structural dimensions were chosen to represent a building of medium to high rise. The center-to-center span length of slab panels were 7320 mm (24 ft) in both directions, the columns were 610 mm x 610 mm (24 in. x 24 in.) with no capital, the slab was 180 mm (7 in.)thick, and the beams were 610 mm x 310 mm

(24 in. x 12 in.) in their cross sections. A portion of the
plan view of the prototype floor system is shown in Fig. 3.1.

The basic test specimen chosen for this experimental
study represented an interior panel of the prototype building
and was supported on one edge by a shearwall and on the opposite
edge by columns. The fabricated test specimen consisted of three
consecutive panels supported by two shearwalls and four columns.
Overhanging slabs, equal to one quarter of the panel dimension,
were added on all non-continuous sides to represent parts of the
floor slabs of the adjacent bays. (Fig. 3.2) Full scale
modelling was abandoned because of economy, space, labor, loading,
and measurement. Small scale modelling with its many disadvantages,
on the other hand, was also unacceptable on account of the diffi-
culties in modelling the aggregate particles, the reinforcing bars,
and the bonding effect between concrete and steel. An inter-
mediate scale ratio of 1 : 4.5 was selected. Fig. 3.2 illustrates
the test specimen and the several support conditions used in the
experiment. The basic panel is 1630 mm x 1630 mm (64 in. x 64 in.)
and 40.0 mm (1.56 in.) thick.

3.2.2 Design of Test Specimen

The prototype floor slab was designed according to the
current ACI Code[1.1] for a service live gravity load of 3.8 kPa

(80 psf). The direct design method described in Section 13.6

of the Code was employed. The columns were designed for combined

axial force and bending moment caused by the vertical load at an

intermediate floor level. The test specimen then was designed

by scaling down these forces and moments. The shearwalls, on

the other hand, were designed so that they would possess sufficient

strength to carry the expected maximum load which may emerge

during the testing. This design was performed to insure failure

in the slabs. Based on a preliminary analysis, the design shear

force for the shearwalls was selected to be 230 kN (50 kips).

Adopted concrete strength was: 27.6 MPa (4000 psi) for the floor

slabs and walls and 34.5 MPa (5000 psi) for the columns. The

yield strength of reinforcing bars was taken to be 410 MPa

(60 ksi). Table 3.1 lists the critical dimensions of the

specimen.

Special care was given to the size of reinforcing bars.
The smallest bars available were larger than what was needed by
the adopted scale ratio (1 : 4.5). Fig. 3.3 shows the arrange-
ment of the reinforcing bars.

Table 3.3 lists the dimension, the design moment, and
the area. The next to the last column of the table shows the
ratio of the amount of steel provided in each individual strip

to the amount of steel required by the Code. The last column
lists the ratio of the amount of steel provided in the strip
to the amount of steel required to carry the design moment. The
table shows that the temperature requirement (0.0018 times the
gross area) controls the amount of steel required at many critical
sections. The average over-supply ratio of reinforcement is
28 percent for one direction and 21 percent for the other direction.
In comparison with the flexural requirements, the amount of
reinforcement used is 3.42 and 2.81 times larger respectively
than that required.

Table 3.4 lists the amount of steel provided in the
beams. Additional reinforcing bars were placed in the bottom
layer of negative moment regions and in the top layer of positive
moment regions in order to meet the requirement stipulated in
Appendix A of the Code.

3.2.3 Fabrication of Specimen

After cutting and bending reinforcing bars, strain
gages were placed in specified locations. Reinforcing bars
then were placed and tied together in a form work. In addition
to reinforcing bars, a total of fifty five inserts also were
installed. These inserts were placed in the specimen to serve
as hooks through which vertical loads can be applied. Additional
explanation of the function of the inserts and the application of

vertical loads will be given in Section 3.4.2. The formwork

was elevated about 1.2 m (4 ft) from the floor level of the

testing laboratory in order to facilitate construction of the

specimen.

Two specimens were constructed and casted at the same

time by using concrete mixed at the testing laboratory. The two

specimens are labelled B-1 specimen and B-2 specimen. Two kinds

of concrete were prepared: 27.6 MPa (4000 psi) for the floor slabs

and the walls and 34.5 MPa (5000 psi) for the columns. Table 3.5

shows the detail of concrete mix. A slump of 130 mm (5 in.)

was specified in view of the maze of reinforcement in the speci-

mens. Plastisizer was added to further facilitate the placement

of concrete around closely spaced reinforcing bars. The added

plastisizer was WRDA-19, which is formulated to comply with ASTM

Specification Designation C 494, a Type A water reducing admix-

ture. The aggregate size was limited to 6.4 mm (0.25 in.) in

order to preserve approximately the prototype relationship

between the aggregate size and the slab thickness. Separate

batches of concrete were used for each specimen.

Sixteen 76 mm x 150 mm (3 in. x 6 in.) and ten 150 mm x

300 mm (6 in. x 12 in.) concrete test cylinders were made from

each batch of concrete. They were placed next to the freshly

cast test specimens so that both the specimens and test cylinders

-33-

would experience the same curing conditions. The specimens and cylinders were cured for fourteen days under moist burlap at room temperature. On the fifteenth day after the placing, the burlap was removed, and the cylinders were stripped. The specimens and concrete test cylinders were then air-cured until tested. Table 3.6 lists the slump, the 7-day strength, and the 28-day strength of the concrete.

Mechanical properties of concrete and reinforcing bars were obtained by the concrete cylinder test at appropriate intervals and by the steel tension test. Section 3.3 describes these properties in further detail.

3.3 Mechanical Properties of Materials

3.3.1 Reinforcing Bars

Deformed reinforcing bars of three sizes were used in the test slab specimens: D2.0, D2.5, and D3.0. The mechanical characteristics of these bars were determined by basic tension tests. The test was repeated four times for each size of reinforcing bar. An electric extensometer with a 57 mm (2.25 in.) gage length was used to measure the strain. Table 3.7 lists the yield stress, the yield strain, the ultimate stress, the ultimate strain, and the modulus of elasticity of these bars. The values listed in the table represent the averages of the results of the four tests.

-34-

3.3.2 Concrete

Two kinds of concrete were used in the test specimens:
27.6 Mpa (4000 psi) concrete and 34.5 MPa (5000 psi) concrete
for each of the two specimens, B-1 and B-2. Standard cylinder
tests were performed at ages of seven and twenty eight days. On
the first day of slab specimen testing, four more concrete test
cylinders were tested to obtain modulus of elasticity, Poisson's
ratio, and compressive strength. The ages of concrete at these
tests were fifty two days for specimen B-1 and 109 days for
specimen B-2.

In order to calculate the modulus of elasticity and
Poisson's ratio, the longitudinal strain of the concrete cylinder
was measured by a pair of clip gages mechanically attached to the
cylinder, while the transverse strain was measured by two electric
strain gages mounted on the cylinder in its circumpherential
direction. After the cylinder was preloaded three times with
90 kN (20 kips), the load was monotonically increased until the
cylinder failed. The split cylinder test was carried out during
the same time. Table 3.8 lists the compressive strength, the
tensile strength, the modulus of elasticity, and the Poisson's
ratio of the concrete at the beginning of slab specimen testing.
The ratios indicated in the table are those in the initial stage.

3.4 Testing Procedure

3.4.1 Test Setup

A group of special fixtures was developed to perform the experiment effectively. In order to facilitate the application of vertical load and provide access to the underside, the specimen was supported on four heavily reinforced concrete pedestals anchored to the floor of the testing laboratory. The tops of these pedestals were equipped to receive either a wall or a pair of columns. In either case, a variety of support fixidity was provided. A wall can be attached to the pedestal by means of twelve bolts along each side of the wall. Assisted by two pairs of heavy steel braces, these bolts completely prevented the wall from moving in the floor plane. Under this support condition, no force can be transmitted between slab panels on opposite sides of the wall. The slabs were effectively isolated from each other, thus enabling the testing of single panels. (Fig. 3.4) On the other hand, by removing the braces and loosening all anchoring bolts, the wall can be supported on several sets of ball bearings and, therefore, can become free to move about on top of the pedestal in any horizontal direction. The third alternative was to secure only four of the twenty four bolts near the middle of the wall to eliminate all translatory movements, while allowing the walls essentially free to rotate about a vertical axis. The column base fixtures were also adjustable to provide either a free sliding or a fixed

condition. The column in the free sliding condition did not offer any resistance to the applied lateral load and provides only a vertical reaction to the gravity load. With a fixed base, the only possible freedom was rotation about a horizontal hinge in the fixture, located 405 mm (16 in.) below the slab center plane. The columns in this condition participated in resisting lateral load. An overall view of the test setup is shown in Fig. 3.5.

3.4.2 Loading System

The in-plane load was generated by a double-acting mechanical jack placed at the slab center-plane and acting against a heavy steel frame. To simulate the desired shear action, a steel frame was used to distribute the jack load to five embedded studs along the loading line at uniformly spaced distances of 540 mm (21.3 in.). (Fig. 3.6 and 3.7) The frame and studs were carefully designed so that each stud would transmit approximately one fifth of the total applied load and the action would lie in the slab center-plane. Fig. 3.7 shows the dimensions of both the frame and studs. The total jack load was measured by a concentric loadcell between the loading jack and distribution frame. (Fig. 3.8) The load on each stud was not individually measured.

The out-of-plane (vertical) load was applied as a series of concentrated forces, spaced at 540 mm (21.3 in.) (one-third panel dimension) center-to-center in each direction. Inserts were placed at the center of each ninth portion of each panel for the application of these loads. (Fig. 3.9) All point loads within one panel width, including those in the quarter panel extension portions, were controlled by a single vertical (gravity) load simulator. A series of statically determinate levers was devised so that all point loads would be equal. (Fig. 3.10) A preliminary elastic analysis showed that a series of concentrated forces could reasonably simulate the uniformly distributed vertical load on the slabs. The vertical (gravity) load simulator was designed so that substantial displacement of the specimen would be permitted in the direction of the in-plane loading without affecting either the direction or the magnitude of the applied vertical load. The out-of-plane (vertical) load was monitored by two loadcells installed between the loading jack and the distribution levers.

3.4.3 Instrumentation and Recording of Data

Deflections and strains were monitored throughout the test. In-plane deflections were measured by linear variable differential transformers (LVDT's) connected to selected reference points. Figs. 3.11 and 3.12 show the arrangement of LVDT's at different phases of the experiment. All LVDT's were

connected to a single data aquisition system, and signals from the LVDT's were recorded on paper tapes. Several of the LVDT's also were connected to X-Y plotters together with the loadcell measuring in-plane loading, and the load-displacement relationship was continuously monitored. Fig. 3.13 schematically shows the whole system of instrumentation established at the single panel strength test.

Out-of-plane (vertical) deflections were measured at several points by means of a transit. A scale was fixed to the top of the tested slab panel at each measuring points. Fig. 3.14 illustrates the target locations as well as the measuring technique. W32 paper electrical wire strain gages were used to measure strains in reinforcing bars. After smoothing the surfaces of reinforcing bars, the strain gages were carefully mounted, protected, and waterproofed to avoid damage before and during the testing. A total of 196 strain gages were installed in each specimen: sixty strain gages in each slab panel and four gages in each column. Fig. 3.15 shows the location of the strain gages. The strain gages were connected to the data aquisition system, and their signals were recorded on paper tapes. Six sets of rosette gages were mounted on the surface of the tested slab immediately before the load was applied. Fig. 3.16 indicates the location of the rosette gages.

3.5 Testing Program and Sequence

A series of testing was programmed for each of the two specimens. The program's sequence was carefully planned to maximize information that can be obtained from the testing but minimize the time and effort required to prepare for each testing program.

The testing program consisted of four kinds of tests: the stiffness test, the strength test, the repaired strength test, and the free vibration test. In the stiffness, test, each specimen was tested as a whole unit, and elastic in-plane stiffness characteristics of the floor system were examined. In the strength test, each slab panel of specimens was tested separately according to predetermined loading and boundary conditions. Ultimate strength, stiffness in post-elastic regions, and ductility of the panel were examined. The panel damaged after the strength test was repaired by using the epoxy-injection technique and tested again under the same testing procedures used in the strength test, labelled the repaired strength test. In this test, the performance of the repaired panel on ultimate strength, stiffness and ductility was investigated. In the free vibration test, each slab panel of specimen was examined about its vibration characteristics such as frequency and damping. The vibration test was repeated several times at various stages in the entire testing

process of each panel: the initial stage, after strength test when the panel was severely damaged, after repair, and after repaired strength test. The changes in vibrational characteristics at these stages were examined.

This report deals with the first two tests only, namely, the stiffness test and the strength test. The description of the entire testing program as well as the test results are presented elsewhere.[3.2]

3.5.1 Stiffness Test

For each specimen, a stiffness test was carried out prior to the strength tests. Each specimen was tested as a whole unit, with both walls supported in the free-to-rotate condition and all columns in the free-to-slide condition. Small in-plane loads were applied simultaneously along both column lines (Fig. 3.11). Under these loading and boundary conditions, the specimen behaved like a simply supported beam with overhanging ends. Two loading conditions were used, both with loads of equal magnitudes. First, the loads were applied in the same direction, causing a symmetrical loading condition in the specimen, as shown in Fig. 3.11(a). In the second test, the loads were applied in opposite directions, causing an anti-symmetrical loading condition as in Fig. 3.11(b). The loads applied were limited to 15 kN (3.5 kip), 12 percent of the ultimate load, to ensure that the specimen would remain in its linear

-41-

elastic range. Deflection of the panels and rotation of the walls were measured with LVDT's, as shown in Fig. 3.11. In this figure, Θ is the rotation of the wall measured in the plane of the slab specimens. The LVDT pair, #9 and #10, or #11 and #12, measured this rotation. The displacement δ, monitored by the LVDT #1 or #5, was measured parallel to the loading at the end of the specimen.

3.5.2 Strength Test

In the strength test, the wall supporting the slab panel to be tested was securely fastened to a pedestal by means of bolts and braces. The other wall and all columns were supported on pedestals in the free-to-slide condition. The in-plane load was applied along the column line parallel to the fastened wall and through the horizontal load distribution frame described in Section 3.4.2. The out-of-plane (vertical) load was also applied when required by the testing program. LVDT's were installed at critical locations and monitored throughout the test as shown in Fig. 3.12. Signals from all strain gages both inside and on the surface of the tested panel were also recorded.

Two types of in-plane loads were used in the strength tests: monotonic loading and cyclic loading. In monotonic loading tests, the in-plane load was gradually increased until the resistance of the test panel decreased significantly after

-42-

reaching the ultimate strength. The load then was released and applied in the opposite direction until failure again took place in a similar manner. The load then was released again, and the test was completed. In the subsequent discussion, the first direction of loading is referred to as positive, and the second as negative. In cyclic loading tests, the in-plane load followed the spectrum shown in Fig. 3.17. The load was applied in complete cycles with gradually increasing displacement amplitudes. Three complete cycles were used at each amplitude. The spectrum was controlled by the displacement along the loading line. The amplitudes specified in the spectrum were: 0.25 mm, 0.76 mm, 1.3 mm, 2.8 mm, 4.3 mm, 5.8 mm, 7.6 mm, and 8.9 mm. This type of loading spectrum most effectively provides data regarding the hysteretic behavior of members or structures when the number of test specimens is limited.

For the tests including vertical (out-of-plane) loading, the total load was chosen to simulate full service dead and live loads. It is noted that the relative weight of the scaled model was less than that of the prototype. Therefore, the vertical load applied to the test panels represented, in addition to full service live load of 3.8 kPa (80 psf), also a supplement of service deal load of 3.9 Pa (83 psf). The total vertical load applied to the entire panel was 45.8 kN (10.3 kip).

The test was conducted according to the following procedure:

1. Initial readings were taken from all measuring devices: loadcells, LVDT's, strain gages, and vertical scales.

2. The out-of-plane (vertical) load up to the specified load level was applied if required. This load was held constant throughout the remaining steps of the test.

3. Strain and displacement readings were taken again after the application of out-of-plane loading. The data provided the characteristics of the test panel subjected to the design service vertical load.

4. The test panel was then preloaded by several cycles of a small in-plane load. The load was limited to 9 kN (2 kip) for tests without vertical load and to 5 kN (1.5 kip) for tests with vertical load. The purpose of this operation was to ensure that all instruments were working properly and make the whole testing system to stablize by adjusting itself.

5. After preloading, in-plane load was applied according to the specified load spectrum. The in-plane load was applied quasi-statically and stopped at frequent

load or displacement increments for strain and displacement measurements. During the in-plane loading, the vertical load was continuously monitored and adjusted to maintain its specified level.

6. The test was terminated when a significant drop in in-plane load resistance was observed, or when it became impossible to maintain the desired vertical load.

7. At the end of each test, a set of final readings were taken from all measuring devices after complete unloading.

3.5.3 Designation of Testing Programs

For the sake of convenience, each test in the program is identified by a five character alphanumeric code. The first character of the code is always B, signifying Beam-supported slab specimens. The second is either H or V. H indicates that no vertical load is applied (in-plane, Horizontal load only), while V indicates that Vertical load is applied together with in-plane load. The third character identifies the slab being tested. Numerals 1, 2, and 3 respectively refer to panels 1, 2, and 3. (Refer to Fig. 3.2) The stiffness test, in which specimens were tested as whole units, is identified by numeral 6 as the third character. A combination of the fourth and fifth characters defines the loading condition: MN for MoNotonic loading, CY for

CYclic loading, SS for Symmetrical loading in the stiffness test, and AS for Anti-Symmetrical loading in the stiffness test. A chart of the alphanumeric codes used in the testing program is tabulated in Table 3.9(a) with an example code. This table also summarizes the entire testing program and gives brief explanations of the characteristics of each testing program.

3.6 Test Results

3.6.1 Results of Stiffness Tests

A stiffness test was executed for each of the two specimens B-1 and B-2 . The displacements (δ) along the edges parallel to the loading and the rotation of the wall (Θ) were measured respectively by the LVDT pair #1 and #5 and the LVDT pairs #9 and #10, and #11 and #12. Table 3.10 lists the average values of the displacement and rotation per unit load as shown in Fig. 3.11. Specimens B-2 has slightly larger displacements and rotations than specimen B-1, hence lower stiffness. Shrinkage cracks were observed in specimen B-2 before the testing and they were believed to have contributed to the lower stiffness. The modulus of elasticity of concrete in the two specimens on the other hand, were nearly the same. (Table 3.8)

3.6.2 Behavior of Test Slab under Service Vertical Load

The service vertical load was applied to panels 1 and 2 of specimen B-2 prior to in-plane loading. Table 3.11 lists the vertical displacements of the panels under this condition measured at three points as shown in Fig. 3.14. Fig. 3.18 illustrates the strain distribution under the service vertical load. At this stage, two lines of cracks were observed on the top surface of the slab, one along the slab-wall junction, and the other along the column line parallel to the wall. (Fig. 3.19) Apparently, negative bending moment due to the service vertical load exceeded the cracking moment of the slab.

3.6.3 Results of Strength Test

The extreme loads and displacements from the strength tests are listed in Table 3.12. The displacements are measured at a point directly opposite the in-plane loading as shown in Fig. 3.12 (LVDT #3). The displacements shown in the figures represent the true deflections of the tested slab panels. All contributions of the fixed edge's movements were removed from the displacement measured by LVDT #3. Consequently, the true displacement spectrum applied to these test panels was slightly less severe than intended. Figures 3.20 through 3.25 show the load-displacement curve of the test slab panels.

-47-

Table 3.13 lists the stiffness of the panels under

small in-plane loads applied at the beginning of the test step

No. 4, Section 3.5.2. The elastic stiffness is defined as the

load per unit displacement along the loading line (LVDT #3).

The stiffness in post-elastic regions, on the other hand, is

not clearly defined since it varies according to load levels

as well as previous loading histories. In order to evaluate

the stiffness and stiffness degradation of the panels subjected

to cyclic loading, five different values are selected and

observed as schematically shown in Fig. 3.26. They are:

1) the slope labelled the secant stiffness 1, defined by the

line linking the points corresponding to the extreme dis-

placements of a hysteretic loop, 2) the slope labelled the secant

stiffness 2, defined by the line linking the points corres-

ponding to the maximum positive displacement and preceding

zero displacement of a hysteretic loop, 3) the slope labelled

the secant stiffness 3, defined by the line linking the points

corresponding to the maximum negative displacement and preceding

zero displacement of a hysteretic loop, 4) the slope labelled

the tangent stiffness 1, defined by the line linking the points

corresponding to zero and 1.3 mm (0.05 in.) displacements

intersected on the way to the maximum positive displacement of

a hysteretic loop, and 5) the slope labelled the tangent

stiffness 2, defined by the line linking the points corres-

ponding to zero and -1.3 mm (-0.05 in.) displacements intersected
on the way to the maximum negative displacement of a hysteretic
loop. The secant stiffness 1 measures the total load change
as the panel is subjected to a complete reversal of cyclic
displacements. The tangent stiffness 1 or 2 represents the
stiffness when a small reversed load is applied after a severe
load cycle. Test results have verified that the stiffness is
almost constant in the region between zero and ±1.3 mm displace-
ments. The secant stiffness 2 and 3 measure two additional
stiffness values referring to positive or negative loading only.
The difference between the secant stiffness 2 or 3 and the
tangent stiffness 1 or 2 reflects the pinching effect of the
hysteretic loop. Figures 3.27 through 3.29 show the stiffness of
the tested slab panels subjected to cyclic loading.

Figures 3.30 to 3.35 show the crack pattern of the
tested panels when the tests were completed. Numerals attached
to cracks represent the loads when the cracks were observed.
Solid lines indicate cracks developed during positive loading, and
broken lines indicate cracks developed during negative loading.
In addition, bold solid lines indicate "major cracks", which are
defined later. Only the top surfaces are shown for slab panels
tested with in-plane load alone since the crack patterns of both top
and bottom surfaces are nearly identical. For panels tested

with both vertical and in-plane loads, crack patterns of the top
and bottom surfaces were significantly different. Both top and
bottom crack patterns, therefore, are shown for these panels.

Figs. 3.36 and 3.37, respectively, show the vertical
deflections of BV1MN and BV1CY at measured locations. (Fig. 3.14)

For each strength test, comments and discussions are
given below.

BH2MN The utlimate load, 120 kN (27.0 kip), was reached
when several cracks, started at lower load levels, suddenly
started growing. This development was followed by a signifi-
cant loss in resistance of about 31 kN (7.0 kip). Although the
load again increased, approaching the ultimate load level
116 kN (26.0 kip), this time its stiffness was less. Another
significant loss of resistance took place when several rein-
forcing bars broke at a total displacement of 7.62 mm. After
the bars broke, the system regained its equilibrium at a load
of 70 kN (16 kip) and at a displacement of 8.6 mm. During
negative loading, defined as loading in the negative direction,
the maximum load attained was 89 kN (19.9 kip). At this point,
several reinforcing bars broke (-7.24 mm of displacement), and
the resistance was reduced greatly.

At 36 kN (8 kip), a crack developed along the slab-wall junction, extending from the edge of the slab to the beam. At 116 kN (26.0 kip), a point near the ultimate load, three cracks developed at the slab edge and rapidly extended inward. One of the cracks, which increased its width significantly, primarily controlled the behavior of the panel in the post-ultimate load region. This crack was labelled the major crack. Additional cracks developed diagonally between the first and second significant losses in resistance. The breaking of several reinforcing bars caused the second significant loss in resistance. One bar embedded in the quarter overhang and two in the beam broke at their intersections with the major crack. The major crack extended parallel to the wall at a distance of approximately 360 mm (14 in.). This line nearly coincided with the boundary between the column and middle strips of the panel, where a number of negative and positive reinforcing steel were cut off. During negative loading, the resistance decreased several times by about 5 to 8 kN (1.0 to 1.5 kip). These losses in resistance corresponded to the development of new cracks. When the load reached 89 kN (19.9 kip), one reinforcing bar in the overhang and two bars in the beam broke, which caused the resistance to decrease about 27 kN (6.0 kip).

BH3MN The ultimate load was obtained at 56.9 kN (12.8 kip),
followed by a decrease in resistance of 13 kN (3 kip). Afterward,the
load was unchanged,while the displacement increased from 2 to 7 mm.
Cracks were accumulated in the post-ultimate load region, and ano-
ther significant loss in resistance of about 13 kN (3 kip) caused
critical damage to the panel. During negative loading, the
load gradually increased to 39 kN (8.9 kip), followed by a
sudden decrease by 11 kN (2.5 kip).

At the load of 19 kN (4.3 kip), a crack which had
developed along the slab-wall junction extended from the tension
edge to the beam. The development of a second crack parallel
to the wall caused a significant loss in resistance immediately
after the ultimate load was reached. This crack, which later in-
creased in width, controlled the deformation in the post-ultimate
load region. At 5.1 mm (0.20 in.) of displacement, one
reinforcing bar in the overhang broke, causing a slight decrease
in resistance of 2 kN (0.5 kip). At 7.3 mm (0.29 in.) of
displacement, three bars in the beam and two additional bars
in the slab broke, reducing the resistance significantly. The
width of the major crack at the slab edge was 9.5 mm (3/8 in.)
at this displacement. During negative loading, the first crack
was observed at the load of 22 kN (5.0 kip). A second crack
which developed at 24 kN (5.5 kip) later merged with the major

crack developed during positive loading. After resistance
decreased slightly several times due to the development of new
cracks, three bars in the beam and two bars in the slab broke
at 6.2 mm (0.24 in.) of displacement. At this point, the load
decreased from 30 kN (6.8 kip) to 20 kN (4.5 kip), which was 52
percent of the negative ultimate load.

BH1CY   The resistance never decreased in each of the cycles
with the three lowest amplitudes: 0.25 mm, 0.76 mm, and 1.3 mm.
The hysteretic loops, then, were stable during these cycles.
The resistance decreased twice during the loading in each of
the 2.8 mm, 4.3 mm, and 5.8 mm amplitudes. The resistance
decreased once during the negative loading of the first cycle
and again during the positive loading of the second cycle in
the 2.8 mm amplitude. During the positive and negative load-
ings of the first cycle in the 4.3 mm and 5.8 mm amplitudes,
the resistance decreased again. The development of cracks
caused these losses of resistance. In the first cycle of the
5.8 mm amplitude, the critical cycle, both positive and negative
ultimate loads were attained [94.7 kN (21.3 kip) for the
positive ultimate load and 96.5 kN (21.7 kip) for the negative
ultimate load]. A crack extending parallel to the wall at a
distance of 360 mm (14 in.) developed during this cycle (the
major crack). During later loadings, new cracks did not develop,
and the major crack controlled the deformation. During cycles

-53-

of the 7.6 mm (0.23 in.) amplitude, the resistance decreased

gradually to 52 percent of the ultimate resistance for positive

loading and 63 percent of the ultimate resistance for negative

loading. The breaking of reinforcing bars at their intersections

with the major crack caused losses in resistance in this cycle.

A crack developed along the slab-wall junction at

28 kN (6.3 kip) during positive loading and at 28 kN (6.3 kip)

during negative loading. The major crack began at 38 kN (8.5

kip) from the edge subjected to tension under negative loading

and at 69 kN from the edge subjected to tension under positive

loading. The cracks, which developed at the edges of the panel,

extended inward while shifting their directions toward the

wall; these cracks developed substantially during the cycles

of the 4.3 mm (0.17 in.) amplitude for positive loading and

during the cycles of the 5.8 mm (0.23 in.) amplitude for negative

loading. The complete formation of the major crack, which

occured during the first cycle of the 5.8 mm (0.23 in.) ampli-

tude, prevented the development of other cracks. During

negative loading in the first cycle of the 7.6 mm (0.23 in.)

amplitude, one reinforcing bar in the slab broke, causing a

loss in resistance of 6.7 kN (1.5 kip). During positive load-

ing in the second cycle of the 7.6 mm (0.23 kip) amplitude,

one bar in the slab broke, causing a loss in resistance of

19 kN (4.3 kip). During the succeeding cycles of this ampli-
tude, several additional bars in the beams and slab broke.

BV1MN Unlike the previous strength tests, no substantial
loss in resistance was observed during testing. The load reached
95 percent of the ultimate load, 97 kN (22 kip), at 6.3 mm
(0.25 in.) of displacement. The panel deformed farther by about
2.5 mm (0.1 in.) without any loss in resistance. The ultimate
load, 102 kN (23 kip), was reached at 8.4 mm (0.33 in.) of dis-
placement and followed by a small portion having a slight
negative slope. The in-plane load was then removed at 8.8 mm
(0.35 in.) of displacement since the loading device arrived at
its limit. During negative loading, the resistance gradually
increased to 90 kN (20.3 kip), followed by a slight loss in
resistance. The test was terminated after the panel reached
-8.8 mm (-0.35 in.) of displacement.

Vertical deflections measured by the scales gradually
increased under positive loading as shown in Fig. 3.36. The
deflection at the center of the panel was 5.4 mm (0.21 in.)
immediately before unloading. Upon unloading of the in-plane
load, the deflections did not decrease but increased slightly.
They continued to increase under negative loading until near the
end of the test. The maximum deflection, reached immediately
before unloading, was 7.8 mm (0.31 in.) at the panel's center.

As mentioned in Section 6.3.2, the vertical load
caused two cracks on the top surface of the panel. One of these
cracks, developed along the slab-wall junction, extended down-
ward and finally reached the bottom surface at 22 kN (4.9 kip).
As evidenced from Fig. 3.34, the crack patterns between the top
and bottom surfaces differed significantly. Many cracks on
the bottom surface extended from the center of the panel in
radial direction, whereas cracks on the top surface were con-
fined near the slab-wall junction and more parallel to the wall.
The major crack, however, was observed almost simultaneously
on both top and bottom surfaces. At 27 kN (6.0 kip), a crack
(the major crack) developed and extended from the edge of the
slab at a distance of 330 mm (13 in.). During negative loading,
the major crack was observed for the first time at 35 kN (7.8
kip). This crack rapidly extended inward and merged with the
major crack developed during positive loading. No reinforcing
bars broke during this test.

BH3CY The resistance never decreased in each of the cycles
with the three lowest amplitudes: 0.25 mm, 0.76 mm, and 1.3 mm.
The hysteretics loops, then, were stable in these cycles. Dur-
ing the first cycle of the 2.8 mm (0.11 in.) amplitude, a crack,
which eventually became the major crack, developed parallel to
the wall at a distance of 280 mm (11 in.), and a slight decrease
in resistance occurred for the first time. The hysteretic

loops remained stable during the succeeding cycles of the 2.8 mm
(0.11 in.) amplitude as well as the three cycles of the 4.3 mm
(0.17 in.) amplitude. The pinching effect was appreciable during
the cycles of the 4.3 mm (0.17 in.) amplitudes. The maximum
resistance reached during the second and third cycles of the
4.3 mm (0.17 in.) amplitude was slightly lower than that reached
during the first cycle. The first cycle of the 5.8 mm (0.23 in.)
amplitude yielded the ultimate load for both positive and
negative loadings. [41.8 kN and 40.5 kN (9.4 kip and 9.1
kip)]. The resistance continuously decreased during the succeed-
ing two cycles of this amplitude and was only about 60 percent
of the ultimate resistance in the third cycle. Additional
cracks did not develop during the second and third cycles of
the 5.8 mm (0.23 in.) amplitude. At the end of the first cycle
of the 7.6 mm (0.30 in.) amplitude, the resistance was reduced
to 14.9 kN (3.36 kip), 36 percent of the ultimate resistance,
and the test was terminated.

A crack along the slab-wall junction was observed at
18 kN (4.2 kip) during positive loading and at 14.2 kN (3.2
kip) during negative loading. Most of the other cracks develop-
ed from the edge of the slab and extended inward during the 2.8 mm
(0.11 in.) amplitude. They extended almost directly across
the panel without shifting their directions. During negative
loading in the first cycle of the 5.8 mm (0.23 in.) amplitude,

a reinforcing bar in the overhang broke at 38.6 kN (8.68 kip).
During negative loading in the second cycle of the 5.8 mm
(0.23 in.) amplitude, two bars in the beam broke at 29.5 kN
(6.65 kip), causing a loss in resistance of 10.2 kN (2.3 kip).
During positive loading in the first cycle of the 7.6 mm
(0.30 in.) amplitude, one reinforcing bar in the slab and two
bars in the beam broke at 26.2 kN (5.91 kip). All of the broken
bars were cut off at their intersections with the major crack.

BV2CY The hysteretic loops remained stable in cycles
with the four lowest amplitudes: 0.25 mm, 0.76 mm, 1.3 mm, and
2.8 mm. A crack, which eventually became the major crack,
developed during the first cycle of the 1.3 mm (0.05 in.) ampli-
tude at a distance of 250 mm (10 in.) and extended parallel to
the wall. During negative loading in the first cycle of the
4.3 mm (0.17 in.) amplitude, a loss in resistance was observed
for the first time from 82.8 kN (18.6 kip) to 77.8 kN (17.5 kip).
During the succeeding two cycles of this amplitude, the maximum
resistance was slightly lower than that during the first cycle.
The ultimate loads were reached during the first cycle of the
5.8 mm (0.23 in.) amplitude [85.0 kN (19.2 kip) and 83.1 kN
(18.7 kip)]. The resistance then decreased significantly during
the succeeding two cycles of this amplitude. Two cycles with
the 7.6 mm (0.30 in.) amplitude were further applied. At the
end of this amplitude's second cycle, the resistance measured
about half of the ultimate resistance.

Vertical deflection increased during the loading.

At the end of the third cycle of the 5.8 mm (0.23 in.)

amplitude, the deflection at the center of the panel was

6.4 mm (0.25 in.), which was measured by the scale #2 in

Fig. 3.14. The deflection rapidly increased by 2.5 mm (0.10

0.10 in.) during the loading of the 7.6 mm (0.30 in.) amplitude.

Permanent deflection after both in-plane and vertical loads

were completely released was 5.3 mm (0.21 in.). (Fig. 3.37)

The deflections on the beams, which were measured by the

scales #1 and #3, showed the behavior similar to the deflect-

ion at the center of the panel. These deflections also

rapidly increased during the cycles with the 7.6 mm (0.30 in.)

amplitude as shown in Fig. 3.37 (a) and (c). The permanent

deflections were 4.1 mm (0.16 in.) for the scale #1 and 3.5 mm

(0.14 in.) for the scale #3.

Two cracks developed under the vertical load. One

of the cracks, developed along the slab-wall junction during the

first cycle of the 0.76 mm (0.03 in.) amplitude at the load of

22 kN (14.9 kip). Cracks were completely formed by the end

of the first cycle of the 5.8 mm (0.23 in.) amplitude;

afterward, the opening and closing of the major crack

controlled the deformation of the panel. During positive loading

in the first cycle of the 7.6 mm (0.30 in.) amplitude, one

reinforcing bar in the overhang and one bar in the beam broke,
causing a loss in resistance from 80.0 kN (18 kip) to 70 kN
(15.7 kip). During negative loading in the first cycle of
the 7.6 mm (0.30 in.) amplitude, one reinforcing bar in the
overhang and two bars in the beam broke, and the resistance
decreased from 71.6 kN (16.0 kip) to 60.9 kN (13.7 kip).

3.7 Discussion

3.7.1 Stiffness Test

In-plane stiffnesses of the slab panels were calcul-
ated by an elastic finite element analysis in order
to be compared with the experimental results. The standard
SAP IV[3.1] finite element program was used with the following
assumptions and specifications:

1. Inelastic action was not considered.

2. The concrete material was taken to be isotropic
    and homogeneous. Reinforcing bars were not included.

3. The material properties for concrete: the modulus
    of elasticity and poisson's ratio, were assigned
    values as obtained from concrete cylinder tests.
    (Table 3.8)

4. The analysis was treated as a two dimensional plane
    stress problem. Forces, stresses, and deflections
    in the third direction were ignored.

-60-

5. Slabs were represented by a number of square plane stress elements. Beams were represented by flexural beam elements. The eccentricity between the neutral axes of slabs and beams was neglected. Then, no consideration was made on the effect of out-of-plane deformation caused by the in-plane loading on the in-plane stiffness.

6. A rather coarse discretization was used as shown in Fig. 3.38. This is referred to as Type I.

The third column of Table 3.10 lists the deflection (δ) and rotation (Θ) obtained from the finite element analysis. The ratio of the values from this analysis to the experimental results range from 0.87 to 1.03 for the B-1 specimen and from 0.83 to 0.95 for the B-2 specimen. The analysis produces greater stiffnesses than the test by an average of 8 percent for the B-1 specimen and 12 percent for the B-2 specimen. The fact that the finite element method gives an upper bound of the solution is responsible for a fraction of the discrepancy. The remainder of the discrepancy can be attributed to minute cracks caused by shrinkage or accidental forces which might have been applied

during the transportation of the specimens. In addition,

the material properties used in the analysis, based upon the

concrete cylinder tests, may not have represented the

material properties in the specimens. In general, however,

the correlation between the stiffness test and elastic

finite element analysis is considered reasonable.

3.7.2 Behavior Under Design Service Vertical Load

An elastic finite element analysis using SAP IV

was carried out on the behavior of a single slab panel

subjected to design service vertical load. In this analysis,

assumptions with respect to the concrete material properties

followed those described in Section 3.7.1. This time,

however, the panel was solved as a plate problem, and square

plate elements were used. The panel was discretized as shown

in Fig. 3.38, referred to as Type II.

The strain distribution obtained by the analysis

as well as the strains measured in the tests are shown in

Fig. 3.18. The analysis shows that the strain in the middle

portion of the slab-wall junction exceeds the cracking strain,

which is calculated based upon the modulus of rupture, $7.5\sqrt{f_c'}$,

and the elastic modulus. The strain, however, is less than the cracking strain in the remaining portion of the panel. Once a part of the panel falls into the inelastic region, the stress is completely redistributed; therefore, elastic analysis is no longer valid. The strains measured in the tests, on the other hand, apparently exceed the cracking strain in the middle portions of the slab-wall junction (Section 1-1 in Fig. 3.18) and the column line parallel to the loading (section 3-3 in Fig. 3.18). Both the elastic finite element analysis and test results show evidence of the crack development under the design service vertical load.

As shown in Table 3.11, measured vertical deflections are greater than the vertical deflections obtained in the analysis. The difference between the analytical and measured deflections is appreciable particularly at points #1 and #3 which were directly above the beams (Fig. 3.14); the measured deflections are nearly twice the calculated values. The two cracks that developed in the panels probably caused additional deflection.

The difference between the analysis and test results could be attributed primarily to any non-linear and/or inelastic action of the panel, which was not considered in the analysis.

In order to further evaluate the stress and deflection of the panel subjected to the design service vertical load, various non-elastic behaviors such as cracking of concrete and yielding of concrete or steel should be incorporated into the analysis.

3.7.3 Strength

Test results show that the type of loading (monotonic vs. cyclic loading), the moment-to-shear ratio, and the intensity of vertical load all affect the ultimate strength of the slab panels. In all cases, the ultimate strength was reached immediately preceding the development of the major crack which extended parallel to the wall at a distance of about 350 mm (14 in.). This major crack extended along the boundary between the column and middle strips of the slab panel. Many reinforcing bars which function as either positive or negative reinforcement were terminated at this location. (Fig. 3.3) The panels' resistance decreased after the formation of the major crack. Very few new cracks developed afterwards, while the overall deformation of the panel was controlled primarily by the opening and closing of the major crack. (The section at the major crack acted like a plastic hinge).

3.7.3.1 Effect of Type of Loading or Strength

The three pairs of test panels: BH2MN and BH1CY,
BV1MN and BV2CY, and BH3MN and BH3CY, were compared to determine
the effect of the type of loading on the ultimate strength.

Cyclic loading resulted in a significant decrease of
the ultimate resistance approximately by 20 to 25 percent. The
ratio of the ultimate load under cyclic loading to that under
monotonic loading was 0.79 (BH1CY/BH2MN), 0.83 (BV2CY/BV1MN),
and 0.73 (BH3CY/BH3MN) respectively, for the three pairs.
Cumulative damages such as cracks were considered the most
probable reason for such a reduction in the ultimate load.
Under cyclic loading, the ultimate strength would depend upon
the compressive strength of concrete which has been cracked
previously. Even though the cracks are closed, the bearing
may not be complete, and the effective strength may be reduced.

In monotonic loading tests, the ultimate load under
negative loading was always lower than under positive loading.
The ratios of the ultimate load under negative loading to that
under positive loading were 0.74 (BH2MN), 0.88 (BV1MN), and
0.68 (BH3MN), respectively. This strength reduction was
attributed to damages caused during the last stage of positive
loading. By the time positive loading was completed, many

cracks had developed, and major cracks had extended almost
to the opposite edges of the panels. Several reinforcing bars
also had broken. These damages would logically have weakened
the panel under negative loading.

In cyclic loading tests, on the other hand, the
ultimate loads under positive and negative loadings were
almost identical. The ratios of the ultimate load under
positive loading to that under negative loading were 1.01
(BH1CY) 0.98 (BV2CY), and 0.97 (BH3CY). Here, damages were
accumulated gradually by cyclic loading, and directional pre-
ference was minimal.

3.7.3.2 Effect of Vertical Load on Strength

The effect of vertical (out-of-plane) loading on the
in-plane strength was studied by comparing the results of test
panels BH2MN vs. BV1MN and BH1CY vs. BV2CY. As might be expected,
the vertical load lowered the ultimate in-plane resistance.
The ratio of the ultimate load with the vertical load to that
without such load was 0.85 for positive loading and 0.98 for
negative loading from the pair BV1MN/BH2MN and 0.89 for positive
loading and 0.86 for negative loading from the pair BV2CY/BH1CY.
The design service vertical load reduced the resistance by no
more than 15 percent.

3.7.3.3 Effect of Moment-to-Shear Ratio on Strength

Two moment-to-shear ratios were used in the strength

tests of various panels. For panels 1 and 2, the ratio was

1.63 m (64 in.), while for panel 3, the ratio was doubled.

Two sets of tests can be compared to determine the effect of the

moment-to-shear ratio on their strength: BH2MN and BH3MN, and

BH1CY and BH3CY. Direct comparison showed strength ratios of

0.47 for positive loading and 0.44 for negative loading for

panels tested monotonically (BH3MN/BH2MN) and 0.44 for positive

loading and 0.42 for negative loading for panels under cyclic

loading (BH3CY/BH1CY). The doubling of the moment-to-shear

ratio is seen to reduce the resistance to about 40 to 45 percent.

Interestingly, this ratio of 0.40 to 0.45, agrees closely to

the ratio of distances of the major cracks from the applied in-

plane load. As described in Section 3.7.1, the major crack

developed along the boundary between the column and middle

strips. The distance from the loading line to the major crack

is 1220 mm (48 in.) for panels 1 and 2, and 2840 mm (112 in.)

for panel 3. The ratio of the distances is 1220/2840 or 0.43,

which is nearly the same as the experimental ultimate strength

ratio, 0.40 to 0.45. This correspondence implies that the

ultimate strength of the slab panel was controlled primarily

by the flexural capacity at the major crack section. The trans-

verse shear force had only a secondary effect.

-67-

3.7.4 <u>Stiffness</u>

3.7.4.1 <u>Changes in Stiffness under Monotonic Loading</u>

The tangent stiffness of BH2MN and BH3MN continuously decreased as load increased until the maximum resistance was reached. Several times in the post-ultimate load region, resistance decreased suddenly as each new crack opened. However, each time the load was recovered quickly, and, consequently, the level of resistance remained relatively stable until the breaking of reinforcing bars drastically reduced the resistance. The initial tangent stiffness, the tangent stiffness immediately before the ultimate loads, and the secant stiffness at the ultimate loads were 218 MN/m, 33.8 MN/m, and 42.9 MN/m for BH2MN and 166 MN/m, 22.2 MN/m, and 28.5 MN/m for BH3MN. The tangent stiffness at the ultimate load was 16 percent of the initial tangent stiffness for BH2MN and 13 percent for BH3MN. As evidenced in Fig. 3.24, the behavior of BV1MN is significantly different from that of BH2MN or BH3MN. The tangent stiffness was 222 MN/m initially and monotonically decreased to practically zero. The ultimate load was reached at a rather large displacement, and there was no sudden changes of resistance as displacement continued to increase with the formation of additional cracks. The vertical load apparently prompted the development of cracks. This process, in turn, resulted in a more rapid stiffness degradation for BV1MN than for BH2MN or BH3MN. When

-68-

cracking occurs, the force carried by concrete at the interface

of the crack before cracking must be transferred to reinforcing

bars. The early development of cracks in BV1MN apparently

enabled a more gradual transfer of force from concrete to

reinforcing bars. The gradual transfer of force not only pre-

vented the sudden loss in resistance caused by cracking, but

also retarded the attainment of the ultimate load.

Stiffness was substantially recovered during unload-

ing. For BH2MN, the tangent stiffness at the beginning of un-

loading was 67.2 MN/m, approximately 31 percent of the initial

tangent stiffness and nearly double the tangent stiffness

before unloading. For BH3MN and BV1MN ,the tangent stiffnesses

at the instant of unloading were 33.7 MN/m and 83.3 MN/m, which

were 21 and 37 percent of their respective initial tangent

stiffnesses. As the load was applied in the negative direction,

stiffness degraded until the load reached approximately 50 per-

cent of the ultimate strength. Unlike the development during

positive loading, the tangent stiffness remained nearly cons-

tant for loads above this level. The tangent stiffness in

this region was 4.2 MN/m for BH2MN, 2.8 MN/m for BH3MN, and

3.2 MN/m for BV1MN, less than 2 percent of the initial tangent

stiffness.

The load level in which the initial tangent stiffness was applicable did not exceed 36 kN (8 kip) for BH2MN, 10 kN (4.3 kip) for BH3MN, and 13 kN (3 kip) for BV1MN, which represent 13 to 20 percent of the ultimate resistance. Table 3.14 tabulates the stiffness values at various load stages.

3.7.4.2 Changes in Stiffness under Cyclic Loading

For all cyclic loading tests, BH1CY, BV2CY, and BH3CY, stiffness rapidly degraded during the cycles with two lowest amplitudes, 0.25 mm and 0.76 mm. At the end of the sixth cycle, the stiffness had reduced to 90 MN/m for BH1CY and BV2CY, and 50 MN/m for BH3CY. During the succeeding cycles, stiffness continued to decrease as amplitude increased. At the end of tests, the secant stiffness 1, as defined in Section 3.6.3, was 6.5 MN/m for BH1CY, 8.6 MN/m for BV2CY, and 3.9 MN/m for BH3CY. These values represent only 2 to 4 percent of the respective initial stiffnesses.

With few exceptions, stiffness remained the same for the three cycles at each amplitude. Occasionally, a significant crack developed, and stiffness decreased during the succeeding cycles. Damage like the breaking of reinforcing bars and the widening of cracks, on the other hand, caused continual degradation of stiffness in greater amplitudes (5.6 mm and 7.6 mm amplitudes).

As shown in Figs. 3.28 and 29, the two types of
stiffness defined in Section 3.6.3, the secant stiffness 2 and
3, were almost identical for BH3CY and BV2CY, indicating that
the stiffness degraded symmetrically in both positive and
negative directions during cyclic loading. In addition, secant
stiffness 1 also did not differ much from the other secant
stiffnesses, indicating that the widths of hysteretic loops were
narrow and that energy absorption in a complete cycle was
small. Specimen BH1CY behaved quite differently; the three
secant stiffnesses were all different. Secant stiffness 3
degraded more quickly than secant stiffness 2 and was about
40 percent of the secant stiffness 2 in the cycles of the
five lowest amplitudes (0.25 mm, 0.76 mm, 1.3 mm, 2.8 mm, and
4.3 mm). The test of BH1CY also showed that cracks
developed more often under negative loading than positive
loading during these cycles. Secant stiffness 1 of BH1CY
corresponded to the average of secant stiffnesses 2 and 3.

The difference between secant stiffness 1, 2, or 3
and tangent stiffness 1 or 2 was small for BV2CY, while for
BH1CY and BH3CY, tangent stiffness 1 and 2 were relatively
smaller than secant stiffness 1, 2, and 3 particularly during
cycles of larger amplitudes. The difference resulted
primarily from the pinching effect of hysteretic loops.   The

difference was appreciable during the cycles of the 5.8 mm
and 7.6 mm amplitudes for BH1CY and the cycles of the 2.8 mm,
4.3 mm, and 5.8 mm amplitudes for BH3CY. During these cycles,
tangent stiffness 1 or 2 was about 50 percent of secant
stiffness 1, 2, or 3.

3.7.4.3 Effect of Vertical Load on Stiffness

In monotonic loading tests, the trends of stiffness
degradation on BH2MN and BV1MN are substantially different as
described in Section 3.7.4.1. In BV1MN, stiffness gradually
degraded smoothly without sudden decreases of resistance, measur-
ing near zero at the ultimate load. In BH2MN, on the other hand,
stiffness was approximately 15 percent of the initial stiffness
when the ultimate load was reached. Afterward, resistance
fluctuated without significant decrease, while displacement
increased many fold until the resistance was drastically reduced
by the breaking of reinforcing bars.

In cyclic loading tests, the trends of stiffness de-
gradation in BH1CY and BV2CY are similar. In fact, values of
secant stiffness 1 in these tests are close particularly
for amplitudes 1.3 mm or greater. In these ranges, secant
stiffness 1 gradually degraded from 50 MN/m to 10 MN/m as
amplitudes increased and continued to degrade during each load-
ing cycle of the 7.6 mm amplitude.

As listed in Table 3.13, the initial stiffness was
218 MN/m for BH2MN, 272 MN/m for BH1CY, 222 MN/m for BV1MN, and
201 MN/m for BV2CY. During initial loading stages, all
conditions were identical for BH2MN and BH1CY and for BV1MN
and BV2CY. The initial stiffness of BH2MN, however, was 80
percent of that of BH1CY, while the initial stiffnesses of
BV1MN and BV2CY were nearly the same. The reason for BH2MN to
have a 20 percent lower initial stiffness than BH1CY was not
clear although imperfection or damage was strongly suspected
for BH2MN at the beginning of the testing. Referring to the
initial stiffness of BH1CY, 272 MN/m, as a datum, the initial
stiffness was reduced by about 20 percent due to the design
service vertical load.

3.7.4.4 Effect of Moment-to-Shear Ratio on Stiffness

As described in Section 3.7.4.3, the initial stiffness
of BH2MN was suspiciously smaller than the initial stiffnesses
of other tested slabs and, therefore, not appropriate for the
use in meaningful comparisons. In monotonic loading, however,
the tangent stiffnesses of BH3MN and BH2MN at all other stages:
under positive loading, at the beginning of unloading, and under
negative loading (except the initial stiffness), showed very
consistent relationship. The stiffness of BH3MN ranged from
50 to 60 percent of that of BH2MN.

In cyclic loading, the relative stiffness ratio of BH1CY to BH3CY was 0.61 initially and ranged from 0.47 to 0.60 during the succeeding loading cycles, based on secant stiffness 1, 2, or 3. The ratio had a tendency to gradually decrease as amplitudes increased. The relative stiffness ratio, however, decreased about 0.25 to 0.30 in amplitudes equal to or greater than 4.3 mm (0.17 in.) if tangent stiffness 1 or 2 was substituted. In these amplitudes, the pinching effect was more appreciable for BH3CY than for BH1CY as shown in Fig. 3.23.

3.7.5 Behavior in Post-Ultimate Region

3.7.5.1 Definition of Deformability and Ductility

Table 3.15 facilitates the discussion of deformability and ductility of tested slab panels. The first two columns list the displacements, labelled critical displacements, at which the resistance of panels decreased substantially. The first and second columns respectively list the critical displacements under positive and negative loadings. As described in Section 3.6.3, critical displacements are much greater than the displacements corresponding to the maximum resistance and immediately followed by the breaking of reinforcing bars.

Ductility, listed in the third and fourth columns, is defined as the ratio of the critical displacement to the displacement at which 90 percent of the ultimate resistance was first reached. The load-deflection curves of all tested panels except

-74-

BV1MN had some plastic plateaus. The curve of BV1MN did not have a plastic plateau in either direction as shown in Fig. 3.24, indicating that stiffness gradually degraded as load increased. Ductility was not calculated for BV1MN since the test was terminated before any reinforcing bars broke. The table's final column lists the deflections, labelled total deflections, which equal the sums of the positive and negative critical displacements.

3.7.5.2 Monotonic Loading vs. Cyclic Loading

The comparison between BH2MN and BH1CY shows that total deflection and ductility respectively are 10 percent and 45 percent larger for monotonic loading. The ductility of the two panels differed primarily because the deflection at which 90 percent of the ultimate resistance reached for the first time was larger for BH1CY than for BH2MN. The comparison of BH3MN and BH3CY shows the same tendency. BV1MN, on the other hand, deformed more than BV2CY by about 60 percent.

3.7.5.3 Effect of Vertical Load

Ductility was nearly the same for BH1CY (without vertical load) and BV2CY (with vertical load), while BH1CY deformed about 15 percent more than BV2CY. A comparison between BH2MN (without vertical load) and BV1MN (with vertical load), on the other hand, shows that BV1MN deformed 25 percent more than BH2MN.

Note, however, that BV1MN deformed more than any other tested panels. In general, the design service vertical load affected ductility slightly.

3.7.5.4 Effect of Moment-to-Shear Ratio

The slab panels with a moment-to-shear ratio of 3.25 m (128 in.) (BH3MN and BH3CY) were 1.2 times more ductile than the slab panels with a moment-to-shear ratio of 1.63 m (64 in.). Apparently, ductility was improved for panels in which bending moment (flexural deformation) was dominant. Total deflection, on the other hand, is less in BH3MN and BH3CY than in BH2MN and BH1CY by about 15 percent.

3.8 Summary and Remarks

The experimental work has provided information about the in-plane characteristics of the slab panels under various supporting and loading conditions. Elastic analysis by means of the finite element method has provided some verifications and comparisons. The results of these comparisons are summarized below.

1. The elastic finite element analysis predicted a slightly higher stiffness of the 3-panel test specimens under symmetrical and anti-symmetrical in-plane loads. (Section 3.7.1) The analysis

produced stiffnesses 10 to 20 percent higher than
the experiments. Minute residual stresses due to
shrinkage or accidental loads prior to the testing
are believed to be responsible for these discrepan-
cies.

2. Two cracks, one along the slab-wall junction and the
other along the column line parallel to the wall,
developed on the top surface of the panel when
subjected to the design service vertical load.
(Section 3.6.2) Plate analysis confirmed the occur-
ence of these cracks. (Section 3.7.2)

3. The development of a crack, labelled a major crack,
which extended parallel to the wall at a distance
of about 350 mm, controlled the ultimate in-plane
resistance of the test slab panel. (Section 3.6.3)
This location of the major crack coincided with the
boundary between the column and middle strips of the
slab panel. The ultimate load was reached when the
major crack extended completely across the panel.
Afterward, the opening and closing of the major crack
controlled the deformation. The flexural capacity
of the section through which the major crack extended
primarily governed the ultimate resistance. The
magnitude of shear affected the ultimate resistance
very slightly. (Section 3.7.3.3)

4. Cyclic loading, specified by the spectrum shown
    in Fig. 3.17, reduced the ultimate resistance of
    the panels by 20 to 25 percent. (Section 3.7.3.1)
    Cumulative damages like cracks most likely caused
    this reduction.

5. The application of the design service vertical load
    reduced the ultimate in-plane resistance by not more
    than 15 percent. (Section 3.7.3.2) The vertical
    load, however, did not alter the general behavior of
    the slabs; the major crack still developed along the
    boundary between the column and middle strips, and
    the complete formation of the major crack governed
    the ultimate resistance.

6. In panels under monotonic in-plane loading, tangent
    stiffness gradually degraded until the ultimate
    resistance was reached. (Section 3.7.4.1) The tan-
    gent stiffness immediately before this occurred was
    10 to 15 percent of the initial tangent stiffness.
    After reaching the ultimate resistance, resistance
    decreased several times due to the development of
    cracks. The load, however, was recovered and the
    level of resistance remained relatively constant
    until the breaking of reinforcing bars drastically
    reduced the resistance. (Figs. 3.20 and 3.22)

7. In panels under monotonic in-plane loading, the design
   service vertical load significantly affected the
   pattern of stiffness degradation. (Section 3.7.4.3)
   Tangent stiffness degraded gradually, measuring near
   zero at the ultimate load. The vertical load apparently
   enhanced the development of cracks, and cracking in
   low load levels made the transfer of forces from con-
   crete to reinforcing bars more gradual. (Fig. 3.24)

8. For cyclic loading, stiffness continually degraded as
   amplitude increased. During each cycle having a
   small to medium amplitude, stiffness remained cons-
   tant. During cycles with a larger amplitude, in which
   some reinforcing bars broke, stiffness continuously
   degraded as the load was reversed. (Section 3.7.4.2)

9. Three kinds of stiffness, secant stiffness 1, 2, and
   3, defined in Section 3.6.3 differed little, indicating
   that stiffness changed only slightly in a complete
   cycle. (Section 3.7.4.2) In the panels with no
   vertical load, the pinching effect was appreciable
   during the cycles with large amplitudes but confined
   in relatively small regions (in the vicinity of neu-
   tral displacement). In the panels with vertical load,
   on the other hand, the pinching effect was not
   evident. (Section 3.7.3.4)

10. Regardless of the loading condition, the definition
    of stiffness, or the level of deflection, the increase
    of the moment-to-shear ratio from 1.63 m (64 in.) to
    3.25 m (128 in.) reduced the in-plane stiffness by
    approximately 40 to 50 percent.

11. Compared with monotonic loading, cyclic loading reduced
    the range of deformation (total deflection defined in
    Section 3.7.5) by about 10 percent and the range of
    ductility by about 45 percent. (Section 3.7.5.2) The
    design service vertical load reduced neither total
    deflection nor ductility. (Section 3.7.5.4)

12. The panels with a moment-to-shear ratio of 3.25 m
    (128 in.) were 1.2 times more ductile than the slabs
    with a moment-to-shear ratio of 1.63 m (64 in.).
    Total deflection, on the other hand, was approximately
    15 percent less in the panels with the larger moment-
    to-shear. (Section 3.7.5.3)

IV ANALYTICAL STUDY

4.1 General

This chapter deals with the development of an analytical model, which can predict the behavior of concrete floor slabs beyond the linear elastic range. The experimental study described in Chapter III has provided valuable information on the behavior of floor slabs under various loadings. Because of the limited number of tests, however, experimental data were insufficient for the development of appropriate design procedures. The analytical study was needed to supplement the experimental findings.

It is difficult to obtain closed-form solutions for the behavior of reinforced concrete members because of the non-linear inelastic material behavior as well as the composite behavior of the two components. It is necessary to simulate the changing of concrete modulus, the developing of cracks, and the yielding of reinforcing bars. The finite element method was used to develop the model.

The characteristics and formulation of the proposed model are described in Sections 4.4 and 4.5. In Section 4.6, the model is applied to various example problems, and the accuracy of this model is evaluated by comparing the analytical solutions with the experimental result and other available data.

4.2 Review of Application of the Finite Element Method to Problems of Reinforced Concrete Structures

The finite element method has been applied to the study of reinforced concrete structures ever since this method was deviced. Many studies have dealt with beams, frames, walls, plates, and shells. Scordelis,[4.24] Darwin,[2.14] and Ngo[4.21] have reviewed extensively the literatures describing the application of this method.

4.2.1 Application to Two-Dimensional Problems, (I) Crack-Line Approach

Ngo and Scordelis[4.20] were the first to demonstrate the application of the finite element method to reinforced concrete beams. They modelled concrete and steel as linear elastic materials connected by linear elastic 'bond links'. Cracks were predefined as the separation of nodal points. Nilson[4.19] extended this method to include non-linear material properties and a non-linear bond-slip relationship. He used an incremental load procedure to analyze reinforced concrete members subjected to concentric or eccentric loads. Whenever cracking was indicated, the tracing of the crack development was performed manually. The finite element mesh layout was modified accordingly, and the analysis was started again from zero load and incrementally loaded to the next stage of failure. Later, Ngo[4.21] extended this method to automatically produce crack-lines to simulate progressing crack growth. He developed an finite element program which was capable of automatically generating nodal points in one continuous execution.

-82-

Kawai et al.[4.12, 4.13, 4.15] proposed another method
to analyze reinforced concrete members. Their model represented
a concrete plate as an assembly of triangular elements inter-
connected by normal and shear springs. Each triangular finite
element was assumed to be rigid, and therefore displacements
at any point in this element were expressed by the displacements
and rotations at its centroid. The coefficients of springs at
the interfaces were determined to reflect the material properties
of the concrete plates. The development of cracks was then
simulated by reducing the spring constants at cracked interfaces.
The concept of this model is somewhat equivalent to the yield line
theory. These researchers executed nonlinear incremental analyses
of plane concrete members subjected to direct tension.[4.14]

4.2.2 Application to Two-Dimensional Problems, (II) Crack-Zone Approach

Cervenka and Gerstle[1.6, 2.10, 4.7] developed the
idea of employing a finite element with composite concrete-steel
material properties at uncracked, cracked, and plastified stages.
They carried out the non-linear incremental analysis of reinforced
concrete panels under both monotonic and cyclic loadings. The
program included the closing and re-opening of cracks within the
finite element. They treated the concrete as an elasto-plastic
material in compression and as an elastic brittle material in
tension. Once a crack was opened, stiffness perpendicular to the

-83-

crack and shear stiffness parallel to the crack were set at zero.
The program had a capacity of automatically altering these
material properties in one continuous execution. The newly
defined orthotropic material could take stress parallel to the
crack only. The same general approach was used by later studies.
Valliappan and Doolan,[4.26] and Suidan and Schnobrich[4.25]
applied this method to cantilever beams. Yuzugullu and Schnobrich
[2.48] used Cervenka's and Gerstle's procedure for shearwall
problems. Yuzugullu and Schnobrich pointed out that better
results were obtained if a finite value was employed for shear
stiffness parallel to the open cracks instead of zero. Salem[4.23]
also applied this method to solve shear panel and beam problems.
He incorporated the hardening rule into the formulation of the
concrete constitutive relationship. Adham et al.[4.1] included
bond slips and the dowel action in this model.

The studies already mentioned produced workable results
for monotonic loading. The investigations which attempted to
determine the behavior of reinforced concrete members under cyclic
loading, [2.10, 4.7] however, met with indifferent results. While
the experimental results showed a continuous loss of stiffness
and strength with each cycle of load, the analytical model did
not show such degradation. Darwin and Pecknold[2.14, 4.9]
developed a new material model to represent the hysteretic
behavior of concrete under biaxial loading. The constitutive law
of concrete derived form this material model was expressed in
terms of the stress-increment and the strain-increment depending

-84-

upon the current stress state as well as the previous history of concrete. Darwin and Pecknold combined this constitutive law with the procedures developed by Cervenka[2.10] and solved several shear panel problems under cyclic loading. Aktan[4.2] later used this constitutive law to investigate shearwall behavior under cyclic loading.

4.2.3 Application to Plate Problems

While aforementioned studies deal with reinforced concrete beams and panels subjected to in-plane loadings, the finite element method has also been used to analyze the reinforced concrete plates under out-of-plane loadings. Jofriet and McNeice[4.11] combined the finite element analysis with the concept of the effective moment of inertia, originally offered by Branson[4.6] and Beeby,[4.5] in order to analyze reinforced concrete slabs subjected to out-of-plane loadings. In their analysis, the effective moment of inertia calculated the stiffness of cracked plate elements because setting the flexural stiffness for the cracked elements at zero usually leads to underestimates of the flexural rigidity. Hand et al.,[4.10] on the other hand, solved reinforced concrete plate and shell problems by using layered finite elements. In their analysis, each plate or shell element was divided into several layers through the thickness, and each subdivided element was treated as a two dimensional plane stress element. Kirchhoff-Love's hypothesis was employed to satisfy

the compatibility of these subdivided elements. Like Suidan's and Schnobrich's[4.25] and Yuzugullu's and Schnobrich's[2.48] studies, their analysis also adopted non-zero shear stiffness for cracked elements. The results of their analysis showed that the magnitude of the shear stiffness in cracked elements was not crucial for the overall behavior as long as a non-zero value was used. Bashur and Darwin[4.4] also used the layered finite elements for their study, combining these elements with the material model proposed by Darwin and Pecknold[4.9].

4.3 Modelling of Material Properties

4.3.1 Inelastic Behavior of Material

<u>Concrete</u> Many of the previous studies[2.10, 2.14, 4.1, 4.24,4.26] modelled concrete as a linear-elastic perfectly-plastic material and applied the Von Mises yield criterion and the associated flow rule to develop the elasto-plastic constitutive equation formulated by Zienkiewicz et al.[4.29] Salem[4.23] modified that model, introducing the hardening rule first developed by Ziegler.[4.28] Kupfer and Gerstle[4.17] and Liu,[4.18] proposed constitutive models for monotonic biaxial loading of plane concrete based upon their experimental investigations. Darwin and Pecknold[4.9] formulated a constitutive

equation of concrete subjected to biaxial cyclic stresses.
Aktan[4.3] and Bashur and Darwin[4.4] later used that model
for their studies.

Steel Many studies treated reinforcing bars as
uniaxially loaded members, idealizing the stress-strain relation-
ship of those bars to be linear-elastic perfectly-plastic[2.10, 2.14, 4.4, 4.23, 4.25, 4.26] or bilinear.[2.48, 4.1, 4.3]
Peterson and Kostem,[4.22] on the other hand, used the Ramberg-
Osgood material model for representing the stress-strain relation-
ship of reinforcing bars. Aktan et al.[4.3] studied the cyclic
behavior of reinforcing bars, concluding that the Ramberg-Osgood
or linear-elastic perfectly-plastic models satisfactorily dupli-
cates the experimental hysteretic stress-strain curves.

Bond Slip Some studies investigating the behavior of
bond slips[4.19, 4.20, 4.21] introduced special link elements
representing the bond slip between concrete and reinforcing bars.
The bond slip, however, was neglected in most research studies
of the general behavior of structural elements.

Cracks Two types of models for the crack development
were used in the previous studies. One was the crack-zone model,
in which cracking was assumed to take place within a finite
region of the structure.[1.6, 2.10, 4.1, 4.2, 4.7, 4.9, 4.10, 4.25, 4.26, 4.44] Cracks in a finite element modified the element

stiffness matrix to reflect the loss of tensile concrete strength in the direction perpendicular to the cracks. The second model represented cracks as lines between two nodes.[4.12, 4.13, 4.14, 4.15, 4.19, 4.20, 4.21] Whenever cracks developed, the interface tractions along the cracked lines were released.

4.3.2 Related Experimental Findings

The experimental study described in Chapter III has offered specific information about the post-elastic behavior of the floor slabs, which was used to select appropriate models. The post-elastic behavior of the slab panels was controlled primarily by the development of cracks and the yielding of reinforcing bars. The region in which concrete was compressed beyond its elastic limit was small. The strength of the slab panel was controlled by the flexural capacity of the critical section into which the major crack penetrated, while the shear force had little effect.

The dowel action of reinforcing bars also had very little influence on the ultimate capacity of the slab panels since the diameters of reinforcing bars were small (not more than 4.6 mm), and the slab panels were lightly reinforced. The experimental investigation did not assess the effect of bond slips on the strength or ductility. The development length and surface condition of reinforcing bars primarily control the

performance of bond between the bars and concrete. Even though all reinforcing bars in the slab panel were deformed, many of them were cut off. In addition, the points of termination were selected according to the out-of-plane bending moment rather than the in-plane bending moment applied to the slab panel. In this regard, the bond performance in the slab panel under in-plane loadings was not clearly understood.

The opening and closing of the major cracks controlled the behavior in post-elastic regions; consequently, few cracks were developed in those regions. The ductility of the floor slabs depended upon the deformability of the reinforcing bars at the critical sections. The breaking of bars at those sections brought about the ultimate failure of the slab panels.

4.4 Proposed Model

Based on the findings cited above, it was decided to use the model developed by Kawai et al.[4.16] because this model easily simulates the development of cracks, which has been proven to be of primary importance to the post-elastic gehavior. This decision, however, is irrelevant to the argument that the crack line model could be more accurate than the crack zone model or vice versa. In both models, the accuracy of solution depends a great deal on the size of finite elements and can only be checked by numerical experimentation and existing data such as experimental results. The method developed by Ngo[4.21] also is appealing be-

cause of its capacity to directly trace the development of cracks.
This method, however, was not used because the stiffness matrix
tends to be sparsely populated as additional nodes are generated in
the process of computation. The algorithms of automatically gen-
erating nodal points and solving a sparse matrix are extremely
complicated. The proposed model does not take either the dowel
action or bond-slip into account.

The analyzed floor slabs consist of three different com-
ponents: the concrete slab, the reinforcing bar, and the concrete
beam. The concrete plate is represented as an assemblage of rigid
triangles interconnected by normal and shear springs, as proposed
originally by Kawai et al.[4.16] Each triangle with springs is
labelled the triangular element in this study. The proposed program
has two options for representing the reinforcing bars in slabs. In
the first option, each bar is treated as a bar element, labelled the
truss element, which resists axial forces but has no flexural ri-
gidity. In the second option, all reinforcing bars in the slab are
smeared together and treated as an orthotropic plate. This ortho-
tropic plate is then divided into rigid triangles with springs in
the same manner as for the concrete panels. These triangle elements
are referred to as "smeared triangular elements". The spring
constants are determined so that they can reflect the orthotropic
properties of the reinforcing bars. Concrete beams running under-
neath the concrete plate are modelled as truss elements resisting
axial forces only. The total neglection of the flexural resistance

of the beams was justified by the following reasons. First,

the experimental investigations have shown that reinforcing

bars at the four corners of each beam are strained almost

equally at the several gaged cross sections, indicating that

the axial deformation of the beam is dominating. Second, elastic

finite element analyses were performed to investigate the effect

of the bending of the beams on the overall behavior. One of the

available finite element programs[3.1] was used for this purpose.

Truss members with no flexural rigidity represented the beams

in one execution, whereas beam elements with appropriate flexural

rigidity were used in the other execution. The two executions

yielded practically the same results. Hence, the flexural

rigidity of these beams is significantly smaller than the in-

plane rigidity of the concrete plate.

4.4.1 Formulation of Triangular Elements

In Fig. 4.1 are shown two rigid triangular elements with

nodes 1-2-4 (element 1) and 3-2-4 (element 2). The elements are

connected along their interface (24) by uniformly distributed

normal and shear springs, with spring constants k_d and k_s res-

pectively. (see Fig. 4.4) G_1 and G_2 are the centroids of the

elements. Since the elements are assumed to be rigid, the dis-

placements at any point in an element are characterized by the

translations (u, v) of the centroid, and the rotation (Θ) of

the element (Fig. 4.2). Point W, located at the interface in the

two elements before displacement, will be moved to separate

locations W_1' and W_2' after displacement (Fig. 4.3). These

displacements, $< U_1, V_1, U_2, V_2 >$ can be related with the dis-

placements at both cetroids $< u_1, v_1, \Theta_1, u_2, v_2, \Theta_2 >$ as follows:

$$
\begin{Bmatrix} U_1 \\ V_1 \\ -- \\ U_2 \\ V_2 \end{Bmatrix} =
\begin{bmatrix}
1 & 0 & (y - y_{g1}) & & & \\
0 & 1 & (x_{g1} - x) & & 0 & \\
\hline
 & & & 1 & 0 & (y - y_{g2}) \\
 & 0 & & 0 & 1 & (x_{g2} - x)
\end{bmatrix}
\begin{Bmatrix} u_1 \\ v_1 \\ \Theta_1 \\ -- \\ u_2 \\ v_2 \\ \Theta_2 \end{Bmatrix}
\quad (4\text{-}1)
$$

or $\qquad\qquad \{U\} = [Q]\ \{U_i\}$

Subscripts 1 and 2 indicate that the displacements belong to the

triangular element 1 with nodes 1, 2, and 4 and the triangular

element 2 with nodes 2, 3 and 4. As shown in Fig. 4.3, the

separation of W_1' and W_2' after displacement, measured in the normal and tangential directions of the interface, are:

$$\begin{Bmatrix} \delta_d \\ \delta_s \end{Bmatrix} = \begin{bmatrix} -1 & 0 & 1 & 0 \\ 0 & -1 & 0 & 1 \end{bmatrix} \begin{Bmatrix} \bar{U}_1 \\ \bar{V}_1 \\ \bar{U}_2 \\ \bar{V}_2 \end{Bmatrix} \qquad (4\text{-}2)$$

or $\qquad\qquad \{\delta\} = [M]\{\bar{U}\}$

Here, δ_d and δ_s are measured with respect to the local co-ordinates $(\bar{X}, \bar{Y})$ as shown in Fig. 4.3. The displacement components $< \bar{U}_1, \bar{V}_1, \bar{U}_2, \bar{V}_2 >$ also are measured with respect to the local coordinates. A transformation matrix $[R]$ relates the displacement vector in the local coordinates $\{\bar{U}\}$ to the displacement vector in the global coordinates $\{U\}$:

$$\begin{Bmatrix} \bar{U}_1 \\ \bar{V}_1 \\ \hline \bar{U}_2 \\ \bar{V}_2 \end{Bmatrix} = \left[\begin{array}{cc|cc} n_1 & m_1 & & \\ n_2 & m_2 & & 0 \\ \hline & & n_1 & m_1 \\ & 0 & n_2 & m_2 \end{array} \right] \begin{Bmatrix} U_1 \\ V_1 \\ \hline U_2 \\ V_2 \end{Bmatrix} \qquad (4\text{-}3)$$

or
$$\{\bar{U}\} = [R] \{U\}$$

where:
$$n_1 = \cos (\bar{x}, x)$$

$$n_2 = \cos (\bar{x}, y)$$

$$m_1 = \cos (\bar{y}, x)$$

$$m_2 = \cos (\bar{y}, y)$$

According to equations, 4-1 to 4-3, the relative displacement
vector $\{\delta\}$ is:

$$\{\delta\} = [M] [R] [Q] \{U_i\} = [B] \{U_i\} \qquad (4\text{-}4)$$

$$[B] = [M] [R] [Q]$$

The normal strain (ε_d) and the shear strain (ε_s) corresponding
to the separation are defined as:

$$\{\varepsilon\} = \begin{Bmatrix} \varepsilon_d \\ \varepsilon_s \end{Bmatrix} = \frac{1}{h_1 + h_2} \begin{Bmatrix} \delta_d \\ \delta_s \end{Bmatrix} = \frac{1}{h} \times \{\delta\} \qquad (4\text{-}5)$$

h_1 and h_2 are the legs from the centroids of elements 1 and 2
to the interface, and h is the total distance between the centroids.
The constitutive law between the stress and the strain is defined
as:

$$\begin{Bmatrix} \sigma_d \\ \tau_s \end{Bmatrix} = \begin{bmatrix} k_d & 0 \\ 0 & k_s \end{bmatrix} \begin{Bmatrix} \varepsilon_d \\ \varepsilon_s \end{Bmatrix} \qquad (4\text{-}6)$$

-94-

or $\qquad \{\sigma\} = [D] \{\varepsilon\}$

The total strain energy stored in the springs distributed
along line (24), therefore, is:

$$V_c = \frac{1}{2} \int_{A_c} \{\delta\}^T [D] \{\varepsilon\} ds$$

(4-7)

$$= \frac{1}{2} \{U_i\}^T \int_{A_c} \frac{1}{h} [B]^T [D] [B] ds \{U_i\}$$

Here, A_c is the area of the interface (24), and ds indicates
an infinitesimal length. By applying Castiligano's theorem,
the displacements at the centroids $\{U_i\}$ can be related to two
forces (P_x, P_y) and moment (M) at the centroids as follows:

$$\begin{Bmatrix} P_{x1} \\ P_{y1} \\ M_1 \\ \hline P_{x2} \\ P_{y2} \\ M_2 \end{Bmatrix} = \begin{bmatrix} K_{11} & & & & & \\ K_{21} & K_{22} & & & \text{SYM.} & \\ K_{31} & K_{32} & K_{33} & & & \\ \hline K_{41} & K_{42} & K_{43} & K_{44} & & \\ K_{51} & K_{52} & K_{53} & K_{54} & K_{55} & \\ K_{61} & K_{62} & K_{63} & K_{64} & K_{65} & K_{66} \end{bmatrix} \begin{Bmatrix} u_1 \\ v_1 \\ \theta_1 \\ \hline u_2 \\ v_2 \\ \theta_2 \end{Bmatrix}$$

(4-8)

or. $\{P\}$ = $[K]$ $\{U_i\}$

Where: [K] is a 6 x 6 element stiffness matrix. Although each

component of [K] matrix can be drived in a closed form, the three-

point Gaussian integration is employed for the computation of

the matrix. Once $\{U_i\}$ is known, the stress vector $< \sigma_d, \sigma_s >$ is

computed in the following form:

$$\{\sigma\} = [D] \frac{t}{h} [B] \{U_i\} \qquad\qquad (4\text{-}9)$$

The same procedure can be used to formulate the element

stiffness matrix of smeared reinforcing bars. Fig. 4.5 shows two

triangular elements representing reinforcing bars which are

arranged orthogonally and inclined by Θ_x from the global coor-

dinates. The axes of the local coordinates parallel to the

reinforcing bars. Equations 4-1 to 4-4 are used to formulate

this stiffness matrix. Equation 4-5, however, are modified to:

$$\varepsilon_1 = \delta_1 / \ell_1$$
$$\qquad\qquad (4\text{-}5')$$
$$\varepsilon_2 = \delta_2 / \ell_2$$

ℓ_1 and ℓ_2 respectively are the distances between the two centroids

projected on the local $\bar{x}$ and $\bar{y}$ axes. The separation, δ_1 and δ_2,

also are measured with respect to the local coordinates. The new

stress-strain relationship is:

$$\sigma_1 = E_{s1} \times \varepsilon_1$$

$$\sigma_2 = E_{s2} \times \varepsilon_2 \tag{4-6'}$$

In the above expressions, E_{s1} and E_{s2} are the modului of elasticity of steel in directions, 1 and 2. The total strain energy stored in the springs which are distributed along the interface is:

$$V_s = \frac{1}{2} \sum_{i=1}^{2} \int (\delta_i \times E_{si} \times \varepsilon_i) ds \tag{4-7'}$$

Where A_i is the area of reinforcing bars placed in the i direction and intersecting the interface. The element stiffness matrix is then obtained by applying Castiligano's theorem to equations 4-4, 4-5', 4-6' and 4-7'.

4.4.2 Formulation of Truss Elements

Fig. 4.6 shows a typical truss element connecting two rigid triangular elements. This truss element interconnects these triangular elements at their centroids rather than at their nodal points. The flexural rigidity of the truss element is not considered ; that is, this element behaves as a uniaxial tension and compression member. Buckling under compressive force is not considered, either. The strain (ε_b) is:

$$\varepsilon_b = \frac{1}{\ell} \times < -\ell_3 - m_3 \quad 0 \mid \ell_3 \quad m_3 \quad 0 > \begin{Bmatrix} u_1 \\ v_1 \\ \theta_1 \\ \overline{u_2} \\ v_2 \\ \theta_2 \end{Bmatrix} \qquad (4\text{-}10)$$

or
$$\varepsilon_b = \frac{1}{\ell} [B_b] \{U_i\}$$

where: ℓ = Length of the truss element

$$n_3 = \cos \alpha = \frac{x_{g2} - x_{g1}}{\ell}$$

$$m_3 = \sin \alpha = \frac{y_{g2} - y_{g1}}{\ell}$$

The strain (σ_b) is:

$$\sigma_b = E_b \times \varepsilon_b = E_b \times \frac{1}{\ell} [B_b] \{U_i\} \qquad (4\text{-}11)$$

E_b = Axial stiffness of the truss member

The strain energy stored in the truss element, therefore:

$$V_b = \frac{1}{2} \int_0^\ell \sigma_b^{\;T} \times E_b \times \varepsilon_b d\ell$$

$$\qquad (4\text{-}12)$$

$$= \frac{A_b E_b}{2\ell} \times \{U\}^T [B_b]^T \{U_i\}$$

-98-

Here, A_b is the cross sectional area of the truss member.
According to equation 4-12, the displacements $\{U_i\}$ and forces
$\{P\}$ at the centroids can be related as follows:

$$\{P\} = \frac{A_b E_b}{\ell} [B_b]^T [B_b]\{U_i\} \tag{4-13}$$

or

$$\{P\} = [K_b]\{U_i\}$$

$$[K_b] = \frac{A_b E_b}{\ell} [B_b]^T [B_b]$$

4.4.3 Material Model of Concrete Slab in Compression

Concrete under compression is assumed to be isotropic
and linear-elastic and perfectly-plastic. The constitutive matrix
of the triangular elements representing concrete slab in the
elastic range is defined as:

$$[D_e] = \begin{bmatrix} D^e_{11} & 0 \\ 0 & D^e_{22} \end{bmatrix} \tag{4-14a}$$

$$D^e_{11} = \frac{E}{1-\nu^2} \tag{4-14b}$$

$$D^e_{22} = \frac{E}{2(1+\nu)} \tag{4-14c}$$

E and ν respectively are the modulus of elasticity and poisson's ratio of concrete. As long as the concrete is in the elastic range the spring constants k_d and k_s are respectively:

$$k_d = D_{11}^e$$

$$k_s = D_{22}^e$$

(4-15)

The compressive yielding of concrete is assumed to follow a yield criterion with an associated flow rule. The yield function defined here is:

$$f = \left(\frac{\sigma_d}{\sigma_p}\right)^2 + \left(\frac{\tau_s}{\tau_p}\right)^2 = 1$$

(4-16)

$$\sigma_p = \sigma_y$$

$$\tau_p = \sigma_y/\sqrt{3}$$

σ_y is the yield stress of concrete under uniaxial compression. If $d\varepsilon_p$ denotes the increment of plastic strain, then:

$$\{d\varepsilon_p\} = \lambda\left\{\frac{\partial f}{\partial \sigma}\right\}$$

(4-17a)

or for each component 1 and 2:

$$d\varepsilon_d^{\,p} = \lambda \, \frac{\partial f}{\partial \sigma_d} \qquad\qquad d\varepsilon_s^{\,p} = \lambda \, \frac{\partial f}{\partial \tau_s} \qquad\qquad (4\text{-}17b)$$

where:
$$d\varepsilon_p^{\,p} = \left\{ \begin{array}{c} d\varepsilon_d^{\,p} \\[2ex] d\varepsilon_s^{\,p} \end{array} \right\}$$

λ is a proportionally constant, as yet undetermined in these equations. During an infinitesimal increment of stress, changes of strain are assumed to be divisible into elastic and plastic parts:

$$\{d\varepsilon\} = \{d\varepsilon_e\} + \{d\varepsilon_p\} \qquad\qquad (4\text{-}18)$$

The elastic strain increments are related to stress increments by the elastic matrix $[D_e]$:

$$\{d\sigma\} = [D_e]\{d\varepsilon_e\} \qquad\qquad (4\text{-}19)$$

According to the yield criterion:

$$df = \frac{\partial f}{\partial \sigma_d}\, d\sigma_d + \frac{\partial f}{\partial \tau_s}\, d\tau_s = 0 \qquad\qquad (4\text{-}20)$$

From equations 4-17 and 4-20, we can derive λ as:

$$\lambda = \frac{D_{11}^{\,e}\left(\dfrac{\partial f}{\partial \sigma_d}\right) d\varepsilon_d + D_{22}^{\,e}\left(\dfrac{\partial f}{\partial \tau_s}\right) d\varepsilon_s}{D_{11}^{\,e}\left(\dfrac{\partial f}{\partial \sigma_d}\right)^2 + D_{22}^{\,e}\left(\dfrac{\partial f}{\partial \tau_s}\right)^2} \qquad\qquad (4\text{-}21)$$

The derivation of equation 4-21 is illustrated in Appendix.

According to equations 4-17 through 4-21, the elasto-plastic constitutive equation can be expressed in an incremental form as:

$$\{d\sigma\} = [D_{ep}]\{d\epsilon\} \qquad (4-22)$$

$$[D_{ep}] = \begin{bmatrix} D^e_{11} & 0 \\ 0 & D^e_{22} \end{bmatrix} - \frac{1}{s}\begin{bmatrix} S_1^2 & S_1 S_2 \\ S_2 S_1 & S_2^2 \end{bmatrix}$$

where:

$$S_1 = D^e_{11}\left(\frac{\partial f}{\partial \sigma_d}\right) \qquad S_2 = D^e_{22}\left(\frac{\partial f}{\partial \tau_s}\right)$$

$$S = D^e_{11}\left(\frac{\partial f}{\partial \sigma_d}\right)^2 + D^e_{22}\left(\frac{\partial f}{\partial \tau_s}\right)^2$$

As long as the concrete stress is in the yield condition (equation 4-16), equation 4-22 is used to relate the stress to the strain. Unloading is assumed to occur if λ is negative. Strain hardenings such as kinematic and isoparametric hardenings are ignored, as evidenced from the yield function equation 4-15. Zienkiewitz et al.[(4.29)] presented the formulation of the elasto-plastic matrix in further detail.

4.4.4 Material Model of Concrete Slab in Tension

Concrete is assumed to be linear elastic until cracks occur, and tension cracking follows the maximum normal stress theory. Once cracks take place, the normal spring constants (k_d)

is set at zero. The shear spring constants (k_s), on the other
hand, hold a finite value in order to maintain numerical stability
throughout the matrix algebra. Recontact of cracked surfaces
under unloading or reloading is considered by introducing a
criterion, $\delta_d < 0$. Once two cracked surfaces contact, both the
normal and shear constants of the springs located in the interface
are assumed to regain their elastic values. The spring
constants maintain these values as long as the interface
remains closed.

4.4.5 Material Model of Reinforcing Bars

The stress-strain relationship for the reinforcing bars
is assumed to be linear-elastic perfectly-plastic in both
tension and compression, taking neither strain hardening nor
the Baushinger effect into account. These bars are assumed
to break under tension when they reach their ultimate strains.
The buckling of bars under compressive force is ignored.

4.4.6 Accuracy of the Proposed Model

As described in Sections 4.4.1 and 4.4.2, the proposed
model is considerably different in its formulation of potential
energy from most other finite element analyses.[2.14, 2.48, 4.7, 4.23] In this section, the accuracy of the model in the elastic
range is demonstrated by comparing the model with one of the

-103-

Table 4.1 lists the ratios of the displacements at several selected points shown in Fig. 4.8. The deflection ratio of the proposed model to SAP IV, ranges from 1.01 to 1.07; the model always gives larger displacements than SAP IV. The discrepancy, however, appears to be minimal despite the difference in models' mesh size and shape and procedure for formulating potential energy. The proposed model is suitable for solving elastic plane stress problems.

4.5 Procedure of Analysis

4.5.1 Scheme of Computation

The basic input for the analysis procedure consists of a description of the topology and material properties of the structure. The loads are expressed as forces acting on the centroids of triangular elements. The material properties for concrete as well as reinforcing bars are specified for each element. The first step in the analysis is to form the structure stiffness matrix from the individual element stiffness matrices. Initially, the element stiffness matrices are determined based on the virgin material properties of the concrete and steel.

The structure is then analyzed under monotonically increasing loads. For each load level, the solution is derived through several iterations after specific convergence criteria are met. The structure is assumed to behave linearly within

-104-

existing elastic finite element programs, SAP IV.[3.1] For

this purpose, a plane stress problem is solved by means

of the two programs. The analyzed structure is a 64 (in.) x

64 (in.) square panel with the thickness of 1 (in.) as shown in

Fig. 4.8. One of the edges is clamped, while the others are

held free. The panel is homogeneous and isotropic with a

modulus of elasticity of 3,500 (ksi) and a poisson's ratio of

0.15. The dimensions and material properties, similar to those

of the tested concrete panels, however, do not matter since the

analysis is made for comparison between two different finite

element models. Two cases of loading are considered. In load-

ing case 1, equally distributed forces are applied along the

free edge opposite the clamped edge. In loading case 2, these

forces are applied along all three free edges, resulting in a

pure shear condition in the panel. The intensity of the forces

is chosen arbitrarily. The panel is discretized to finite

elements as shown in Fig. 4.9. It is known that the size of

finite elements significantly affects the accuracy of solutions.

The finite element sizes shown in the figure are selected after

several executions with different element sizes. Although

a square finite element in SAP IV is four times greater in area

than a triangular element in the proposed model, this difference

does not necessarily leads to a conclusion that the proposed model

is more accurate than SAP IV; the formulation of the stiffness

matrix, after all, is different.

an iteration. Following each iteration, the structure stiffness matrix is reconstructed using the tangent stiffness properties of the material, and forces within the structure are corrected to reflect the nonlinear behavior of the material model. The force correction procedure, which is explained below, uses the Initial Stress Method of Zienkiewicz et al. [4.29] Following the solution of the element equilibrium equations, the element displacements are used to obtain the strains within each element. The material strains then determine the apparent changes in stresses for the concrete and steel. These changes are corrected to reflect the nonlinear properties of the materials. The differences between the apparent stresses and corrected stresses are the residual stresses used to calculate residual element loads. With each iteration, the state of each material is updated, stresses are corrected, and a new tangent stress-strain matrix is calculated. The element and structure stiffness matrices are reconstructed, and the residual loads are applied until the solution for that load step converges. This force correction procedure is shown schematically in Fig. 4.7.

The analysis, on the other hand, is terminated when the structure reaches its maximum load. When the imposed load approaches the structure's maximum resistance level, the load

increment becomes too large to converge. If it takes place, the load increment at the present load step is reduced by one third, and the iteration is restarted. Once the load increment is lowered to within a specified fraction of the load reached in the previous load step, the execution then stops, assuming that this load be the ultimate load.

4.5.2 Solution Technique of the Nodal Equilibrium Equations

Wilson, et al. [4.27] have developed an efficient computer program for the direct solution of large numbers of simultaneous linear equations. Basically, the program used the Gauss elimination in order to solve positive-definite symmetrical systems. The specific features are that systems of very large size and bandwidth can be solved and that operations on zero elements are effectively eliminated to reduce the time for computation. This program is used as a subroutine in the analysis.

4.6 Numerical Examples

4.6.1 Selection of Examples

In order to evaluate the usefulness and applicability of the proposed finite element model, several numerical examples are presented in this section. For this purpose, the model is used to analyze the tested panels for both monotonic and cyclic loadings, and the results are compared with the test results: BH2MN, BH3MN, and BH1CY. To achieve close match between the analysis

and experiment, material properties used in the analysis are determined based upon the results of the concrete cylinder test and steel tension test. In the proposed model, concrete subjected to compression is assumed to be linear-elastic perfectly-plastic, while concrete subjected to tension is assumed to be linear up to a specified cracking stress. The yield strength and tensile strength obtained by the concrete cylinder test are used to represent the yield stress and cracking stress respectively. The yield stress and ultimate strain of reinforcing bars are assumed to be those derived from the steel tension test. (Table 3.7)

4.6.2 Monotonic Loading on Beam-Supported Slab Panels (BH2MN and BH3MN)

The ability of the proposed model to simulate the behavior of floor slabs under monotonic in-plane loading is demonstrated by using two tested slab panels (BH2MN and BH3MN). In order to save the time required for computation, the individual panel under test is analyzed. (Fig. 4.10) For simulating the behavior of BH2MN, a 410 mm (16 in.) overhang of the slab panel, outside of the load line, is ignored. The significance of the overhang is minimal because this neglection only disregards the effect of the self-equilibrium stresses acting on the panel section along the load line. A preliminary elastic analysis of BH2MN has also shown that this ignored part has

little effect on the overall behavior of the panel. The
edge connected to the vertical wall (refer to Fig. 3.2) is
clamped, and, therefore, the wall is not included in the
analysis. The other three edges are assumed to be stress-free.
The concrete panel is discretized to 216 triangular elements.
(Fig. 4.11) Three concrete beams, two running perpendicular
and one running parallel to the loading direction, are re-
presented by truss elements. Since the truss elements are
jointed at the centroids of triangular elements, the eccen-
tricity between the neutral axes of slab and beams are neglec-
neglected. Reinforcing bars are represented by truss elements
in one execution (case 1) and by smeared triangular elements
in another execution (case 2). In the case 1 analysis, all
reinforcing bars located along the interface of two triangular
elements are treated as one truss element for each direction
(X and Y directions in Fig. 4.11). The applied load is assumed
to be distributed uniformly along the loading line parallel to
the clamped edge. The distributed load, therefore, is represented
by nine equal element forces along the loading line. (Fig. 4.11)
The proportion of the forces remains unchanged during the loading.

In order to simulate the behavior of BH3MN, the entire
middle panel (1630 mm x 2440 mm) is analyzed (Fig. 4.10). The
edge connected to the fixed vertical wall (refer to Fig. 3.2) is
clamped, while the remaining edges are stress-free; therefore,

the walls also do not appear in the analysis. The concrete

panel is discretized to 216 triangular elements like BH2MN.

Three concrete beams are treated as truss elements, and rein-

forcing bars are treated as smeared triangular elements. In

order to simulate the loading employed in BH3MN, both moment

and shear force are applied to the free edge parallel to the

clamped edge. The applied moment equals the shear force

multiplied by a 1630 mm moment arm. The shear force is re-

presented by nine equal element forces in the y direction,

and the moment by nine linearly distributed element forces in the

x direction. These directions follow those specified in

Fig. 4.11. The element forces are increased proportionally in

the analysis.

The results of the analyses are compared to the experimental

load-displacement and load-rotation curves in Figs. 4.12 and

4.13. For BH2MN, analyses of cases 1 and 2 constantly show a

higher load than the experiment. Once the load exceeds 100 kN

(80 percent of the experimental ultimate load), however, the

analytical curves approach the experimental curve rapidly and

meet it at 120 kN, which is 95 percent of the experimental ulti-

mate load. The analytical curves reach the ultimate loads

at 116 kN (case 1) and 115 kN (case 2), which are 97 and 96

percent of the experimental ultimate load, respectively. The

experimental curve shows a sudden decrease of resistance at the displacement of 2.8 mm, and after the decrease takes place, the resistance does not reach its maximum again. Since the analytical model is loaded with a series of imposed load increments, it is not possible to deal with structural unloading, and the curves rise continuously until the ultimate load, defined in Section 4.5.1, is reached. According to the case 1 analysis, in which the reinforcing bars are treated as truss elements, the displacement corresponding to the ultimate load is 3.0 mm, while 2.8 mm is obtained from the experimental curve. In the second analysis (case 2), in which the smeared triangular elements are used for the reinforcing bars, the transfer of stresses caused by the cracking of concrete is more gradual than in the case of the real slab panel, which contained discrete reinforcing bars. The smooth transfer of forces appears to retard the onset of instability. The case 2 analytical curve, however, reaches 99 percent of its ultimate load at 2.6 mm and travels on additional 0.9 mm with a load increase of 1 percent. The region between 2.6 mm and 3.5 mm can be said as a plastic plateau. Except for the displacement of the ultimate load, the load-displacement curves in cases 1 and 2 practically are the same. In later analyses, the smeared triangular elements are used to represent reinforcing bars, for the use of these elements reduces the band-widths of global stiffness matrices and improves the numerical stability particularly near the ultimate load.

For BH3MN, the experimental and analytical load-displacement curves show agreement up to about 30 kN, which is 60 percent of the ultimate load. At this load level, the slope of the experimental curve decreases suddenly, while the analytical curve shows a smooth reduction of the slope up to the ultimate load. The analytical ultimate load is 51.1 kN, which is 93 percent of the experimental ultimate load. The analytical curve reaches 99 percent of the maximum load at 2.0 mm displacement, followed by a 1.6 mm plastic plateau. On the other hand, the experimental curve reaches the ultimate load of 56.9 kN at 1.9 mm displacement, and a sudden decrease of resistance, which is never fully recovered as the panel undergoes an additional 4.9 mm of displacement. In both BH2MN and BH3MN, the experimental and analytical load-end rotation curves show agreement up to about 90 percent of the ultimate loads (Fig. 4.13). At this load level, the analytical curves depart from the experimental curves, showing a rapid decrease of the slopes. The characteristics of the experimental curves, the loss and recovery of resistance in the post-ultimate load regions are replaced by the smooth transition of the slopes in the analytical curves.

The ability of the proposed model to duplicate experimental crack patterns is demonstrated in Fig. 4.14. The experimental and analytical crack patterns are compared at three different load levels for both BH2MN and BH3MN. Since the pro-

posed model assumes that cracks occur at interfaces between
two triangular elements, cracks can develop in only one of the
three directions: the direction parallel to the loading, the
direction perpendicular to the loading, and the direction in-
clining by 45 degrees from the loading direction. Considering
this limitation on the crack direction, the model simulation
of the crack development is good.

In general, the proposed model successfully simulates
the overall behavior of the slab panels. The model offers a
close duplication of the ultimate resistance as well as the
deformation corresponding to the ultimate resistance. The
model also duplicates the deformation of most tested panels;
it did not, however, duplicate the displacement of BH2MN. For
BH2MN, the analytical load-displacement curve always shows
higher load than the experimental curve. Several reasons for
this discrepancy can be noted. Material properties used in the
model, based upon the concrete cylinder tests and steel tension
tests (Tables 3.7 and 3.8), may not be the same as those of
the tested slab panels. The tested slab panels might have
initial minute cracks because of the shrinkage of concrete or the
accidental forces applied during the process of setting the
specimen. Significant residual stress due to creep or shrinkage
might exist since the slab panels were tested more than two
months after they were cast. The analyses, on the other hand,

do not consider any of such possibilities. Additional experiments are required to discuss more specifically the reasons for this discrepancy.

The analytical curves do not reach the experimental failure displacements: 7.6 mm for BH2MN and 6.9 mm for BH3MN. The reason is clear; the experimental curves show that the resistance is never completely recovered after the first significant loss of resistance. That is, the region after the point corresponding to the ultimate resistance is a post-ultimate load region. On the other hand, the analytical model can simulate the behavior only up to the ultimate load. The experimental results verify that the breaking of the reinforcing bars embedded in the concrete beam subjected to tension causes the ultimate failure. To evaluate the breaking of reinforcing bars in cracked regions, however, is difficult since the strains of these bars depend heavily upon various local effects such as bond slips and dowel action. The model, on the other hand, has been developed to simulate the overall behavior rather than to investigate the local behavior of individual components.

Nevertheless, the failure displacements are evaluated by using the stiffness of the structure as well as the stress and strain of concrete and reinforcing bars at the ultimate load. Assuming that the stiffness at the ultimate load remains unchanged in the post-ultimate load region, the displacement

at which the strain of the reinforcing bars in the concrete
beam located 400 mm from the tension edge reaches the ultimate
strain can be computed. In other words, the model is assumed
to be linear, having the same stiffness as that of the ultimate
load. This assumption is rather reasonable because the experi-
mental results show that few cracks take place once the ultimate
load is reached and that the behavior in the post-ultimate load
region is controlled primarily by the opening of the major crack.
The computed failure displacements are 6.65 mm for BH2MN and
6.60 mm for BH3MN as shown in Fig. 4.12. They are 88 and 93
percent the experimental failure displacements respectively. The
correlation seems reasonable for the considerably crude assumption.

4.6.3 Cyclic Loading on Beam-Supported Slab Panels (BH2MN and BH1CY)

The ability of the proposed model to simulate the
behavior of floor slabs under reversed or cyclic loading
tested with two tested slab panels (BH2MN and BH1CY). For BH2MN,
the tested panel was unloaded after it reached failure and re-
loaded in the opposite direction (defined as the negative
direction in Chapter III) until another failure occured. The
analytical model follows this loading pattern; first it is un-
loaded after the ultimate load is reached and then reloaded in
the opposite direction until another ultimate load is
reached. For BH1CY, the panel was subjected to a series of load

reversals in both directions with gradually increasing displacement specified by the loading spectrum in Fig. 3.17. Since enormous computation time is required to completely duplicate the loading spectrum, a simplified loading spectrum is selected for the analytical model. It contains one complete cycle with the 1.3 mm amplitude, followed by one cycle with the 2.8 mm amplitude. In the third cycle, the load continues to increase until failure occurs. The discretization of the slab panel is identical to that used for BH2MN subjected to monotonic loading. Smeared triangular elements are used for reinforcing bars in this analysis.

The analytical load-displacement curve of BH2MN under the reversed loading is compared with the experimental curve in Fig. 4.15. Since the analytical curve does not reach the experimental failure displacement in the initial loading as mentioned in Section 4.6.3, these two curves are far apart on the unloading. In the reloading, the analytical curve consistently shows a higher slope than the experimental curve and reaches the ultimate load at -4.0 mm displacement as compared with the -6.0 mm experimental displacement. The curve also shows a clear pinching effect in the neighborhood of zero displacement. Since the ultimate displacement which the analytical model can reach is substantially less than the experimental failure displacement, the model fails to simulate the experimental curve in the reloading region. In addition, the analytical curve

reaches the same ultimate resistance in both directions (115 kN for positive loading and 110 kN for negative loading), although the experimental curve shows a substantial decrease in ultimate resistance due to the reversed loading by about 26 percent. The analytical ultimate load in the negative direction is 110 kN, which is 96 percent of the analytical positive ultimate load and 125 percent of the experimental negative ultimate load. The damage that the tested slab panel (BH2MN) received during the first half cycle of loading is not simulated properly by the analytical model. This unsatisfactory simulation explains the discrepancy on the ultimate loads.

In Fig. 4.16, the analytical crack pattern at the negative ultimate load is compared to the experimental crack pattern at the point of failure in the negative direction. Despite the discrepancy between the analytical and experimental curves, the two crack patterns are considerably alike.

The analysis for cyclic loading of test panel BH1CY resulted in a load-displacement curve unlike the experimental curve. The analytical ultimate load after two complete cycles is 107 kN, which is 112 percent of the experimental ultimate load of BH1CY. As shown in Fig. 4.17, the analytical curve consistently shows a higher load than the experimental curve. The difference is probably caused because the analytical model does not

accurately evaluate the damage accumulated in the slab during

the cyclic loading. The tested slab panel experienced six

complete cycles immediately preceding the first cycle of the

1.3 mm amplitude. In the analysis, on the other hand, load

up to this displacement level is applied from the virgin state.

Furthermore, the tested panel reached the ultimate load at

4.3 mm displacement after twelve cycles were completed, while

in the analysis, only two complete cycles are employed before

the ultimate load. It is suspected that the model does not pro-

perly represent the causes for cumulative damage. In cyclic loading

with increasing amplitudes, cracks develop gradually from both

sides. The cracks open and close alternately as the load is

reversed. The stiffness of the panel changes at each opening

and closure of the cracks. It is also known that load reversal

commonly enhances bond slips. The proposed model does not

simulate these potential sources of cumulative damage.

4.6.4 Concluding Remarks

In summary, the proposed model properly simulates the

behavior of slab panels subjected to in-plane loading when they

are loaded monotonically. The model accurately predicts both

the ultimate resistance and the corresponding displacement. The

analytical load-deformation curves reasonably coincide with the

experimental curves. The analytical curves do not reach the

the experimental failure displacements since these displacements are in post-ultimate load regions. Nevertheless, an evaluation of the failure displacement based upon the stiffness at the ultimate load is still workable.

On the other hand, the ability of the model to simulate the cyclic behavior of floor slabs is not satisfactory. For BH2MN, the model does not duplicate the damage that the tested slab panel possessed upon unloading and, consequently, fails to simulate either the weakened stiffness or the reduced strength which the tested panel disclosed during the reversed loading. The model fails to simulate the behavior of the floor slab under cyclic loading with gradually increasing amplitudes (BH1CY). The deficiency of the model to simulate cumulative damages due to cyclic loading most likely creates the discrepancy.

V PARAMETRIC STUDY

5.1 General

In this chapter, the experimental findings described in Chapter III are further examined in order to define the parameters which control the in-plane behavior of floor slabs and evaluate the effects of these parameters on the in-plane characteristics of floor slabs. This study focuses on three major characteristics: strength, stiffness, and ductility. Parameters which may affect these characteristics are chosen carefully, and the significance of each parameter is examined. The selected parameters are: 1) the aspect ratio of floor slabs, 2) the relative beam size, 3) the amount of reinforcing steel, 4) the arrangement of reinforcing bars, 5) the boundary condition, 6) the loading condition (monotonic, reversed, or cyclic loading), and 7) the intensity of gravity load.

This Chapter also describes a simplified representation of the floor slab subjected to in-plane loading as a deep beam considering both flexural and shear deformations. The appropriateness and accuracy of this representation are discussed in detail.

5.2 Elastic Characteristics

The stiffness test and accompanying elastic finite
element analysis, described in Chapter III, have shown that the
in-plane stiffness characteristics of floor slabs in the elastic
region can be reasonably estimated by the finite element
analysis. When the analysis of the entire structure is needed,
however, dividing each slab panel to smaller elements is
impractical. A more practical representation of the floor slabs,
in which they are treated as deep beams, is demonstrated in this
section. The effect of several parameters such as the relative
beam size or the aspect ratio on the stiffness characteristics
is discussed.

5.2.1 Comparison with Stiffness Test

In order to simulate the stiffness test by a simpli-
fied beam model, the tested specimen, composed of three panels
separated by two walls (refer to Fig. 3.2),is treated as a
simply supported beam with a projection at each end, labelled
an equivalent beam. As shown in Fig. 5.1, two forces are
applied to the equivalent beam at the distance (ℓ) from the
supports. The forces are applied in the same direction
to simulate the symmetrical loading test and in opposite
directions to simulate the anti-symmetrical loading test.
Fig. 5.1 also illustrates the resulting moment and shear dia-
grams created by these forces. Both bending and shear de-

-121-

formations are included to calculate the deflection of the equivalent beam. The following equations, 5-1 to 5-4, determine the rotations (Θ_s, Θ_a) at the supports and the deflection (δ_s, δ_a) at the edges of the beam.

For symmetrical loading:

$$\Theta_s = \frac{\ell^2}{2EI} \times P \tag{5-1}$$

$$\delta_s = \left(\frac{5\ell^3}{6EI} + \frac{\ell}{AG}\right) \times P + \frac{\ell^2}{EI} \times (\ell_1 - \ell) \times P \tag{5-2}$$

For anti-symmetrical loading:

$$\Theta_a = \left(\frac{\ell^2}{6EI} + \frac{2}{AG}\right) \times P \tag{5-3}$$

$$\delta_a = \left(\frac{\ell^3}{2EI} + \frac{3\ell}{AG}\right) \times P + \left(\frac{2\ell^2}{3EI} + \frac{2}{AG}\right) \times (\ell_1 - \ell) \times P \tag{5-4}$$

where: P = applied force

E = modulus of elasticity of the equivalent beam

G = shear modulus of the equivalent beam

I = moment of inertia of the equivalent beam

A = shear area of the equivalent beam

ℓ = span length (1630 mm)

ℓ_1 = length of the projection (2030 mm)

-122-

In the application of equations 5-1 to 5-4, the material properties, E and G are taken as those of concrete obtained from the cylinder test. (Table 3.8) The effect of reinforcement as well as the stiffening beams are ignored. The moment of inertia is taken to be that of the gross section of the panel, including the two beams running parallel to the span (or perpendicular to the loading) as shown in Fig. 5.5. The nominal shear area is taken to be 0.833 times the area of the same cross section, 0.833 being the theoretical coefficient for the shear area of a rectangular cross section.

The results based upon these properties are listed in Table 3.14. For symmetrical loading, the equivalent beam calculation gives an approximately 20 percent higher stiffness than the experiment but closely approximates the finite element analysis. For anti-symmetrical loading, on the other hand, the equivalent beam calculation gives an 40 percent higher stiffness than the experiment or the finite element analysis. Note that the finite element analysis correlates well with the stiffness test for anti-symmetrical loading. Further investigation revealed that the combined effect of the high shear force applied in the middle panel and the boundary condition employed for the stiffness test and finite element analysis caused additional rotations in the walls. Since the tested panels were supported only at walls' mid-points, at a distance of 1220 mm (48 in.) from the

-123-

panel edges perpendicular to the loading, the shear force applied
to the walls forced them to either contract or elongate in the
direction parallel to the shear force. The equivalent beam cal-
culation, however, did not account for such deformation due to
the shear force. Further finite element analysis verified that
this additional rotation of the walls due to the shear force
disappeared when the walls were prevented from deforming in the
direction parallel to the shear force. In this finite element
analysis, artificially stiff beams were substituted for the walls
to restrict the deformation along their lines. As indicated by
Table 3.14, the stiffnesses of the slab specimen were increased
significantly, and the results were nearly the same as the
equivalent beam calculation. In most building structures in
which two adjoined floor slabs are separated by shearwalls or
frames, either elongation or contraction of the boundary
between the two slabs is unlikely to occur. The equivalent beam
calculation, therefore, seems to give reasonable evaluation in
most cases.

In general, the technique which treats floor slabs
as deep beams is acceptable to simulate the in-plane
stiffness characteristics of floor slabs. First, the equivalent
beam calculation reasonably duplicates the finite element
results. Second, the finite element results indicate good

correlation with the stiffness test results. Chapter III

describes the comparison between the stiffness test and finite

element analysis in detail.

5.2.2 Effective Moment of Inertia and Effective Shear Area

In the previous section, the suitability of the equi-

valent beam calculation to evaulate the in-plane stiffness

characteristics of floor slabs is demonstrated. In order to

properly evaluate the in-plane stiffness characteristics,

however, the moment of inertia (I) and the shear area (A) of

equivalent deep beams should be selected carefully. Although

an equivalent beam calculation using the nominal moment of

inertia and shear area reasonably simulates the results of the

stiffness test and finite element analysis, a floor slab with

a different combination of aspect ratio and relative beam size

may require a different set of moment of inertia and shear area.

A parametric study was made to determine the moment

of inertia and shear area of equivalent beams so that the equi-

valent beam calculation would properly reflect the true in-plane

characteristics of floor slabs. The moment of inertia and shear

area determined by this parametric study are labelled the

effective moment of inertia (I_e) and the effective shear area

(A_e) respectively. Elastic finite element analysis was made

to provide the data necessary for computation.   In the

previous section, this analysis has been verified to be capable

of properly simulating the true behavior of slab panels under in-

plane loadings. As in the finite element analyses described

in Chapters III and IV, eccentricities between the mid-planes

of floor slabs and beams were neglected; therefore, the floor

slabs with beams were analyzed as two-dimensional plane stress

problems. Cantilever floor slabs were analyzed instead of three

panel floor system analyzed in the previous section. This

treatment is reasonable because the finite element analysis also

simulated adequately the behavior of the specimens' outer panels

in the stiffness test. The aspect ratio and the relative

beam size were selected as parameters. The relative beam size

was defined as the ratio of the nominal moment of inertia of

a floor slab with beams to the nominal moment of inertia of the

floor slab without such beams. The relative beam size of 1.0,

then, indicated a flat slab. The width of floor slabs, or

likewise, the depth of the equivalent beams, designated as

d in Fig. 5.2, was defined as the distance between the center

lines of the two beams. The beams were placed at the

edges of the slab panels.   This parametric study did not

include floor slabs with projecting parts. The dimensions and

material properties of the analyzed floor slabs are listed in

Table 5.1.

The following procedure was adopted to compute the effective moment of inertia (I_e) and shear area (A_e):

1. A cantilever floor slab with a particular set of aspect ratio and relative beam size was selected. (Fig. 5.2)

2. A unit rotation (Θ) without allowing any translation at the free edge was applied and the shear force (P) and the end moment (M) at the edge were computed.

3. I_e and A_e were calculated from the following equations:

$$I_e = \frac{\ell}{2E} (2M - P\ell)$$

$$A_e = \frac{3P(2M - P\ell)}{G(3M - 2P\ell)}$$

(5-5)

These equations can be derived by means of the basic beam theory which takes both flexural and shear deformations into account.

The values used in this parametric study ranged from 0.25 to 3.0 for the aspect ratio and from 1.0 to 2.7 for the relative beam size. The calculated I_e and A_e are listed in Table 5.2.

According to Table 5.2, the values of I_e are very close to the nominal moment of inertia regardless of the aspect ratio or the relative beam size. On the other hand, both the aspect

-127-

ratio and relative beam size affect the effective shear area; a smaller aspect ratio or a larger relative beam size gives a larger effective shear area. This change in the effective shear area is consistent with the generally accepted concept of the shear area. For the flat slab (the relative beam size is 1.0) with 3.0 of the aspect ratio, the ratio of the effective shear area to the cross sectional area 0.872, is very close to the standard 0.833 value for a beam with a rectangular cross section. For the floor slab with 0.25 of the aspect ratio and 2.7 of the relative beam size, the effective shear area nearly is the same as the cross sectional area of the floor slab (not including the area of the beams). The shear area of cross sections with stiff edges like wide-flange cross sections, is the area of the part between the edges.

For practical design purposes, nevertheless, the cross sectional area of floor slabs reasonably represents the shear area. The area of beams, if any, need not to be added to the area of the floor slab. This simplification creates less than a 12 percent error in the aspect ratio and relative beam size covered in this study. Since the stiffness of equivalent beams are computed on the basis of the sum of flexural and shear deformations and thereto the computation based upon the nominal moment of inertia properly provides flexural deformation, the total

error brought about by considering the cross sectional area
of floor slabs as the shear area can be further reduced.
Although the analysis was made only for the slabs with edge
beams, supplemental analysis disclosed that the use of nominal
moment of inertia and shear area is also suitable to evaluate
the stiffness of slabs in which beams are attached inside the
slab edges (like the tested slab panels).

5.3   Strength of Floor Slabs

5.3.1   Description of Problems

The proposed finite element model described in Chapter
IV was used to predict the strength of eight slab panels with
a variety of loading conditions, boundary conditions, relative
beam sizes, and reinforcing bar arrangements. These analyzed
panels are designated as cases 1 to 8 in the following dis-
cussion.

All eight cases dealt with a slab panel 1630 mm x
2440 mm in plane dimensions with one of the long edges clamped
and the other three edges free. Three beams of 96 mm x 68 mm
cross section were attached to the slab panel. Two beams were
placed symmetrically in the short direction, 1630 mm apart
(405 mm from the edges). A beam was placed along the loading
line. These dimensions followed those of the tested slab
panels. Cases 1 and 2 respectively were the original tested
floor slab, BH2MN and BH3MN. In BH2MN, the basic slab panel was

analyzed with distributed shear forces along the free edge. In BH3MN, the slab panel was analyzed with a combined shear force and bending moment along the free edge. In case 3, the slab panel was subjected to bending moment at the free edge. Unlike cases 1 and 2, the slab panel was under pure bending, and no shear force existed. Case 4 was similar to case 1 except that the loaded edge was prevented from rotating. This boundary condition simulates floor slabs supported by vertical members whose torsional rigidity is very large. The cases 1 and 4, therefore, marked the upper and lower bounds of the strength of floor slabs supported by vertical members with finite torsional rigidity. In case 5, uniformly distributed forces were applied along the three free edges so that the floor slabs would be subjected to pure shear. Case 6 had the same boundary and loading conditions as case 1 (BH2MN), but the area of longitudinal reinforcing bars, which extended perpendicular to the loading, was doubled while the area of transverse reinforcing bars remained unchanged. The slab's flexural strength was expected to increase. Case 7 also had the boundary and loading conditions of case 1. Additional reinforcing bars, however, were placed near the floor slab's edges so that its flexural strength could be increased. In case 8, the dimensions of the concrete beams were doubled, while their locations remained unchanged. A detailed explanation about the

analysis procedures of these slab panels has already been made

in Chapter IV. In addition, Fig. 5.3 schematically shows the

conditions employed to analyze each of the eight floor slabs.

5.3.2 Ultimate Strength and Failure Mode

In cases 1, 2, 3, and 8, cracks developed on the finite

element boundary parallel to the loading and at a distance of

270 mm (10.5 in.) from the clamped edge, and the ultimate loads

were reached when the cracks nearly penetrated the floor slabs

(Fig. 5.4). Most reinforcing bars intersecting the cracks yielded

at the ultimate loads. These cracks and cross sections corres-

ponded to the major cracks and the critical sections defined in

Chapter III. These failures were then labelled flexural failures.

In cases 4 to 7, on the other hand, the slab panel

developed diagonal crack which completely separated a triangular

portion from the remainder of the slab at the failure point.

All reinforcing bars crossing the diagonal crack also yielded.

This failure was designated as shear failure. It was felt that

this failure would be inhibited in a slab supported by a shearwall

or a strong beam attached along the loading edge because the shear-

wall or the beam would function as a link between the two parts

(Fig. 5.4). Even after a diagonal crack completely penetrated

the floor slab, the two parts can remain connected at the loading

edge. To test this speculation, three additional analyses were

made, designated cases 4', 6', and 7'. These were identical
to cases 4, 6, and 7,respectively, except that a stiffer and
stronger beam was added along the loading edge. (100 times
stiffer than the normal beam) (Fig. 5.4)   Table 5.3 also lists
the strength of these floor slabs. The shear failure was
completely prevented because the beam-was stronger and stiffer
and the ultimate resistance of these floor slabs was controlled
by flexural failure. The major crack locations at ultimate
load levels coincided with those of cases 1, 2, 3, and 8
(Fig. 5.4).

5.3.3 Evaluation of Flexural Capacity

Since the flexural capacity of cross sections in which
major cracks developed (critical sections) seemed to control the
flexural failure of floor slabs, an attempt was made to evaluate
the ultimate resistance of floor slabs on the basis of the
theoretically computed flexural capacity of the critical sections.
Assumptions and procedures used to calculate the flexural capa-
city of critical sections are described below.

1.   The Navier-Bernoulli hypothesis, that a plane section
     remains plane after deformation, was adopted to specify
     the strain distribution in the critical section.

2. The stress-strain relationship of reinforcing steel
   was assumed to be linear-elastic perfectly-plastic.
   The yield stress and modulus of elasticity of the
   steel were taken as those derived from the tension
   tests (Table 3.8).

3. The stress-strain relationship of concrete in com-
   pression was expressed by a cubic equation. Four
   constants were selected from the report published by
   Rao,[5.1] in which the values were determined by the
   curve-fitting of stress-strain curves originally pro-
   posed by Kriz and Lee.[5.2] The original curves were not
   used because the stress therein was not expressed as an
   explicit function of strain and, therefore, not suit-
   able for trial-and-error computation. The cubic
   equation to represent the stress-strain relationship
   of 27.6 MPa (4000 psi) concrete is:

$$f_c = 31.5 \, e - 11.0 \, e^2 + 0.980 \, e^3 \qquad (5-5)$$

f_c = stress of concrete   (MPa)
e = strain of concrete   (m/m)

Many equations defining the stress-strain relationship
of concrete under uniaxial compression and bending are
available in both explicit and implicit forms.[5.3] No

attempt was made to calibrate the propriety of

these equations on this flexural capacity calcul-

ation. Nevertheless, the discrepancy which could be

caused by using different equations appears to be mini-

mal. For example, the computation by using a linear

stress-strain relationship instead of equation 5-5

gave only a 15 percent discrepancy.

4. The tensile strength of concrete was completely neg-

lected. Consequently, concrete did not carry any

stress as long as the strain was in tension.

5. Strain was specified at the cross section's outer-

most fiber in tension, and a neutral axis which satis-

fied the equilibrium of axial force on the cross

section (resulting axial force of zero) was located

by trial-and-error. The corresponding moment then

was computed from the stresses in concrete

and reinforcing steel. The procedure was repeated

by alternating the level of strain at the outer-most

fiber in tension. Finally, the maximum moment obtained

was taken as the flexural capacity of the cross section.

Figure 5.5 schematically shows the procedure used to

compute the moment with a specified strain.

As listed in Table 5.3, the ultimate strength computed
from the flexural capacity of critical sections reasonably
approximates the ultimate strength computed from finite element
analyses. In case 4', the finite element analysis gave a 20
percent higher strength. This difference may have occurred
because the slab panel in case 4' was divided into elements
too large to guarantee the accuracy of the analysis. Moment
gradient in case 4', in which the loading edge was prevented from
rotating, was twice as large as in case 1. The length from zero to
maximum moment locations was divided into three sections in case
case 4', whereas the length in case 1 was divided into six
sections. (Fig. 4.11) Case 1 then may have reflected the
moment gradient more reasonably than case 4'. Except for
the slight discrepancy in case 4', however, the strength derived
from the finite element analysis agrees with the strength cal-
culated according to the flexural capacity of critical sections.
The comparison between cases 1 and 8 indicates that the larger
concrete beams increased the elastic in-plane stiffness and the
load corresponding to the onset of the post-elastic behavior of
the slab panel; however, they did not affect the ultimate resis-
tance. Once the major crack penetrated the concrete beam
subjected to tension, the beam no longer contributed to the
flexural resistance of the critical section.

5.3.4 Evaluation of Shear Capacity

Cases 4, 5, 6, and 7, exhibited a shear mode of failure. In each of the four cases, the amount as well as the arrangement of transverse reinforcing bars, equivalent to stirrups in beams, were the same. The shear capacities, however, differed. Table 5.3 shows that the shear capacity increases as the moment-to-shear ratio becomes greater. This increase may be caused by the flexural compressive stresses in concrete which tend to retard the onset of development of the diagonal crack. The ratio of compressive force to shear force increased in slab panels with large moment-to-shear ratios; such compressive force did not exist in case 5'.

Since all reinforcing bars intersecting the diagonal crack yielded when failure occurred, the shear force (V_s) resisted by the reinforcing bars could be evaluated by the standard ACI Code formula (11.5.6.2):

$$V_s = \frac{A_v \times f_y \times d}{S}$$

A_v = area of shear reinforcement within a distance s, or area of shear reinforcement perpendicular to flexural tension reinforcement within a distance s for deep flexural members

s = spacing of shear or torsional reinforcement in direction parallel to longitudinal reinforcement

d = distance from extreme compression fiber to
         centroid of longitudinal tension reinforcement
         but need not be less than 0.80h for pre-
         stressed members

    f_y = specified yield strength of non-prestressed
         reinforcement.

According to this formula, the shear force (V_s) in cases 4, 5,
6, and 7 equals 122 kN, which closely corresponds to the maximum
shear resistance in case 4. The ACI code also presents a formula
(11.3.1.1) for the shear force carried by cracked concrete (V_c):

$$V_c = 0.17 \times \sqrt{f'_c} \times b_w \times d$$

    b_w = web width

    f'_c = specified compressive strength of concrete   (MPa)

This formula calculates 67 kN of V_c. On the other hand, the
results derived from cases 4, 5, 6, and 7 show that V_c does not
exceed 33 kN, less than 50 percent of the value suggested by
the ACI code. The formula (11.3.1.1), therefore, is not suit-
able to evaluate the effect of cracked concrete on shear resis-
tance in the slab panels covered by this study.

A comparison between cases 4, 6, and 7 and cases
4', 6' and 7' stipulates another criterion for the shear
capacity of floor slabs. If floor slabs are integrated with
shearwalls or strong beams along their boundaries (Fig. 5.4),
the shear failure, in which a triangular portion is separated
from the remainder of the floor slab did not occur. As a
result, the flexural capacity controls the ultimate resistance
of the floor slabs. In floor slabs whose aspect ratio is more
than 1.0, however, the shear failure could still take place
even when the slabs are supported by shearwalls. As shown in
Fig. 5.4, full penetration of diagonal cracks can occur in the
floor slabs without being affected by the supporting shearwalls.
In these slabs, therefore, the shear capacity controls the
ultimate resistance.

5.4 Evaluation of Stiffness

5.4.1 Elastic Limit

As described in Chapter III, the in-plane stiffness of
slab panels significantly degraded as loads increased. The
elastic in-plane stiffness of floor slabs defined in the
Section 5.2, therefore, is not applicable if loads exceed a
certain limit.

First, the range within which the elastic stiffness
can be applied was evaluated. The experimental results reported
in Section 3.6.3 show that the development of cracks along

-138-

slab-wall junctions significantly reduces the stiffness of the
tested panels for the first time. The load levels at which the
cracks developed were 36 kN (8.0 kip) for BH2MN and 19 kN
(4.3 kip) for BH3MN, 30 and 34 percent of the ultimate load,
respectively. The load which would cause cracking along the
slab-wall junction was calculated based upon the following
assumptions:

1. Strain was distributed linearly along the junction.
   (Navier-Bernoulli's hypothesis)

2. Stress-strain relationship was linear.

3. Cracking occurred when the strain exceeded a cracking
   strain.

4. Reinforcing bars were not included in the calculation
   of moment at the junction.

The modulus of elasticity (E) and the split cylinder tensile
strength (σ_t) were used to compute cracking strain (ε_t). Thus
calculated, the cracking strain was 0.00010. The calculated
cracking load was 64 kN (15 kip) for BH2MN and 32 kN (7.3 kip)
for BH3MN, which are substantially higher than the experimental
cracking loads.

An elastic finite element analysis was carried out
to further investigate the strain distribution along the wall-
slab junction. Assumptions and procedures for the analysis

-139-

followed those described in Section 3.7.1. The analyzed slab

referred to as Type II was discretized as shown in Fig. 3.38.

Fig. 5.6 illustrates the analytical strain distribution along

the slab-wall junction together with the strain distribution

derived from Navier-Bernulli's hypothesis. This diagram indi-

cates that the analytical strain is 1.5 times larger at the slab

edges than the strain derived from this hypothesis. If the analyti-

cal strain is adopted, the cracking load is 43 kN (9.7 kip) for

BH2MN and 21 kN (4.8 kip) for BH3MN, 120 and 110 percent of the

experimental cracking load, respectively. Minute cracks

and residual stress which may have existed in the test panels

before testing are likely to have reduced the cracking load

by about 15 percent.

In summary, the cracking along the slab-wall junction

most probably gives the upper limit of the elastic behavior.

The strain distribution, however, is highly non-linear;

consequently, linear strain distribution significantly under-

estimates the strain at the slab edges (by about 40 percent

for the tested slab panels).

5.4.2 Stiffness in Post-Elastic Regions

The evaluation of the in-plane stiffness of floor slabs with various loading conditions as well as previous histories is complicated particularly in post-elastic regions. Here, the technique of treating floor slabs as deep beams for the stiffness estimation is extended to post-elastic regions. Seven slab panels, each of which had a particular set of geometrical, loading and boundary conditions, were selected to investigate their in-plane stiffnesses. The seven slab panels were: 1) the tested slab panel, BH2MN, 2) case 1 of the finite element analysis (Section 5.3.1), 3) the tested slab panel, BH3MN, 4) case 2 of the finite element analysis (Section 5.3.1), 5) case 3 of the finite element analysis (Section 5.3.1), 6) case 6 of the finite element analysis (Section 5.3.1), and 7) case 4 of the finite element analysis (Section 5.3.1).

In order to evaluate the elastic in-plane stiffness of floor slabs, as described in Section 5.3, the slabs were represented by deep beams that had particular combinations of effective moment of inertia and shear area, and the elastic material properties E and G. To extend this procedure to post-elastic regions, two hypothetical properties, named equivalent flexural stiffness $(EI)_e$ and equivalent shear stiffness $(AG)_e$

were introduced. The in-plane stiffness of floor slabs in post-elastic regions then was evaluated by combining the basic beam theory with these hypothetical stiffnesses. The calculation of these stiffnesses followed the procedure explained below:

1. $(EI)_e$ and $(AG)_e$ of the investigated floor slab are assumed to be constant throughout the length, from the clamped edge to the loading edge. Either $(EI)_e$ or $(AG)_e$ varies obviously depending upon the bending moment and shear force applied to the cross section. The calculated $(EI)_e$ and $(AG)_e$, therefore, represent the averaged stiffnesses of the floor slab rather than the actual properties.

2. According to the loading condition imposed on the floor slab, load-deformation relationships are defined as:

$$\Theta = \frac{P\ell^2}{2(EI)_e} \tag{5-6}$$

$$\delta_f = \frac{P\ell^3}{3(EI)_e} \qquad \text{for BH2MN, case 1, and case 6} \tag{5-7}$$

$$\delta_s = \frac{P\ell}{(AG)_e} \tag{5-8}$$

$$\Theta = \frac{3P\ell^2}{2(EI)_e} \left.\vphantom{\begin{array}{c} \\ \\ \\ \\ \\ \\ \\ \end{array}}\right\} \text{for BH3MN and case 2} \qquad (5\text{-}9)$$

$$\delta_f = \frac{5P\ell^3}{6(EI)_e} \quad \text{for BH3MN and case 2} \qquad (5\text{-}10)$$

$$\delta_s = \frac{P\ell}{(AG)_e} \qquad (5\text{-}11)$$

$$\Theta = \frac{M\ell}{(EI)_e} \qquad (5\text{-}12)$$

$$\delta_f = \frac{M\ell^2}{2(EI)_e} \quad \text{for case 3} \qquad (5\text{-}13)$$

$$\delta_s = 0 \qquad (5\text{-}14)$$

$$\Theta = \frac{P\ell^2}{8(EI)_e} \qquad (5\text{-}15)$$

$$\delta_f = \frac{P\ell^3}{12(EI)_e} \quad \text{for case 4} \qquad (5\text{-}16)$$

$$\delta_s = \frac{P\ell}{(AG)_e} \qquad (5\text{-}17)$$

$$\delta = \delta_f + \delta_s \qquad (5\text{-}18)$$

Θ = rotation at the loading edge for equations
5-6, 5-9, and 5-12 and the rotation at the
middle section for equation 5-15 (Refer to
Fig. 5.7)

δ_f = deflection due to bending along the loading
line

δ_s = deflection due to shear along the loading line.

δ = total deflection along the loading line

ℓ = length of the slab

P = external force applied at the edge

M = external bending moment applied at the edge

The equations 5-6 through 5-18 equal those derived
from the basic elastic beam theory except that equi-
valent flexural and shear stiffnesses substitute for
the elastic flexural and shear stiffnesses. Fig. 5.7
shows the loading and boundary conditions of the
seven investigated slab panels.

3. Θ and δ are measured at various load levels, and at
each load level, a pair of $(EI)_e$ and $(AG)_e$ are computed
by substituting the measured Θ, δ, and P or M in the
proper equations. Since total deflections and total
load rather than deflection increments and load incre-

ment are used to compute the equivalent flexural
and shear stiffnesses, these stiffnesses are associ-
ated with the secant stiffness of the floor slab at
specified load levels.

In Figs. 5.8 and 5.9, the computed $(EI)_e$'s and $(AG)_e$'s
are plotted against the largest bending moments, which were
applied at the clamped edges. The $(EI)_e$'s and $(AG)_e$'s, and the
bending moments are non-dimensionalized respectively by the
initial (EI)'s and (AG)'s, and the measured ultimate moments.
The curves of BH2MN and case 1 or the curves of BH3MN and case 2
match closely in the figures, demonstrating the ability of the pro-
posed finite element model described in Chapter IV to simulate the
in-plane behavior of slab panels in post-elastic regions. Figs.
5.8 and 5.9 show rapid decrease in equivalent flexural and
shear stiffnesses once elastic limits are exceeded. The stiff-
nesses continuously decrease as the moment increase. With the
exception of case 6, investigated slab panels have stiffnesses
that are about 30 percent of their initial stiffnesses when the
moments reach about 40 percent of the ultimate moments. At the
ultimate stages, both equivalent stiffnesses range from 10 to 13
percent of the initial elastic stiffnesses. In case 6, on the
other hand, the equivalent stiffnesses degrade less than in the
other slabs. They are reduced to about 30 percent of the initial

stiffness when the moment reaches about 70 percent of the
ultimate moment, and to approximately 15 percent of the initial
stiffnesses at the ultimate moment.

Fig. 5.10 shows the composition of the total deflec-
tions in the flexural and shear components for the investigated
slab panels. It is seen that the compositions remain relatively
constant regardless of load level; in BH2MN and cases 1 and 6,
the shear proportion ranges from 0.5 to 0.7. In BH3MN and case 2,
it ranges from 0.35 to 0.45, and in case 4, from 0.8 to 0.9.
On the other hand, the proportions are 0.62 in BH2MN and cases
1 and 6, 0.39 in BH3MN and case 2, and 0.87 in case 4 in the
elastic range. These values are calculated from the equations,
5-6 to 5-17, combined with the elastic material properties and
effective moment of inertia and shear area defined in Section
5.2. These values are shown by dotted lines in Fig. 5.10. It
is interesting to note that the proportions remain unchanged
from elastic to inelastic ranges. In Fig. 5.11, the same com-
positions are plotted against total displacement for BH2MN and
BH3MN, showing the trend in the post-ultimate load ranges. As
pointed out previously, behavior beyond the ultimate load point
was not obtained by the finite element analysis. The propor-
tions essentially remain unchanged even in the post-ultimate
load ranges.

-146-

Two important characteristics of the equivalent
flexural and shear stiffnesses can be inferred from this study.
First, the observation that the proportions remain constant
indicates that the equivalent flexural stiffness degrades in the
same proportion as the equivalent shear stiffness. That is,
at a given load, the identical coefficient to represent the
stiffness reduction, referred to as the reduction factor (α),
can be used to evaluate both stiffnesses. Second, the obser-
vation that the proportion in the post-elastic region is the
same as that in the elastic region makes it convenient to use
the basic elastic beam theory considering both flexural and
shear deformations. The total deformation of floor slabs
subjected to in-plane loads in post-elastic regions, then,
can be calculated by means of the beam theory together with
the degradation factor α.

Although the discussion so far has been devoted to
evaluating the secant stiffness of floor slabs, the tangent
stiffness of floor slabs can also be evaluated by using the
same procedures; the proportions of flexural and shear
deformations to total deformation in the elastic range do not
change in post-elastic regions.

5.4.3 Degradation Factor α

The discussion in Section 5.4.2 has verified that the
in-plane stiffness of floor slabs in post-elastic regions can
be approximated by using the fundamental beam theory which
includes both flexural and shear deformations together with the
stiffness degradation factor α. The evaluation of α is developed
.by examining of the flexural stiffness in post-elastic
regions. As shown in Fig. 5.8, the flexural stiffness degrad-
ation curves of all investigated slab panels except case 6 are
confined in a narrow band. This situation suggests that the
moment gradient in the panel has little effect on the degrad-
ation of the equivalent flexural stiffness. (Fig. 5.7)   The
parameter which differentiated case 6 from the others was the
amount of reinforcement; the amount of longitudinal (flexural)
reinforcement in this panel was twice the amount in the other
panels. On the other hand, the amount of flexural reinforcement
is known to control the flexural stiffness of cracked cross
sections. The observation that the flexural reinforcement con-
trols both the equivalent flexural stiffness in the post-
elastic regions and the flexural stiffness at cracked cross
sections infers the possibility to evaluate the equivalent
stiffness of floor slabs in post-elastic regions based upon the
flexural characteristics at their cracked (critical) sections.
A simple method to compute the equivalent flexural stiffness of
floor slabs in post-elastic regions is proposed below:

According to Fig. 5.12, the end rotation of the
slab panel in the post-elastic region is the sum of the elastic
rotation due to bending and the hinge rotation at the critical
section. The end rotation is:

$$\Theta = \Theta_f + \phi \times \ell_p \qquad (5\text{-}19)$$

Θ = total end rotation

Θ_f = rotation due to elastic bending

$$\Theta_f = \frac{P\ell^2}{2(EI)_{e,\ elastic}} \qquad \text{for BH2MN and cases 1 and 6}$$

$$\Theta_f = \frac{3P\ell^2}{2(EI)_{e,\ elastic}} \qquad \text{for BH3MN and case 2}$$

$$\Theta_f = \frac{M\ell}{(EI)_{e,\ elastic}} \qquad \text{for case 5}$$

ϕ = curvature at the critical section

ℓ_p = length of the hinge

Although the hinge introduced at the critical section is hypo-
thetical but represents the sum of non-elastic rotations caused
by flexural cracks in the slab panel. The procedure described
in Section 5.3.3 computes ϕ's at various load levels. Fig. 5.13

-149-

illustrates the moment-curvature relationship of two critical

sections: the critical section of cases 1, 2, 3, and 4,

and the critical section of case 6. The technique used to

divide the total deformation into elastic deformation and hinge

deformation is analogous to the tequnique which Mattock[2.28]

and Corlay[2.13] deviced to determine the ductility of rein-

forced concrete flexural members. Knowing the elastic rotation

Θ_f, hinge length ℓ_p can be calculated from the total end

rotation Θ derived from either the experiment or finite element

analysis and from the curvature ϕ calculated according to the

procedure described in Section 5.3. As shown in Fig. 5.14, the

calculated ℓ_p's range from 190 mm to 300 mm. The range is

limited to a relatively narrow band despite the wide variations

of the parameters such as load level, loading condition, and

amount of sttel among the investigated cases.

The average of the ℓ_p's, 250 mm, is used to reconstruct

the equivalent flexural stiffness $(EI)_e$ in post-elastic regions.

Once the ℓ_p is specified, data from either experiments or analyses

are not needed to compute $(EI)_e$. The procedure to compute $(EI)_e$

is explained for BH2MN:

$$\Theta = \frac{P\ell^2}{2(EI)_{e, \text{ elastic}}} + \phi \times \ell_p \qquad (5-20)$$

ϕ is selected from Fig. 5.15, and ℓ_p = 250 mm.

$$(EI)_e = \frac{2P\ell^2}{\Theta} \qquad\qquad (5\text{-}21)$$

$$\alpha = (EI)_e / (EI)_{e, \text{ elastic}} \qquad\qquad (5\text{-}22)$$

As evidenced in Figs. 5.8 and 5.15, the calculated equivalent
flexural stiffness and consequently the degradation factor rea-
sonably duplicate those derived by means of vigorous experiments
or finite element analyses. It should be pointed out, however,
that 250 mm of the hinge length ℓ_p is valid within the range
covered in the investigated slabs. Mattock[2.28] and Corlay[2.13]
found that the depth of beams and the moment gradient primarily
controlled the hinge length. On the other hand, the observation
in this section does not show that the moment gradient signi-
ficantly influences the hinge length. Further investigation is
needed to define the hinge length ℓ_p more precisely for floor
slabs with different geometry, loading, and reinforcement.

5.5 <u>Ductility of Floor Slabs</u>

To evaluate the ductility of reinforced concrete
members is difficult because of the interaction of several compli-
cated phenomena like cracking of concrete, the yielding or slip-
ping of reinforcing bars, or the crusing of concrete. Mattock[3.28]
and Corlay[2.13] produced two of the earliest works discussing
the ductility of reinforced concrete flexural beams. Their basic

-151-

procedures used to evaluate the ductility of a simply

supported beam with a concentrated force at mid-span are:.

1) to assume that the total deflection of the beam consists

of elastic deflection and inelastic deflection caused by a

plastic hinge at the mid-span, 2) to compute the ultimate cur-

vature at the critical section (the section at the mid-span) of

the beam by specifying the ultimate compressive strain of con-

crete, 3) to assume that the ultimate curvature spreads over

a finite length, and next to compute the inelastic rotation at

the critical section, and 4) to relate the total inelastic

deformation to the inelastic rotation at the hinge according to

an empirical formula. Mattock reported that the plastic hinge

length was controlled by the effective depth of beam, the

gradient of the applied bending moment measured by the distance

between the locations of the maximum and zero moments, and the

degree of confinement which limits the ultimate compressive

strain. Mattock offered the following formula that defines

the hinge length:

$$\ell_p = 0.4d + 0.05z \qquad\qquad (5\text{-}23)$$

d = the effective depth of beams

z = the distance along span from section of

maximum moment to adjacent section of zero moment

Fiorato et al.[(2.19)] computed the ductility of their tested

slender shearwalls by using the procedures devised by Mattock·

They found that experimental and computed ductilities were

comparable.

The formula 5-23 and the moment-curvature curve

shown in Fig. 5.13 calculates 14.9 mm of the ultimate deflection

for both BH2MN and BH3MN. The calculated deflection is

approximately twice as large as the ultimate deflection observed

during the tests. The breaking of reinforcing bars controlled

post-ultimate load deformation in the tested slab panels

described in Chapter III, while Mattock's and Corley's studies

assumed that the ultimate compressive strain of concrete limits

the deformation. The reinforcement ratio of the tested slab

panels ranged from 0.0025 to 0.005, while the ratio of the beams

tested in Mattock's and Corley's studies ranged from 0.010 to

0.030. The floor slabs had significantly less reinforcement

than their tested beams.

As shown in Fig. 4.13, the end rotations of BH2MN and

BH3MN are 28×10^{-4} rad. and 43×10^{-4} rad. at the critical

stages at which resistance decreased significantly due to the

breaking of several reinforcing bars. The equivalent flexural

stiffness, described in Section 5.4.2, are $54 \text{ kN} \times \text{m}^2$ for

BH2MN and $49 \text{ kN} \times \text{m}^2$ for BH3MN at the critical stages. These

values are 4.0 and 3.6 percent of the respective initial flexural

stiffnesses. An attempt was made to estimate the ductility of

BH3MN and BH2MN by employing the simplified techniques and

experimental findings noted in the previous sections of this

chapter. Assumptions and procedures used are as follows:

1. Computation of the ultimate strength was based upon

   the flexural capacity of the critical section.

   (Section 5.4.1)

2. The sum of the flexural and shear deformations

   constituted the total deformation. The proportion

   of the flexural or shear deformation to the total

   deformation remained unchanged at all load levels.

   (Section 5.4.2)

3. The degradation factor α at the ultimate load was

   computed based upon the curvature at the critical

   section and an empilical hinge length of 250 mm.

   (Section 5.4.3)

4. The degradation factor α at the critical stage was

   taken as 0.038, the average of experimental values.

   Note that this value was purely empirical.

With the procedures described above, the ductility can be

computed without using any of deflections in the tests. The

displacement at the ultimate load is 2.8 mm (0.11 in.) for

BH2MN and 1.9 mm (0.075 in.) for BH3MN. The critical displacement is 8.6 mm (0.34 in.) for BH2MN and 5.8 mm (0.23 in.) for BH3MN. The ductility then is 3.1 for both slabs, which approximates the experimental ductility listed in Table 3.15. This coincidence, however, is rather obvious because the degradation factor 0.038 was chosen to match the experimental results. The critical displacement is easily affected by the value of degradation factor at the critical stage. A minor change in this factor at the critical stage can easily double or halve the ductility. The precise evaluation of the critical displacement which corresponds to the breaking of reinforcing bars, therefore, is crucial.

The instant when reinforcing bars would break is unpredictable since local conditions such as bond slip and secondary bending due to dowel action significantly affect the strain at critical regions. Although the experimental results show that the slab panels BH2MN and BH3MN can deflect up to about 7 mm without a significant loss in resistance, to expect this level of deflection in floor slabs having various loading conditions is controversial. Furthermore, to rely the ductility on the performance of reinforcing bars appears to be unwise. It is tentatively suggested not to expect ductile behavior of floor slabs unless they are reinforced more heavily than floor slabs with usual reinforcement.

5.6 Effect of Cyclic Loading

5.6.1 Effect on Strength

The experimental results have shown that reversed load-
ing (negative loading in monotonic loading tests) or cyclic
loading (represented by the spectrum shown in Fig. 3.17) reduces
the in-plane strength of the tested slab panels by as much as
20 to 25 percent. The finite element analysis described in
Chapter IV, on the other hand, did not show a reduction in the
strength caused by either reversed or cyclic loading. The
evaluation of the ultimate strength based on the flexural
capacity at the critical sections, described in Section 5.3.3,
did not indicate any such reduction, either.

As several reinforcing bars were broken in the mono-
tonically loaded slab panels at the end of positive loading,
these bars obviously did not function in resisting negative
loading. The flexural capacity of the critical section was
recomputed with these bars removed. The reduction of the ulti-
mate load, however, was not more than 4 percent. All removed
bars, located either in the compression region or the vicinity
of the neutral axis, had very little effect on the ultimate
strength. Clearly, some characteristics not represented by
either the finite element analysis or flexural capacity cal-
culation were responsible for the reduction of the ultimate

strength of the panels under reversed or cyclic loading.
It is suspected that precracked concrete lose some effective-
ness in resisting compressive force even after cracks are
closed.

5.6.2   Effect on Stiffness

5.6.2.1   Elastic Limit

In cyclic loading tests BH1CY and BH3CY, the initial
stiffness listed in Table 3.13 remained unchanged during the
cycles with the 0.25 mm amplitude. During the loading in the
first cycle of the 0.76 mm amplitude, cracks developed along
the slab-wall junctions, causing the stiffness to decrease
significantly as shown in Fig. 3.27 and 3.28. The cracks
occurred in BH1CY at 28 kN (6.3 kip) under positive loading
and at -28 kN (-6.3 kip) under negative loading and in BH3CY
at 18 kn (4.0 kip) under positive loading and -14 kN (-3.2 kip)
under negative loading. These cracks loads were 20 and 25 percent
lower than the cracking loads taken place in the monotonic
loading tests. (Section 5.4.1) The three preceding cycles in
a lower amplitude evidently accelerated the development of the
cracks. Interestingly, the cracking loads and the utli-
mate loads decreased by the same percentage under cyclic
loading. In BH2CY, the cracking load decreased to 78 percent,

while the ultimate load decreased to 79 percent. In BH3CY, the cracking load decreased to 74 percent, while the ultimate load decreased to 73 percent.

5.6.2.2 Stiffness in Post-Elastic Regions

The technique to evaluate the in-plane stiffness of floor slabs by treating them as deep beams was extended to the post-elastic regions for slabs subjected to cyclic loading. Figs. 5.16 and 5.17 show the proportions of flexural and shear deflections to total deflection of BH1CY and BH3CY, respectively. The definitions of the flexural and shear deflections and the procedures used to compute these deflections followed those described in Section 5.4.2. Rotation and deflection increments used in the calculations were taken in three different ways: 1) rotation and deflection increments from the point of the minimum deflection to the point of the maximum deflection of a hysteretic loop, which corresponds to the secant stiffness 1 defined in Section 3.6.3, 2) rotation and deflection increments from the point of zero deflection preceding the maximum deflection to the point of the maximum deflection of a hysteretic loop, which corresponds to the secant stiffness 2 defined in Section 3.6.3, and 3) rotation and deflection increments from the point of zero deflection preceding the minimum deflection to the point of the minimum

deflection of a hysteretic loop, which corresponds to the secant stiffness 3 defined in Section 3.6.3. The proportions of flexural and shear deflections to total deflection are computed for the first cycle of each amplitude based upon these three different types of rotation and deflection increments and plotted against the amplitude in Figs. 5.16 and 5.17.

As evidenced by these diagrams, the proportions are confined in a relatively narrow band and maintain the proportions found in the elastic region (indicated by dotted lines) regardless of amplitude or load (or displacement) level. This finding supports the conclusions derived in Section 5.4.2, which discusses slabs subjected to monotonic loading. First, both the equivalent flexural and shear stiffnesses degraded by the same degree regardless of loading condition, load level, or amplitude. Second, the proportions of flexural and shear deflections to total deflection in the elastic region remained unchanged in post-elastic regions. Consequently, the in-plane stiffness of floor slabs under cyclic loading can also be evaluated by means of the basic beam theory which includes both flexural and shear deformations once the degradation factor α is specified. The degradation factor α is a function of load level, deflection and previous loading history. The following section describes the derivation of the degradation factor α for slabs subjected to cyclic loading.

-159-

5.6.2.3 Degradation Factor for Slabs in Cyclic Loading

Fig. 5.18 plots the secant stiffness 1, defined in Section 3.6.3, of cyclic loading tests BH1CY and BH3CY against specified amplitudes. This diagram also plots the secant stiffness of the monotonic loading tests BH2MN and BH3MN, in which the stiffness is plotted against the deflection corresponding to the amplitudes. During the cycles of the two lowest amplitudes, 0.23 mm and 0.76 mm, the secant stiffnesses between the monotonic and cyclic loading tests are the same. According to Section 3.7.4.3, the initial stiffness of BH2MN is significantly lower than those of all other tests. During these cycles, damage caused by cracks occuring in the previous cycles had not yet reduced the stiffness. During the three cycles of the 1.3 mm amplitude, in which the load reached approximately half of the ultimate load for the first time, the secant stiffness 1 equals approximately 75 percent of the secant stiffness of the corresponding monotonic loading tests. The secant stiffness 1 constantly ranges from 75 to 80 percent of the secant stiffness of the corresponding monotonic loading tests in the succeeding cycles. Both the stiffness and the ultimate load are reduced due to cyclic loading by the same percentage.

Based upon this finding, a rule to evaluate the secant stiffness 1 of slabs under cyclic loading from the secant stiffness of the slabs when they are loaded monotonically is proposed:

1. The secant stiffness 1 of a slab subjected to cyclic loading with a given amplitude is x times the secant stiffness of the slab subjected to monotonic loading at the deflection corresponding to the amplitude.

2. The fraction x is the ratio of the ultimate load which can be reached if the slab is loaded monotonically to the ultimate load which can be reached if the slab is subjected to cyclic loading. The degradation factor α of the slab under cyclic loading, therefore, is x times the degradation factor of the slab under monotonic loading.

3. During the cycles with amplitudes in which the load is less than half of the ultimate load, the secant stiffness 1 may equal the corresponding secant stiffness derived from the monotonic loading.

The secant stiffness 1 represents only a portion of the stiffness of the slab panel subjected to cyclic loading. Nevertheless, this stiffness is one of the most suitable representations of the stiffness of slabs under arbitrary

reversed loadings. As pointed out in Section 3.7.4.2, the

five types of stiffness defined in Section 3.6.3 varied little

regardless of loading condition or load level.

5.6.3 Effect on Ductility

Experimental results show that cyclic loading reduced

critical displacements by about 10 percent and increased

by about 40 percent the deflection at which 90 percent of the

ultimate load was reached for the first time. The approximately

30 percent difference in ductility observed in monotonic and

cyclic loading tests, as shown in Table 3.15, was attributed

primarily to the larger deflection corresponding to 90 percent

of the ultimate load taking place during the cyclic loading

tests. However, it must be noted that the load-deflection

relationship of cyclically loaded panels is heavily dependent

on the loading spectrum. Consequently, significant variations

may take place in the base deflection value for the calcul-

ation of ductility.

The ductility of the slab panels subjected to

cyclic loading also depended upon the performance of rein-

forcing bars. The breaking of several reinforcing bars at

their intersections with major cracks caused significant loss

in resistance. Although the test results show that cyclic

loading reduced the critical displacement by only 10 percent

and that resistance did not degrade in three cycles for most
of the specified amplitudes of the test spectrum, these
performances may not prevail under different loading systems.
The suggestion offered in Section 5.5 can be pointed out again.
With limited data available, we should not allow slabs to
deflect under any loading conditions beyond the deflection
level at which the ultimate load can be reached when the
slabs are loaded monotonically.

5.7 Effect of Vertical Load

5.7.1 Effect on Strength

The design service vertical load reduced the ultimate
resistance of the tested slab by 15 percent. The vertical load
also changed the crack pattern particularly in the middle port-
ion of the bottom surface, where many cracks extended from the
center of the slab in radial direction. Evidently, out-of-
plane bending moment caused these cracks. The vertical load,
however, did not change the general in-plane behavior of the test
panel. The major crack still developed along the boundary
between the column and middle strips, and its complete formation
governed the ultimate resistance. The opening and closing of
the major crack also controlled the deformation of the panel
in post-ultimate load regions.

Under in-plane loading, the major crack developed along
the boundary between the column and middle strips, where a
significant decrease of reinforcement took place. The boundary
was least reinforced because the out-of-plane bending moment
caused by the vertical load was small along the boundary.
In other words, the boundary was the most critical section
under in-plane loading but relatively safe under out-of-plane
(vertical) loading. Along the slab-wall junction, on the other
hand, the bending moment caused by the vertical load was the
greatest; therefore, the junction was heavily reinforced. The
junction with substantial reinforcement, then, increased
the flexural capacity of the slab in its own plane. The junct-
ion, therefore, was the most critical section under vertical
loading but considerably stronger than the boundary against
in-plane loading. The test result indicates that the boundary
between the column and middle strips was still the most
critical section under the combined vertical and in-plane load-
ing.

Cyclic loading reduced the ultimate load further by 18
percent, which is about the same as the reduction on slab panels
not subjected to vertical loading. The cyclic loading changed
neither the crack pattern nor the development of major cracks.

5.7.2 Effect on Stiffness

5.7.2.1 Effect in Post-Elastic Region

In order to determine the suitability of treating
floor slabs as deep beams and evaluating the in-plane stiff-
ness of floor slabs subjected to the design service vertical
load, the porportions of flexural and shear deflections to total
deflection were computed for BV1MN and BV2CY. The procedures
used to calculate the flexural and shear deflections were those
described in Section 5.4.2. Three types of rotation and
deflection increments (BV2CY), were employed to compute equations
5-6 through 5-8, as described in Section 5.6.2.2. According
to Fig. 5.19, the proportions are confined in a relatively
narrow band. They maintain the proportion in the elastic
region regardless of amplitude or load level. This finding
again supports the extension of the calculation procedure
described in Section 5.4.2 for evaluating the in-plane stiffness
of floor slabs under combined in-plane and out-of-plane load-
ings. The in-plane stiffness of floor slabs subjected to
combined vertical and in-plane loads (either monotonic or
cyclic) can be evaluated by means of the fundamental beam theory
which includes both flexural and shear deformations once the
degradation factor α is specified. The degradation factor
can be a function of in-plane load level, vertical load level,
deflection, and previous loading history.

5.7.2.2 Degradation Factor of Slabs with Vertical Load

The test results show that the design service vertical load reduced the initial in-plane stiffness by about 20 percent. (Section 3.7.4.7) The reduction was caused primarily because cracks developed under the vertical load. (Fig. 3.19) Unlike slab panels without vertical load, slab panels with vertical load immediately lost their initial in-plane stiffness. Afterward, the stiffness gradually degraded as the load increased or reversed.

For BH2MN, BV1MN, and BV2CY, the ratio of equivalent flexural stiffness $(EI)_e$ to the elastic flexural stiffness is plotted against the displacement. (Fig. 5.20) This ratio matches the degradation factor. The equivalent flexural stiffness of BV1MN ranged from 60 to 85 percent of that of BH2MN. The difference between these equivalent flexural stiffnesses was appreciable particularly in the vicinity of the deflection at which BH2MN reached its ultimate load. (2.9 mm of deflection) The stiffness of BV1MN degraded rapidly in the deflection range in which BH2MN approached its ultimate load, while varying its tangent stiffness slightly. The secant stiffness of the slab panels with the design service vertical load and which were loaded monotonically in their own planes, therefore, comprised 60 to 85 percent of the secant stiffness of the panels with no vertical load.

-166-

. Like the slab panels without vertical load, the slab

panels with the design service vertical load also show a

correlation between the secant stiffnesses under cyclic and mono-

tonic loadings. For a deflection of less than 1.1 mm, the point

at which BV2CY first reached about half of the ultimate load,

each of the secant stiffnesses 1, 2, and 3 of BV2CY almost equalled

the secant stiffness of BV1MN. For a larger deflection, the

secant stiffnesses 1, 2, and 3 of BV2CY ranged from 80 to 90 per-

cent of the secant stiffness of BV1MN. The relationship between

the secant stiffnesses of BV1MN and BV2CY was identical to those

between BH2MN and BH1CY, and BH3MN and BH3CY. The rule stipula-

ted in Section 5.6.2.3, therefore, can be used to evaluate the

secant stiffness 1 of slabs with vertical load.

The degradation factor of a slab to which vertical load

is first applied and held constant during in-plane cyclic

loading is x times y times the degradation factor of the slab

to which only in-plane load is applied monotonically. The factor

x is the ratio of the ultimate load which may be reached if

the slab is loaded monotonically to the ultimate load which may

be reached if the slab is subjected to cyclic loading. The

factor y is the ratio of the ultimate load which may be reached

if the slab is loaded monotonically with vertical load to the

ultimate load which may be reached if the slab is loaded

monotonically without vertical load. For the slab panels investigated in this study, x and y are 0.80 and 0.85 respectively. Data, however, are limited, and further research is indispensable to the proper evaluation of the combined effect of the intensity of vertical load and loading history on these factors, x and y.

As in panels without vertical load, the secant stiffness 1 also is a reasonable representation of the stiffness in slabs with vertical load and subjected to cyclic loading. The five types of stiffness defined in Section 3.6.3 differed little regardless of load level, indicating that the secant stiffness 1 reasonably matches the tangent stiffness of a hysteretic loop in most regions.

5.7.3 Effect on Ductility or Deformability

As indicated in Section 5.6.3, ductility in cyclic loading tests is questionable because it is difficult to pinpoint the deflection at which 90 percent of the ultimate resistance could first be reached. In addition, ductility was not computed for BV1MN since the test was terminated before the panel reached the critical displacement. The design service vertical load, on the other hand, reduced critical displacement by about 15 percent when the slab panel was subjected to cyclic loading, but increased critical displacement by about 25 percent when the panel. was subjected to mono-

-168-

tonic loading. Like the panels without vertical load, the
panel with vertical load lost its resistance when several
reinforcing bars broke. The vertical load (at least up to the
design service load level) cannot be a major parameter reducing
the deformability of the slabs if the uncertainty of computing
ductility as well as the slab's allowable deflection are taken
into account.

5.8 Summary

In this Chapter, the critical in-plane characteristics
of floor slabs: strength, stiffness, and ductility,were examined
based on the experimental findings and data provided by the
proposed finite element analysis (Chapter IV). Practical proce-
dures to predict the ultimate in-plane strength and in-plane
stiffness of floor slabs have also been proposed. The important
findings can be summarized as follows:

Findings Concering Strength

(1) Two failure modes were observed in the analyzed
slab panels depending on imposed loading and
boundary conditions. In the flexural failure mode,
the major crack developed parallel to the clamped
edge at a distance of about a quarter panel length
(350 mm) and controlled the ultimate in-plane
resistance. This location of major crack, labelled

-169-

the critical section, was very near the boundary

between the column and middle strips of the panel.

Many reinforcing bars were terminated here, according

to out-of-plane bending considerations. The

flexural capacity of the critical section governed

the ultimate resistance.

(2)   In the shear failure mode, slab panels reached their

ultimate loads when a diagonal crack completely

separated a triangular portion from the remainder

of the panel. A strong beam attached to the

loading edge of the slab panel, simulating the

situation where slabs are supported by shearwalls

would prevent the diagonnal separation of the panel

and promote the flexural failure mode.

(3)   Increasing the amount of flexural reinforcement improved

the in-plane strength of slab panels. On the other

hand, increasing the size of concrete beams increased

the elastic in-plane stiffness and the elastic

limit load, but did not affect the ultimate resis-

tance.   When panels failed in the flexural mode,

the effect of the magnitude of shear on the ultimate

strength was minimal, indicating that the moment-

to-shear ratio did not influence the flexural capacity

of the critical sections.

(4)   Cyclic loading represented by the spectrum shown

        in Fig. 3.17 reduced the in-plane strength of slab

        panels by as much as 25 percent. Cumulative damage

        like cracking was responsible for the reduction.

        The effectiveness of concrete in resisting compress-

        ion was reduced by cracking even after the cracks

        had been closed. The application of the design

        service vertical load reduced the ultimate in-plane

        resistance of slab panels by not more than 15 per-

        cent. Vertical load did not alter the general

        behavior of the panels; the major crack still de-

        veloped along the boundary between column and middle

        strips.

(5)   The in-plane flexural strength of slab panels loaded

        monotonically without vertical load can be reasonably

        evaluated by using the theoretically calculated

        flexural capacity at the critical section by means of

        the Navier-Bernoulli hypothesis.   (The procedure

        detail is described in Section 5.3.3) The standard

        ACI Code provision (11.5.6.2) for estimating the

        contribution of shear reinforcement to the shear

        capacity is applicable for the slab panels. The ACI

        provision (11.3.1.1) on the contribution of the

        cracked concrete overestimates the shear capacity.

Findings Concerning Stiffness

(1)   Slab panels not subjected to vertical loading started losing their initial in-plane stiffness upon appearance of a crack at the edge of the slab-wall junction; this point, therefore, was defined as the elastic limit. The load corresponding to the elastic limit was approximately 30 percent of the ultimate load, whereas the secant stiffness at this stage was about 30 percent of the initial value. The secant stiffness continuously decreased as load increased, reaching approximately 15 percent of the initial value at the ultimate load stage.

(2)   In cyclically loaded slab panels without vertical load application, the secant stiffness degraded in a similar manner as in monotonically loaded slab panels. Hysteretic load-deflection loops of these panels were narrow in width, indicating that energy absorption in a complete cycle was small. The secant stiffness, therefore, appears to be a relatively suitable representation of the stiffness of slabs subjected to arbitrary reversed loading.

(3)   Upon the application of the design service vertical load, two cracks developed on the slab panel's top surface, one along the slab-wall junction and the other along the loading line. These cracks apparently changed the

pattern of stiffness degradation under monotonic load-
ing. Tangent stiffness of the panel degraded gradually,
measuring near zero at the ultimate load. The verti-
cal load promoted the development of cracks, and
cracking in low load levels made the transfer of forces
from concrete to reinforcing bars more gradual. When
slab panels with the vertical load were loaded
cyclically, however, the effect of the vertical load
on stiffness degradation was small. The slab panel
with the design service vertical load constantly showed
an about 20 percent lower secant stiffness than the
panel without such load.

(4)   In the elastic range, the stiffness characteristics
of the slab panels may be reasonably estimated by
treating them as deep beams considering both flexural
and shear deformations (equivalent beams). The use
of nominal moment of inertia and shear area, those
computed from the gross cross section, is sufficient
for evaluating the in-plane stiffness of floor slabs
regardless of aspect ratio or relative beam size.

(5)   The equivalent beam simulation also can be used in
post-elastic ranges if a hypothetical reduction factor
is introduced. This factor represents a stiffness reduc-
tion of the equivalent beam caused by various inelastic

behavior such as cracking or yielding of reinforcing
bars. Once a reduction factor is known at a given
load level, the in-plane stiffness of a floor slab in
the post-elastic region is computed by using the same
procedure as for elastic deep beams. A simple
procedure to compute the reduction factor is proposed
in Section 5.4.3. This equivalent beam simulation is
proven to be applicable not only for floor slabs sub-
jected to monotonic in-plane loadings but also for
floor slabs subjected to in-plane cyclic loadings or
combined in-plane and out-of-plane loadings.

Findings Concerning Ductility (Deformability)

(1) Once the ultimate load was reached, the deflection of
the tested slab panels was controlled primarily by
the opening and closing of the major crack. Few new
cracks started in this post-ultimate load region,
while the level of resistance remained relatively
constant. Finally, the breaking of reinforcing bars
at the major crack reduced the resistance drasti-
cally. The effect of either cyclic loadings or combined
in-plane and out-of-plane loadings on ductility was
minimal. The slab panels under these loadings de-

formed without a significant change in resistance
to approximately 80 percent of the limit deflection
of monotonically loaded slab panels.

(2)   In-plane ductilities of tested slab panels were com-
pared with theoretical ductilities computed by means
of a conventional procedure. The computed ductilities
were approximately twice as large as the experimental
ductilities. The discrepancy was attributed to the
difference in material behavior controlling the
critical deformation. The breaking of reinforcing
bars controlled deformation in post-ultimate load
regions for tested slab panels. In contrast, the
computational procedure assumes that the reinforcing
bars can yield indefinitely and the ultimate com-
pressive strain of the concrete limits the deformation.

(3)   A technique is proposed to compute the ductility of
floor slabs by using empirically defined ultimate stiff-
ness reduction factors. This technique functions satis-
factorily for the tested panels, but additional confir-
mation is still needed before its usefulness may be ex-
panded. With insufficient data available about the
deflection corresponding to the breaking of reinforcing
bars, it is tentatively suggested that in-plane ductile
behavior of floor slabs should not be expected unless
they are reinforced more heavily than usual.

VI DYNAMIC RESPONSE OF BUILDING INCLUDING IN-PLANE FLOOR SLAB DEFORMATION

6.1 General

This chapter examines influence of in-plane defor-
mation of floor slabs on the total seismic lateral load applied
to a structure as well as on the distribution of this lateral
load to the vertical load resisting elements. Shear forces
and bending moments applied to floor slabs are also inves-
tigated.

A relatively simple building model representing a
reinforced concrete building with usual dimensions was selected,
and the dynamic response of the model was investigated. The
direct integration method was used to obtain the time-history
relationship of this structural model. The ground motion
selected for this study was the N-S component of the El Centro
earthquake recorded in Imperial Valley, May 18, 1940. The var-
ious in-plane characteristics of the floor slabs defined in
Chapter V as well as the stiffness and strength characteristics
of the vertical elements (shearwalls and columns) were incor-
porated into the dynamic analysis.

At the beginning of this investigation, elastic dyna-
mic analysis was executed based on the elastic characteristics
of the floor slabs and vertical elements. The results obtained
from this elastic analysis were used as the basis for comparison

with the results derived from the succeeding analyses. In
these analyses, the stiffness characteristics of the floor slabs
as well as vertical elements altered. First, the propriety
of the rigid floor slab assumption was examined. Then, the
change in the model structure's response due to the non-linear
actions of vertical elements and floor slabs was investigated.

6.2 Building Model Selected

A reinforced concrete building model with seven
stories, six bays in width, and one bay in depth was selected
for this study. Fig. 6-1 illustrates the plan and elevation
views of this building and its critical dimensions. The story
height is 3.0 m from second through seventh stories, while the
first story is 3.75 m in height. The center-to-center span
length is 6.0 m in two horizontal directions. A shearwall is
located at each end, whereas the interior spans are supported
by flexible frames. The thickness of the shearwalls is 320 mm,
and the cross section of the columns is 600 mm x 600 mm with
no capital. The floor slabs are 200 mm in thickness. Beams
(300 mm x 500 mm) are attached to the lower sides of these slabs
and along column lines in both directions. The ground motion was
applied in the transverse direction of the structure.

This model has a relatively slender cross section, whose aspect ratio is 1 : 6. This arrangement was chosen intentionally so that the floor slabs would play a significant role on the distribution of lateral force to vertical elements. As discussed in Chapter II, a slender cross section tends to amplify the bending action of the floor slabs, referred to as bowing. In addition, a great difference in lateral stiffness between adjoined vertical elements increases the force to be transmitted by the floor slab connecting these components. This increase in force may cause severe distortion of the floor slab.

6.3 Analysis of Building Model

6.3.1 Simplification of Model

To investigate the response of the building model, the structure was simplified to a discrete model. In this model, all structural components: floor slabs, frames, and walls, were treated as beams, named equivalent beams. These equivalent beams were assembled and jointed at each connection, forming a seventy-story six-bay frame. Since the ground motion was applied in the transverse direction, equivalent beam properties for the deformation in this direction were needed. The beam properties were determined so that these equivalent beams would appropriately simulate the original properties. Walls were treated as deep beams which have both flexural and shear de-

formations. Floor slabs also were treated as deep beams;
Chapter V has discussed this treatment in detail. Frames,
composed of columns and beams, were represented as beams that
have particular combinations of flexural and shear rigidities.
The selection of both geometrical and material properties of
the equivalent beams is described in further detail in Section
6.4. Since both geometry of the model structure and input
ground motion were symmetrical about the vertical axis (Fig. 6.1),
only half of the structure must be analyzed.

6.3.2 Formulation of Equations of Motion

In dynamic response analysis, the equations of
motion can be written as:

$$[M]\{\ddot{u}\} + [C]\{\dot{u}\} + [K]\{u\} = \{R(t)\} \qquad (6-1)$$

where: $[M]$ = mass matrix

$[C]$ = damping matrix

$[K]$ = stiffness matrix

$\{u\}$ = displacement vector

$\{\dot{u}\} = \dfrac{du}{dt}$

$\{\ddot{u}\} = \dfrac{d^2u}{dt^2}$

$R(t)$ = vector of arbitrary time varying loads

If the structure is uniformly subjected to the ground
motion u_g, the equation can be expressed as:

$$[M]\{\ddot{u}_r\} + [C]\{\dot{u}_r\} + [K]\{u_r\} = -[M] \times u_g \qquad (6\text{-}2)$$

where $\{u_r\}$ is the relative displacement vector of the structure
with respect to the ground, ie $\{u_r\} = \{u\} - \{1\} \times u_g$.

6.3.3 Formulation of Mass Matrix

The mass of the structure was represented by lumped
masses at junctions. Each lumped mass equalled to the mass within
a tributary region of a junction. The mass of the service
design vertical load, 3.8 kPa, acting on the floor slabs was added
to the mass calculated from the structure's dead weight. Since
rotational inertia was neglected, (Section 6.3.4), the lumped
masses caused only translational inertia at the junctions. The
mass matrix [M], then, is a diagonal matrix.

6.3.4 Formulation of Stiffness Matrix

The element stiffness matrix of equivalent beams re-
presenting floor slabs and walls can be expressed in terms of
the deflections and rotations at end points:

$$
\left\{\begin{array}{c} P_i \\ \\ M_i \\ \\ P_j \\ \\ M_j \end{array}\right\} = \frac{1}{A\ell^2 + 2B} \left[\begin{array}{cc|cc} 2 & \ell & -2 & \ell \\ \ell & \frac{2}{3}\ell^2 + \frac{B}{3A} & -\ell & \frac{\ell^2}{3} - \frac{B}{3A} \\ \hline -2 & -\ell & 2 & -\ell \\ \ell & \frac{\ell^2}{3} - \frac{B}{3A} & -\ell & \frac{2}{3}\ell^2 + \frac{B}{3A} \end{array}\right] \left\{\begin{array}{c} \delta_i \\ \\ \Theta_i \\ \\ \delta_j \\ \\ \Theta_j \end{array}\right\} \quad (6\text{-}3)
$$

where:

$$A = \frac{\ell}{6EI_x}$$

$$B = \frac{\ell}{AG}$$

Element stiffness matrices were first assembled for each

floor or vertical span (wall or frame), making a set of sub-

structure stiffness matrices.

The torsional rigidity of walls, frame and floor slabs was

taken to be zero.   Elements associated with rotation (moment)

were then condensed for each substructure stiffness matrix.

This static condensation was permissible since the rotational

inertia has been eliminated.   After the static condensation,

the substructure stiffness matrix, therefore, related trans-

latory displacements to lateral forces. A global stiffness matrix

was   composed by assembling substructure stiffness matrixes

and related the out-of-plane forces at each joint of the planar

frame to the corresponding displacements. The procedure for

making the stiffness matrix is schematically illustrated in

Fig. 6.2.

6.3.5 Formulation of Damping Matrix

The Rayleigh damping was chosen to represent the

viscous damping characteristics of the structure.   The damping

matrix is:

$$[C] = \alpha[M] + \beta[K]$$

α and β are constants to be determined by given damping ratios

that correspond to two unequal frequencies of vibrations. α and

β were calculated by using the two lowest circular frequencies

ω_1 and ω_2 of the structure and then by employing 5 and 10

percent of the critical damping in these two modes. After

applying the mode superposition technique to the original

equations of motion, the relationship between α and β, and

ω_1 and ω_2 can be expressed as:

$$\alpha + \beta \times (0.05)^2 = \omega_1 \times 0.10$$

$$\alpha + \beta \times (0.10)^2 = \omega_2 \times 0.20$$

(6-4)

6.3.6 Method of Integrating Equations of Motion

Various integration techniques have been developed to solve the equations of motion for linear and nonlinear structures. The techniques are divided primarily into two groups. The first group, referred to as the implicit solution technique, includes the techniques such as the Houbolt method, the Newmark method, the Wilson Θ method, and the Park stiffly-stable method. The second group, referred to as the explicit solution technique, includes the central difference method, the two-cycle iteration with the trapezoidal rule, and the Runge-Kutta method. Algorithms for these solution techniques as well as their stability and accuracy have been investigated by many researchers. While the stability and accuracy of these tequniques for linear structures have been evaluated extensively, those for nonlinear structures can be studied only through numerical experimentation. In the present study, the Newmark method[6.6] was chosen to solve the equations of motion. This selection was based upon the investigation completed by Nickell,[6.7] Mondkar and Powel,[6.5] and Adeli et al.[6.1]

Basically, the Newmark integration technique is an extension of the linear acceleration method and makes the following assumptions:

$$\dot{u}_{t+\Delta t} = \dot{u}_t + [(1 - \delta)\ \ddot{u}_t + \delta\ \ddot{u}_{t+\Delta t}]\ \Delta t \qquad (6\text{-}5)$$

$$u_{t+\Delta t} = u_t + \dot{u}_{t+\Delta t} + [(\tfrac{1}{2} - \alpha)\ \ddot{u}_t + \alpha\ \ddot{u}_{t+\Delta t}]\ \Delta t^2 \qquad (6\text{-}6)$$

α and δ are parameters to be chosen by considering integration accuracy and stability. The present study used $\alpha = 1/4$ and $\delta = 1/2$, which Newmark originally proposed as an unconditionally stable constant-average-acceleration method. The equilibrium equations at time $(t+\Delta t)$ are:

$$[M]\{\ddot{u}_{t+\Delta t}\} + [C]\{\dot{u}_{t+\Delta t}\} + [K]\{u_{t+\Delta t}\} = -[M]\{\ddot{u}_g\} \qquad (6\text{-}7)$$

Solving from equation 6-6 for $\ddot{u}_{t+\Delta t}$ in terms of $u_{t+\Delta t}$ and substituting it into equation 6-5 result in two equations for $\ddot{u}_{t+\Delta t}$ and $\dot{u}_{t+\Delta t}$, each in terms of the unknown displacement $u_{t+\Delta t}$ only. These equations for $\dot{u}_{t+\Delta t}$ and $\ddot{u}_{t+\Delta t}$ are then substituted into equation 6-7 to solve for $u_{t+\Delta t}$, after which, using equations 6-5 and 6-6, $\ddot{u}_{t+\Delta t}$ and $\dot{u}_{t+\Delta t}$ can also calculated.

The complete algorithm of the Newmark method is presented in Bathe and Wilson[6.3] and Bathe.[6.2]

6.4 Selected Force-Deflection Relationship

6.4.1 Force-Deflection Model for Floor Slabs

The stiffness of the floor slabs in post-elastic range was determined by using the concept of reduction factor defined in Chapter V. Each equivalent beam representing a floor slab had a particular reduction factor according to the magnitude of the forces being applied to the beam as well as its previous history. As discussed in Sections 5.2.2, 5.4.1, and 5.4.2, the reduction factors for flexural and shear stiffnesses were assumed to be identical at any stage during loading and dependent upon the magnitude of the maximum bending moment applied to the equivalent beam. In the present study, the reduction factor vs. moment relationship was approximated in the following form: the reduction factor is 1.0, indicating that the floor slab is elastic when M/M_{max} is less than 0.3. At 0.3 of M/M_{max} the reduction factor is decreased to 0.3, assuming that cracking occurs. As the moment increases, the reduction factor decreases linearly until the moment reaches its maximum value, at which the reduction factor is 0.15. This reduction factor vs. moment relationship is illustrated by the bold line in Fig. 5.17, which shows that this line reasonably approximates the actual degradation pattern of the reduction factor.   After reaching its maximum value, the moment is assumed to remain unchanged under continued deformation.   On the other hand, the secant stiffness measured when unloading

begins is used for succeeding loading until the moment reaches

the maximum value a second time.   When this takes place, the

stiffness is once again set at zero.   This assumed moment-

stiffness relationship was based on the experimental finding that

the width of the hysteretic loops of slab panels was relatively

narrow and that the tangent stiffness measured from a hysteretic

loop of the slab panel varied only slightly regardless of the

moment (or deformation) level.   Detailed discussion of this charac-

teristics can be found in Sections 3.7.4.2. and 5.6.2.3. Fig. 6.3

illustrates the hysteretic law adopted for the floor slabs.

6.4.2 Force-Deflection Model for Walls

The behavior of shearwalls under seismic loadings

has been investigated extensively as already discussed in

Chapter II.   Here in this study, the experimental work performed

by Oesterle et al.[2.32] was referred to for determining the

characteristics of the model structure's shearwalls.   One of

their tested shearwalls (R-2 specimen in their report), which

did. not have any boundary frame,was utilized to represent the

shearwalls.

A number of analytical force-deflection models have

been proposed for simulating hysteretic behavior of structural

members and systems. These proposed models include for example:

(4)   Cyclic loading represented by the spectrum shown
in Fig. 3.17 reduced the in-plane strength of slab
panels by as much as 25 percent. Cumulative damage
like cracking was responsible for the reduction.

The effectiveness of concrete in resisting compress-
ion was reduced by cracking even after the cracks
had been closed. The application of the design
service vertical load reduced the ultimate in-plane
resistance of slab panels by not more than 15 per-
cent. Vertical load did not alter the general
behavior of the panels; the major crack still de-
veloped along the boundary between column and middle
strips.

(5)   The in-plane flexural strength of slab panels loaded
monotonically without vertical load can be reasonably
evaluated by using the theoretically calculated
flexural capacity at the critical section by means of
the Navier-Bernoulli hypothesis.   (The procedure
detail is described in Section 5.3.3) The standard
ACI Code provision (11.5.6.2) for estimating the
contribution of shear reinforcement to the shear
capacity is applicable for the slab panels. The ACI
provision (11.3.1.1) on the contribution of the
cracked concrete overestimates the shear capacity.

Findings Concerning Stiffness

(1)   Slab panels not subjected to vertical loading started losing their initial in-plane stiffness upon appearance of a crack at the edge of the slab-wall junction; this point, therefore, was defined as the elastic limit. The load corresponding to the elastic limit was approximately 30 percent of the ultimate load, whereas the secant stiffness at this stage was about 30 percent of the initial value. The secant stiffness continuously decreased as load increased, reaching approximately 15 percent of the initial value at the ultimate load stage.

(2)   In cyclically loaded slab panels without vertical load application, the secant stiffness degraded in a similar manner as in monotonically loaded slab panels. Hysteretic load-deflection loops of these panels were narrow in width, indicating that energy absorption in a complete cycle was small. The secant stiffness, therefore, appears to be a relatively suitable representation of the stiffness of slabs subjected to arbitrary reversed loading.

(3)   Upon the application of the design service vertical load, two cracks developed on the slab panel's top surface, one along the slab-wall junction and the other along the loading line. These cracks apparently changed the

pattern of stiffness degradation under monotonic load-
ing. Tangent stiffness of the panel degraded gradually,
measuring near zero at the ultimate load. The verti-
cal load promoted the development of cracks, and
cracking in low load levels made the transfer of forces
from concrete to reinforcing bars more gradual. When
slab panels with the vertical load were loaded
cyclically, however, the effect of the vertical load
on stiffness degradation was small. The slab panel
with the design service vertical load constantly showed
an about 20 percent lower secant stiffness than the
panel without such load.

(4)   In the elastic range, the stiffness characteristics
of the slab panels may be reasonably estimated by
treating them as deep beams considering both flexural
and shear deformations (equivalent beams). The use
of nominal moment of inertia and shear area, those
computed from the gross cross section, is sufficient
for evaluating the in-plane stiffness of floor slabs
regardless of aspect ratio or relative beam size.

(5)   The equivalent beam simulation also can be used in
post-elastic ranges if a hypothetical reduction factor
is introduced. This factor represents a stiffness reduc-
tion of the equivalent beam caused by various inelastic

-173-

behavior such as cracking or yielding of reinforcing bars. Once a reduction factor is known at a given load level, the in-plane stiffness of a floor slab in the post-elastic region is computed by using the same procedure as for elastic deep beams. A simple procedure to compute the reduction factor is proposed in Section 5.4.3. This equivalent beam simulation is proven to be applicable not only for floor slabs subjected to monotonic in-plane loadings but also for floor slabs subjected to in-plane cyclic loadings or combined in-plane and out-of-plane loadings.

Findings Concerning Ductility (Deformability)

(1) Once the ultimate load was reached, the deflection of the tested slab panels was controlled primarily by the opening and closing of the major crack. Few new cracks started in this post-ultimate load region, while the level of resistance remained relatively constant. Finally, the breaking of reinforcing bars at the major crack reduced the resistance drastically. The effect of either cyclic loadings or combined in-plane and out-of-plane loadings on ductility was minimal. The slab panels under these loadings de-

formed without a significant change in resistance to approximately 80 percent of the limit deflection of monotonically loaded slab panels.

(2) In-plane ductilities of tested slab panels were compared with theoretical ductilities computed by means of a conventional procedure. The computed ductilities were approximately twice as large as the experimental ductilities. The discrepancy was attributed to the difference in material behavior controlling the critical deformation. The breaking of reinforcing bars controlled deformation in post-ultimate load regions for tested slab panels. In contrast, the computational procedure assumes that the reinforcing bars can yield indefinitely and the ultimate compressive strain of the concrete limits the deformation.

(3) A technique is proposed to compute the ductility of floor slabs by using empirically defined ultimate stiffness reduction factors. This technique functions satisfactorily for the tested panels, but additional confirmation is still needed before its usefulness may be expanded. With insufficient data available about the deflection corresponding to the breaking of reinforcing bars, it is tentatively suggested that in-plane ductile behavior of floor slabs should not be expected unless they are reinforced more heavily than usual.

VI DYNAMIC RESPONSE OF BUILDING INCLUDING IN-PLANE FLOOR SLAB DEFORMATION

6.1 General

This chapter examines influence of in-plane deformation of floor slabs on the total seismic lateral load applied to a structure as well as on the distribution of this lateral load to the vertical load resisting elements. Shear forces and bending moments applied to floor slabs are also investigated.

A relatively simple building model representing a reinforced concrete building with usual dimensions was selected, and the dynamic response of the model was investigated. The direct integration method was used to obtain the time-history relationship of this structural model. The ground motion selected for this study was the N-S component of the El Centro earthquake recorded in Imperial Valley, May 18, 1940. The various in-plane characteristics of the floor slabs defined in Chapter V as well as the stiffness and strength characteristics of the vertical elements (shearwalls and columns) were incorporated into the dynamic analysis.

At the beginning of this investigation, elastic dynamic analysis was executed based on the elastic characteristics of the floor slabs and vertical elements. The results obtained from this elastic analysis were used as the basis for comparison

with the results derived from the succeeding analyses. In
these analyses, the stiffness characteristics of the floor slabs
as well as vertical elements altered. First, the propriety
of the rigid floor slab assumption was examined. Then, the
change in the model structure's response due to the non-linear
actions of vertical elements and floor slabs was investigated.

6.2 Building Model Selected

A reinforced concrete building model with seven
stories, six bays in width, and one bay in depth was selected
for this study. Fig. 6-1 illustrates the plan and elevation
views of this building and its critical dimensions. The story
height is 3.0 m from second through seventh stories, while the
first story is 3.75 m in height. The center-to-center span
length is 6.0 m in two horizontal directions. A shearwall is
located at each end, whereas the interior spans are supported
by flexible frames. The thickness of the shearwalls is 320 mm,
and the cross section of the columns is 600 mm x 600 mm with
no capital. The floor slabs are 200 mm in thickness. Beams
(300 mm x 500 mm) are attached to the lower sides of these slabs
and along column lines in both directions. The ground motion was
applied in the transverse direction of the structure.

This model has a relatively slender cross section, whose aspect ratio is 1 : 6. This arrangement was chosen intentionally so that the floor slabs would play a significant role on the distribution of lateral force to vertical elements. As discussed in Chapter II, a slender cross section tends to amplify the bending action of the floor slabs, referred to as bowing. In addition, a great difference in lateral stiffness between adjoined vertical elements increases the force to be transmitted by the floor slab connecting these components. This increase in force may cause severe distortion of the floor slab.

6.3 Analysis of Building Model

6.3.1 Simplification of Model

To investigate the response of the building model, the structure was simplified to a discrete model. In this model, all structural components: floor slabs, frames, and walls, were treated as beams, named equivalent beams. These equivalent beams were assembled and jointed at each connection, forming a seventy-story six-bay frame. Since the ground motion was applied in the transverse direction, equivalent beam properties for the deformation in this direction were needed. The beam properties were determined so that these equivalent beams would appropriately simulate the original properties. Walls were treated as deep beams which have both flexural and shear de-

formations. Floor slabs also were treated as deep beams;
Chapter V has discussed this treatment in detail. Frames,
composed of columns and beams, were represented as beams that
have particular combinations of flexural and shear rigidities.
The selection of both geometrical and material properties of
the equivalent beams is described in further detail in Section
6.4. Since both geometry of the model structure and input
ground motion were symmetrical about the vertical axis (Fig. 6.1),
only half of the structure must be analyzed.

6.3.2 Formulation of Equations of Motion

In dynamic response analysis, the equations of
motion can be written as:

$$[M]\{\ddot{u}\} + [C]\{\dot{u}\} + [K]\{u\} = \{R(t)\} \qquad (6-1)$$

where: $[M]$ = mass matrix

$[C]$ = damping matrix

$[K]$ = stiffness matrix

$\{u\}$ = displacement vector

$\{\dot{u}\} = \dfrac{du}{dt}$

$\{\ddot{u}\} = \dfrac{d^2u}{dt^2}$

$R(t)$ = vector of arbitrary time varying loads

If the structure is uniformly subjected to the ground

motion u_g, the equation can be expressed as:

$$[M]\{\ddot{u}_r\} + [C]\{\dot{u}_r\} + [K]\{u_r\} = -[M] \times u_g \qquad (6-2)$$

where $\{u_r\}$ is the relative displacement vector of the structure

with respect to the ground, ie $\{u_r\} = \{u\} - \{1\} \times u_g$.

6.3.3 Formulation of Mass Matrix

The mass of the structure was represented by lumped

masses at junctions. Each lumped mass equalled to the mass within

a tributary region of a junction. The mass of the service

design vertical load, 3.8 kPa, acting on the floor slabs was added

to the mass calculated from the structure's dead weight. Since

rotational inertia was neglected, (Section 6.3.4), the lumped

masses caused only translational inertia at the junctions. The

mass matrix [M], then, is a diagonal matrix.

6.3.4 Formulation of Stiffness Matrix

The element stiffness matrix of equivalent beams re-

presenting floor slabs and walls can be expressed in terms of

the deflections and rotations at end points:

$$\begin{Bmatrix} P_i \\ M_i \\ P_j \\ M_j \end{Bmatrix} = \frac{1}{A\ell^2 + 2B} \begin{bmatrix} 2 & \ell & -2 & \ell \\ \ell & \frac{2}{3}\ell^2 + \frac{B}{3A} & -\ell & \frac{\ell^2}{3} - \frac{B}{3A} \\ -2 & -\ell & 2 & -\ell \\ \ell & \frac{\ell^2}{3} - \frac{B}{3A} & -\ell & \frac{2}{3}\ell^2 + \frac{B}{3A} \end{bmatrix} \begin{Bmatrix} \delta_i \\ \Theta_i \\ \delta_j \\ \Theta_j \end{Bmatrix} \quad (6\text{-}3)$$

where:

$$A = \frac{\ell}{6EI_x}$$

$$B = \frac{\ell}{AG}$$

Element stiffness matrices were first assembled for each

floor or vertical span (wall or frame), making a set of sub-

structure stiffness matrices.

The torsional rigidity of walls, frame and floor slabs was

taken to be zero.   Elements associated with rotation (moment)

were then condensed for each substructure stiffness matrix.

This static condensation was permissible since the rotational

inertia has been eliminated.   After the static condensation,

the substructure stiffness matrix, therefore, related trans-

-181-

latory displacements to lateral forces. A global stiffness matrix

was composed by assembling substructure stiffness matrixes

and related the out-of-plane forces at each joint of the planar

frame to the corresponding displacements. The procedure for

making the stiffness matrix is schematically illustrated in

Fig. 6.2.

6.3.5 Formulation of Damping Matrix

The Rayleigh damping was chosen to represent the

viscous damping characteristics of the structure. The damping

matrix is:

$$[C] = \alpha[M] + \beta[K]$$

α and β are constants to be determined by given damping ratios

that correspond to two unequal frequencies of vibrations. α and

β were calculated by using the two lowest circular frequencies

ω_1 and ω_2 of the structure and then by employing 5 and 10

percent of the critical damping in these two modes. After

applying the mode superposition technique to the original

equations of motion, the relationship between α and β, and

ω_1 and ω_2 can be expressed as:

$$\alpha + \beta \times (0.05)^2 = \omega_1 \times 0.10$$
$$\alpha + \beta \times (0.10)^2 = \omega_2 \times 0.20$$

(6-4)

-182-

6.3.6 Method of Integrating Equations of Motion

Various integration techniques have been developed to solve the equations of motion for linear and nonlinear structures. The techniques are divided primarily into two groups. The first group, referred to as the implicit solution technique, includes the techniques such as the Houbolt method, the Newmark method, the Wilson Θ method, and the Park stiffly-stable method. The second group, referred to as the explicit solution technique, includes the central difference method, the two-cycle iteration with the trapezoidal rule, and the Runge-Kutta method. Algorithms for these solution techniques as well as their stability and accuracy have been investigated by many researchers. While the stability and accuracy of these tequniques for linear structures have been evaluated extensively, those for nonlinear structures can be studied only through numerical experimentation. In the present study, the Newmark method[6.6] was chosen to solve the equations of motion. This selection was based upon the investigation completed by Nickell,[6.7] Mondkar and Powel,[6.5] and Adeli et al.[6.1]

Basically, the Newmark integration technique is an extension of the linear acceleration method and makes the following assumptions:

$$\dot{u}_{t+\Delta t} = \dot{u}_t + [(1 - \delta)\, \ddot{u}_t + \delta\, \ddot{u}_{t+\Delta t}]\, \Delta t \qquad (6\text{-}5)$$

$$u_{t+\Delta t} = u_t + \dot{u}_{t+\Delta t} + [(\tfrac{1}{2} - \alpha)\, \ddot{u}_t + \alpha\, \ddot{u}_{t+\Delta t}]\, \Delta t^2 \qquad (6\text{-}6)$$

α and δ are parameters to be chosen by considering integration accuracy and stability. The present study used $\alpha = 1/4$ and $\delta = 1/2$, which Newmark originally proposed as an unconditionally stable constant-average-acceleration method. The equilibrium equations at time $(t+\Delta t)$ are:

$$[M]\{\ddot{u}_{t+\Delta t}\} + [C]\{\dot{u}_{t+\Delta t}\} + [K]\{u_{t+\Delta t}\} = -[M]\{\ddot{u}_g\} \qquad (6\text{-}7)$$

Solving from equation 6-6 for $\ddot{u}_{t+\Delta t}$ in terms of $u_{t+\Delta t}$ and substituting it into equation 6-5 result in two equations for $\ddot{u}_{t+\Delta t}$ and $\dot{u}_{t+\Delta t}$, each in terms of the unknown displacement $u_{t+\Delta t}$ only. These equations for $\dot{u}_{t+\Delta t}$ and $\ddot{u}_{t+\Delta t}$ are then substituted into equation 6-7 to solve for $u_{t+\Delta t}$, after which, using equations 6-5 and 6-6, $\ddot{u}_{t+\Delta t}$ and $\dot{u}_{t+\Delta t}$ can also calculated.

The complete algorithm of the Newmark method is presented in Bathe and Wilson[6.3] and Bathe.[6.2]

6.4 Selected Force-Deflection Relationship

6.4.1 Force-Deflection Model for Floor Slabs

The stiffness of the floor slabs in post-elastic range was determined by using the concept of reduction factor defined in Chapter V. Each equivalent beam representing a floor slab had a particular reduction factor according to the magnitude of the forces being applied to the beam as well as its previous history. As discussed in Sections 5.2.2, 5.4.1, and 5.4.2, the reduction factors for flexural and shear stiffnesses were assumed to be identical at any stage during loading and dependent upon the magnitude of the maximum bending moment applied to the equivalent beam. In the present study, the reduction factor vs. moment relationship was approximated in the following form: the reduction factor is 1.0, indicating that the floor slab is elastic when M/M_{max} is less than 0.3. At 0.3 of M/M_{max} the reduction factor is decreased to 0.3, assuming that cracking occurs. As the moment increases, the reduction factor decreases linearly until the moment reaches its maximum value, at which the reduction factor is 0.15. This reduction factor vs. moment relationship is illustrated by the bold line in Fig. 5.17, which shows that this line reasonably approximates the actual degradation pattern of the reduction factor.   After reaching its maximum value, the moment is assumed to remain unchanged under continued deformation.   On the other hand, the secant stiffness measured when unloading

begins is used for succeeding loading until the moment reaches the maximum value a second time. When this takes place, the stiffness is once again set at zero. This assumed moment-stiffness relationship was based on the experimental finding that the width of the hysteretic loops of slab panels was relatively narrow and that the tangent stiffness measured from a hysteretic loop of the slab panel varied only slightly regardless of the moment (or deformation) level. Detailed discussion of this characteristics can be found in Sections 3.7.4.2. and 5.6.2.3. Fig. 6.3 illustrates the hysteretic law adopted for the floor slabs.

6.4.2 Force-Deflection Model for Walls

The behavior of shearwalls under seismic loadings has been investigated extensively as already discussed in Chapter II. Here in this study, the experimental work performed by Oesterle et al.[2.32] was referred to for determining the characteristics of the model structure's shearwalls. One of their tested shearwalls (R-2 specimen in their report), which did not have any boundary frame, was utilized to represent the shearwalls.

A number of analytical force-deflection models have been proposed for simulating hysteretic behavior of structural members and systems. These proposed models include for example:

1) the ordinary elasto-plastic model, and 2) the degrading

stiffness models,[6.4, 6.9] which consider such nonlinear

behavior as the Bauschinger effect and the pinching effect.

A comprehensive review and critique of those models has been

made by Riddell and Newmark.[6.8]

It was decided to represent the hysteretic behavior

of the shearwalls by the force-deflection model used for floor

slabs. (Section 6.4.2) This decision was made based upon

the following reasons: (1) Oesterle et al. reported that flexure

dominates the behavior of the shearwall R-2 (2) The load-

deflection relationship of the shearwall R-2 is similar

to those of the tested floor slabs. (However, the pinching

effect is more appreciable in the shearwall.) (3) The algo-

rysm needed for this model is much simpler than those for

other models.[6.9]

6.4.3 Model for Frames

Frames were also assumed to be beams which include both

flexural and shear deformations (equivalent beams). Moment of

inertia of the equivalent beam was taken as that of the

frame's cross section. Shear area of the beam, on the other

hand, was evaluated by equating the shear displacement of the

equivalent beam to the lateral displacement of the frame.

Fig. 6.4 schematically shows the procedure to compute the shear
area of equivalent beams. In this study, the frames were assumed
to behave linear-elastically.

6.5 Input Material and Geometrical Properties

Table 6.1 lists the moment of inertia and shear area
of equivalent beams representing floor slabs, walls, and frames.
This table also shows the maximum moment levels which the critical
sections of floor slabs or walls can reach. The elastic constants
for all elements are: 24.1 GPa for the modulus of elasticity and
0.15 of poisson's ratio. The lumped masses at junctions are listed
in Table 6.2. According to an eigenvalue analysis, the frequencies
of the model structure are 0.355 Hz for the first mode and 0.0852
Hz for the second mode. From these frequencies and equation 6-4,
the damping coefficients α and β are computed to be 0.561 and
0.00362 respectively.

6.6 Results and Discussion

The model structure was analyzed for the following four
cases, referred to as cases 1 through 4: (1) linear elastic
analysis, (2) linear elastic analysis with rigid floor slab
assumption, (3) non-linear analysis, in which floor slabs
are allowed to behave non-linearly as defined in the previous
section, (4) non-linear analysis, in which both floor slabs

and shearwalls are allowed to behave non-linearly. The numerical results including maximum displacement, maximum acceleration, total base shear, base shear distributed in each shearwall or frame, and maximum shear and moment applied to floor slabs are tabulated for the four analyses in Tables 6.3 through 6.5. Fig. 6.5 shows lateral force distribution in shearwalls and frames, while shear forces in floor slabs are plotted in Fig. 6.6. Fig. 6.7 shows several displacement, base shear, bending moment vs. time relationships. For convenience of the following discussion, all comparisons of results are referred to that of the elastic analysis (case 1).

When floor slabs are assumed to be infinitely rigid, the total shear is reduced to 88 percent, while it is increased to 102 percent when slabs behave non-linearly. (Table 6.3) The change in the total base shear, however, is not great despite that basically three different structures (case 1 to 3) are analyzed. As anticipated, the rigid slab assumption causes significant underestimate of the base shear resisted by the frames. (Table 6.4) The base shear in the middle frame (frame 3) is only 23 percent if the rigid slab assumption is adopted. Non-linearity of the floor slabs (case 3) also changes the lateral load distribution significantly. Decreased stiffness of floor slabs in the inelastic range causes frame base shear to increase by nearly 100 percent. Here, the

interaction among the vertical elements is lessened, resulting that each element responds more independently from one another.

In the elastic analyses, shearwalls take a major portion of the shear: 75 and 92 percent in cases 1 and 2 respectively. When slabs and shearwalls behave non-linearly, on the other hand, the base shear transmitted by the shearwalls is decreased significantly (to 65 percent). This reduction apparently is caused by the degraded stiffness in the shearwalls. Frames, in turn, carry approximately 2.5 times larger base shear.

Floor slabs behave like simply supported beams with distributed lateral force, causing maximum shear force at the junctions with shearwalls (exterior bents) and maximum bending moment at the mid-span (at the junction with the middle frame: frame 3). (Fig. 6.7) The shear force transmitted in the floor slabs is much smaller than the shear force which would be considered to be critical. The ACI Code formula, (11.3.1.1) which specifies the lower limit for shear effect consideration, gives 1.05 MN of shear force, while the maximum shear force carried by the floor slabs is not more than 0.428 MN. Bending moment, on the other hand, is significant particularly at the mid spans, and exceeds the specified maximum moment in many occasions. As tabulated in Table 6-5, the bending moments of the floor slabs in

the lowest five stories exceed the maximum moment level at the
mid spans in case 1 (elastic analysis), while the top five stories
reach this level when the floor slabs are allowed to behave
non-linearly. A comparison between cases 3 and 4 reveals that
the level of bending moment decreases as the variation in stiff-
ness among the vertical elements decreases.

As shown in Fig. 6.6, the distribution of lateral
force applied to each story is approximately triangular except
for the roof level. Lateral force is reduced at this level
because masses at this roof level are signficantly smaller than
those in other stories. No live load was assigned to this level.
(Table 6.2) The distribution of lateral force in shearwalls,
however, is far from triangular, rather, shear force is nearly
constant for all floors. The lateral force distribution in
frames is close to triangular although the variation among story
shears decreases considerably when non-linear behavior of floor
slabs or shearwalls is considered (cases 3 and 4). This near rec-
tangular distribution is appreciable particularly in the middle
frame (frame 3). The complexity of the lateral force distri-
bution in frames and shearwalls would be caused by the
change in the relative story stiffness of the vertical
elements (shearwalls and frames) at each story level. The story
stiffness of frames is relatively constant, while the story stiff-
ness in shearwalls decreases significantly in upper stories.

6.7 Summary

The findings in this chapter may be itemized as follows:

1. The effect of the in-plane stiffness of the floor slabs on the base shear applied to vertical elements is appreciable in the analyzed model structure. The rigid floor assumption significantly underestimates the base shear of the frames.

2. The stiffness of the shearwalls (major lateral force resisting elements in the model structure) also affects the base shear. Degraded stiffness of the shearwalls shifts some base shear to the frames.

3. Shear force applied to the floor slabs is very small and practically negligible. Bending moment, however, is significant, particularly at the mid-span of the structure, reaching the maximum moment level in many stories. The degraded stiffness of the floor slabs alters the base shear distribution, placing more load to the frames.

4. The distribution of lateral force applied to each story is approximately triangular. The distribution of lateral force in shearwalls or frames, on the other hand, does not follow the triangular distribution. The change in the relative story stiffness of the vertical elements at each story level most probably causes this complexity.

VII SUMMARY, CONCLUSIONS, AND RECOMMENDED RESEARCH

This report presents a comprehensive study of the in-plane characteristics of reinforced concrete beam-supported floor slabs with various loading and support conditions and studies the effect of those characteristics on seismic building response. The discussion of experimental and analytical results and the application of the results and findings to the evaluation of the in-plane characteristics have been described in Chapters III through V. In Chapter VI, the effect of the in-plane deformation of floor slabs in building response has been examined. Important findings, suggestions and proposals for practical designs, and recommendations for future work are summarized as follows:

Experimental Findings

(1) The development of a crack, labelled a major crack, which developed along the boundary between the column and middle strips, controlled the ultimate in-plane strength of the test slab panels.

(2) The cyclic loading represented by the spectrum adopted in the tests reduced the in-plane strength of the test slab panels by as much as 25 percent. Cumulative damage like cracking was responsible for the reduction.

(3) The application of the design service vertical (gravity) load reduced the in-plane ultimate strength of the test slab panels by about 15 percent.

(4) The test slab panels with in-plane loading lost their initial stiffness after the formation of a crack at the clamped edge. The load at which this crack formed was approximately 30 percent of the ultimate load.

(5) The application of the design service vertical load caused two cracks on the top surface of the test slab panels, one along the slab-wall junction, and the other along the loading line. The vertical load promoted the development of cracks, and cracking in low load levels made the transfer of forces from concrete to reinforcing bars more gradual.

(6) The deflection in the post ultimate load range was controlled by the opening and closing of the major crack, while the breaking of reinforcing bars at the major crack caused the test slab panels to fail.

(7) The effect of cyclic loading or combined in-plane and out-of-plane loadings on ductility of the test slab panels was minimal.

(8) Because of insufficient available data regarding the performance of reinforcing bars which control the ductility of floor slabs, it is tentatively suggested that a high degree of ductility should not be expected unless the slabs are reinforced more heavily than the test slab panels.

Analytical Findings and Proposals for Practical Designs

(1) The in-plane ultimate strength of a floor slab is reached when the slab fails either by flexure or by shear. In the flexural mode of failure, a major crack develops along the boundary between the column and middle strips of the slab.

(2) In the shear mode, on the other hand, the slab reaches the ultimate load when a diagonal crack separates a triangular portion from the remainder of the panel.

(3) The in-plane flexural strength of the slab can be predicted by the theoretical flexural capacity of the critical section of the slab. The detailed procedure is described in Section 5.3.3.

(4) The standard ACI Code Provision (11.5.6.2) gives an accurate estimate of the in-plane shear strength of the slab.

(5) The in-plane stiffness of the floor slab can be evaluated by representing the slab as a deep beam considering both flexural and shear deformations. The use of nominal moment of inertia and shear area is appropriate when computing the initial in-plane stiffness regardless of geometry of the slab. (Section 5.4.1)

(6) The deep beam analogy is also valid when the in-plane stiffness of the floor slab in the post-elastic range is determined. A reduction factor is incorporated into the

computation in order to reflect the stiffness degra-
dation in this range. (Section 5.4.2)

(7) A procedure to compute the reduction factor is proposed.
(Section 5.4.3)   A reduction factor at a given load
level can be estimated on the basis of the curvature at
the critical section and an empirical hinge length.

Effects of Floor Slab In-Plane Deformation on Seismic Building Response

(1) The stiffness of floor slabs and vertical elements, walls
and frames, can significantly affect the base shear
distribution to the vertical elements. The rigid slab
assumption underestimated the base shear distributed to
flexible frames by as much as 75 percent.

(2) Nonlinear action of the floor slabs also altered the
lateral load distribution, causing the frames to take
base shear approximately twice as large as that com-
puted in the elastic analysis.

(3) Shear force applied to the floor slabs was very small
and practically negligible. Bending moment, however,
was significant particularly at the mid-spans of the
building, reaching the specified maximum moment level
in many stories.

(4) The distribution of lateral force applied to each story
was considerably triangular. The distribution

-196-

of lateral force in each vertical element, however,
did not follow the triangular distribution. The change
in the relative story stiffness of the vertical
elements at each story level caused this complexity.

Future Research Needed

(1) The in-plane behavior of floor slabs under cyclic
loadings must be investigated further.
It is known that the load-deflection relationship
of slab panels depends heavily on the loading history.
A different loading spectrum very possibly would affect
the ultimate strength as well as the stiffness
degradation.

(2) The in-plane behavior of floor slabs under combined
in-plane and out-of-plane loadings is also a
subject for further study. The design ser-
vice vertical load reduced the ultimate resistance
but did not change the general pattern of stiffness
degradation or behavior in post-ultimate load regions.
The intensity of the vertical load can yet be a major
parameter to control the in-plane behavior of
floor slabs. Although the critical section was
located at the boundary between the column and middle
strips in the test slab panels, a larger vertical load

or, alternatively, more reinforcement at this boundary may shift the critical section to the center line of the span where out-of-plane bending moment is the greatest.

(3) Future study should be extended to investigate the interaction of floor slabs with supporting elements, that is, the combined effect of frame and diaphragm actions. When floor slabs are supported by columns, lateral load applied to the floor system induces both in-plane and out-of-plane deformations in the slabs. The in-plane characteristics of these slabs may be greatly affected by the out-of-plane bending. If a floor slab is supported by a wall on one edge and by columns on the other, warping can take place in the slab because of the difference between the rotational stiffnesses of the two vertical members. The combined effect of warping and in-plane force on the in-plane characteristics of the floor slab may also be significant. To examine this combined effect, experiment must be performed by using subassemblages of floor systems rather than isolated slab panels.

APPENDIX

The proportionality constant λ used in the flow rule can be derived as follows:

From equations 4-17 and 4-18:

$$d\varepsilon_d^e = d\varepsilon_d - \lambda \frac{\partial f}{\partial \sigma_d} \qquad (A-1)$$

$$d\varepsilon_s^e = d\varepsilon_s - \lambda \frac{\partial f}{\partial \tau_s} \qquad (A-2)$$

The elastic strain increments, $d\varepsilon_d^e$ and $d\varepsilon_s^e$ can be related to the stress increments, $d\sigma_d$ and $d\tau_s$ as:

$$d\sigma_d = D_{11}^e \left(d\varepsilon_d - \lambda \frac{\partial f}{\partial \sigma_d} \right) \qquad (A-3)$$

$$d\tau_s = D_{22}^e \left(d\varepsilon_s - \lambda \frac{\partial f}{\partial \tau_s} \right) \qquad (A-4)$$

Substituting equations A-3 and A-4 to equation 4-20:

$$df = \frac{\partial f}{\partial \sigma_d} D_{11}^e \left(d\varepsilon_d - \lambda \frac{\partial f}{\partial \sigma_d} \right) + \frac{\partial f}{\partial \tau_s} D_{22}^e \left(d\varepsilon_s - \lambda \frac{\partial f}{\partial \tau_s} \right) = 0 \quad (A-5)$$

and $\quad \lambda \left\{ \left(\frac{\partial f}{\partial \sigma_d} \right)^2 + \left(\frac{\partial f}{\partial \tau_s} \right)^2 \right\} = D_{11}^e \left(\frac{\partial f}{\partial \sigma_d} \right) d\varepsilon_d + D_{22}^e \left(\frac{\partial f}{\partial \tau_s} \right) d\varepsilon_s$

Then: $\qquad \lambda = \dfrac{D_{11}^e \left(\dfrac{\partial f}{\partial \sigma_d} \right) d\varepsilon_d + D_{22}^e \left(\dfrac{\partial f}{\partial \tau_s} \right) d\varepsilon_s}{\left\{ \left(\dfrac{\partial f}{\partial \sigma_d} \right)^2 + \left(\dfrac{\partial f}{\partial \tau_s} \right)^2 \right\}} \qquad (4-21)$

NOMENCLATURE

Symbols used in the text are defined where they first appear. A summary of frequently used symbols is presented below for convenience. Symbols with dual meanings are listed twice.

A shear area of equivalent beam

A_e effective shear area

A_s area of steel

A_v area of reinforcement within a distance s(ACI Code)

A_1, A_2 areas of steel placed in 1 and 2 directions and intersecting interface

$(AG)_e$ equivalent shear stiffness

$[B]$ matrix relating centroidal displacements to concrete strains

$[B_b]$ matrix relating centroidal displacements to truss element's strain

b_w web width (ACI Code)

$[C]$ viscous damping matrix

$[D]$ constitutive matrix

D dead load

$[D_e]$ elastic constitutive matrix

$[D_{ep}]$ elasto-plastic constitutive matrix

$D_{11}{}^e$, $D_{22}{}^e$ coefficients of elastic constitutive matrix

d	distance from extreme compression fiber to centroid of tension reinforcement (ACI Code)
E	modulus of elasticity of concrete
E_b	modulus of elasticity of truss element
E_{s1}, E_{s2}	modulus of elasticity of steel in 1 and 2 directions
$(EI)_e$	equivalent flexural stiffness
e	strain in concrete
f	yield function
f_c	concrete stress
f_c'	compressive strength of concrete (ACI Code)
f_y	yield strength of nonprestressed reinforcement (ACI Code)
h	centroidal distance of two triangular elements
h_1, h_2	legs from centroid of element 1 and 2 to interface
I	moment of inertia of equivalent beam
I_e	effective moment of inertia
[K]	element stiffness matrix (Chap. IV)
[K]	stiffness matrix (Chap. VI)
k_d	normal spring constant
k_s	shear spring constant
L	live load
ℓ	length of truss element (Chap. IV)

ℓ	span length (Chap. V)
ℓ_1	length of projecting part in equivalent beam (Chap. V)
ℓ_1, ℓ_2	distances between two centroids projected on local 1 and 2 axes (Chap. IV)
M	external moment applied at edge
[M]	matrix relating element displacements to relative displacements (Chap. IV)
[M]	mass matrix (Chap. VI)
m_1, m_2, n_1, n_2	coefficients of transformation matrix
m_3	direction cosine of orthogonal steel
n_3	direction sine of orthogonal steel
P	applied in-plane load
{P}	external force vector
[Q]	matrix relating centroidal displacements to element displacements
[R]	transformation matrix from global coordinates to local coordinates
s	spacing of shear reinforcement (ACI Code)
t	slab thickness
{U}	vector of element displacements in global coordinates
{$\bar{U}$}	vector of element displacements in local coordinates
{U_i}	vector of centroidal displacements
{u}	displacement vector

$\{\dot{u}\}$	velocity vector
$\{\ddot{u}\}$	acceleration vector
u_g	ground displacement
V_b	total potential energy functional of truss element
V_c	total potential energy functional of triangular element (Chap. IV)
V_c	nominal shear strength provided by concrete (ACI code, Chap. V)
V_s	total potential energy functional of smeared triangular element (Chap. IV)
V_s	nominal shear strength provided by shear reinforcement (ACI Code, Chap. V)
W	design load of floor slab
W, W_1, W_2	arbitrary point at interface
x_g, y_g	coordinates of center of gravity of triangular element
α	degradation factor (Chap. V)
α, β	Rayleigh damping coefficients
δ	deflection along loading line in strength test
$\{\delta\}$	vector of relative displacements
δ_a, δ_s	edge deflections in stiffness test under anti-symmetrical and symmetrical loadings (Chap. III)
δ_f, δ_s	flexural and shear deflections in equivalent beam calculation (Chap. V)
δ_1, δ_2	relative displacements measured with respect to local 1 and 2 axes
$\{\varepsilon\}$	strain vector

$\{d\varepsilon\}$	vector of strain increments
$\{d\varepsilon_e\}$	vector of elastic strain increments
$\{d\varepsilon_p\}$	vector of plastic strain increments
ε_b	strain in truss element
ε_d, ε_s	normal and shear strain coefficients in strain vector
ε_1, ε_2	δ_1/ℓ_1 and δ_2/ℓ_2
ε_t	cracking strain
Θ	end rotation in strength test
Θ_a, Θ_s	wall rotations in stiffness test under anti-symmetrical and symmetrical loadings
Θ_f	end rotation due to flexure in equivalent beam calculation
λ	proportionality constant used in flow rule
ν	poisson's ratio
ξ	vertical deflection in strength test
ξ_1, ξ_2	viscous damping coefficients
$\{\sigma\}$	stress vector
σ_b	stress in truss element
σ_p	yield stress in uniaxial loading
σ_t	tensile strength of concrete
σ_y	compressive strength of concrete
$\{d\sigma\}$	vector of stress increments

τ_p yield stress in pure shear

ϕ curvature at critical section

ω circular frequency

Table 3.1 Dimensions of Test Specimen

Items	Dimensions	
	(mm)	(in.)
Center-to-Center Span Length	1630	64
Exterior Panels	2030 x 2440	80 x 96
Interior Panel	1030 x 2440	64 x 96
Slab Thickness	39.6	1.56
Beam Width	67.8	2.67
Beam Depth (projecting depth)	95.8	3.77
Column Length (from the mid-plane of the slab)	280	11.0
Column Cross Section	136 x 136	5.34 x 5.34
Wall Thickness	136	5.34
Wall Length	3000	118.0
Total Wall Height	612	24.1

Table 3.2   Selected Reinforcing Bar Sizes

Items	Bar Size
Slab Reinforcing Bars	D2.0, D2.5, D3.0
Column Longitudinal Bars	#3
Column Stirrups	D2.0
Beam Longitudinal Bars	D2.0, D3.0
Beam Stirrups	W14
Wall Reinforcing Bars	D5.0, #3, #4

Table 3.3 Design Detail of Concrete Slab

	Strip	Sign	A_s Required (mm^2)	A_s Provided	Required Steel Ratio	Over Rein- forcement Ratio	Over-Strength Ratio
1	Column	Negative	58*	D2.0 x 6	0.0018	1.3	2.9
		Positive	58*	D2.5 x 2 + D2.0 x 4	0.0018	1.5	5.6
	Column	Negative Interior	58*	D2.0 x 6	0.0018	1.3	4.1
	Middle	Negative	61	D2.0 x 6	0.0019	1.3	1.3
		Positive	58*	D2.5 x 2 + D2.0 x 4	0.0018	1.5	5.6
	Middle	Negative Interior	120	D3.0 x 7	0.0038	1.1	1.1
2	Column	Negative	58*	D2.0 x 6	0.0018	1.3	2.8
		Positive	58*	D2.0 x 6	0.0018	1.3	5.0
	Column	Negative Interior	29*	D2.0 x 2	0.0018	1.1	2.2
		Positive Interior	29*	D2.0 x 2	0.0018	1.1	4.1
	Middle	Negative	67	D2.0 x 6	0.0021	1.2	1.2
		Positive	58*	D2.0 x 5	0.0018	1.1	1.9

* Controlled by temperature requirement

** Based on flexural resistance

Table 3.4 Design Detail in Concrete Beam

Region	Required Area	Actual Area	Ratio (Actual/Required)
Negative Moment (Around Columns)	54.3 mm^2 (0.0842 in.^{2})	D3.0 x 3 (58 mm^2)	1.07
Negative Moment (Around Walls)	33.2 (0.0515)	D2.0 x 3 (39 mm^2)	1.17
Positive Moment	27.9 (0.0432)	D2.0 x 3 (39 mm^2)	1.39

Table 3.5   Concrete Mix Proportions

For 1.0 m^3 (1.3 cu.yd) Concrete	27.6 MPa (4,000 psi)	Concrete 34.5 MPa (5,000 psi)
Type 1 Portland Cement	330 kg (730 lbs.)	400 kg (880 lbs.)
6.4 mm Crushed Limestone	770 kg (1700 lbs.)	770 kg (1700 lbs.)
Concrete Sand	1000 kg (2300 lbs.)	1000 kg (2300 lbs.)
Total Water	0.23 m^2 (60 gals.)	0.23 m^3 (60 gals.)
WRDA-19 Plastisizer	0.012 m^3 (110 oz.)	0.015 m^3(130 oz.)
Water Cement Ratio	0.68	0.57

Table 3.6   Concrete Compressive Strength (7 Day and 28 Day Tests)

Type			Slump (mm)	7-Day Strength (MPa)	28-Day Strength (MPa)
27.6 MPa (4,000 psi)	Batch 1 (B-1)		110	23.2	27.7
	Batch 2 (B-2)		120	24.0	28.8
34.5 MPa (5,000 psi)	Batch 1 (B-1)		110	29.9	36.1
	Batch 2 (B-2)		130	26.8	33.1

Table 3.7   Mechanical Properties of Reinforcing Bars

Size	Area (mm^2)	Yield Stress (MPa)	Yield Strain (m/m)	Ultimate Stress (MPa)	Ultimate Strain (m/m)	Modulus of Elasticity (GPa)
D2.0	13.4	368	1.93×10^{-3}	411	78.3×10^{-3}	191
D2.5	17.2	609	3.11×10^{-3}	668	49.2×10^{-3}	196
D3.0	21.5	590	2.72×10^{-3}	590	62.5×10^{-3}	190

Table 3.8 Mechanical Properties of Concrete

Type	Compressive Strength on Testing (MPa)	Tensile Strength Split Test (MPa)	Modulus of Elasticity (GPa)	Initial Poisson's Ratio
27.6 MPa (4,000 psi) Batch 1 (B-1)	28.0	2.13	21	0.13
Batch 2 (B-2)	29.0	2.40	22	0.14
34.5 MPa (5,000 psi) Batch 1 (B-1)	37.3	3.57	30	0.21
Batch 2 (B-2)	35.0	4.90	30	0.20

Table 3.9(a) Designation of Test Program
                (Five character alphanumeric
                 code)

1	2	3	4	5

1	B	slab-on-Beam floor system
2	H	Horizontal (in-plane) loading only
	V	Vertical (out-of-plane) load included
3	1	panel 1
	2	panel 2
	3	panel 3
	6	a whole specimen
4-5	SS	Stiffness test, Symmetrical loading
	SA	Stiffness test, Anti-symmetrical loading
	MN	MoNotonic loading
	CY	CYclic loading

EXAMPLE

BHIMN   slab-on-beam floor system
               horizontal loading only
               panel 1 is tested
               under monotonic loading

-214-

Table 3.9(b) Sequence of Test Program

B-1	BH 6SS	Stiffness test, symmetrical loading
	BH 6SA	Stiffness test, anti-symmetrical loading
	BH 2MN	Strength test, monotonic loading without vertical load, Moment-to-shear ratio of 1.63m
	BH 3MN	Strength test, monotonic loading without vertical load, Moment-to-shear ratio of 3.25m
	BH 1CY	Strength test, cyclic loading without vertical load, Moment-to-shear ratio of 1.63m
B-2	BH 6SS	Stiffness test, symmetrical loading
	BH 6SA	Stiffness test, anti-symmetrical loading
	BV 1MN	Strength test, monotonic loading with vertical load, Moment-to-shear ratio of 1.63m
	BH 3CY	Strength test, cyclic loading without vertical load, Moment-to-shear ratio of 3.25m
	BV 2CY	Strength test, cyclic loading with vertical load, Moment-to-shear ratio of 1.63m

Table 3.10 Stiffness Test Results

	Experiment		SAP IV	Beam Theory
	B-1	B-2		
Symmetrical loading				
δ (m/GN)	6.24	6.50	5.42	5.11
Θ_s (rad./GN)	1.17	1.25	1.08	1.11
Anti-symmetrical loading				
δ (m/GN)	11.60	12.50	11.90 [*] (8.30)	8.02
Θ_a (rad./GN)	4.15	4.32	3.81 [*] (2.42)	2.39

* With artificially stiff beams along the Boundaries

Table 3.11 Vertical Reflection under Design
            Service Vertical Load

Test	Scale #1 (mm)	Scale #2 (mm)	Scale #3 (mm)
BV 1MN	0.76	1.30	1.02
BV 2CY	0.76	0.89	1.52
Elastic Theory	0.42	1.17	0.42

Table 3.12 Strength Test Results (Ultimate
Resistance and Deflection)

Test	Ultimate Load (kN)		Maximum Displacement (mm)	
	Positive	Negative	Positive	Negative
BH 2MN	120.0	− 88.5	8.48	− 7.44
BH 1CY	94.7	− 96.5	8.36	− 8.29
BH 3MN	56.9	− 38.7	7.32	− 6.17
BH 3CY	41.8	− 40.5	6.21	− 5.87
BV 1MN	102.0	− 89.8	9.22	− 9.22
BV 2CY	85.0	− 83.2	6.72	− 7.02

Table 3.13   Initial Stiffness in Strength Tests

Test	Initial Stiffness $(MN/_m)$	Experiment/Theory
BH 2MN	218	0.663
BH 1CY	272	0.796
BH 3MN	166	0.790
BH 3CY	175	0.830
BV 1MN	222	0.675
BV 2CY	201	0.589

Table 3.14 Stiffness Change in Monotonic Loading Tests

	BH 2MN (MN/m)	BH 3MN (MN/m)	BV 1MN (MN/m)
Initial stiffness	218	166	222
Tangent stiffness at ultimate resistance	33.8 (0.16)	22.0 (0.13)	0.0 (0.00)
Secant stiffness at ultimate resistance	42.9 (0.20)	28.5 (0.17)	–
Tangent stiffness upon unloading	67.2 (0.31	33.7 (0.20)	83.3 (o.38)
Tangent stiffness in negative stable range	4.2 (0.019)	2.8 (0.017)	3.2 (0.015)

Table 3.15 Critical Displacement and Ductility in Strength Tests

	Critical Displacement Positive (mm)	Negative (mm)	Ductility Positive	Negative	Total Displacement (mm)
BH 2MN	7.62	− 7.62	3.2	--	14.86
BH 1CY	6.75	− 6.30	2.1	2.0	13.05
BH 3MN	7.11	− 5.72	3.6	---	12.83
BH 3CY	4.60	− 5.42	2.6	2.5	10.02
BV 1MN	9.22*	− 9.22*	--	--	18.44
BV 2CY	6.27	− 5.08	3.1	2.8	11.35

* No breaking of bars, "Critical Displacement" not reached

Table 4.1 Comparison of Proposed Model With
SAP IV (Elastic Analysis)

Load	Selected point (Fig.4.8)	Direction of Displacement	Proposed Model/SAP IV
Case 1	1	x	1.07
		y	1.02
	2	x	1.05
		y	1.03
Case 2	1	x	1.05
		y	1.05
	2	x	1.06
		y	1.06
	3	x	1.07
		y	1.07

Table 5.1(a) Dimensions and Material Properties of Slab
              Panel in Effective Moment of Inertia and
              Shear Area Calculations

Item	Symbol	Dimension
Depth	d	1630 mm
Length	ℓ	1630 x mm (ASPECT RATIO)
Thickness	t	39.6 mm
Modulus of Elasticity	E	22 GPa
Poisson's Ratio	ν	0.15

Table 5.1(b) Relative Beam Size of Slab Panel in Effective
              Moment of Inertia and Shear Area Calculations

Relative Beam Size	Width x Depth (mm x mm)	
1.00	0	0
1.43	68	96 *
1.61	81	114
2.29	118	166
2.71	136	192

* The beam size of the tested slab panels

Table 5.2 Effective Moment of Inertia and Shear Area

RELATIVE BEAM SIZE / ASPECT RATIO	MOMENT OF INERTIA (Ie) (m^4)					SHEAR AREA (Ae) (m^2)				
	1.00	1.43	1.61	2.29	2.71	1.00	1.43	1.61	2.29	2.71
NOMINAL VALUES	0.0141	0.0202	0.0231	0.0323	0.0384	0.0643	0.0736	0.0775	0.0917	0.101
0.25	0.0143 (1.01)	0.0204 (1.01)	0.0233 (1.01)	0.0325 (1.01)	0.0385 (1.00)	0.0606 (0.94)	0.0633 (0.86)	0.0638 (0.83)	0.0639 (0.70)	0.0644 (0.64)
0.50	0.0142 (1.01)	0.0203 (1.01)	0.0232 (1.01)	0.0324 (1.00)	0.0385 (1.00)	0.0580 (0.90)	0.0618 (0.84)	0.0630 (0.82)	0.0634 (0.69)	0.0641 (0.63)
0.75	0.0142 (1.01)	0.0203 (1.01)	0.0231 (1.00)	0.0324 (1.00)	0.0385 (1.00)	0.0577 (0.90)	0.0615 (0.84)	0.0628 (0.81)	0.0632 (0.69)	0.0639 (0.63)
1.00	0.0142 (1.01)	0.0202 (1.00)	0.0231 (1.00)	0.0324 (1.00)	0.0385 (1.00)	0.0571 (0.89)	0.0610 (0.83)	0.0625 (0.81)	0.0630 (0.69)	0.0638 (0.63)
1.25	0.0142 (1.01)	0.0202 (1.00)	0.0231 (1.00)	0.0324 (1.00)	0.0385 (1.00)	0.0568 (0.88)	0.0608 (0.83)	0.0624 (0.81)	0.0629 (0.69)	0.0637 (0.63)
1.50	0.0141 (1.00)	0.0202 (1.00)	0.0231 (1.00)	0.0323 (1.00)	0.0385 (1.00)	0.0566 (0.88)	0.0606 (0.83)	0.0622 (0.81)	0.0628 (0.69)	0.0637 (0.63)
2.00	0.0141 (1.00)	0.0202 (1.00)	0.0231 (1.00)	0.0323 (1.00)	0.0384 (1.00)	0.0564 (0.88)	0.0604 (0.82)	0.0621 (0.80)	0.0626 (0.68)	0.0634 (0.63)
2.50	0.0141 (1.00)	0.0202 (1.00)	0.0231 (1.00)	0.0323 (1.00)	0.0384 (1.00)	0.0564 (0.88)	0.0604 (0.82)	0.0620 (0.80)	0.0625 (0.68)	0.0634 (0.63)
3.00	0.0141 (1.00)	0.0202 (1.00)	0.0231 (1.00)	0.0323 (1.00)	0.0384 (1.00)	0.0563 (0.88)	0.0604 (0.82)	0.0620 (0.80)	0.0625 (0.68)	0.0634 (0.63)

Table 5.3 Maximum Load and Failure Mode of Analyzed Slab Panels

Case	Moment-to-Shear Ratio	Experiment Maximum Load	FEM Model Maximum Load	Failure Mode	Maximum Load Based On Flexural Capacity
1	1.63m (64 in.)	120 kN	116 kN	Flexural Failure	125 kN
2	3.25m (128 in.)	56 kN	53 kN	Flexural Failure	54 kN
3	∞	–	M = 153 kN x m	Flexural Failure	M = 155 kN x m
4	0.812m (32 in.)	–	131 kN	Shear Failure	340 kN
5	0	–	124 kN	Shear Failure	125 kN
6	1.63m (64 in.)	–	153 kN	Shear Failure	239 kN
7	1.63m (64 in.)	–	144 kN	Shear Failure	181 kN
8	1.63m (64 in.)	–	117 kN	Flexural Failure	125 kN
4'	0.812m (32 in.)	–	398 kN	Flexural Failure	332 kN
6'	1.63m (64 in.)	–	224 kN	Flexural Failure	239 kN
7'	1.63m (64 in.)	–	175 kN	Flexural Failure	181 kN

Table 6.1 Sectional Properties and Maximum Moment Levels of
Model Structure

	I (Moment of inertia) (m^4)	A (Shear area) (m^2)	Maximum moment level (MN x m)
Slab	3.63	1.08	2.94
Wall	5.79	1.60	24.5
Frame (1st story)	3.24	0.0265	-
Frame (2nd-7th story)	3.24	0.0414	-

Table 6.2 Lumped Masses in Model Structure

Story \ Span	1	2	3	4 (half)
7	15.9	20.3	20.3	10.2
6	30.1	37.3	37.3	18.6
5	30.1	37.3	37.3	18.6
4	30.1	37.3	37.3	18.6
3	30.1	37.3	37.3	18.6
2	30.1	37.3	37.3	18.6
1	31.9	38.0	38.0	19.0

Unit: k_g

(1) Linear elastic analysis

(2) Linear elastic analysis (rigid floor assumption)

(3) Non-linear analysis (floor slabs can behave non-linearly)

(4) Non-linear analysis (floor slabs and walls can behave non-linearly)

Table 6.3 Maximum Displacement, Acceleration, and Total Base Shear

Case	Maximum Displacement		Maximum Acceleration		Total Base Shear
	①	②	①	②	
	(mm)		(m/sec^2)		(MN)
(1)	34.2(5.00)	33.3(4.78)	9.74(4.98)	9.12(5.00)	8.24(4.78)
(2)	29.6(4.72)	29.6(4.72)	10.0(4.72)	10.0(4.72)	7.29(4.72)
(3)	54.2(5.04)	30.0(5.04)	13.8(2.34)	6.52(4.86)	8.38(5.04)
(4)	63.7(5.08)	53.9(5.10)	13.2(2.34)	8.25(5.04)	8.87(5.04)

Number in parenthesis indicates the time when the maximum value is reached.
① 7th story middle
② 7th story end

Table 6.4 Base Shear in Walls and Frames

Case	Wall (MN)	Frame 1 (MN)	Frame 2 (MN)	Frame 3 (MN)
(1)	3.16	0.322	0.462	0.515
(2)	3.34	0.119	0.119	0.119
(3)	2.43	0.555	0.931	1.09
(4)	2.05	0.795	1.18	1.33

Table 6.5 Maximum Shear and Moment in Floor Slabs

Story	Maximum shear in floor slab (MN)				Maximum moment in floor slab (MN x m)			
	(1)	(2)	(3)	(4)	(1)	(2)	(3)	(4)
7	0.0265	–	0.197	0.176	0.962	–	2.94*	2.81
6	0.194	–	0.261	0.226	2.45	–	2.94*	2.94*
5	0.327	–	0.301	0.255	3.58**	–	2.94*	2.94*
4	0.391	–	0.298	0.245	4.20**	–	2.94*	2.78
3	0.420	–	0.281	0.221	4.52**	–	2.94*	2.56
2	0.428	–	0.255	0.193	4.54**	–	2.52	2.31
1	0.422	–	0.229	0.177	4.06**	–	1.90	1.89

* Reaching the specified maximum moment level

** Exceeding the specified maximum moment level
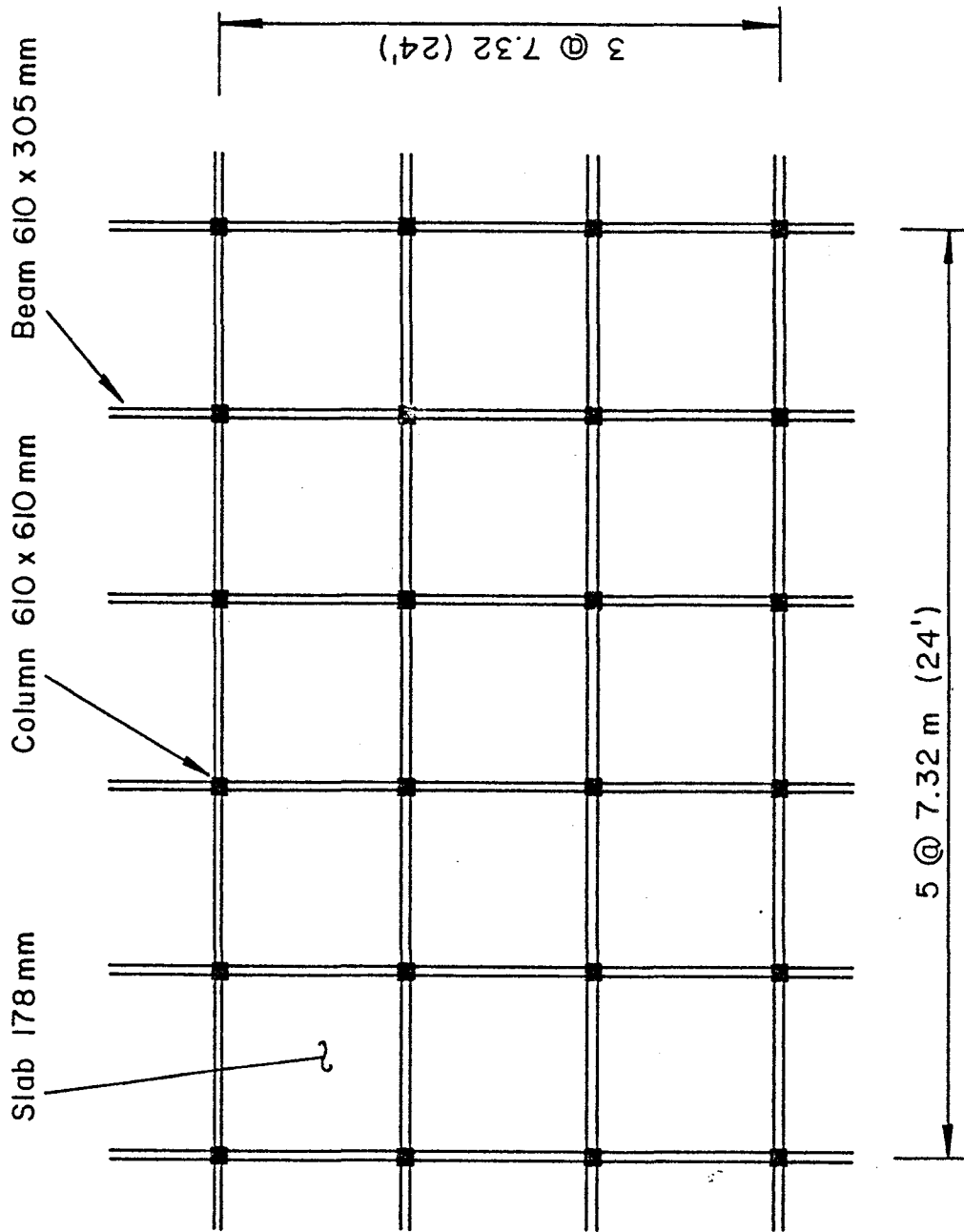
Fig. 3.1 Prototype Dimension

Beam 610 x 305 mm

Column 610 x 610 mm

Slab 178 mm

3 @ 7.32 (24')

5 @ 7.32 m (24')
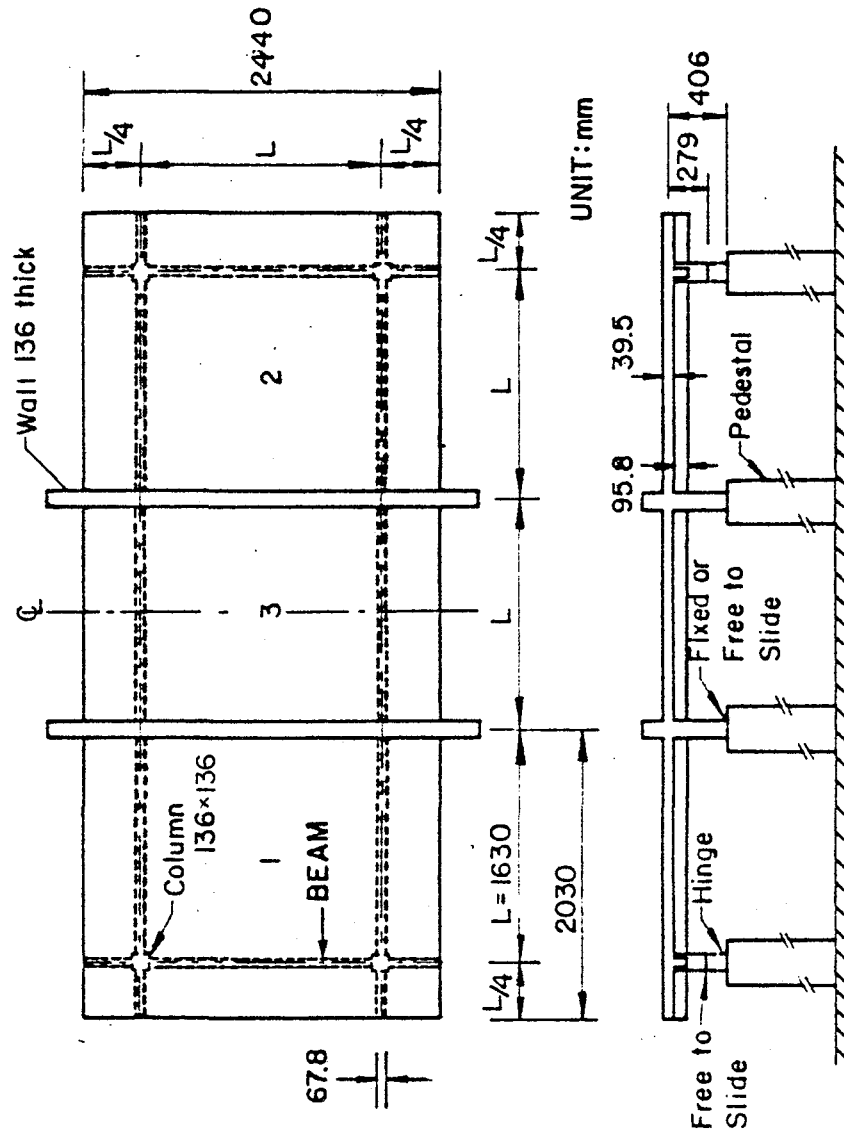
Fig. 3.2 Dimension and Supporting Condition of Test Specimen
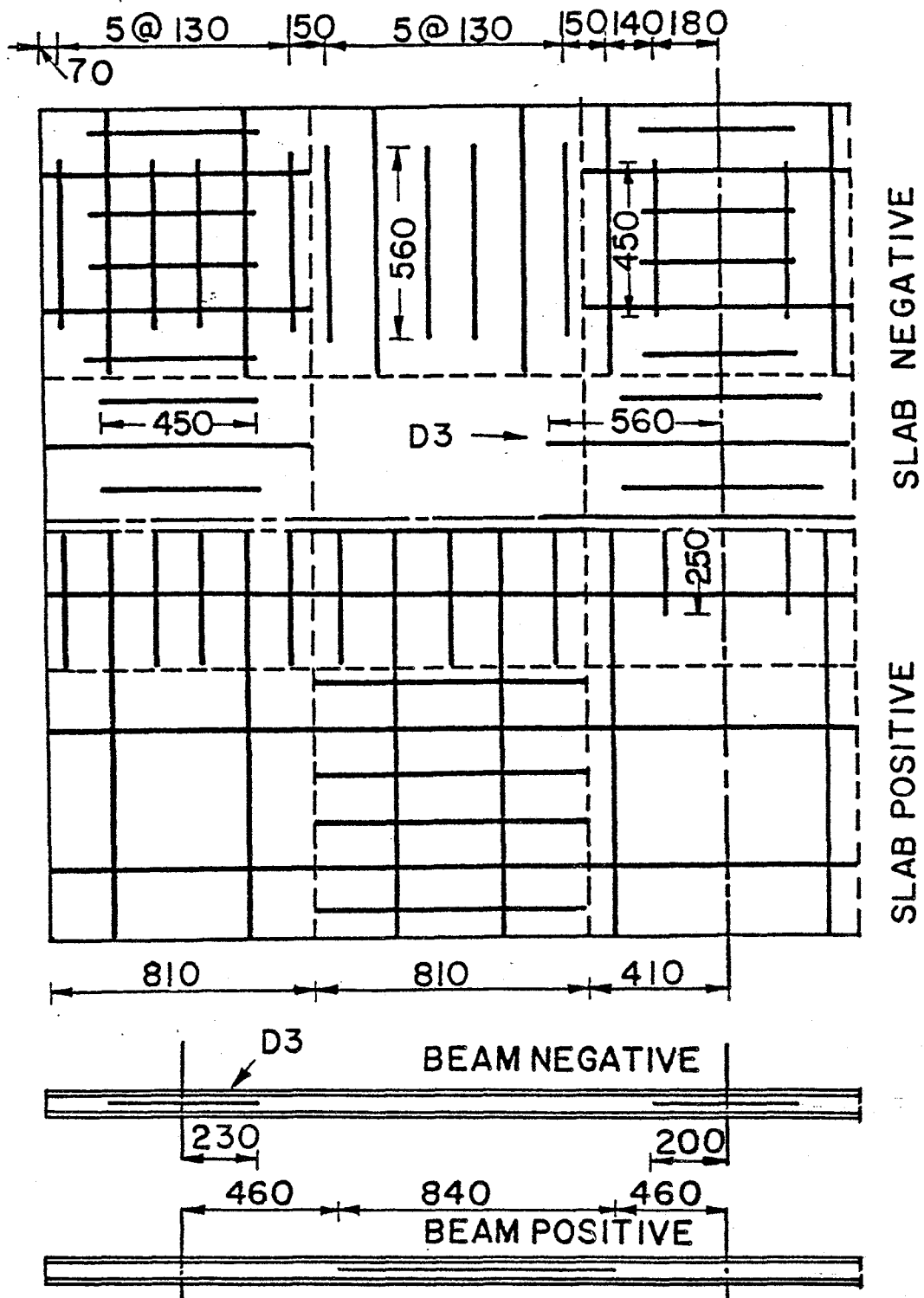
Fig. 3.3 Reinforcement Detail in Concrete Slab and Beam
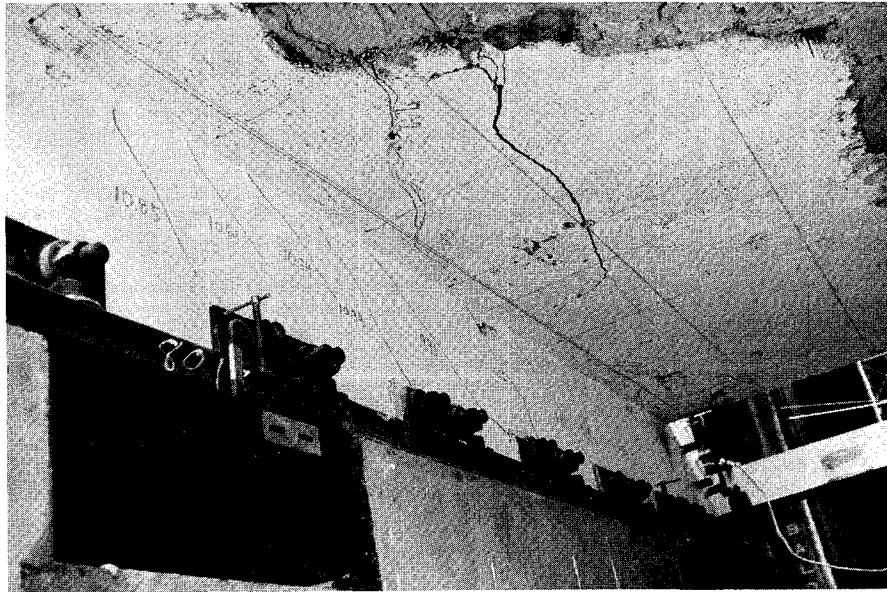
Fig. 3.4 Pedestal-Wall Connection
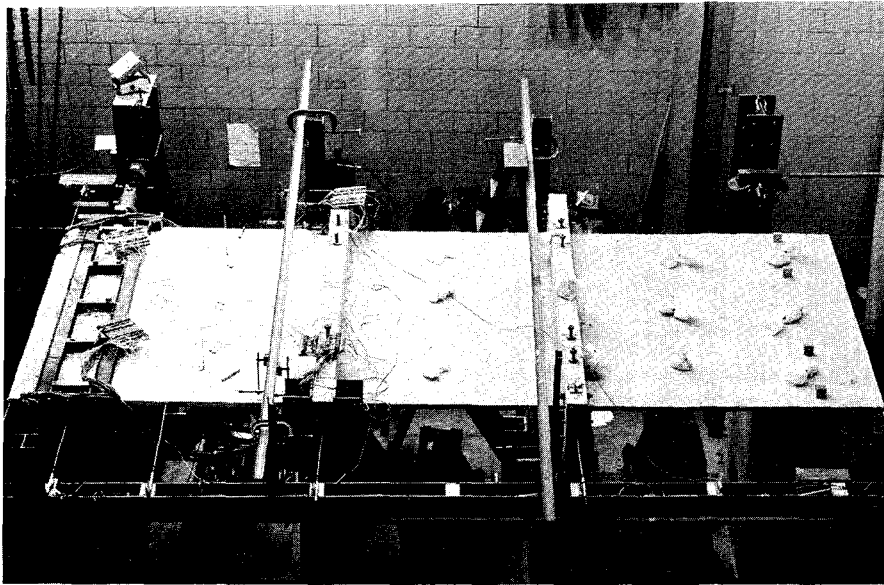
Fig. 3.5 Overall View of Test Setup
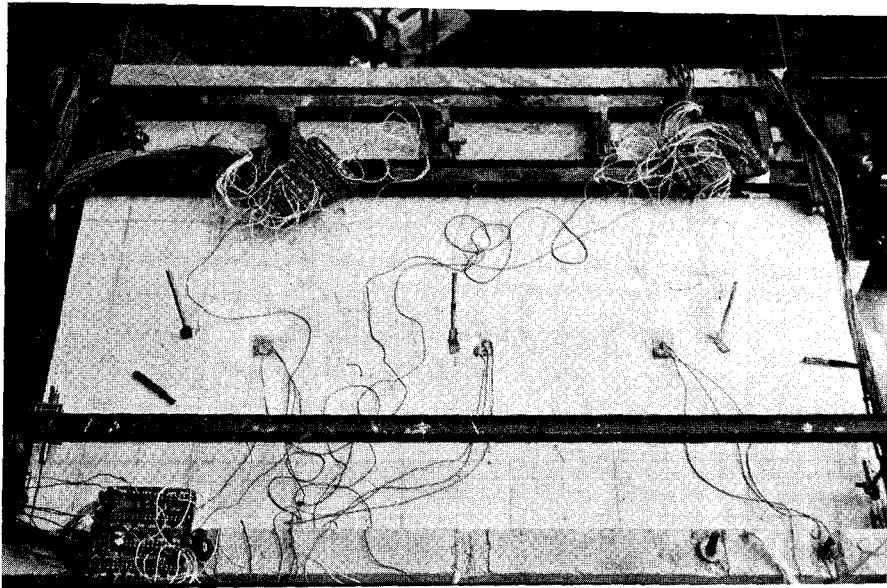
Fig. 3.6   Lateral Load Distribution Frame Placed
           for Strength Test

-234-
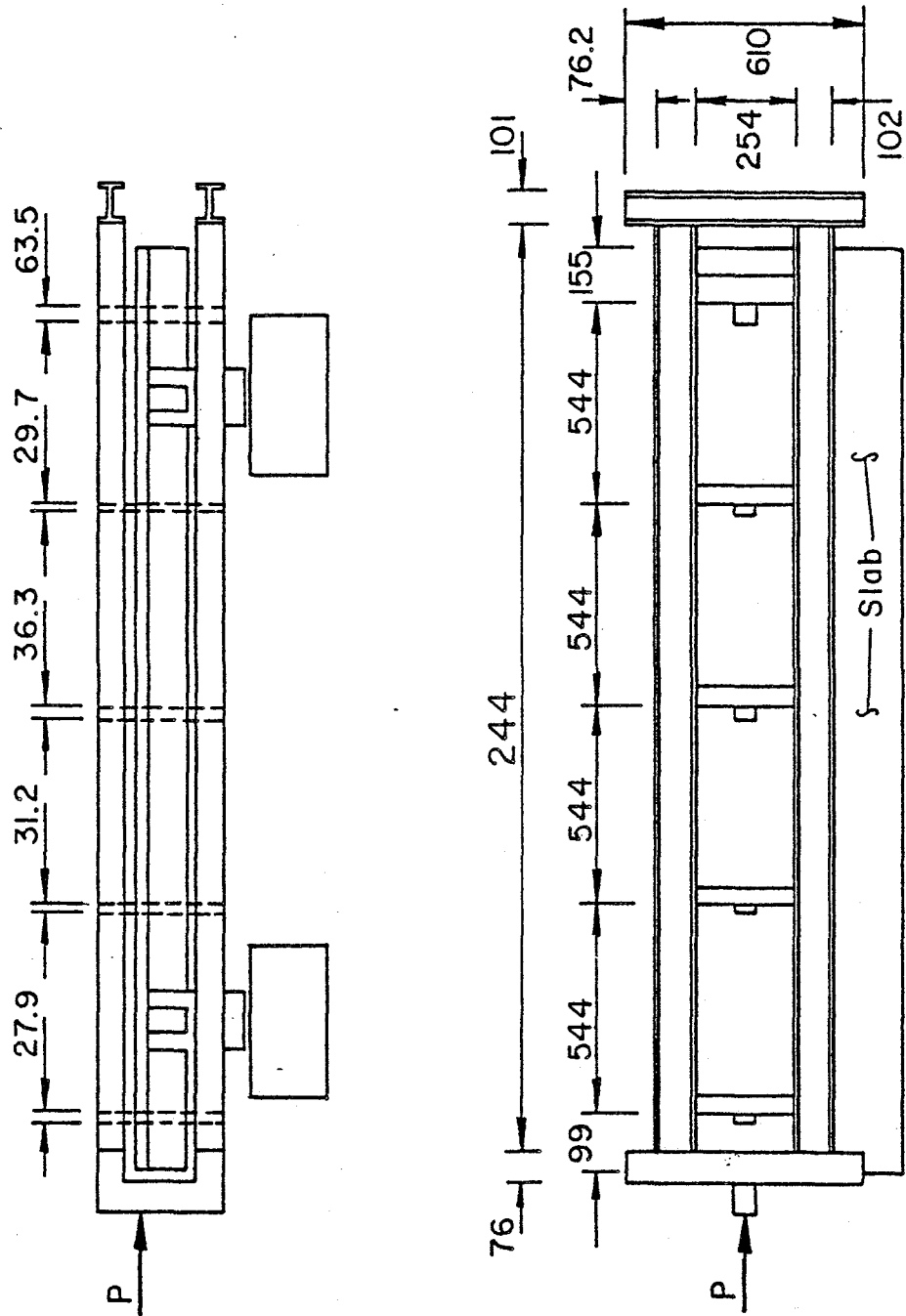
Fig. 3.7 Lateral Load Distribution Frame

UNIT:mm
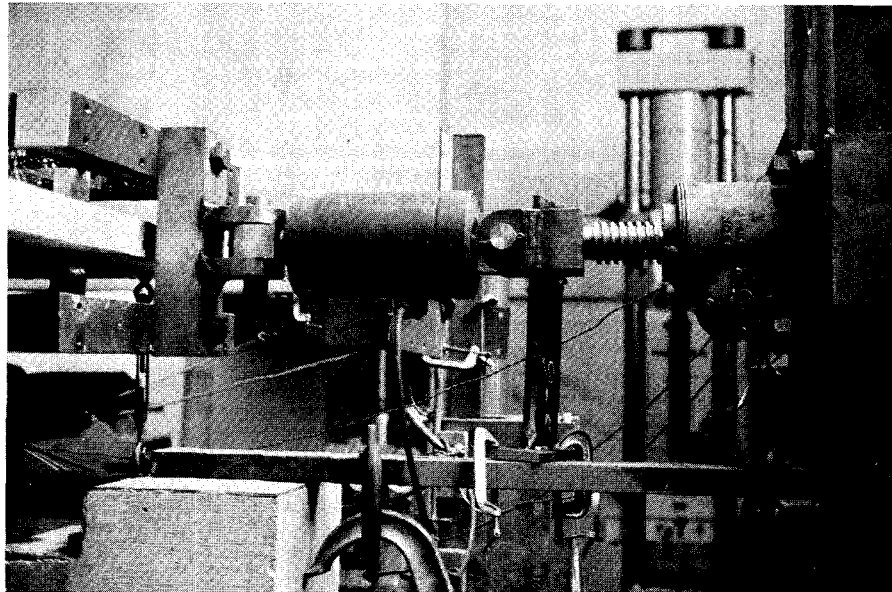
Fig. 3.8 Lateral Loading Jack

31.5 dia.

140

540

540

50

540

540

140

50

140   540   540   540   200

UNIT:mm

40
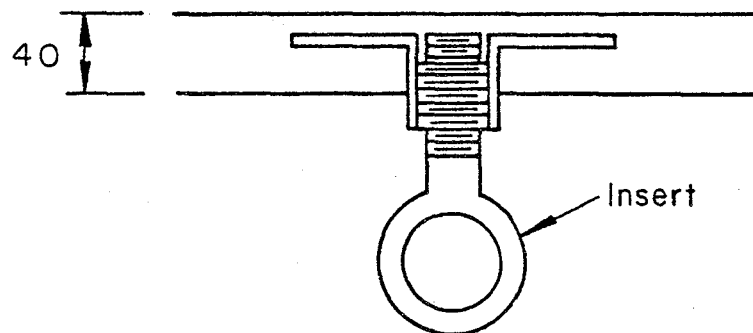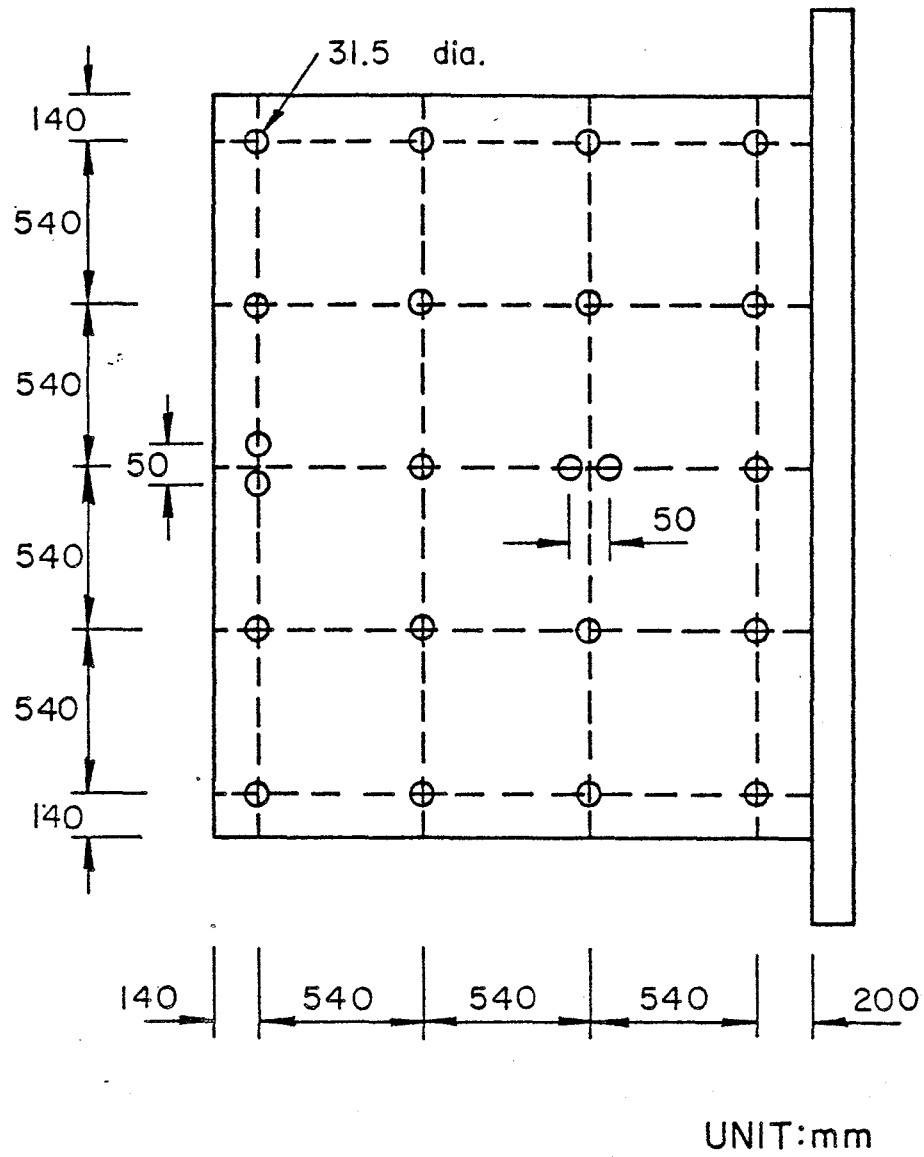
Insert

Fig. 3.9 Inserts embedded in slab

-237-
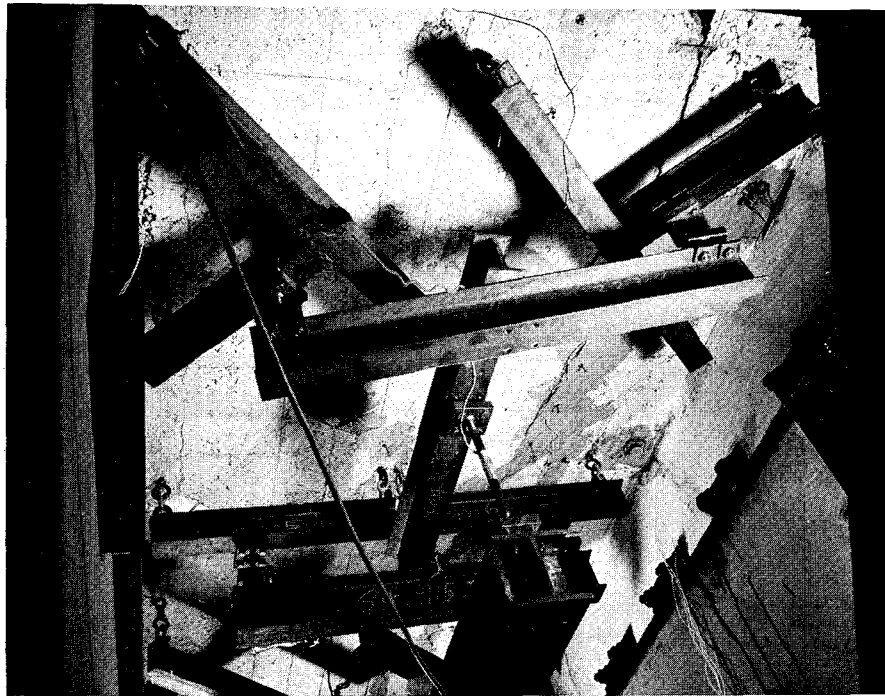
Fig. 3.10 Vertical Loading Frame
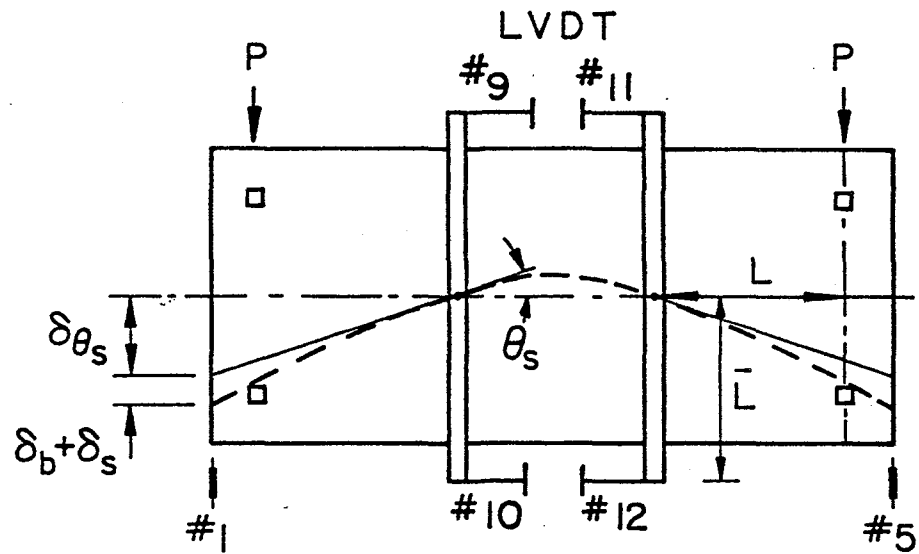
(a) Symmetrical Loading
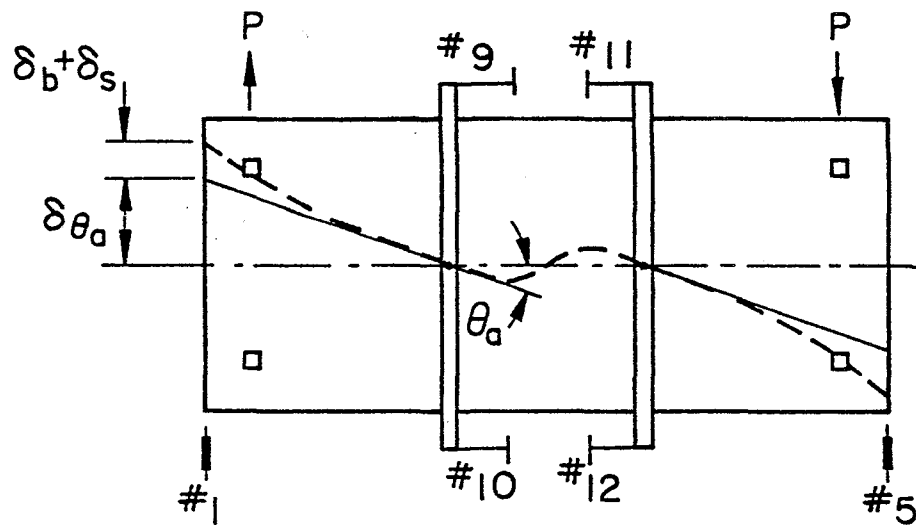
(b) Anti-symmetrical Loading

Walls Allowed to Rotate, Columns Free to Slide

Fig. 3.11 Loading Conditions and Measurement in Stiffness Test
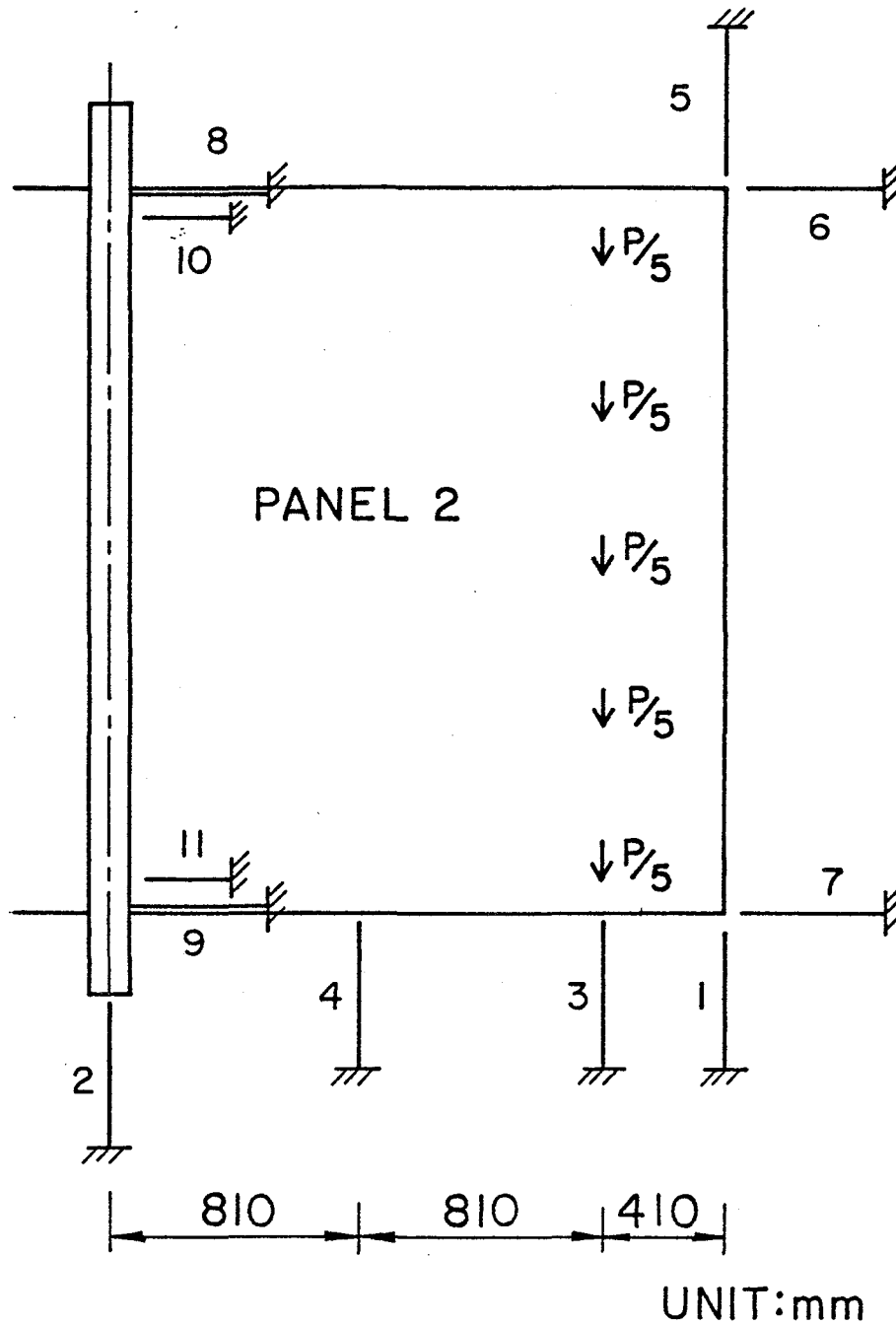
Fig. 3.12 Loading Condition and Measurement
in Strength Test
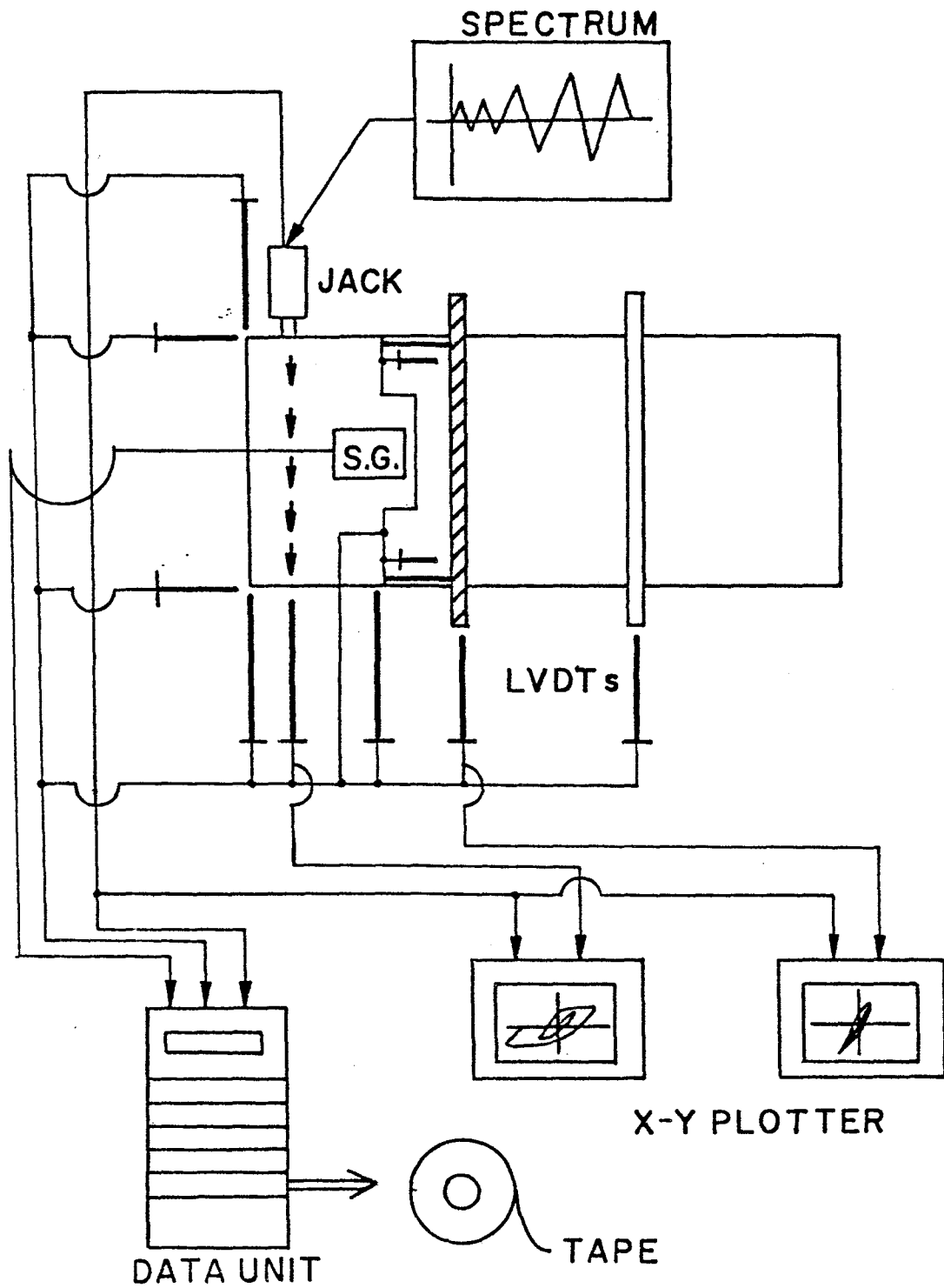
Fig. 3.13 Testing Procedure in Strength Test
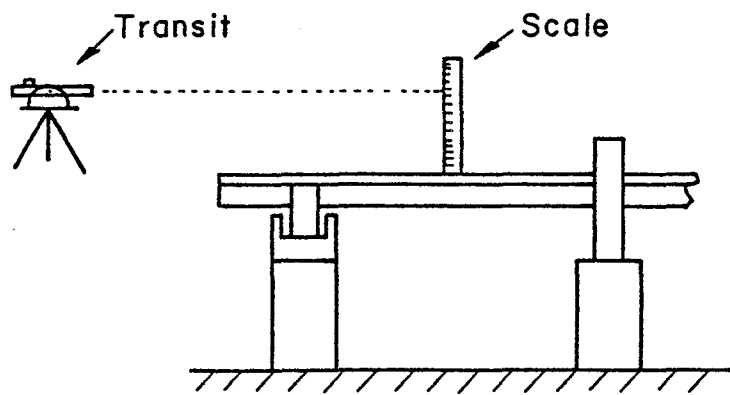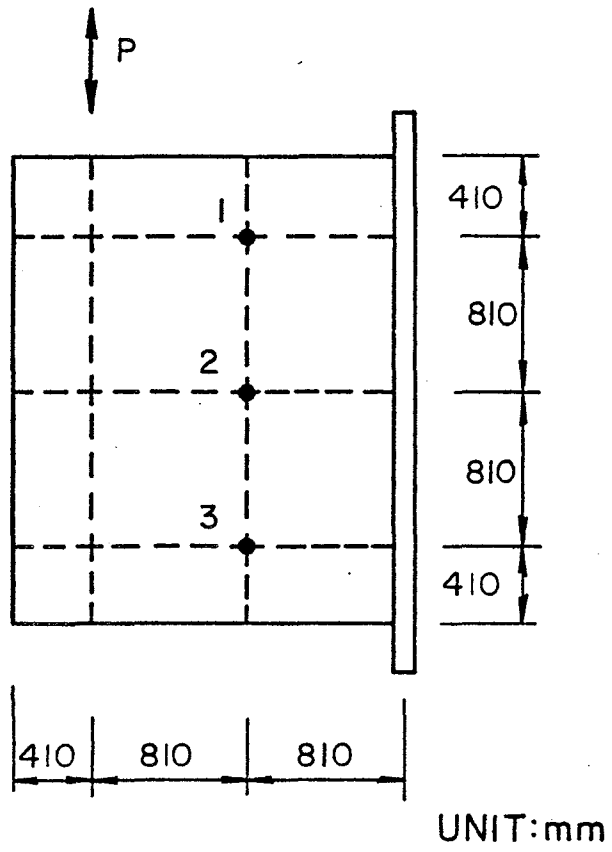
Fig. 3.14 Vertical Deflection Measurement
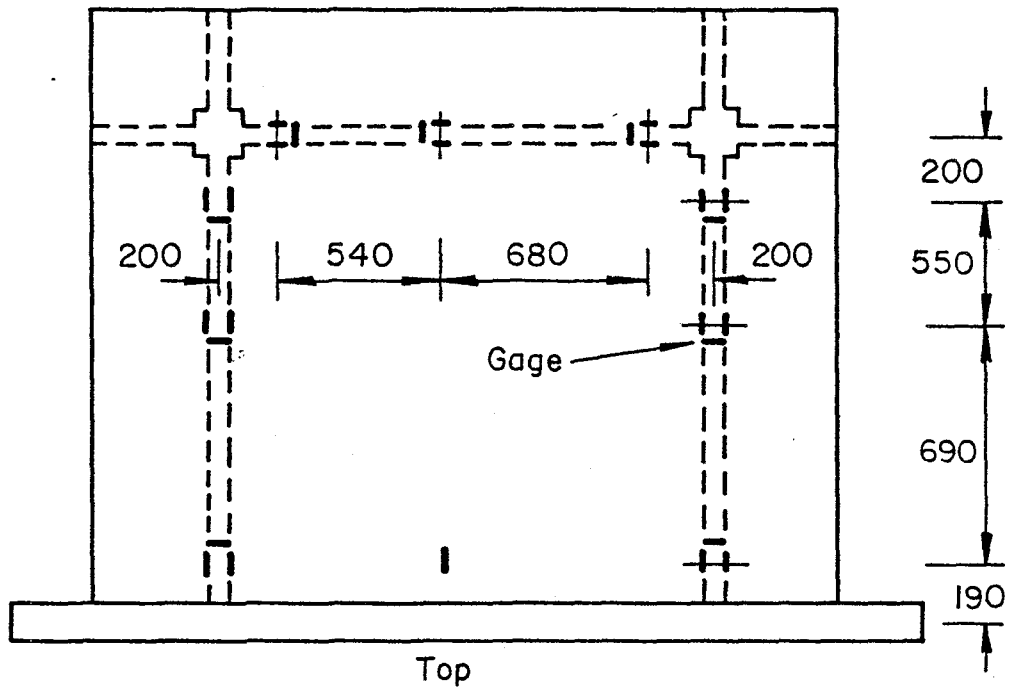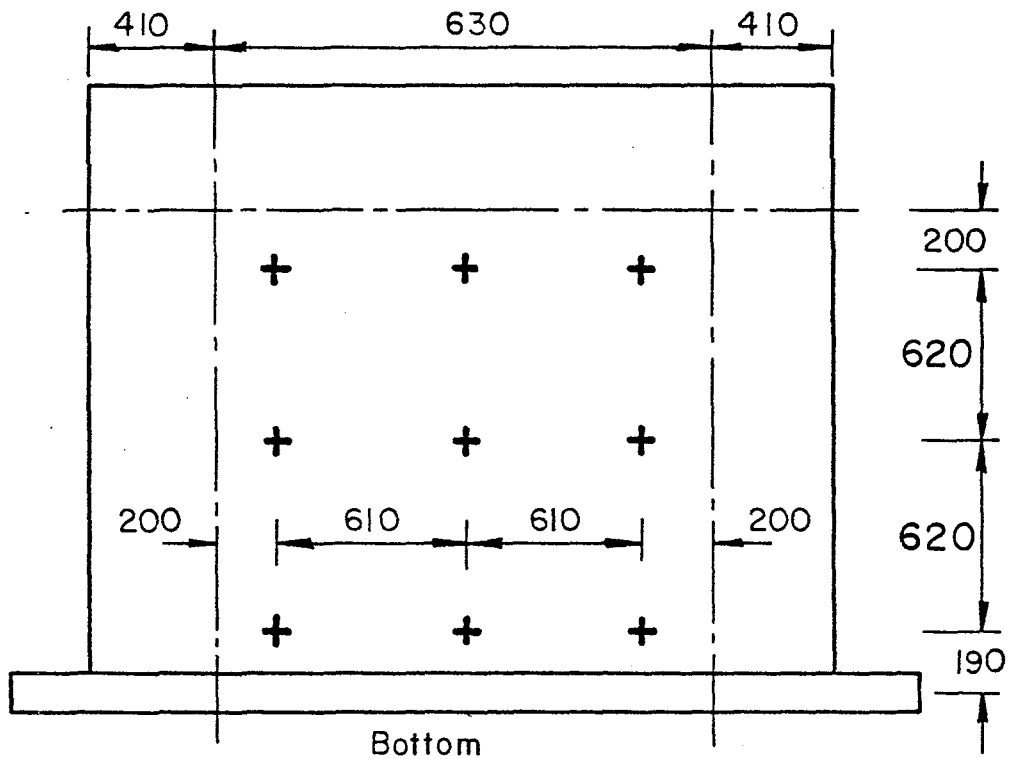
Fig. 3.15 Strain Gages in Slab
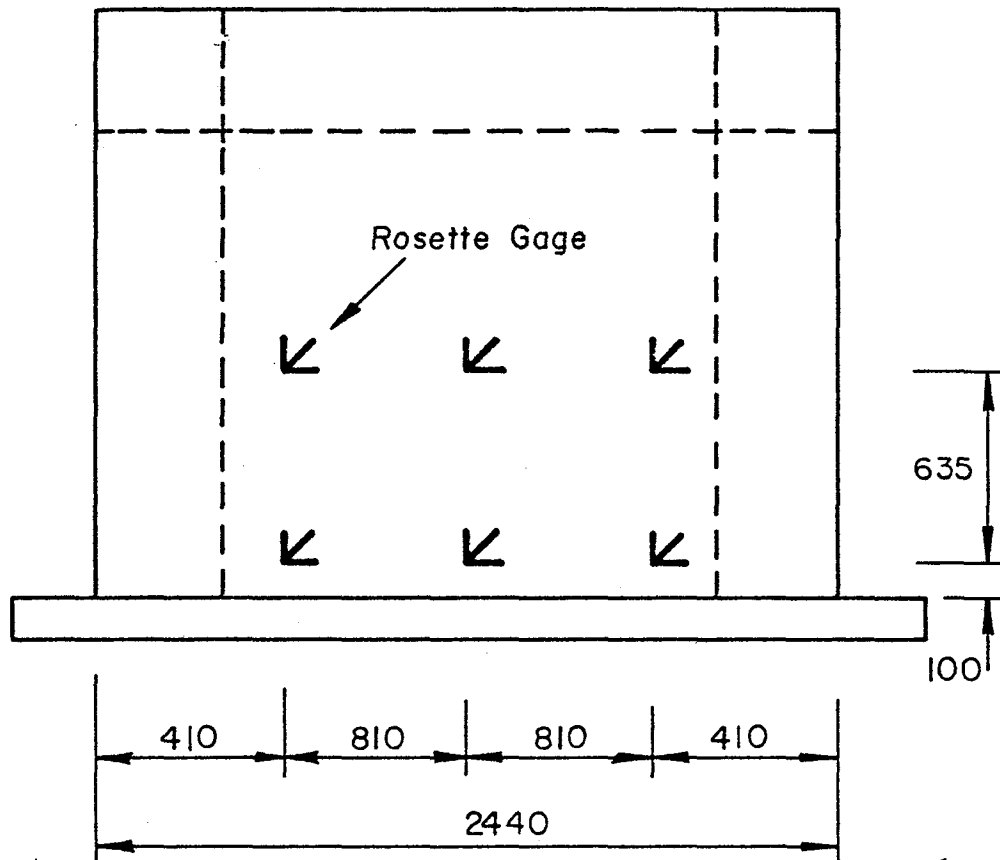
Fig. 3.16 Rosette Gages on Slab
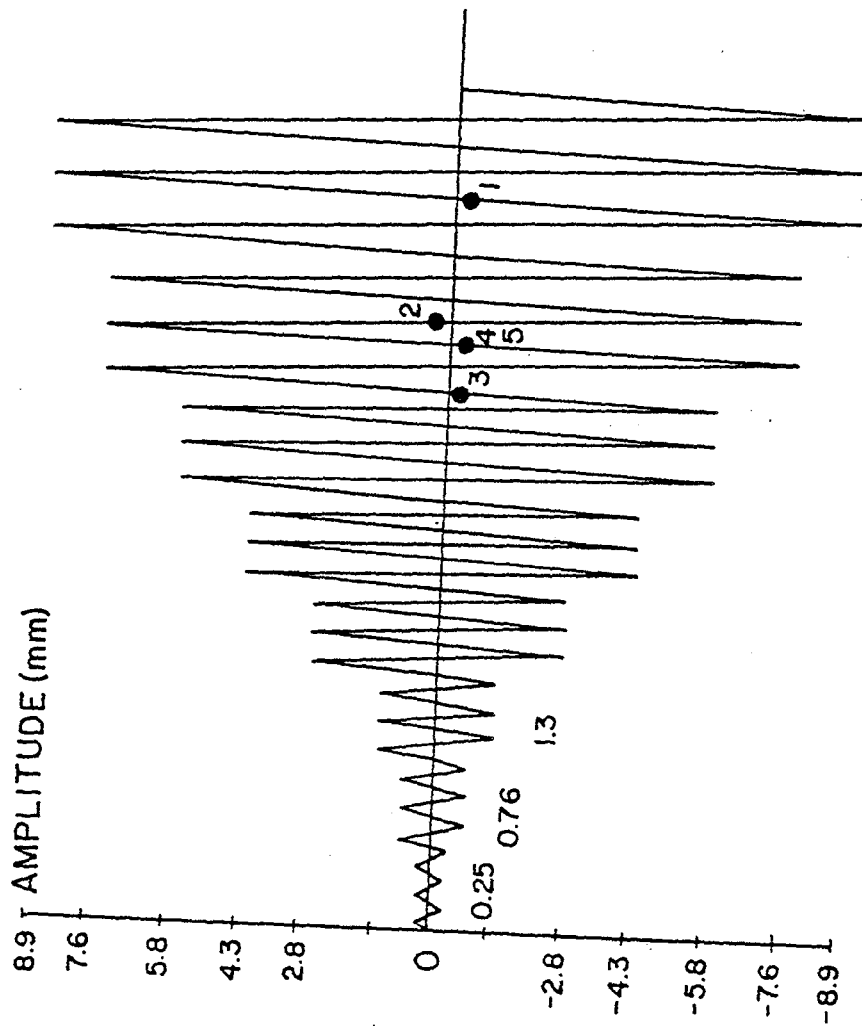
Fig. 3.17 Loading Spectrum for Cyclic Loading Tests
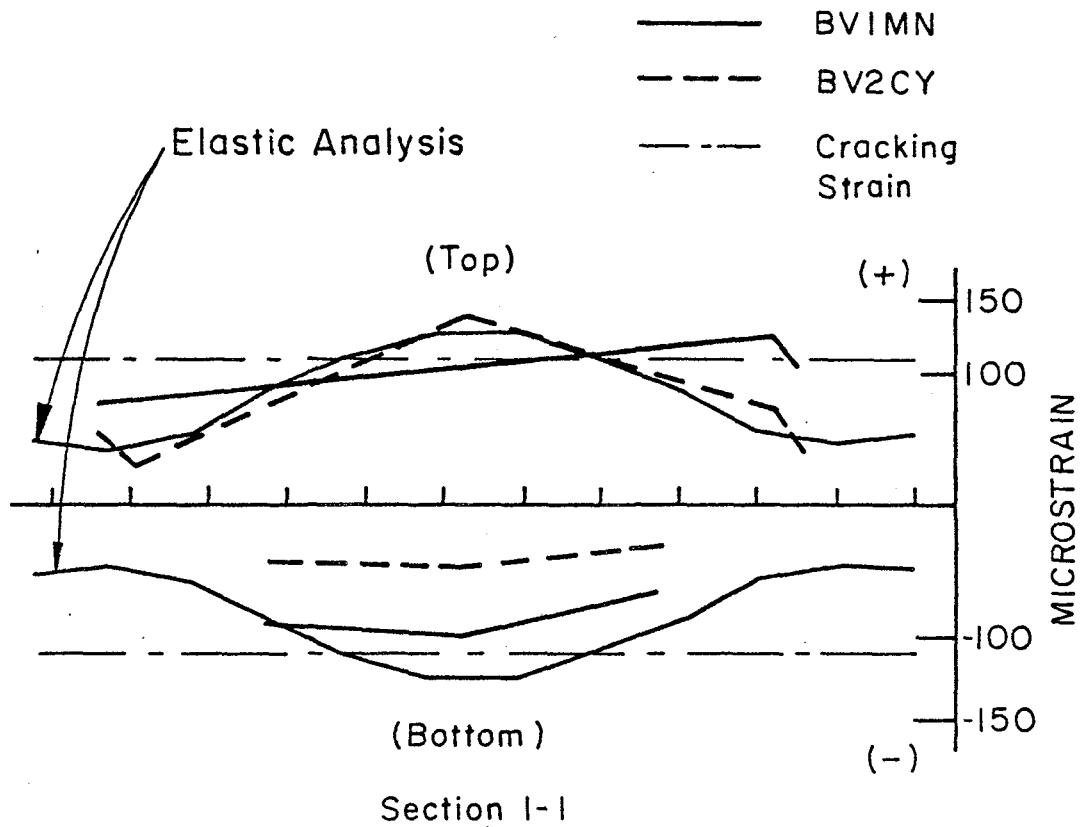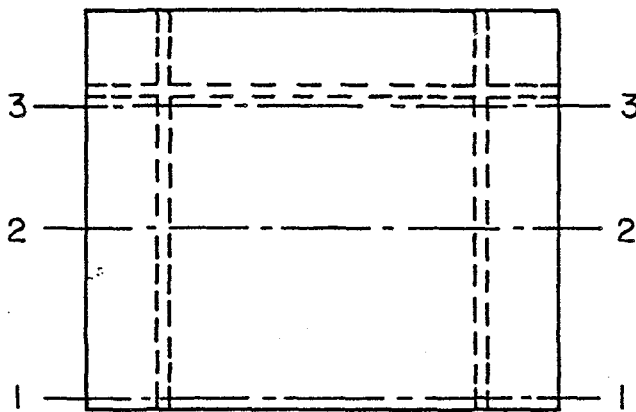
Fig. 3.18   Strain Distribution in Slab Under
Design Service Vertical Load
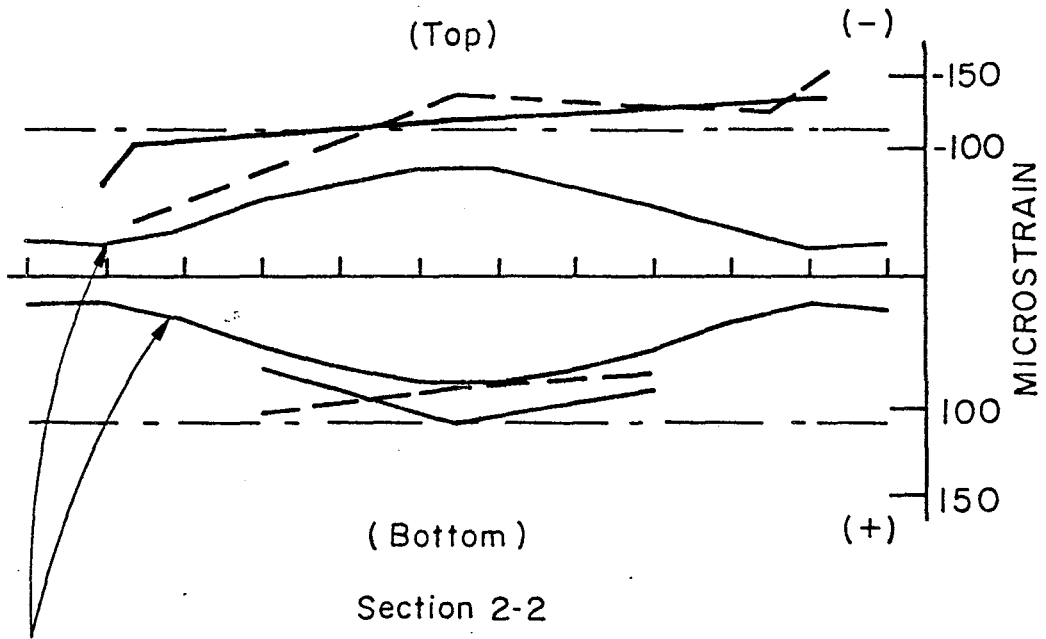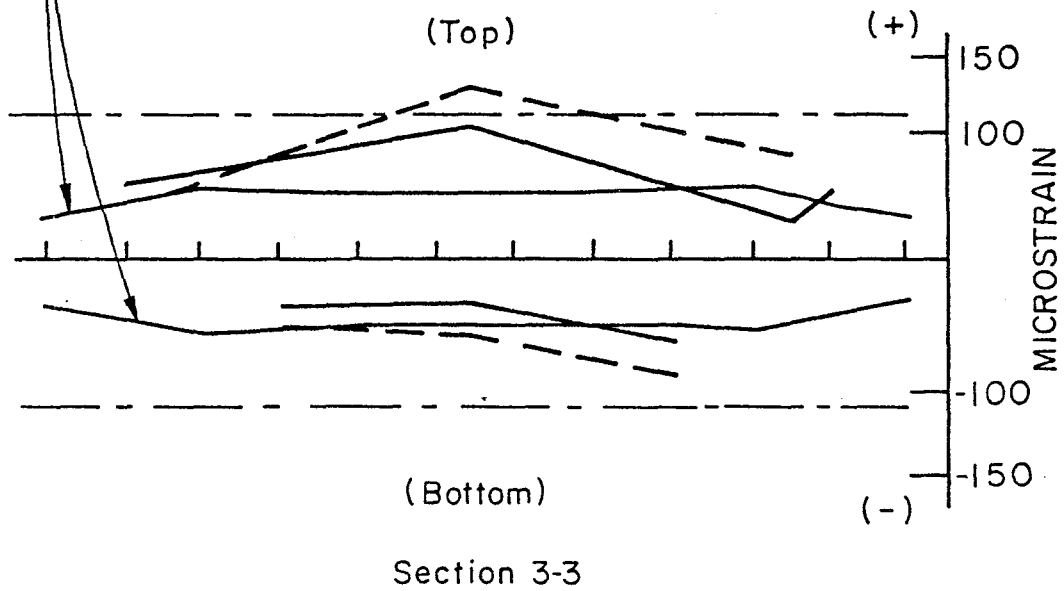
Fig. 3.18(Continued)   Strain Distribution in Slab
Under Design Service Vertical Load

-247-
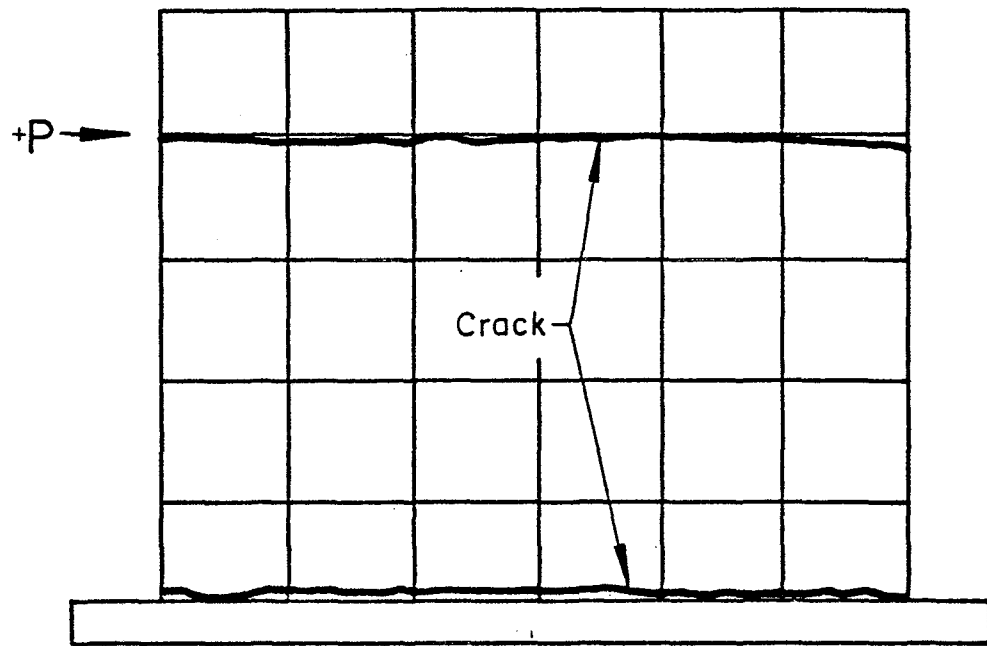
Fig. 3.19   Crack Pattern in Slab Under
            Design Service Vertical Load
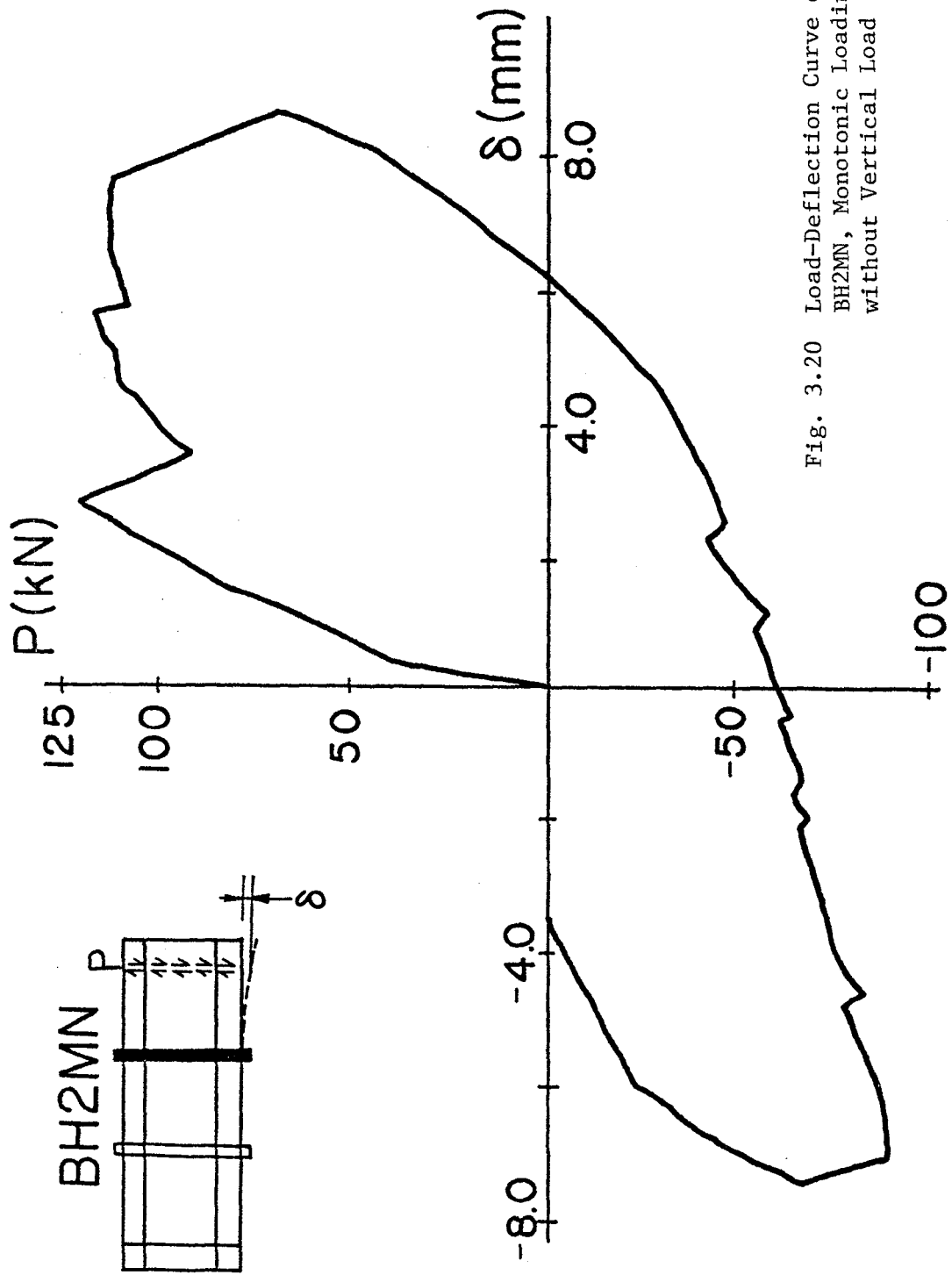
Fig. 3.20 Load-Deflection Curve of BH2MN, Monotonic Loading without Vertical Load
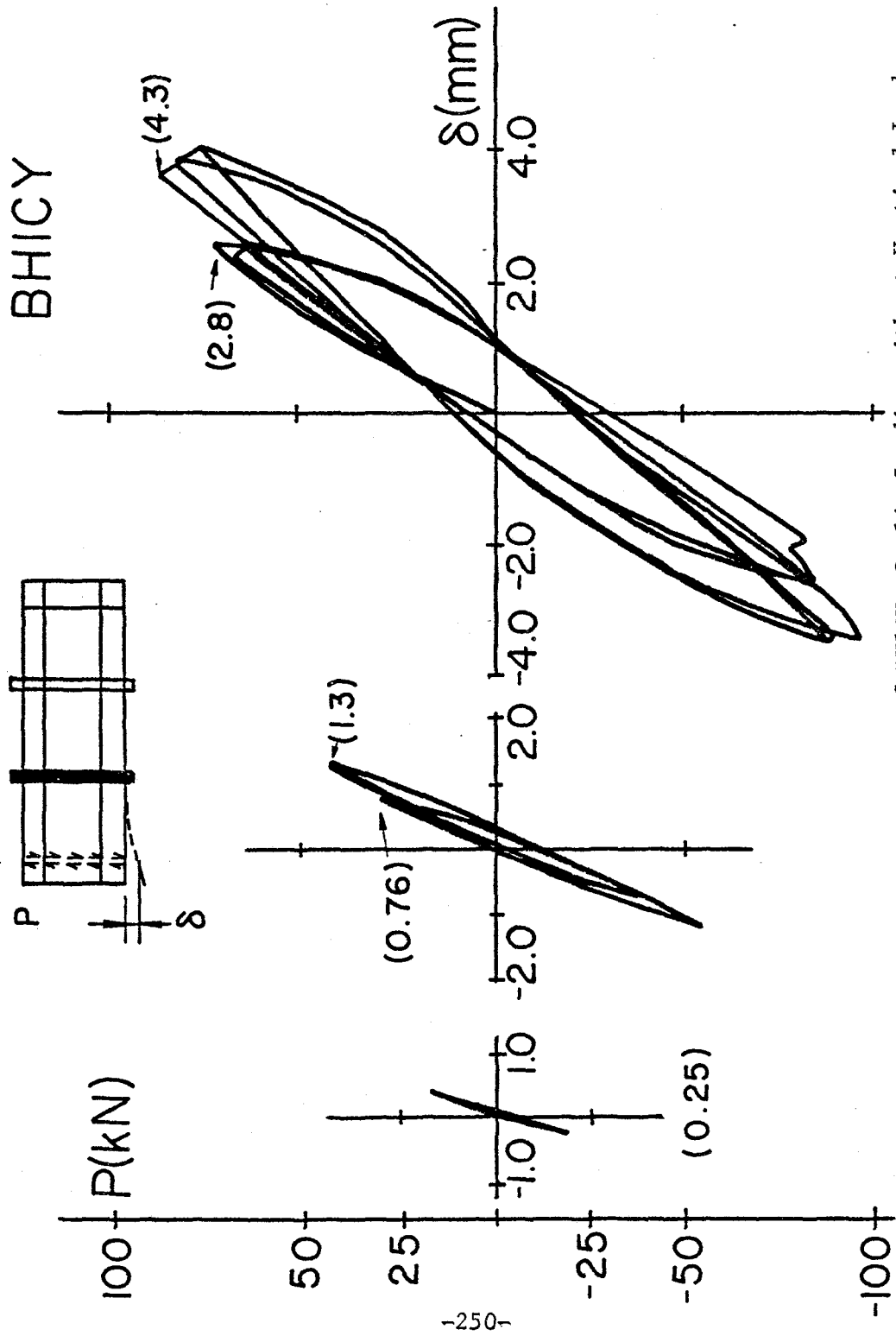
Fig. 3.21 Load-Deflection Curve of BH1CY, Cyclic Loading without Vertical Load

BHICY

Fig. 3.21(continued)
Load Deflection Curve of
BHICY, Cyclic Loading
Without Vertical Load
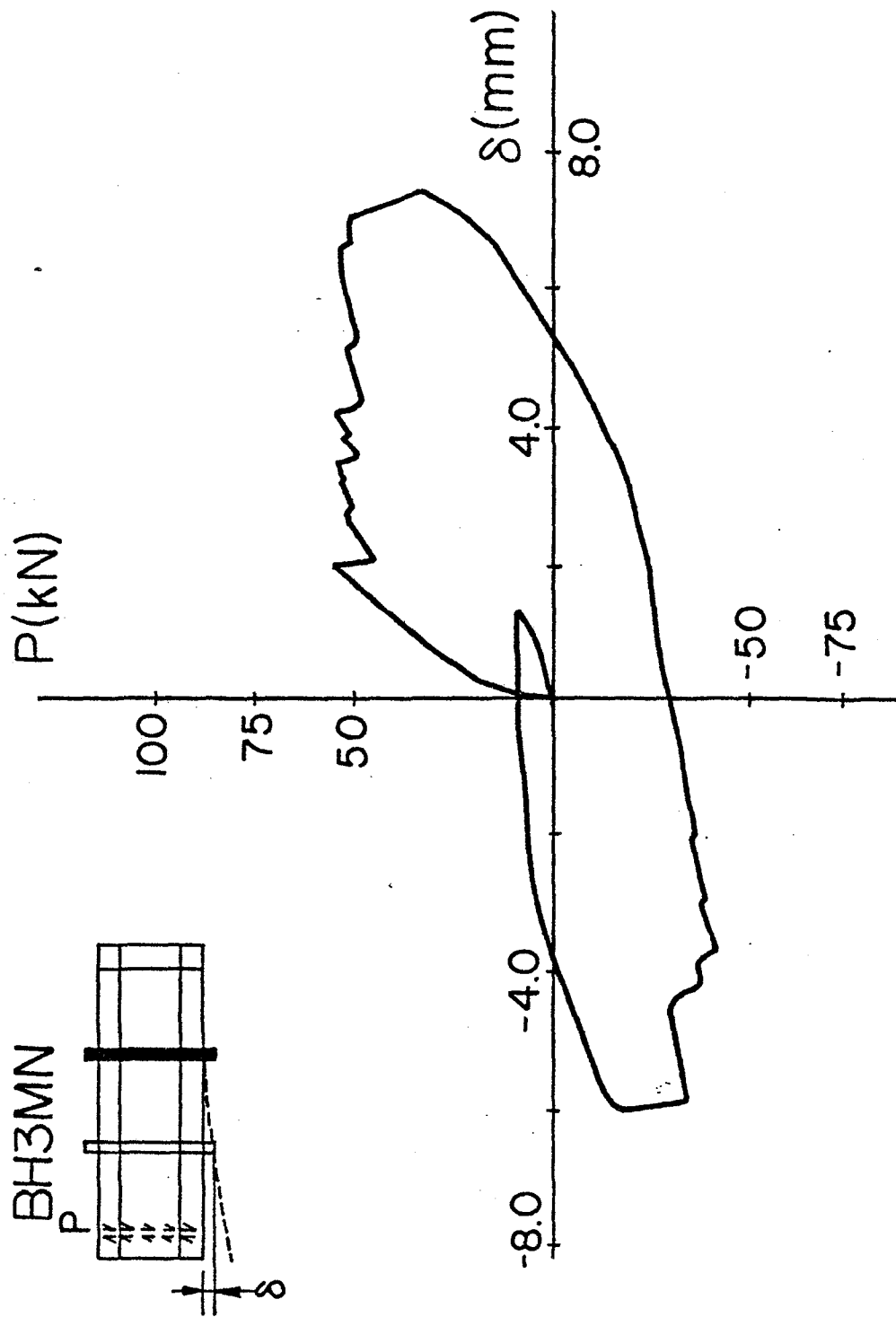
Fig. 3.22 Load-Deflection Curve of BH3MN, Monotonic Loading without Vertical Load
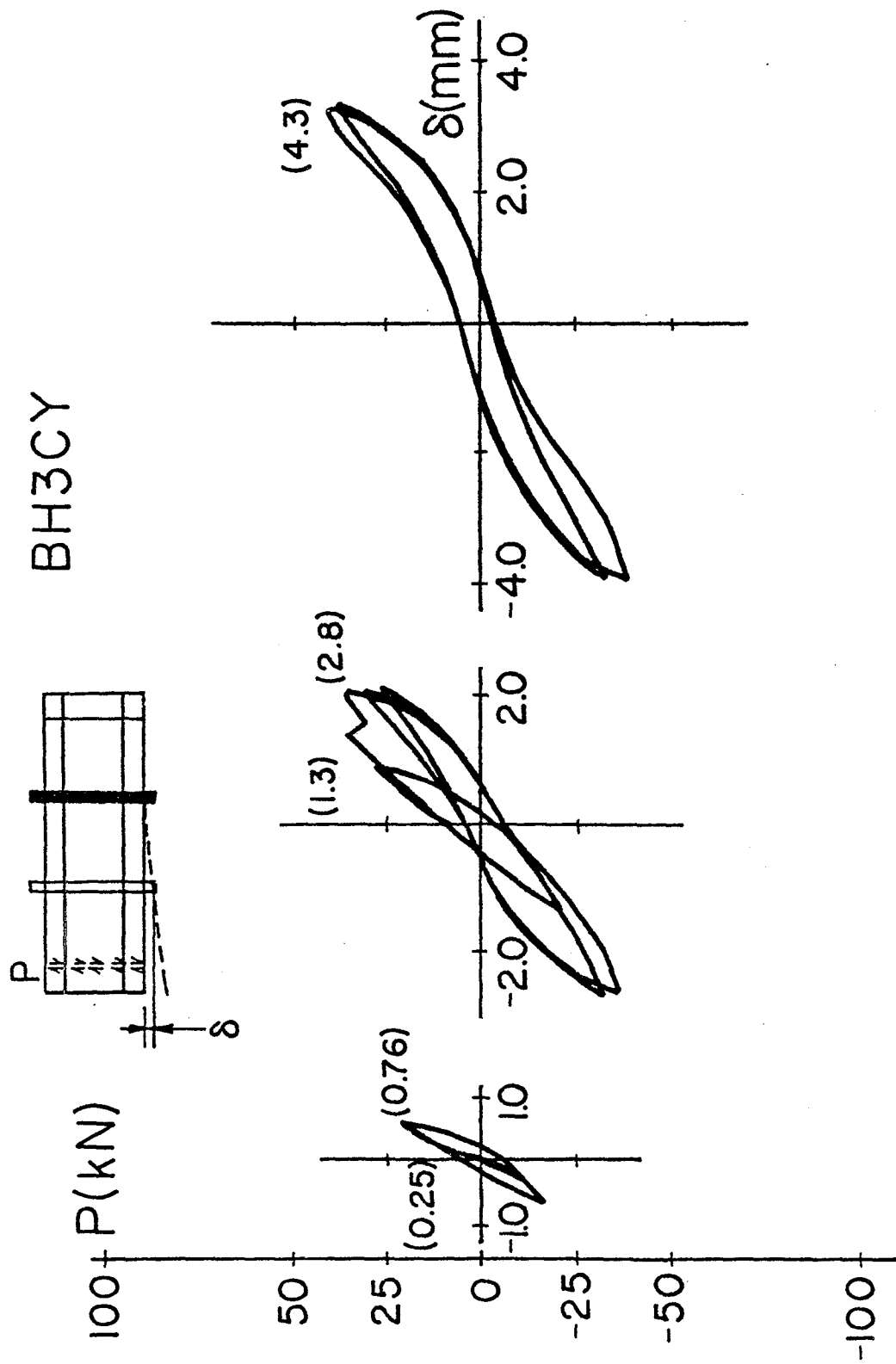
Fig. 3.23 Load-Deflection Curve of BH3CY, Cyclic Loading without Vertical Load
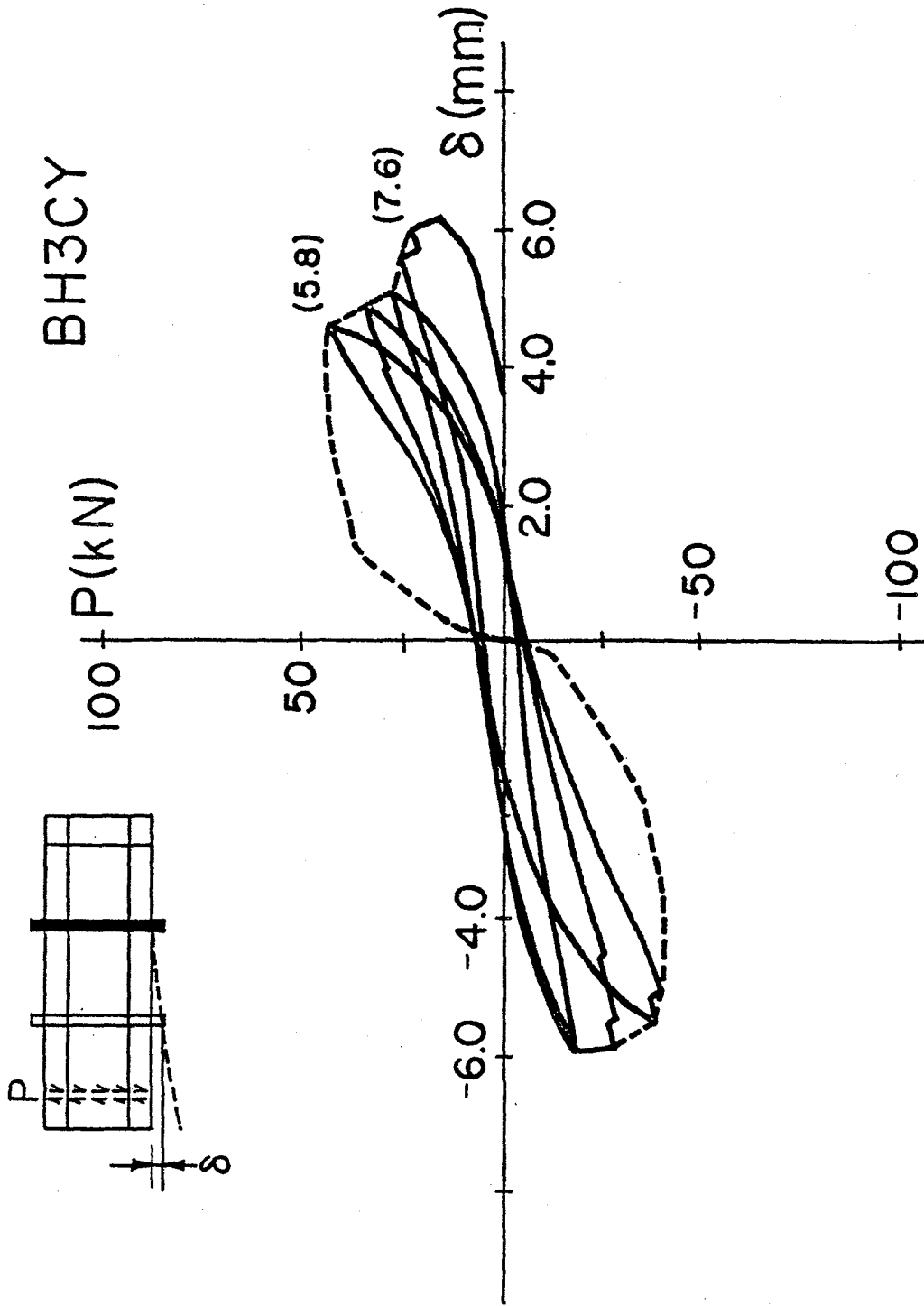
Fig. 3.23(continued) Load-Deflection Curve of BH3CY, Cyclic Loading without Vertical Load
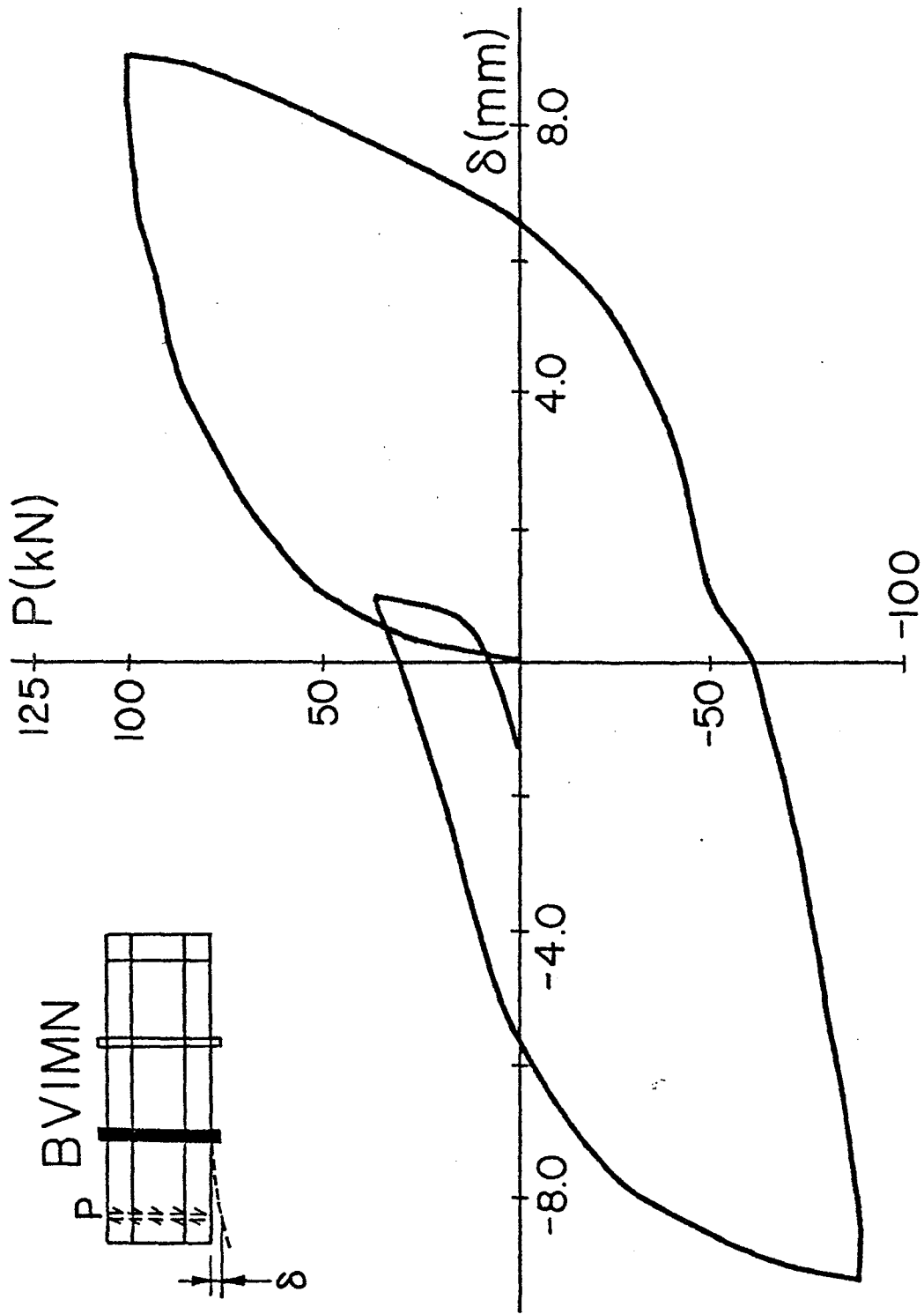
Fig. 3.24 Load-Deflection Curve of BV1MN, Monotonic Loading with Vertical Load
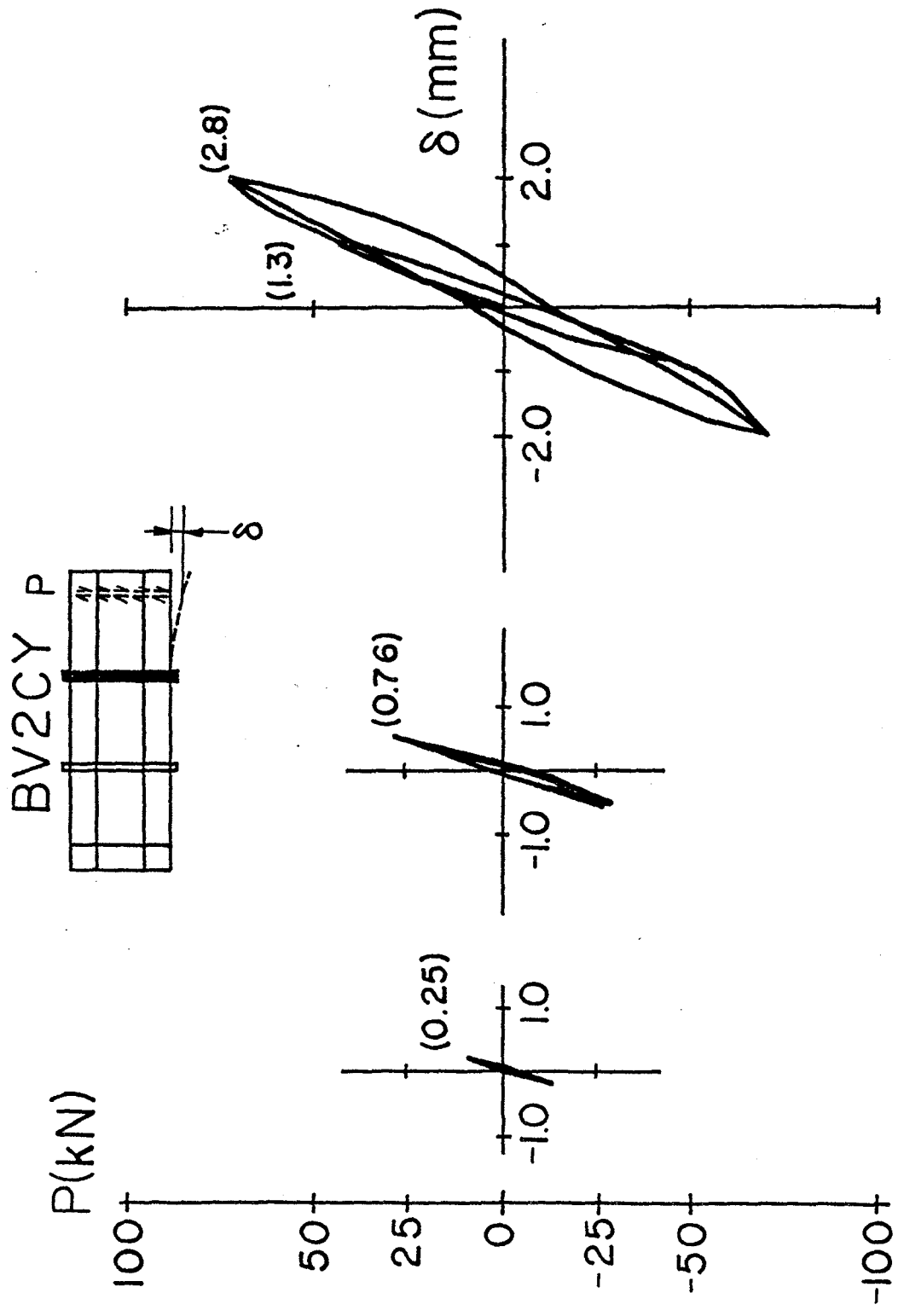
Fig. 3.25 Load–Deflection Curve of BV2CY, Cyclic Loading with Vertical Load
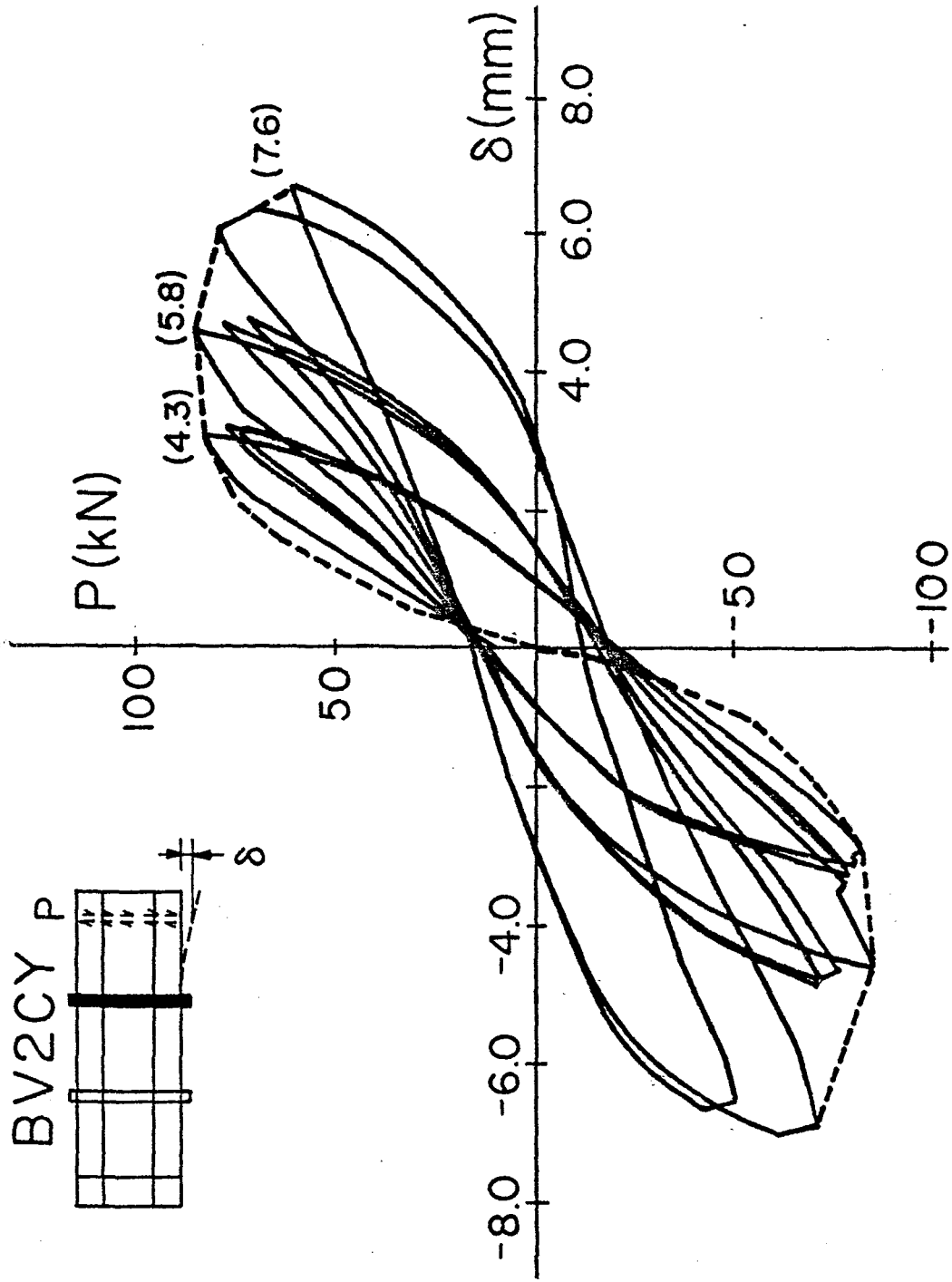
Fig. 3.25(continued) Load-Deflection Curve of BV2CY, Cyclic Loading with Vertical Load
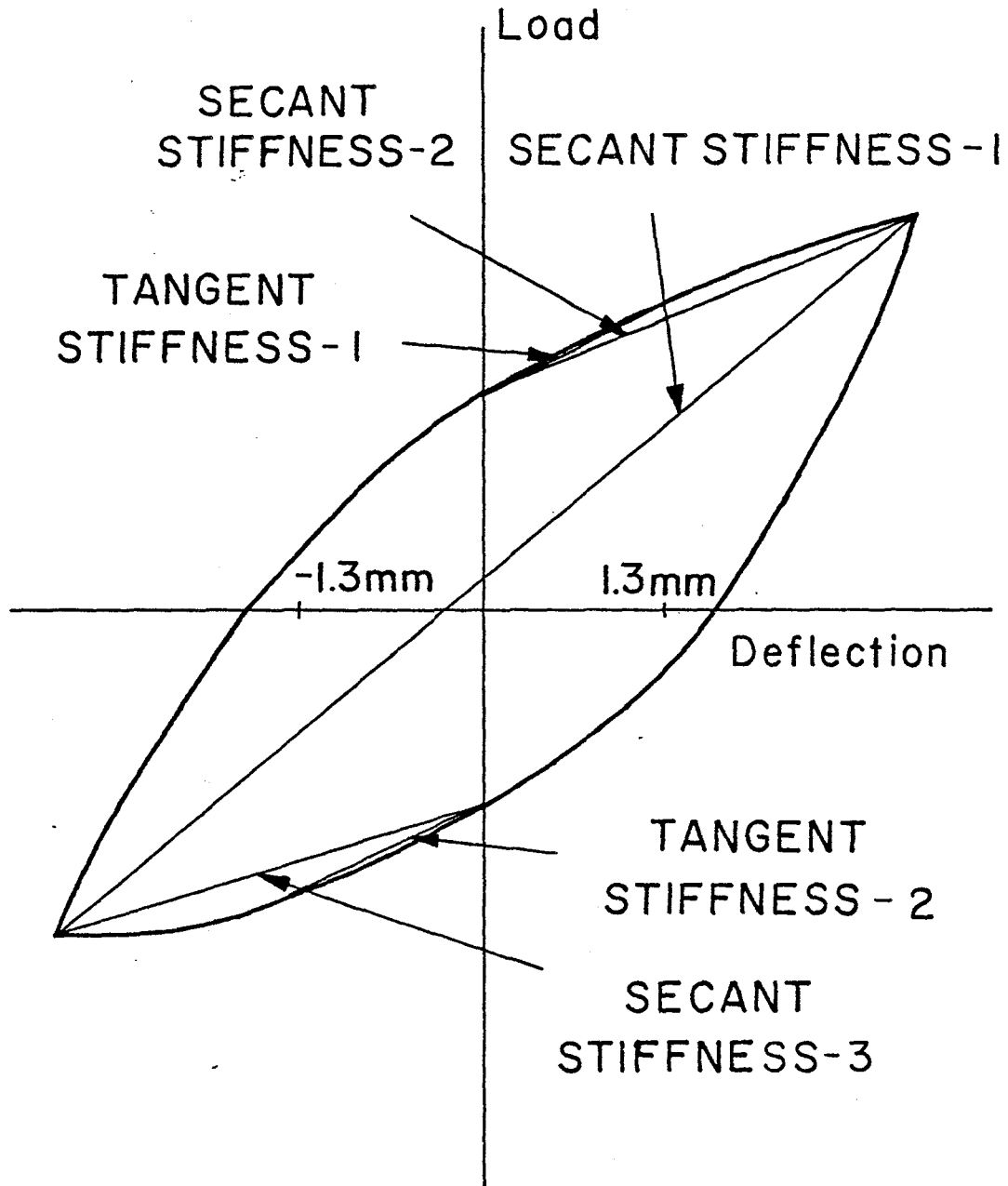
Fig. 3.26   Measured Stiffnesses in Cyclic
Loading Strength Tests
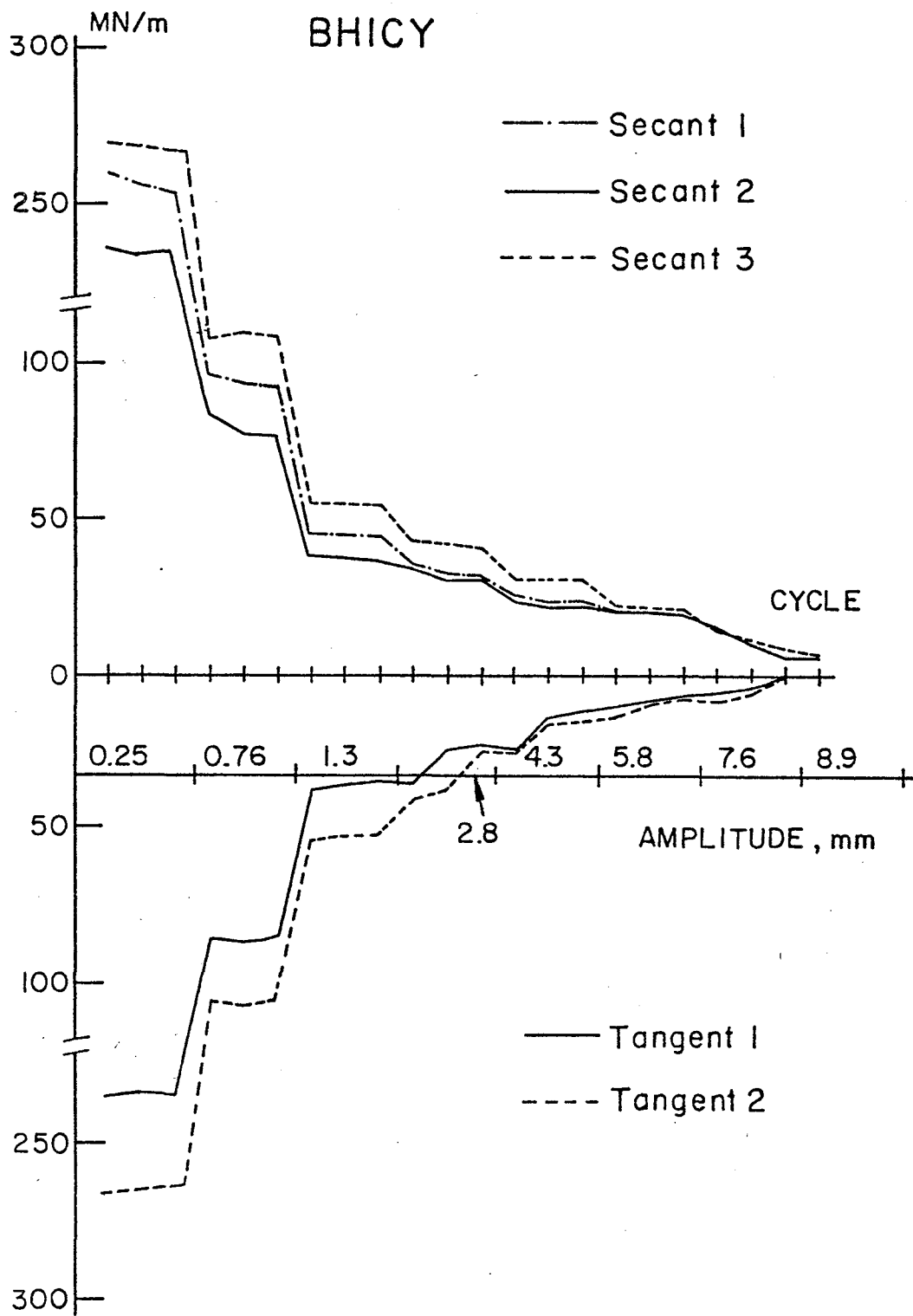
Fig. 3.27   Stiffness Degradation in BH1CY
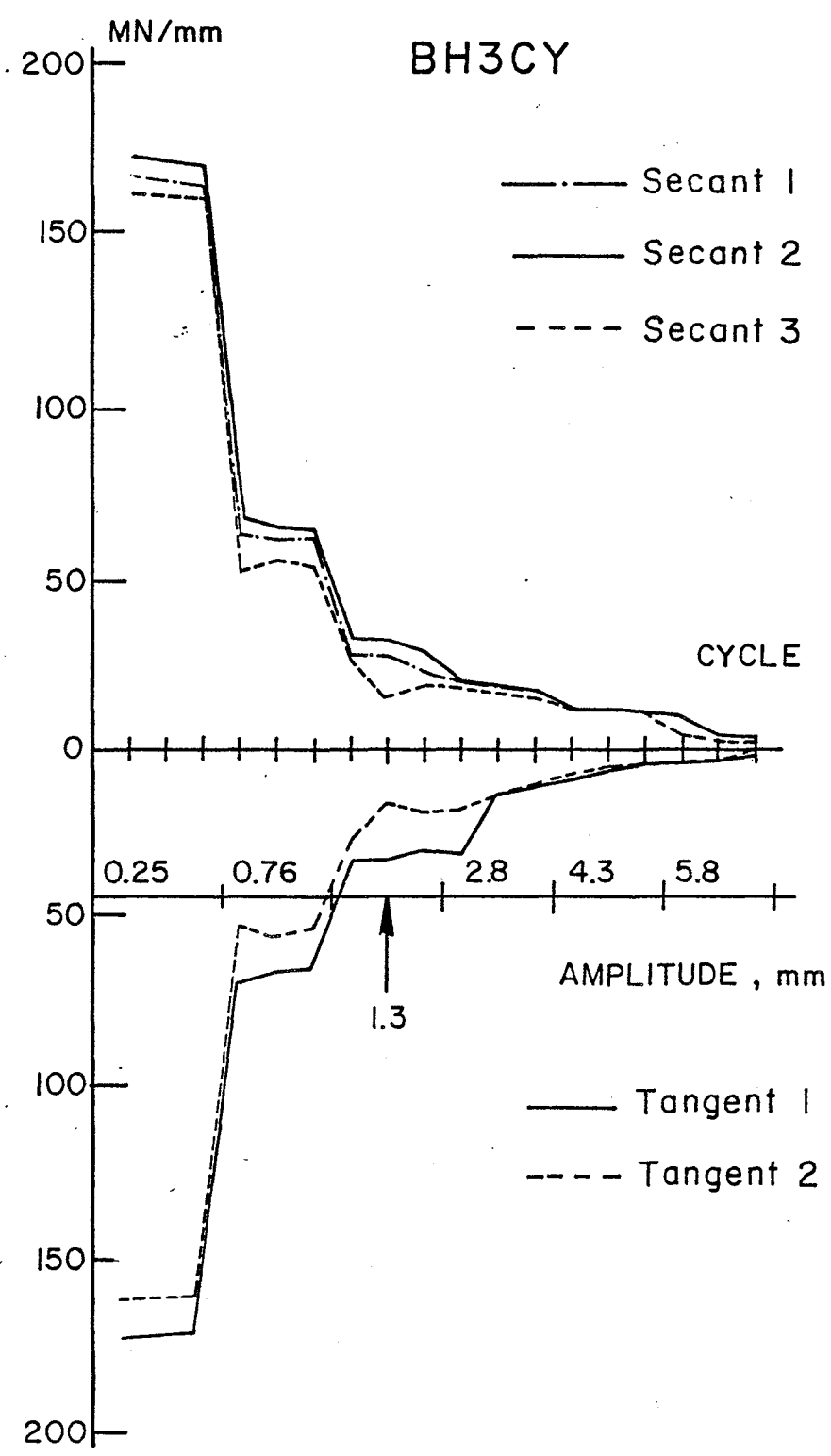
Fig. 3.28 Stiffness Degradation in BH3CY
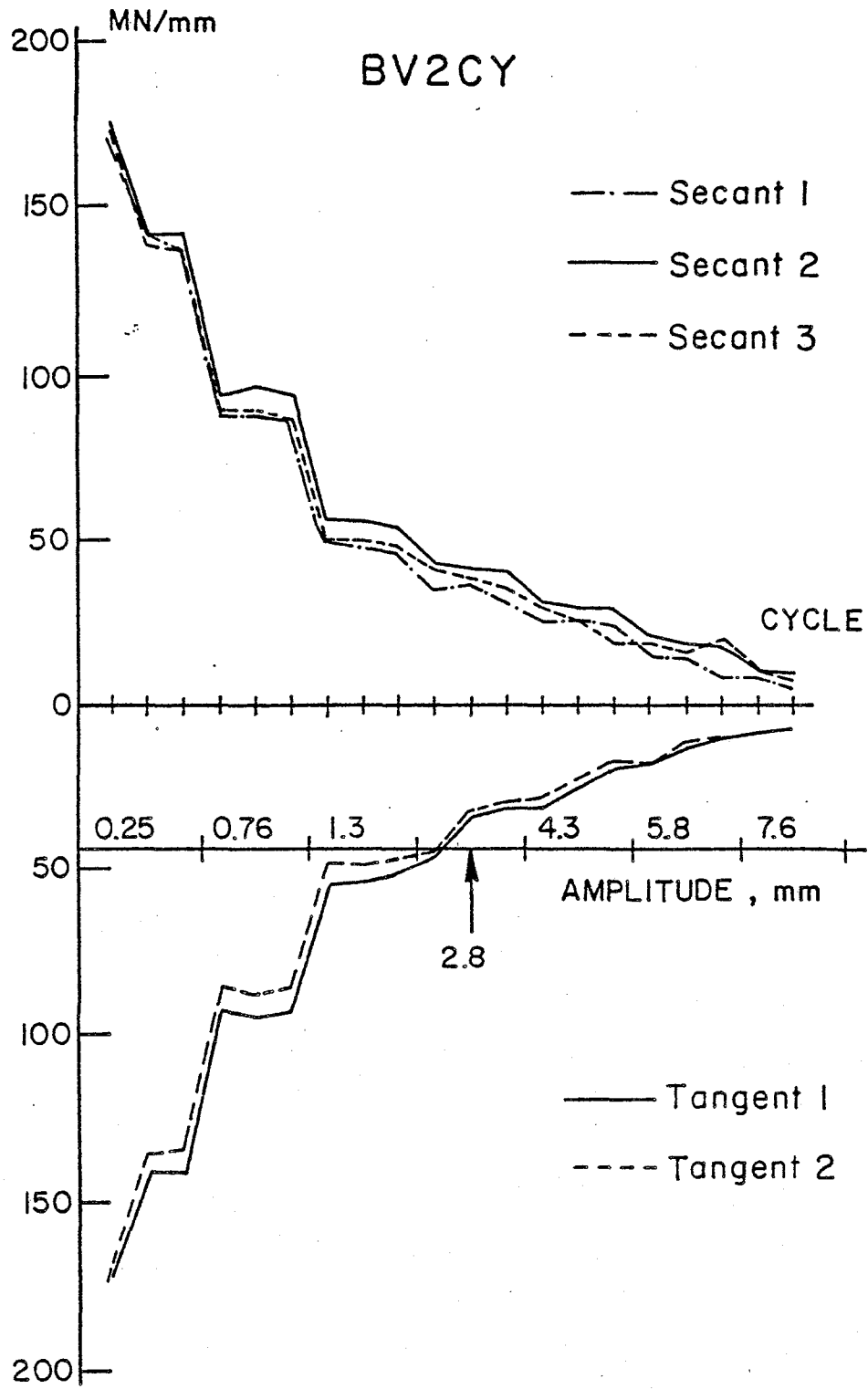
Fig. 3.29   Stiffness Degradation in BV2CY
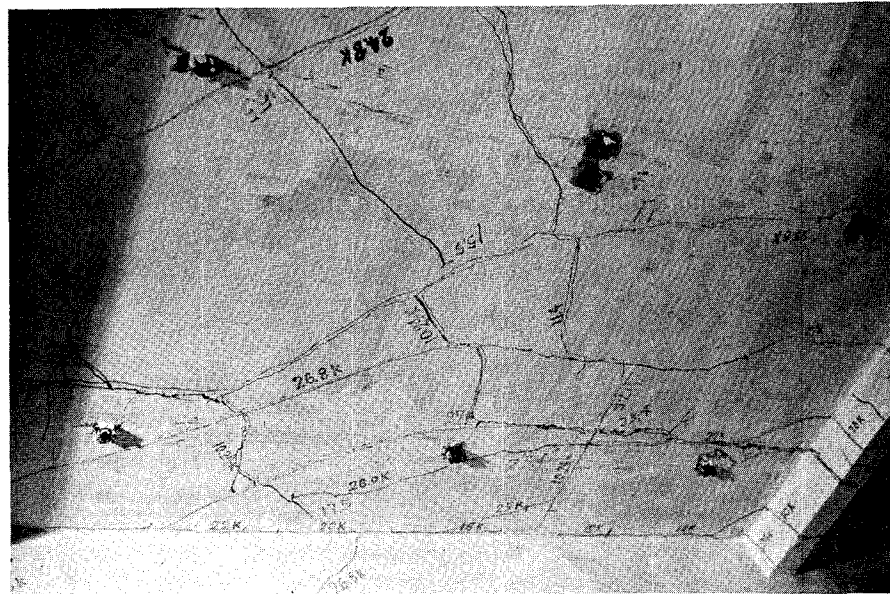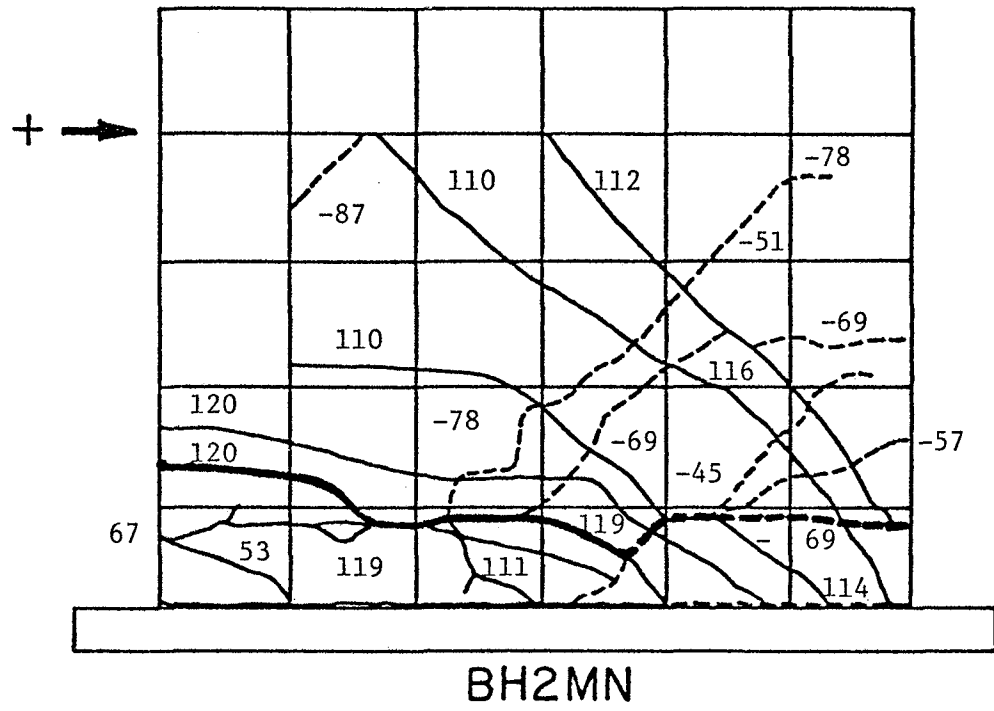
BH2MN

Fig. 3.30 Crack Pattern of BH2MN
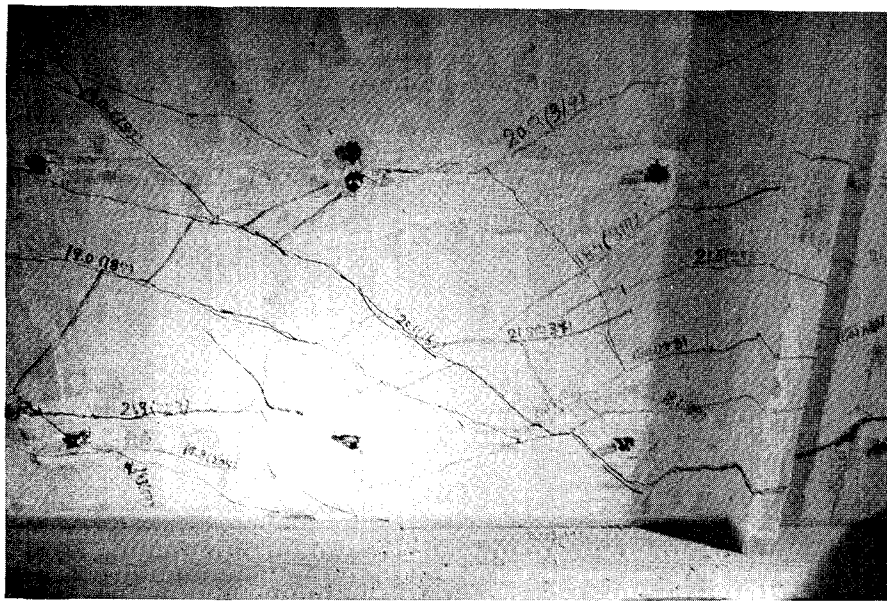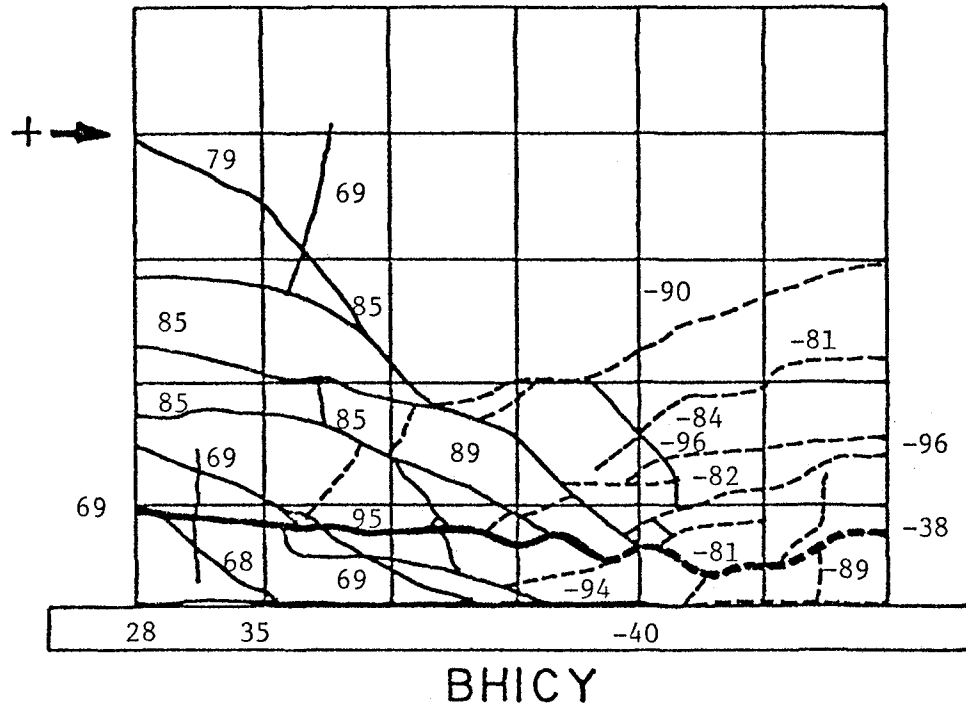
BHICY

Fig. 3.31   Crack Pattern of BH1CY
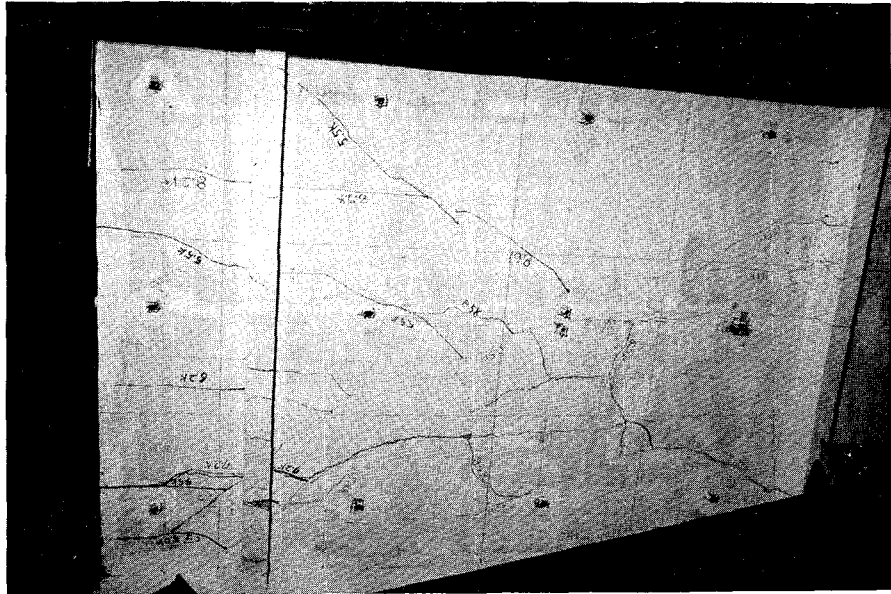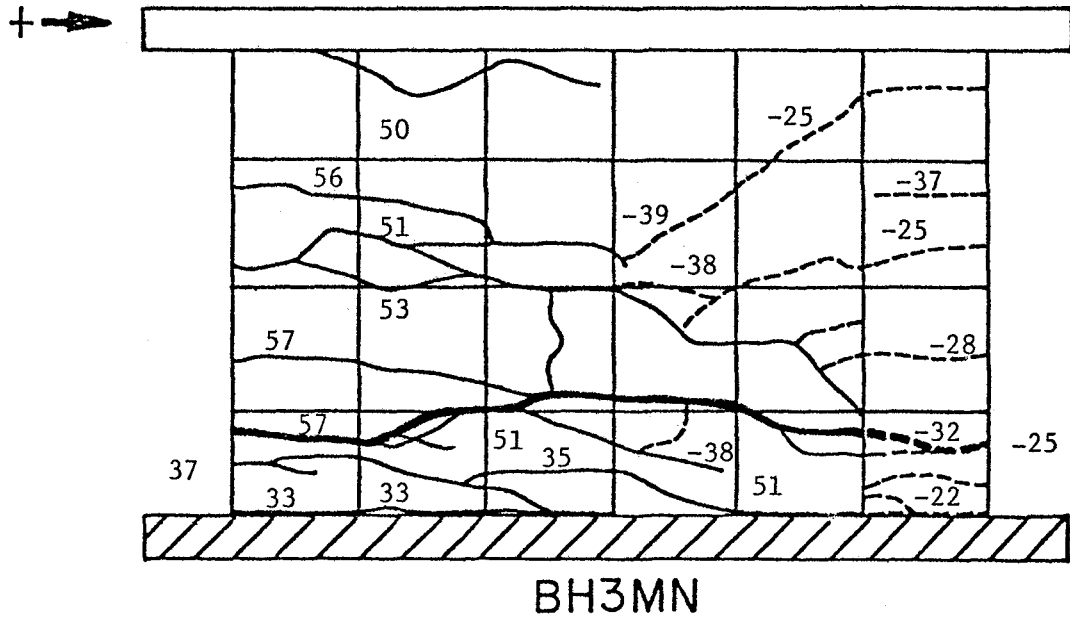
BH3MN

Fig. 3.32   Crack Pattern of BH3MN
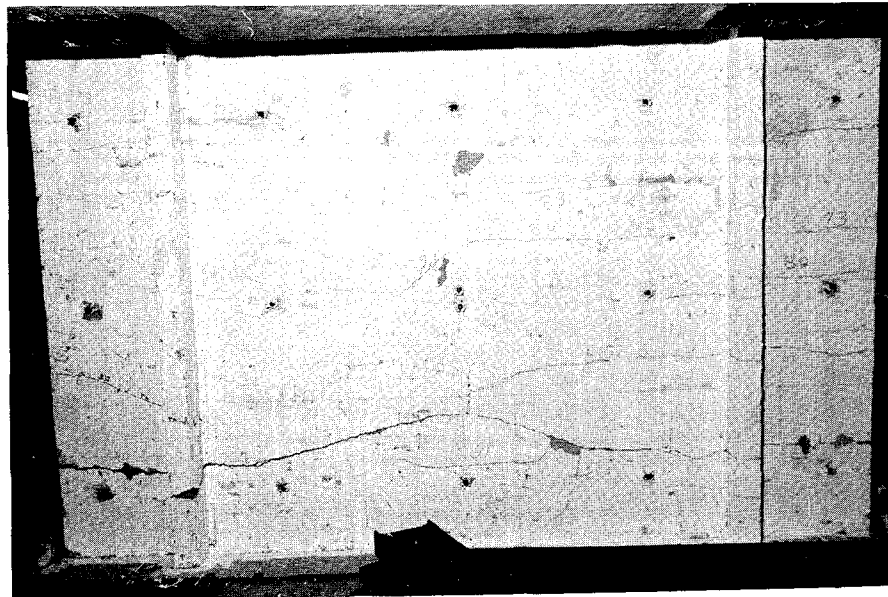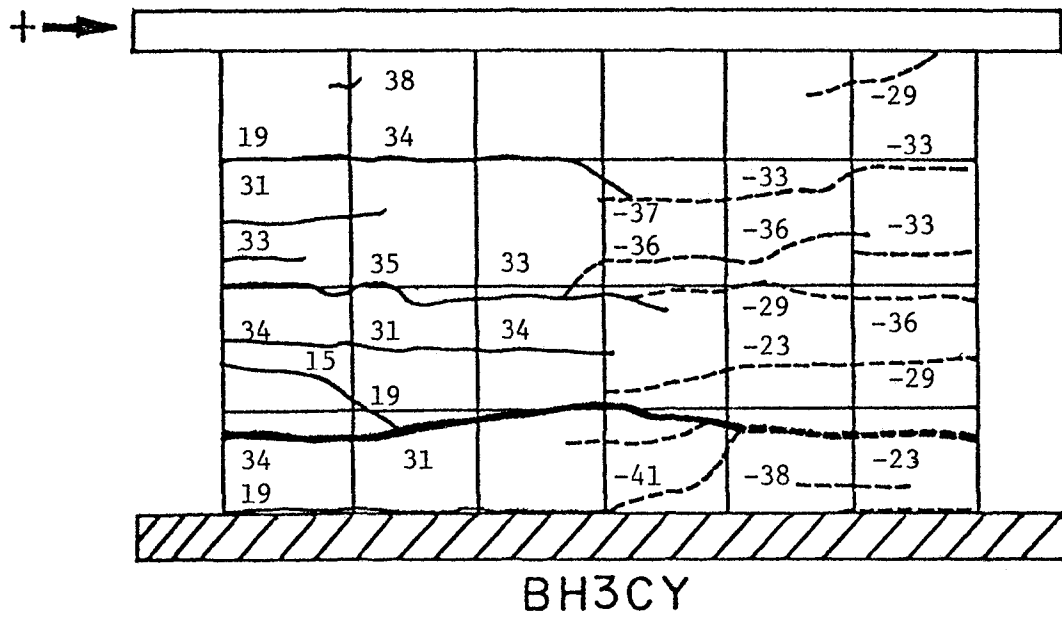
BH3CY

Fig. 3.33 Crack Pattern of BH3CY

BVIMN (top)

BVIMN (bottom)
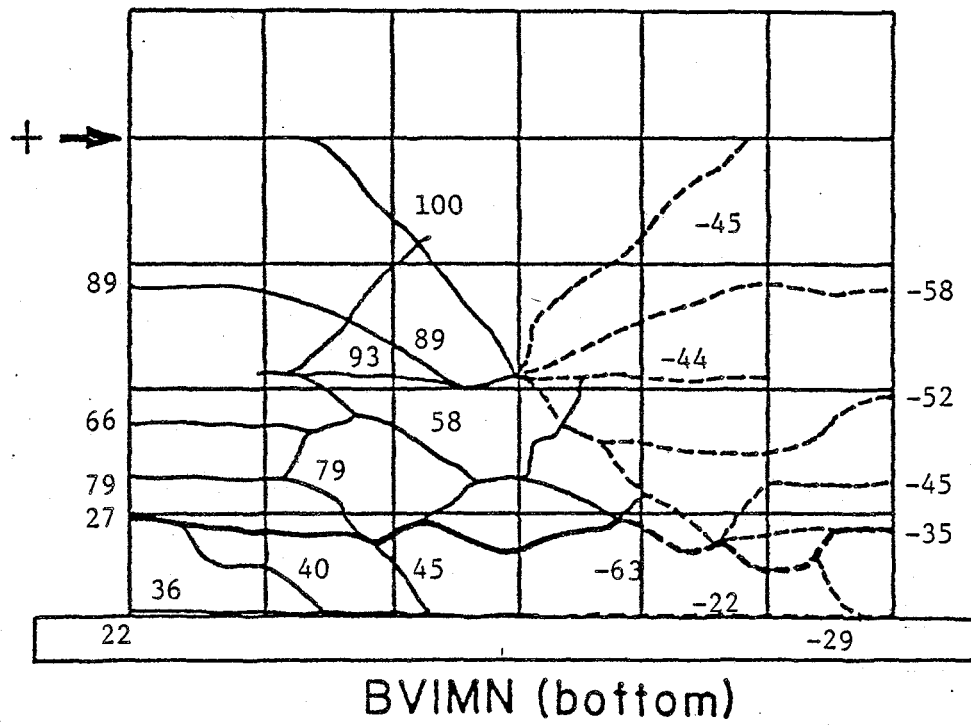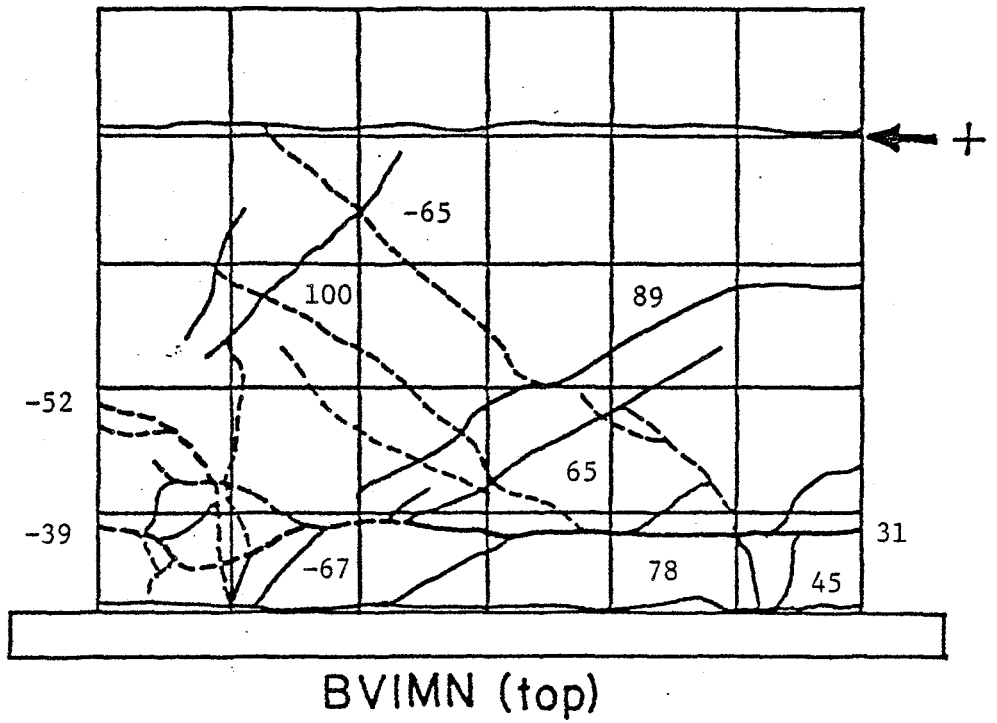
Fig. 3.34   Crack Pattern of BV1MN

BV2CY (top)

BV2CY (bottom)
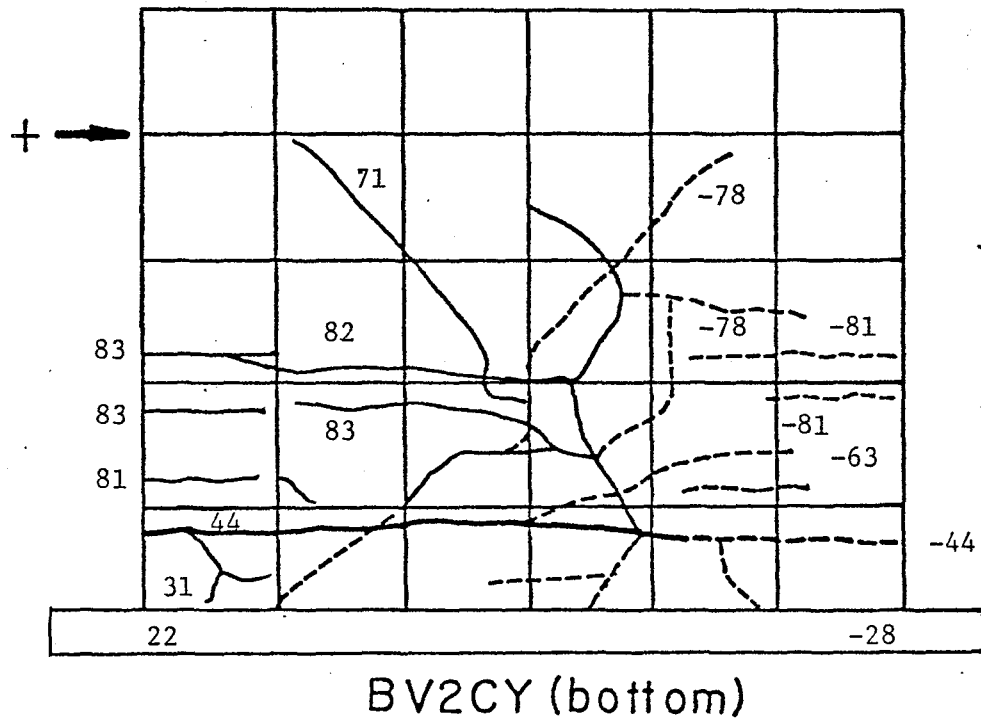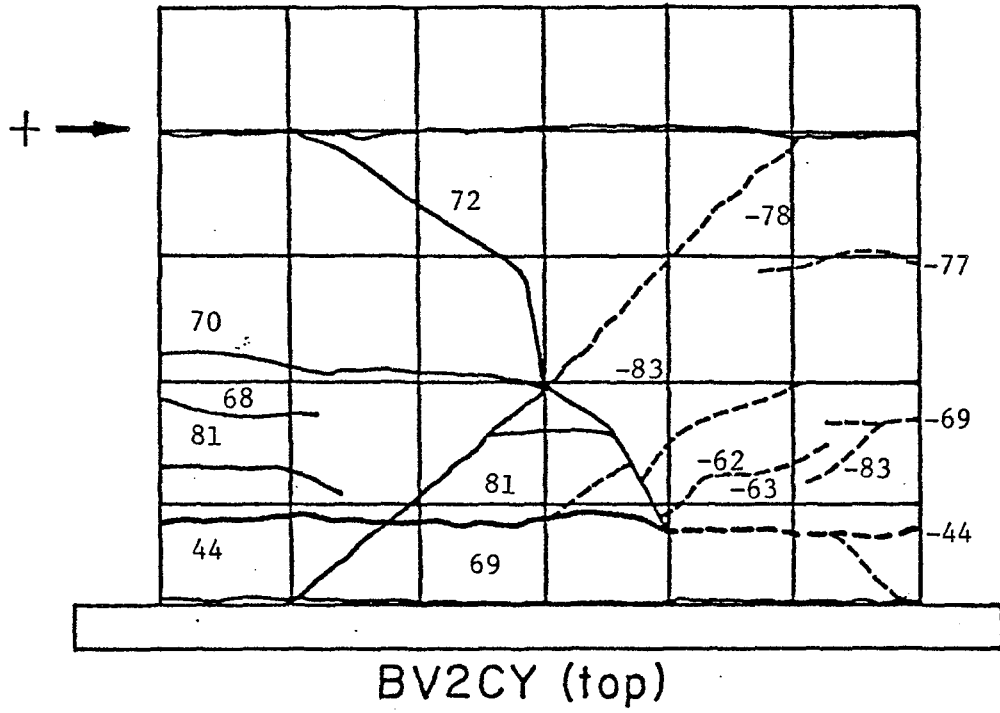
Fig. 3.35 Crack Pattern of BV2CY
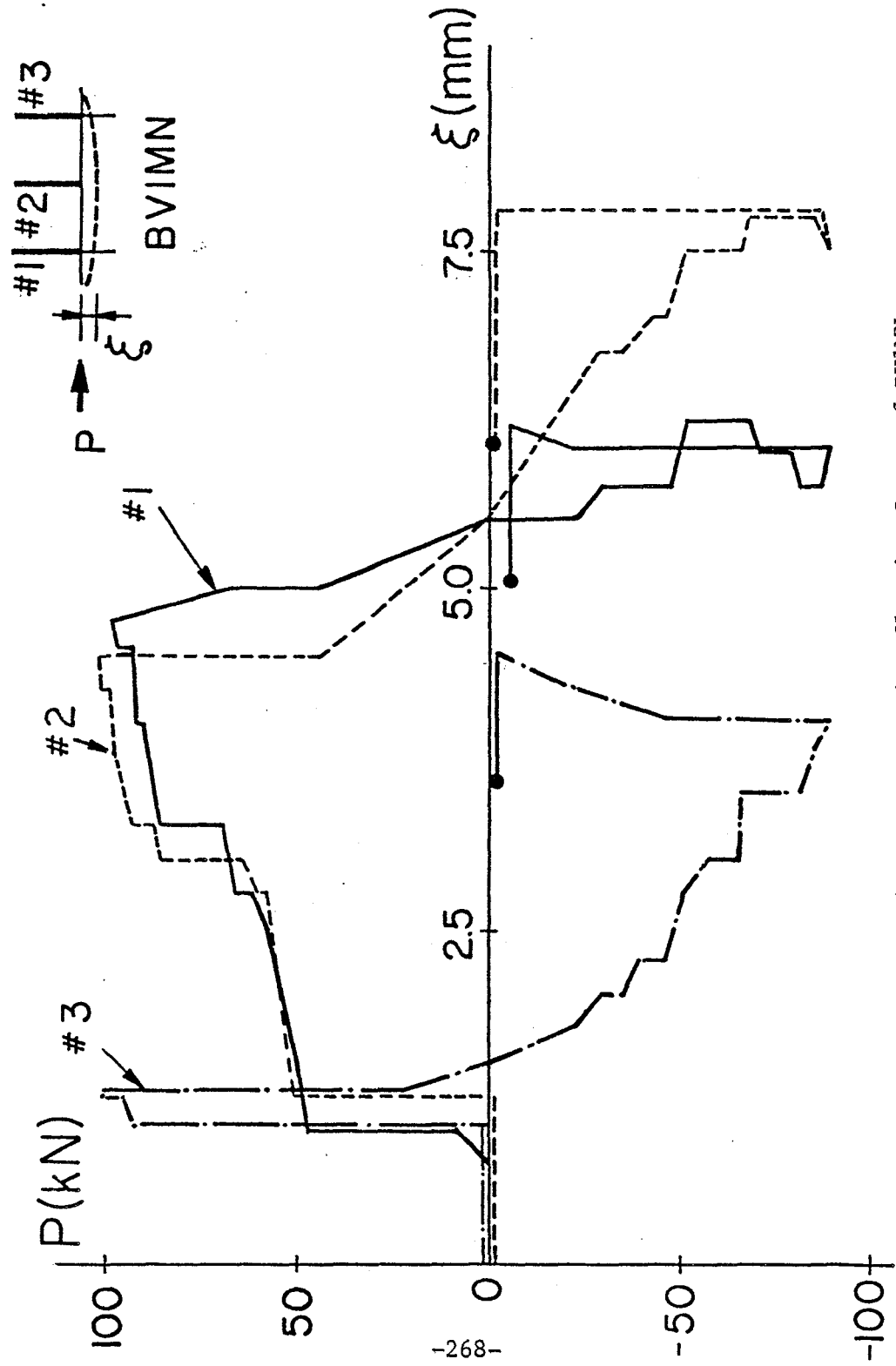
Fig. 3.36 Load-Vertical Deflection Curve of BV1MN
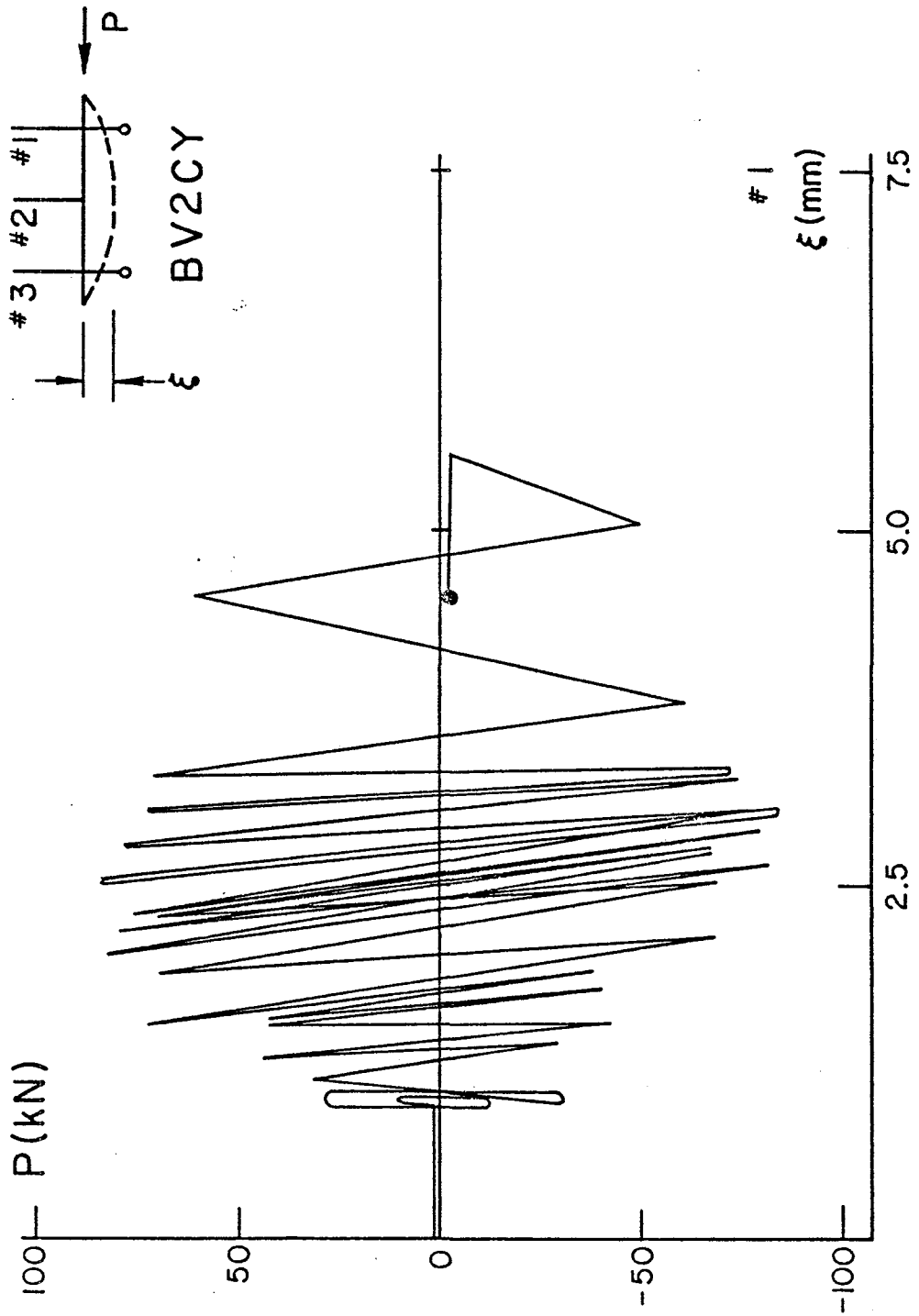
Fig. 3.37(a)   Load—Vertical Deflection Curve of BV2CY (Scale #1)
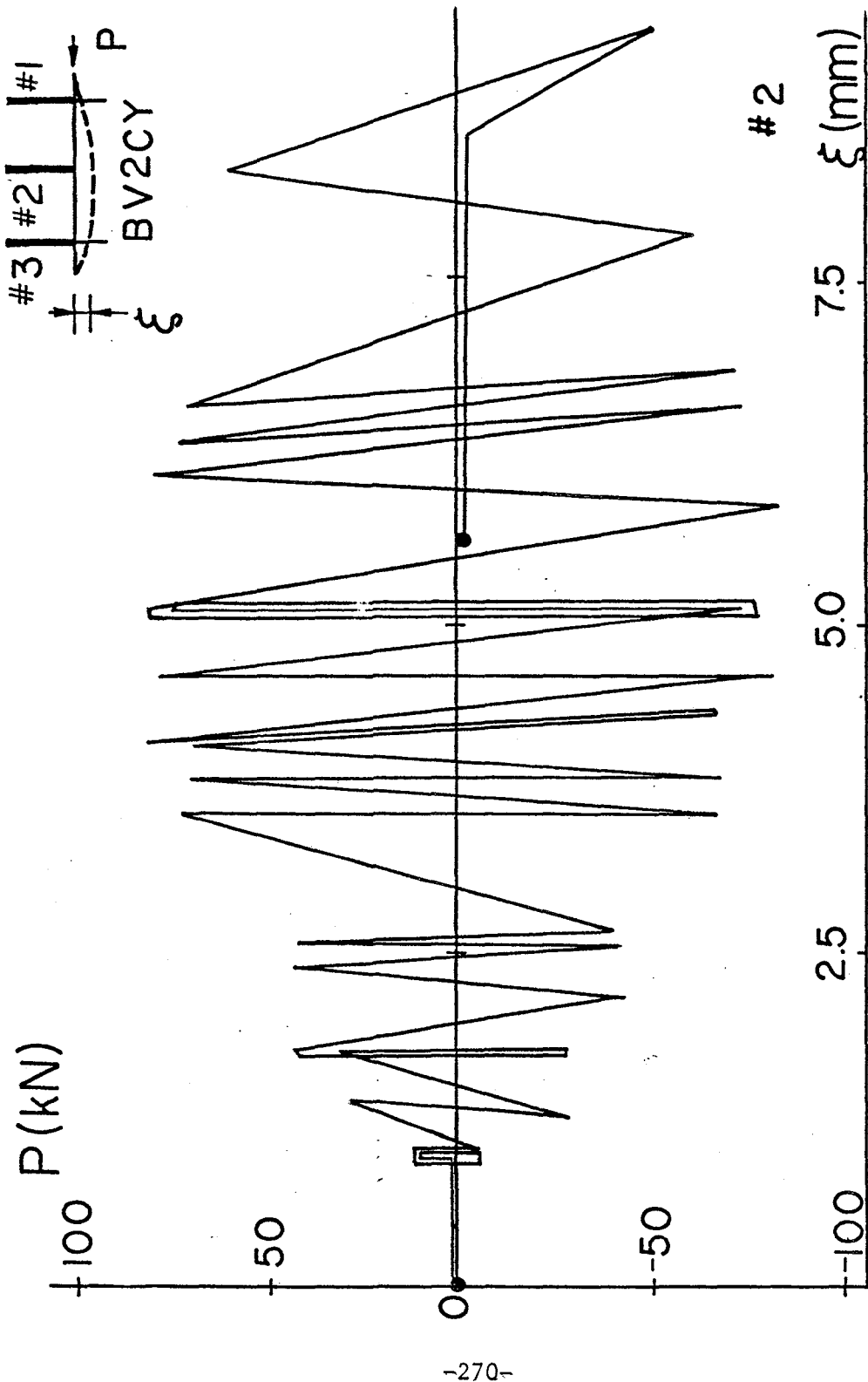
Fig. 3.37(b) Load-Vertical Deflection Curve of BV2CY (Scale #2)
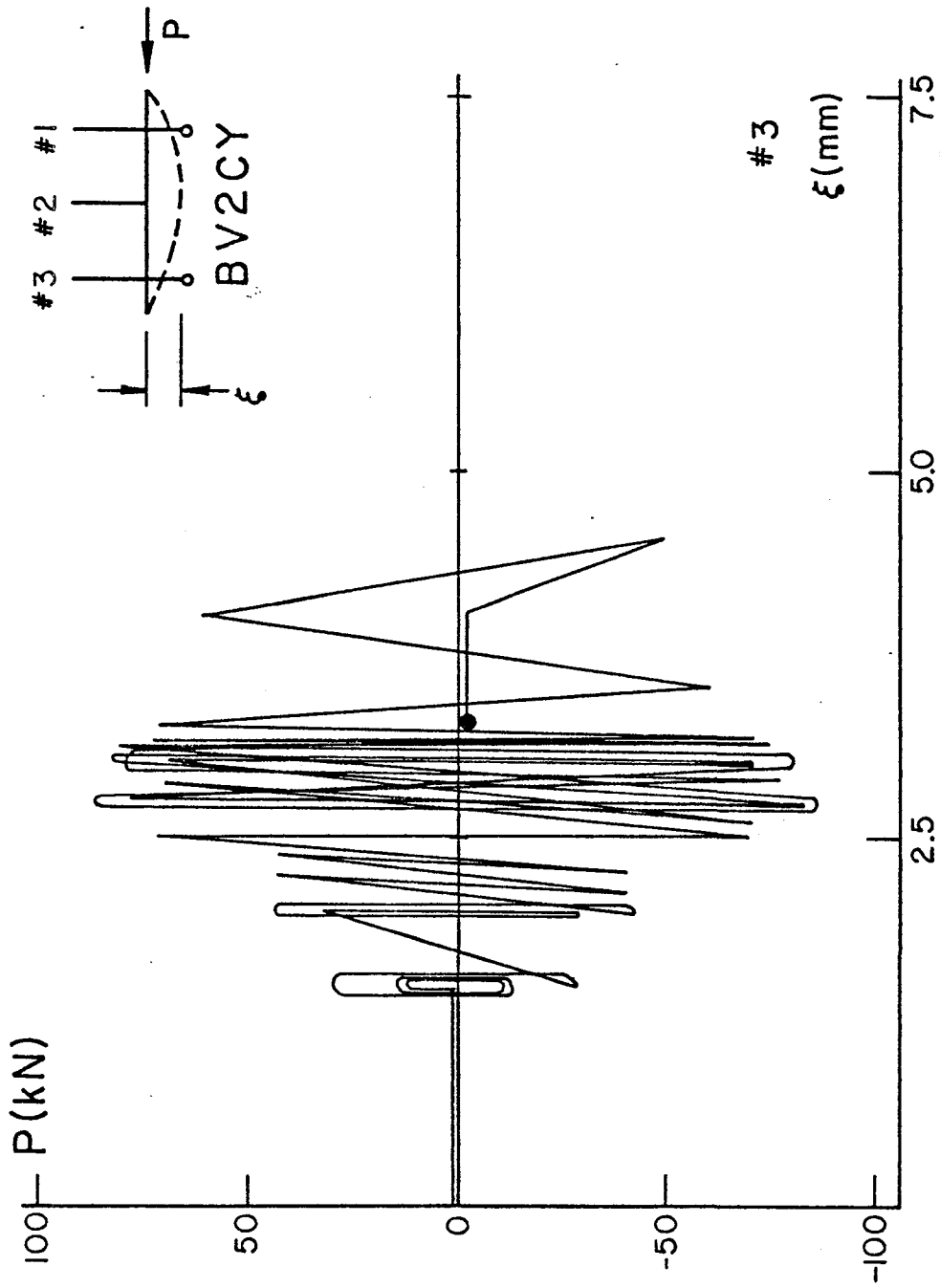
Fig. 3.37(c) Load-Vertical Deflection Curve of BV2CY (Scale #3)
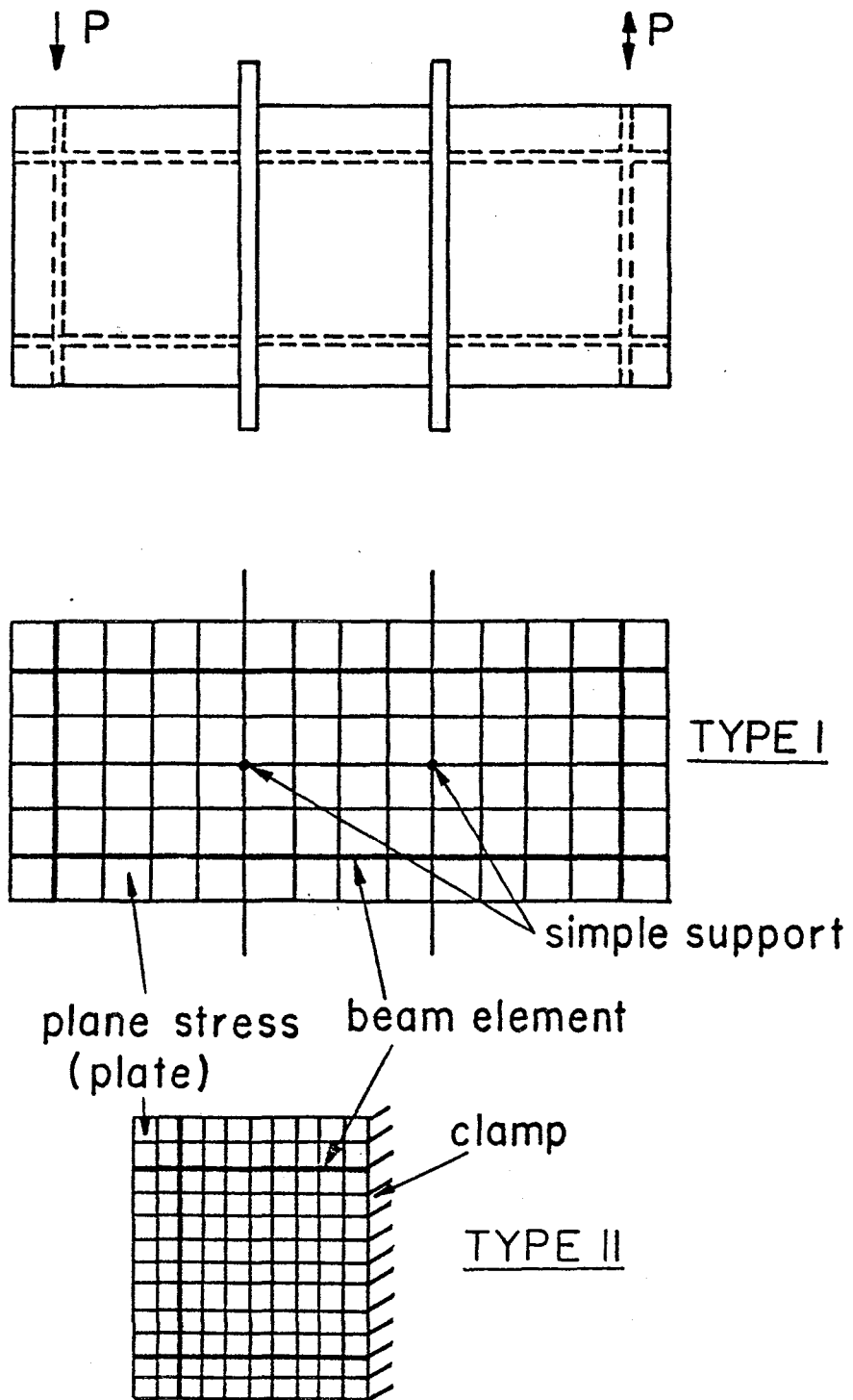
Fig. 3.38 Finite Element Model of Test Slab
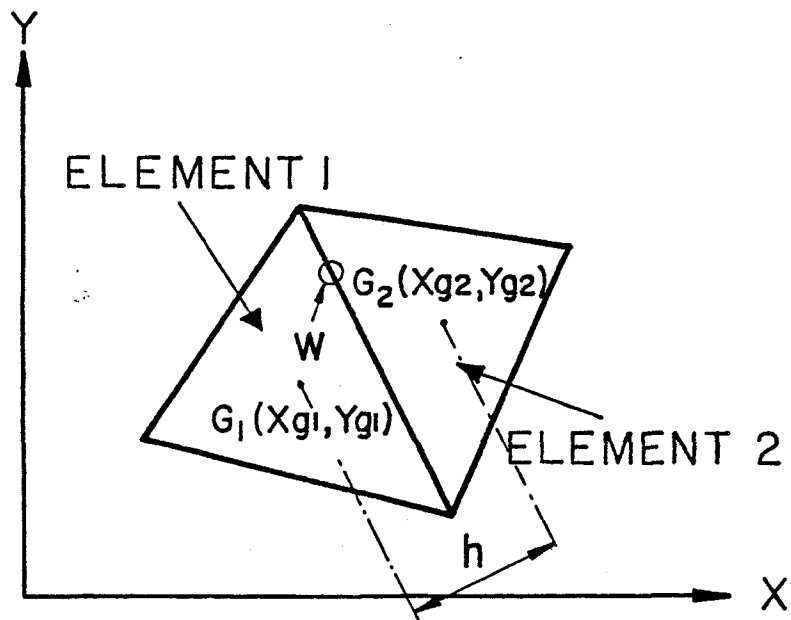
Fig. 4.1   Two Rigid Triangular Elements
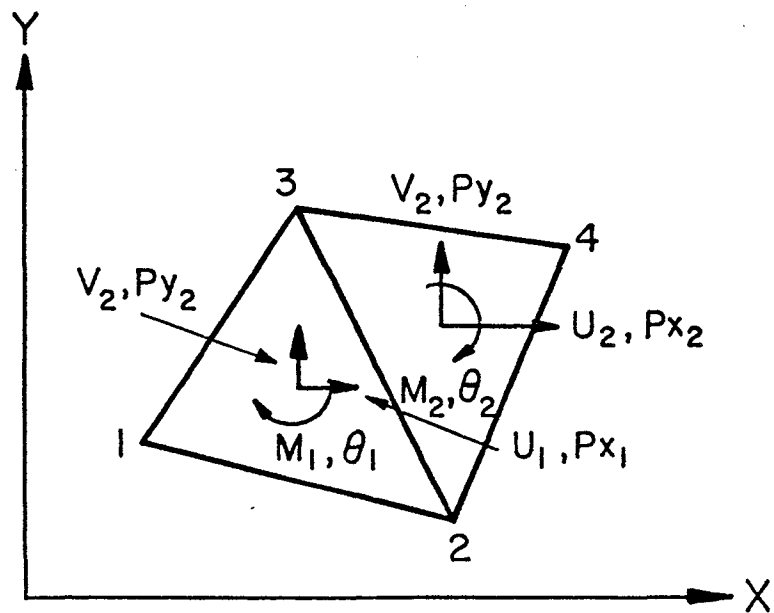
Fig. 4.2   Displacement, Rotation, Force, and
Moment of Triangular Elements
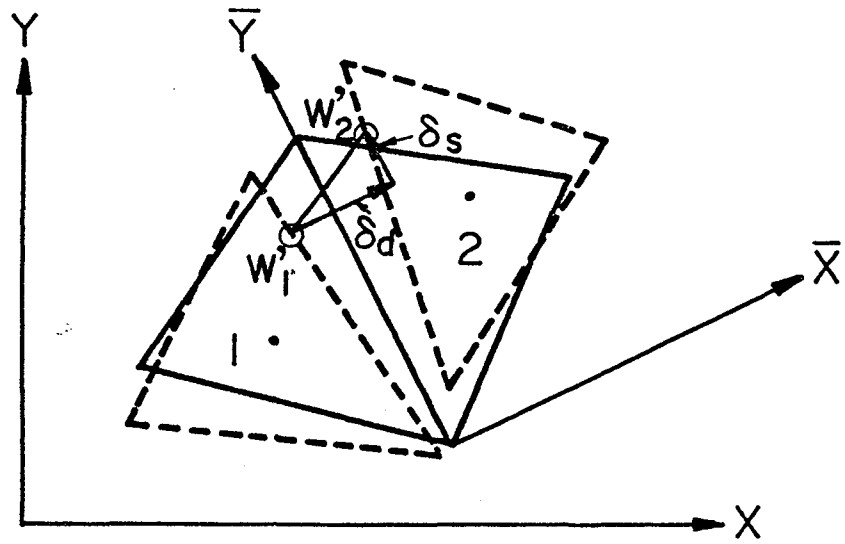
Fig. 4.3 Relative Displacement of Two
Triangular Elements
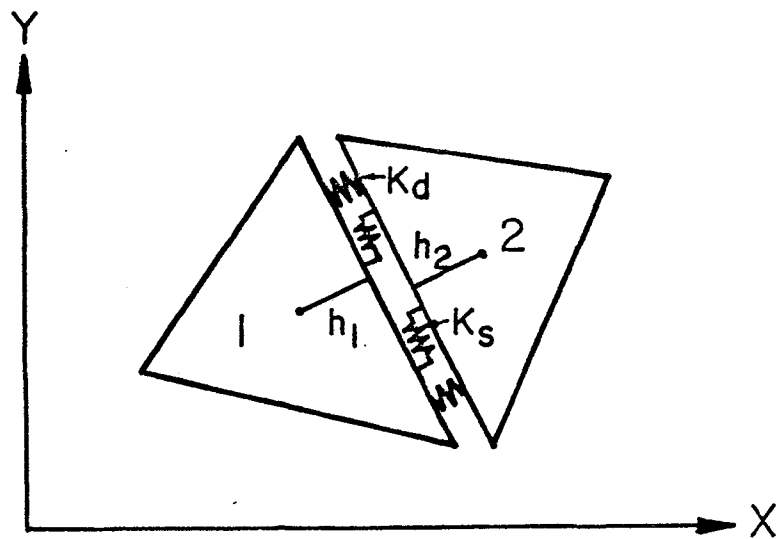
Fig. 4.4 Normal and Shear Springs Along Interface
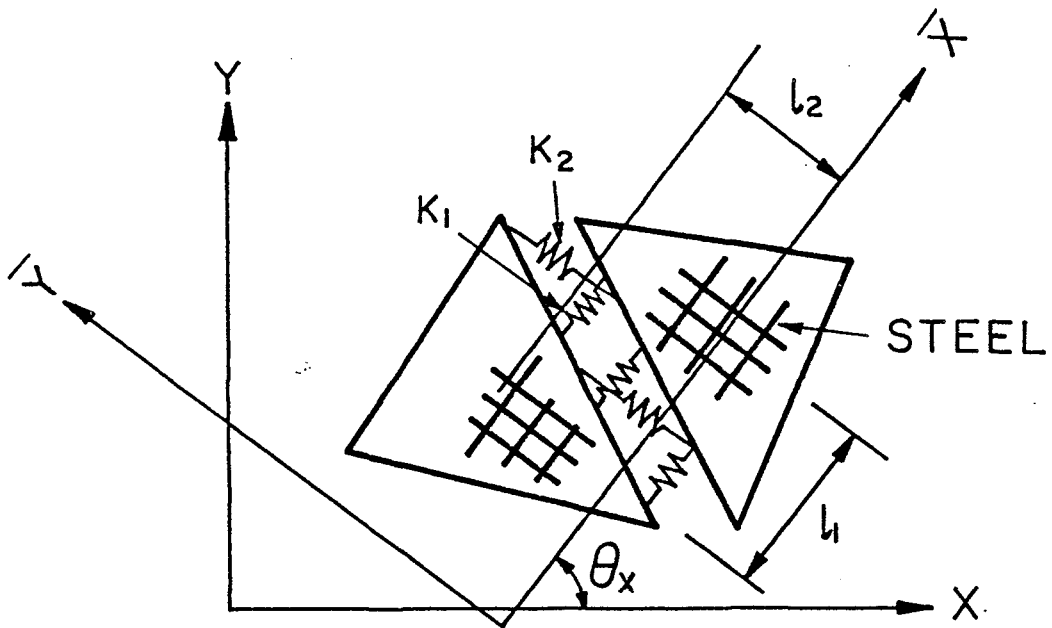
Fig. 4.5   Orthogonal Reinforcement
(Smeard Triangular Elements)
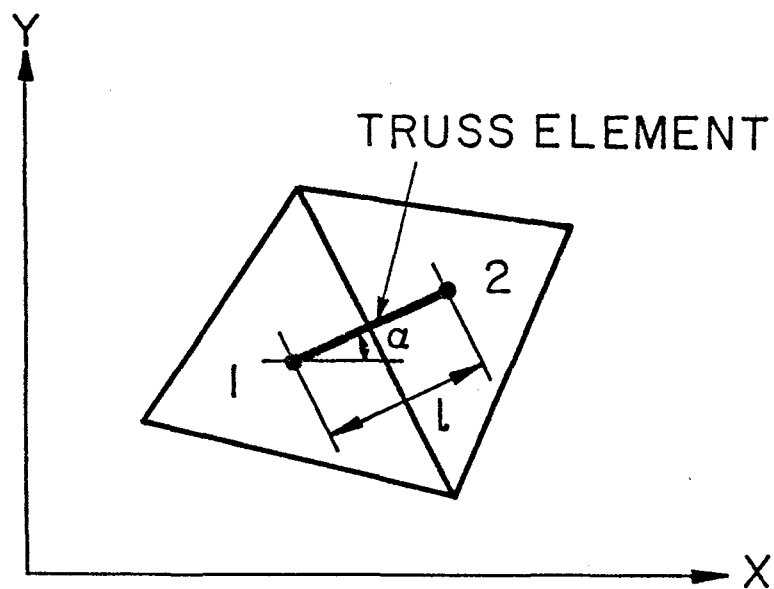
Fig. 4.6   Truss Element
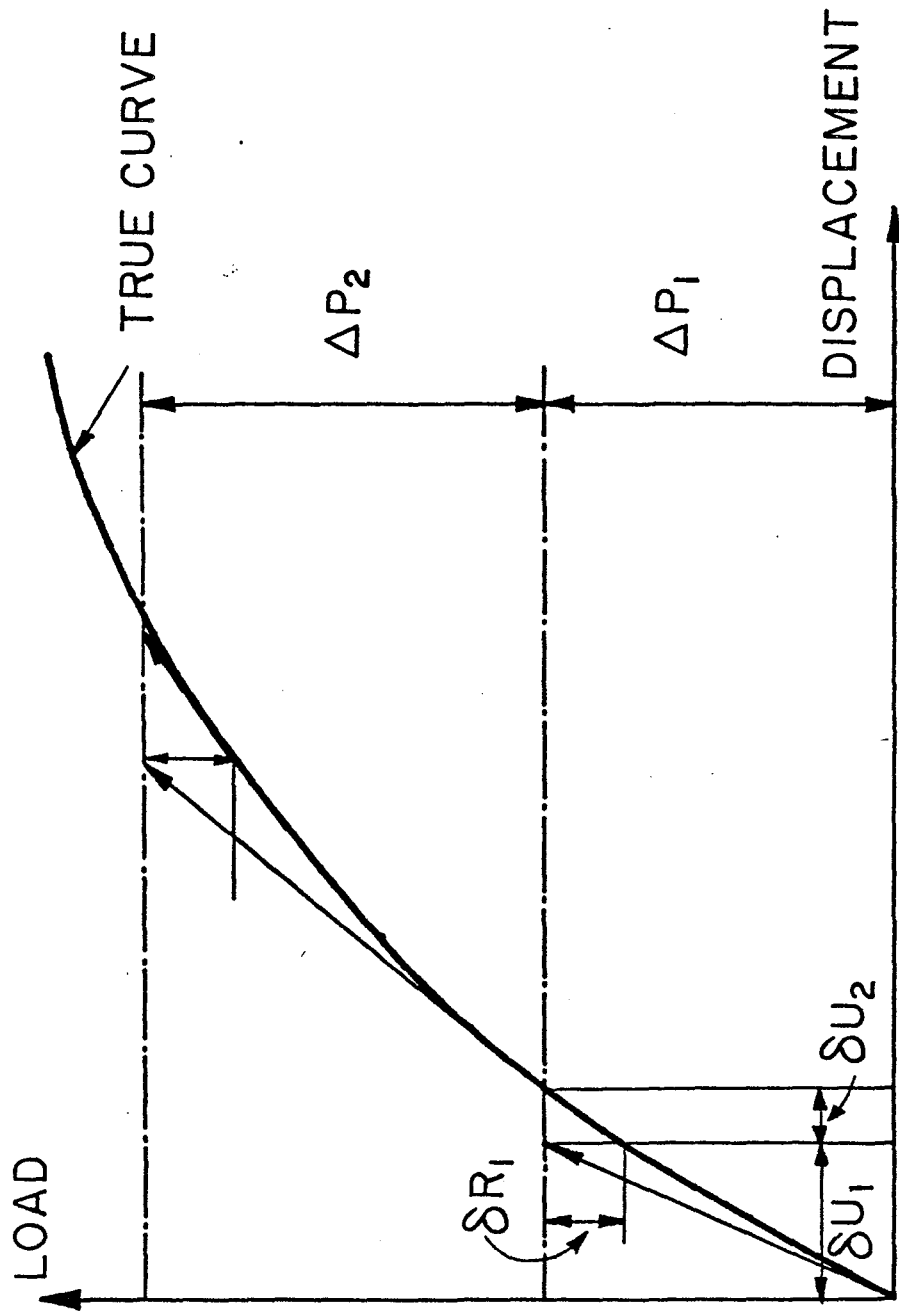
Fig. 4.7 Iteration Procedure (Initial Stress Method)
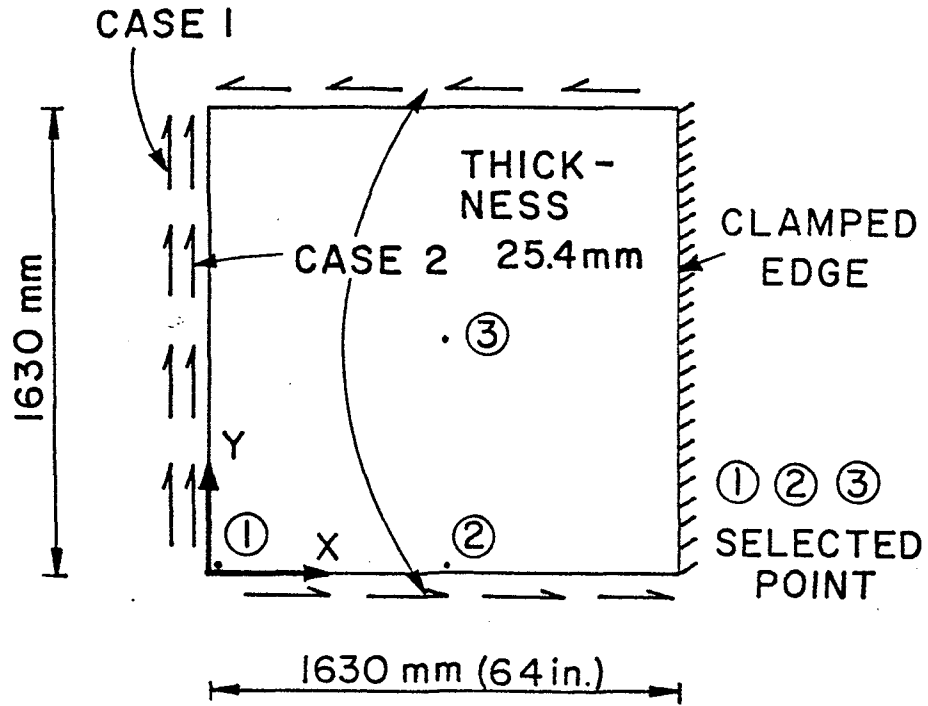
Fig. 4.8   Example Problem, Plate With
a Clamped Edge

PROPOSED MODEL   SAP IV
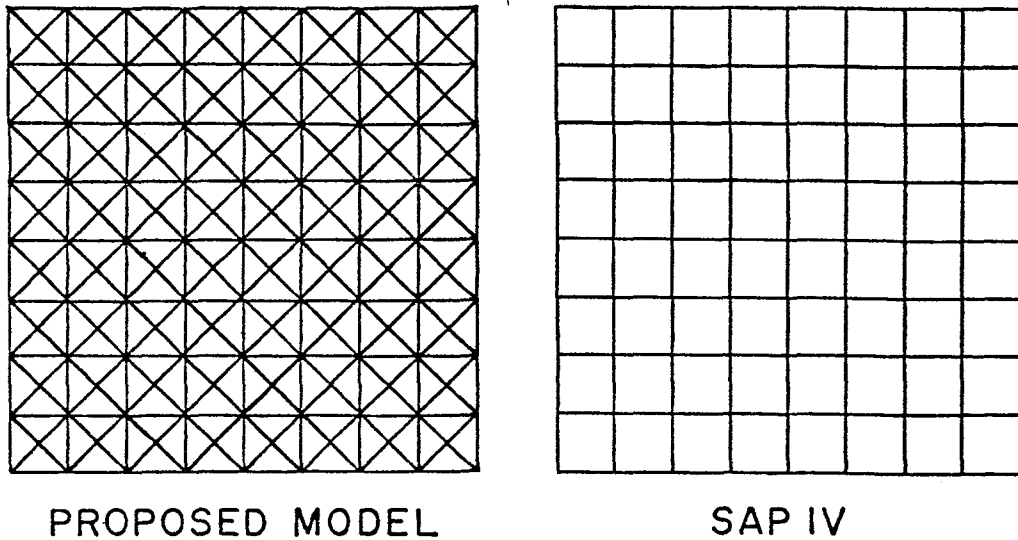
Fig. 4.9   Discretization of Plate (Example Problem)
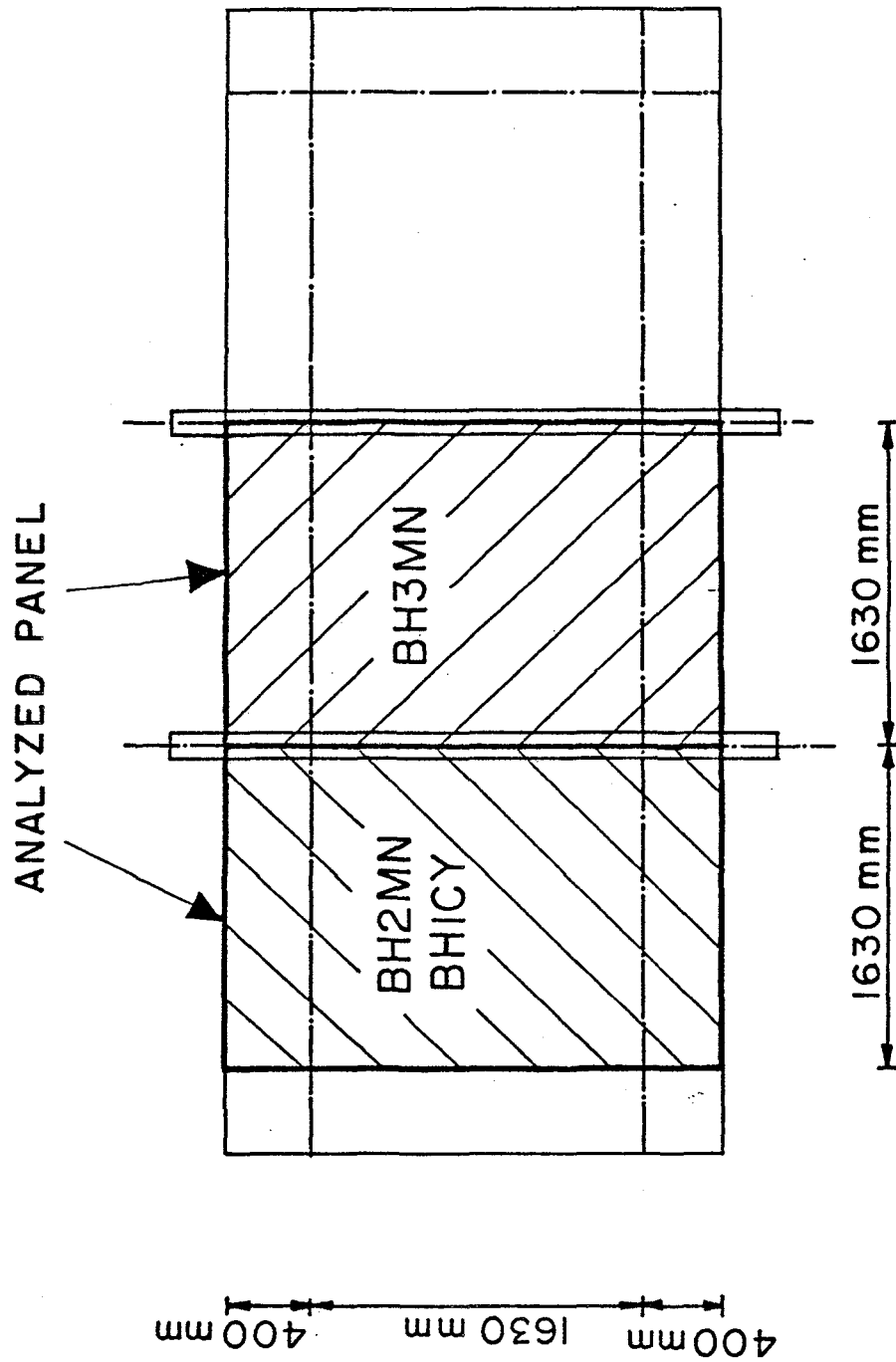
Fig. 4.10 Analyzed Slab Panel (BH2MN, BH3MN, BH1CY)
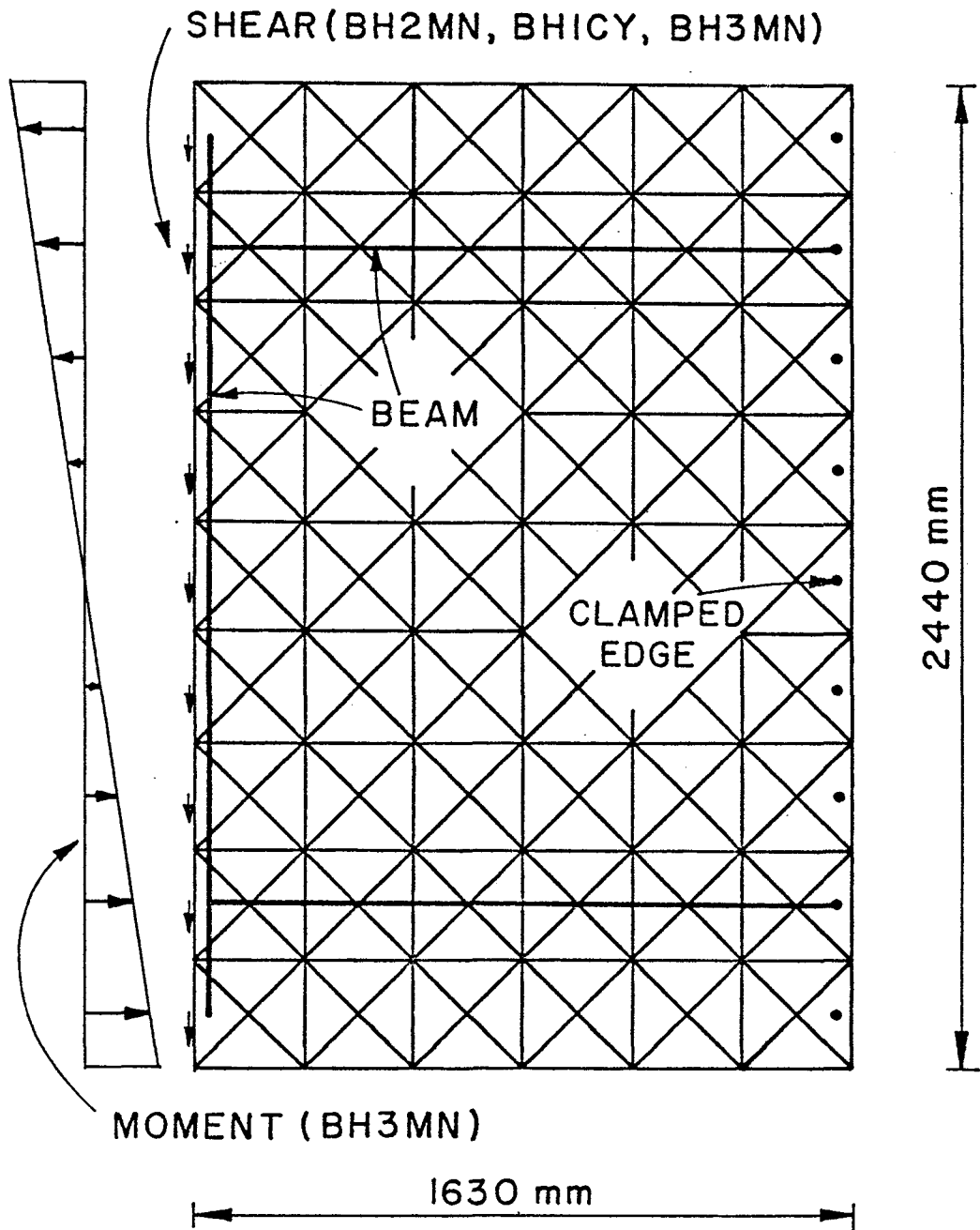
Fig. 4.11 Finite Element Model of Slab Panel
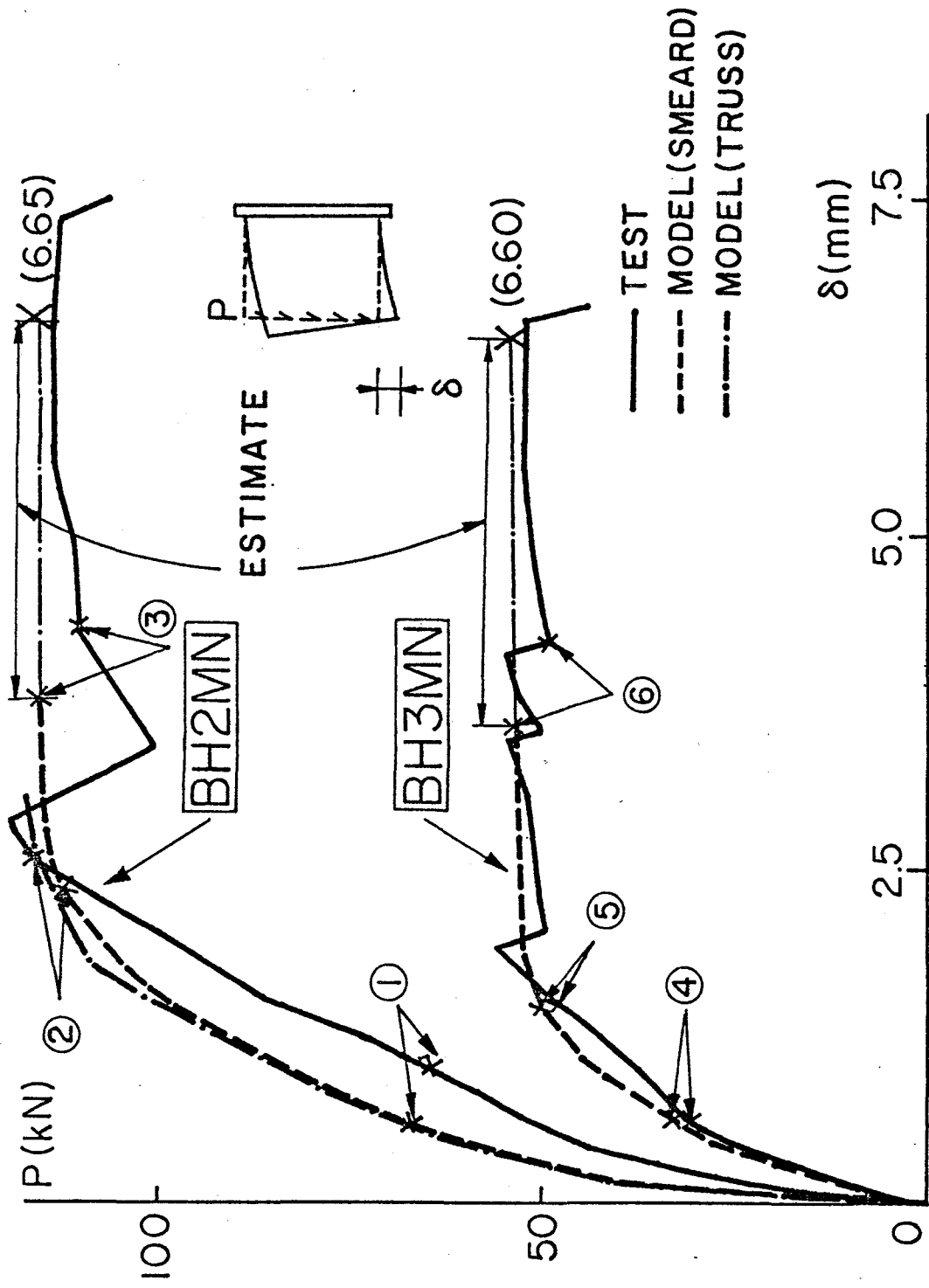
Fig. 4.12 Analytical Load-Deflection Curves (BH2MN, BH3MN)
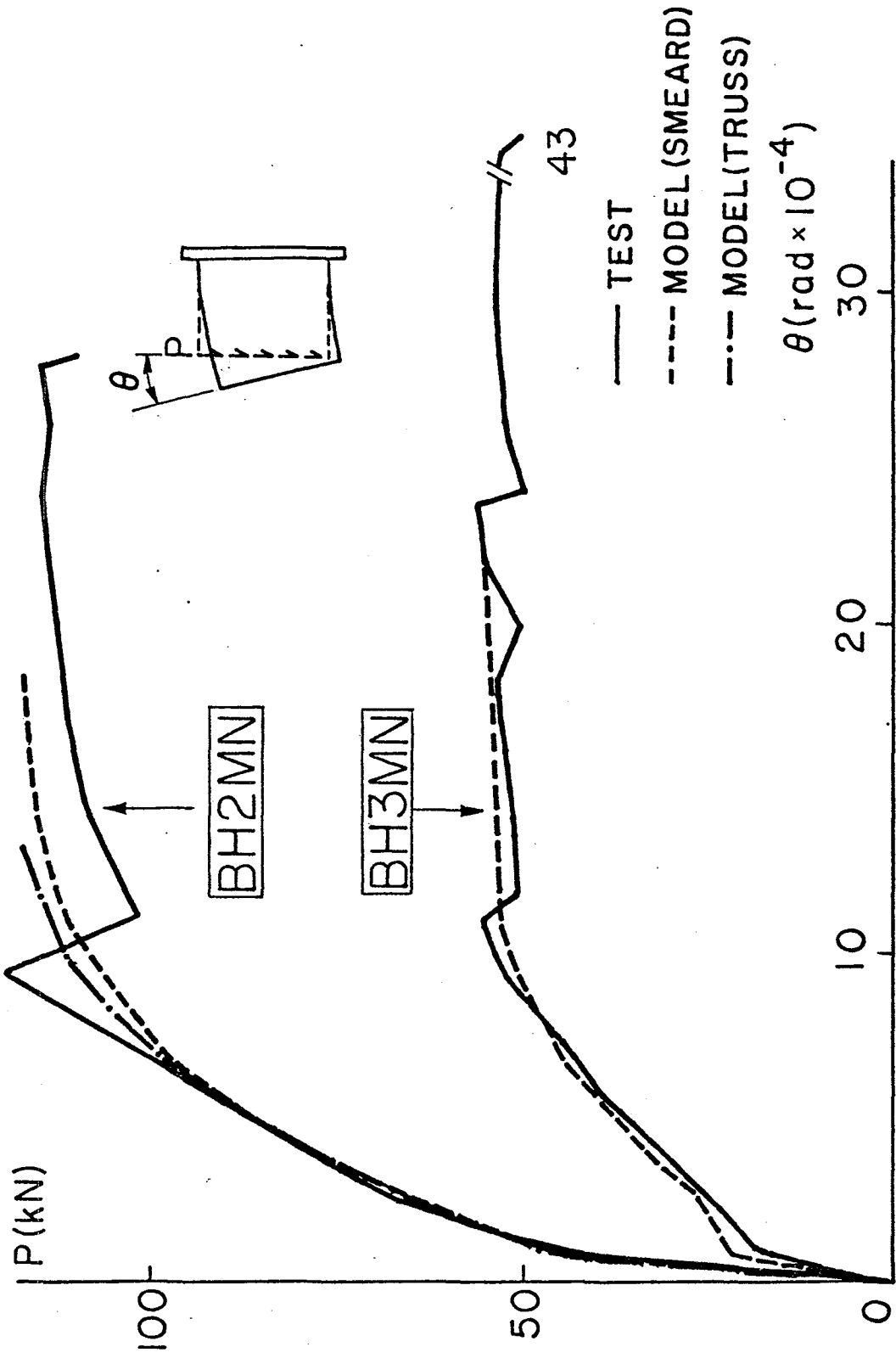
Fig. 4.13 Analytical Load-End Rotation Curves (BH2MN, BH3MN)
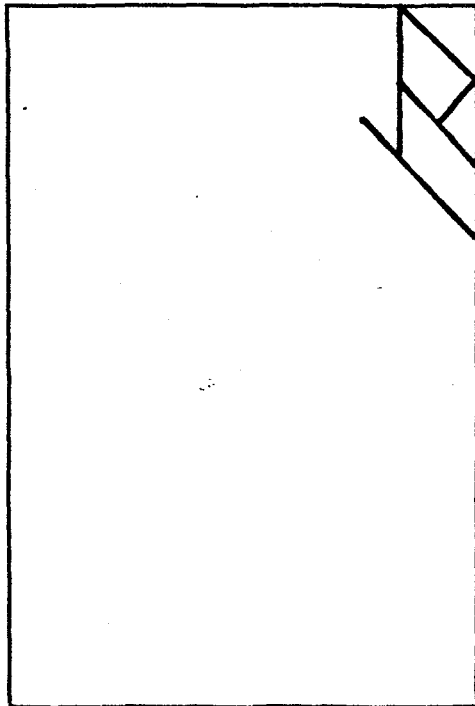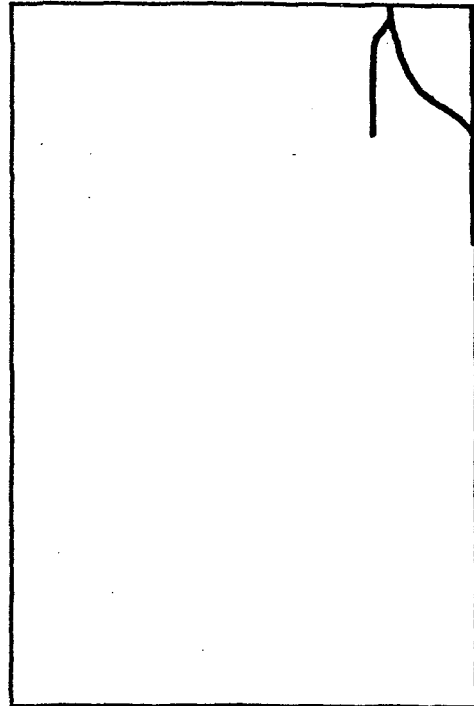
①   P=70kN   BH2MN
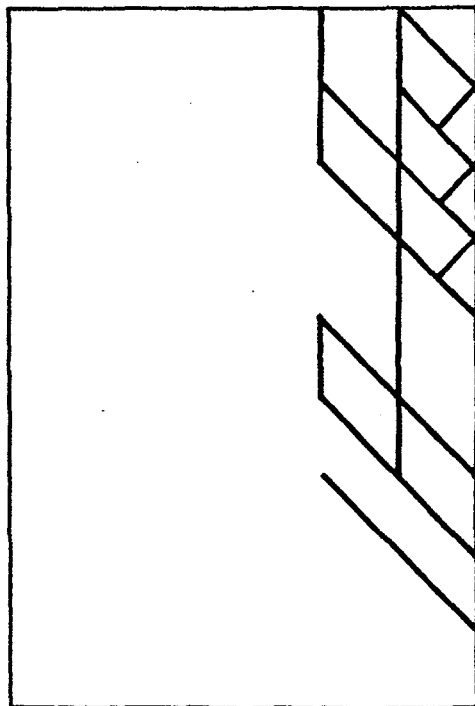
②   P=120kN   BH2MN
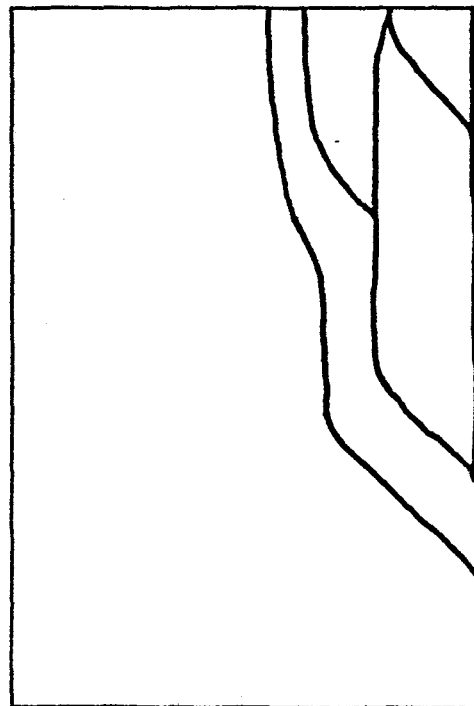
Fig. 4.14   Analytical Crack Patterns (BH2MN)
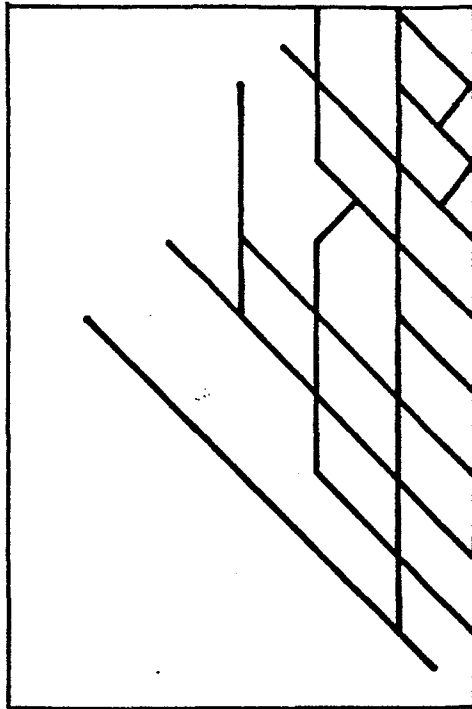
③   P = ULTIMATE   BH2MN
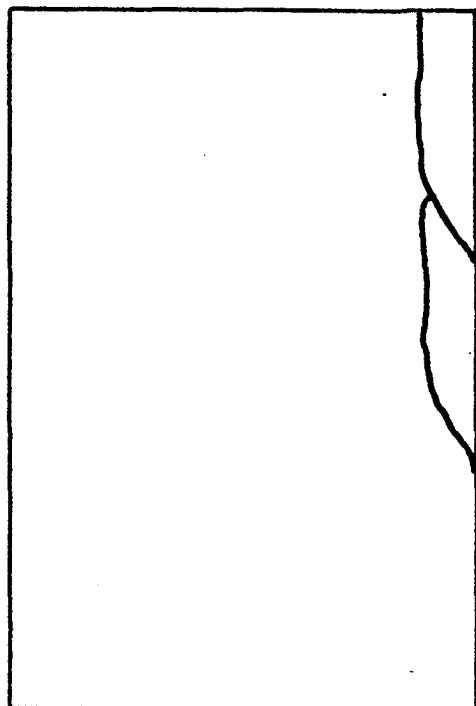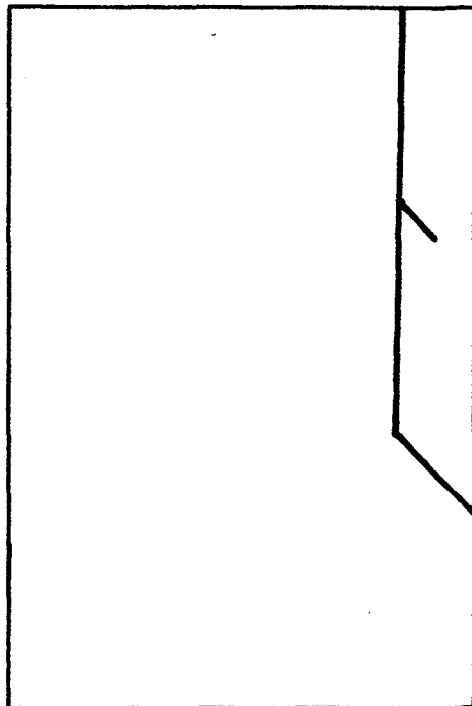
④   P = 36 kN   BH3MN

Fig. 4.14(continued)   Analytical Crack Patterns (BH2MN, BH3MN)
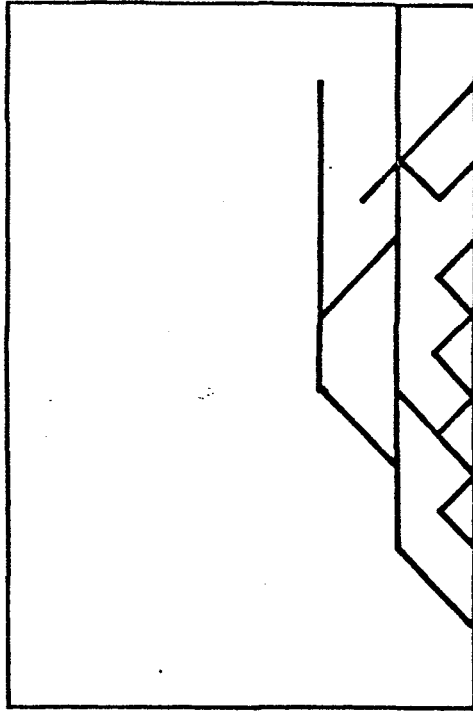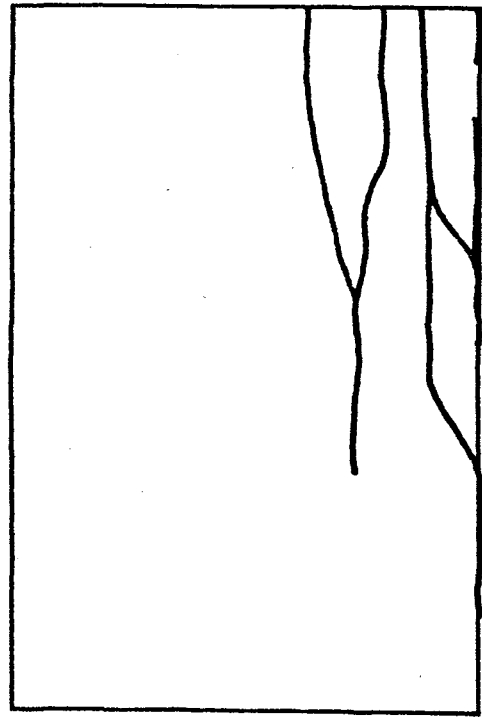
⑤   P = 5lkN   BH3MN
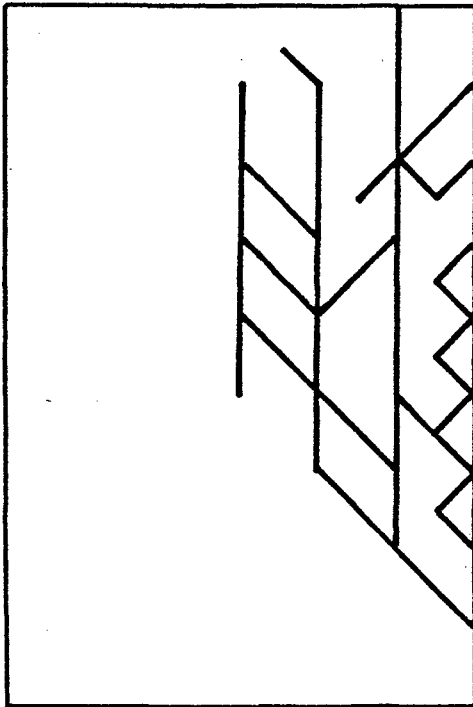
⑥   P = ULTIMATE   BH3MN
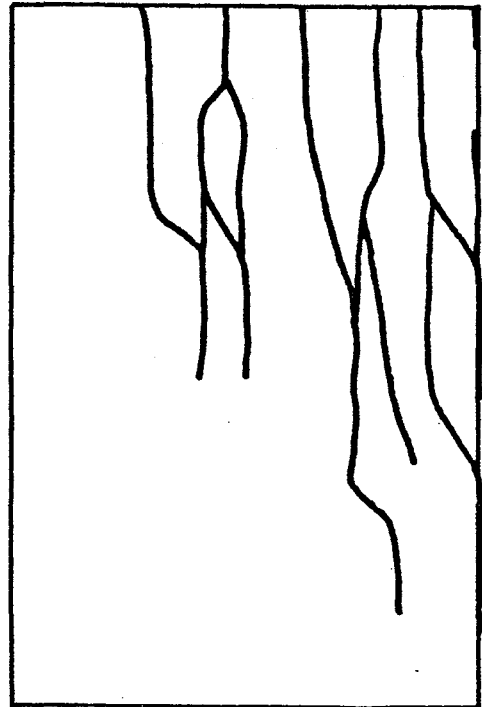
Fig. 4.14(continued) Analytical Crack Pattern (BH3MN)
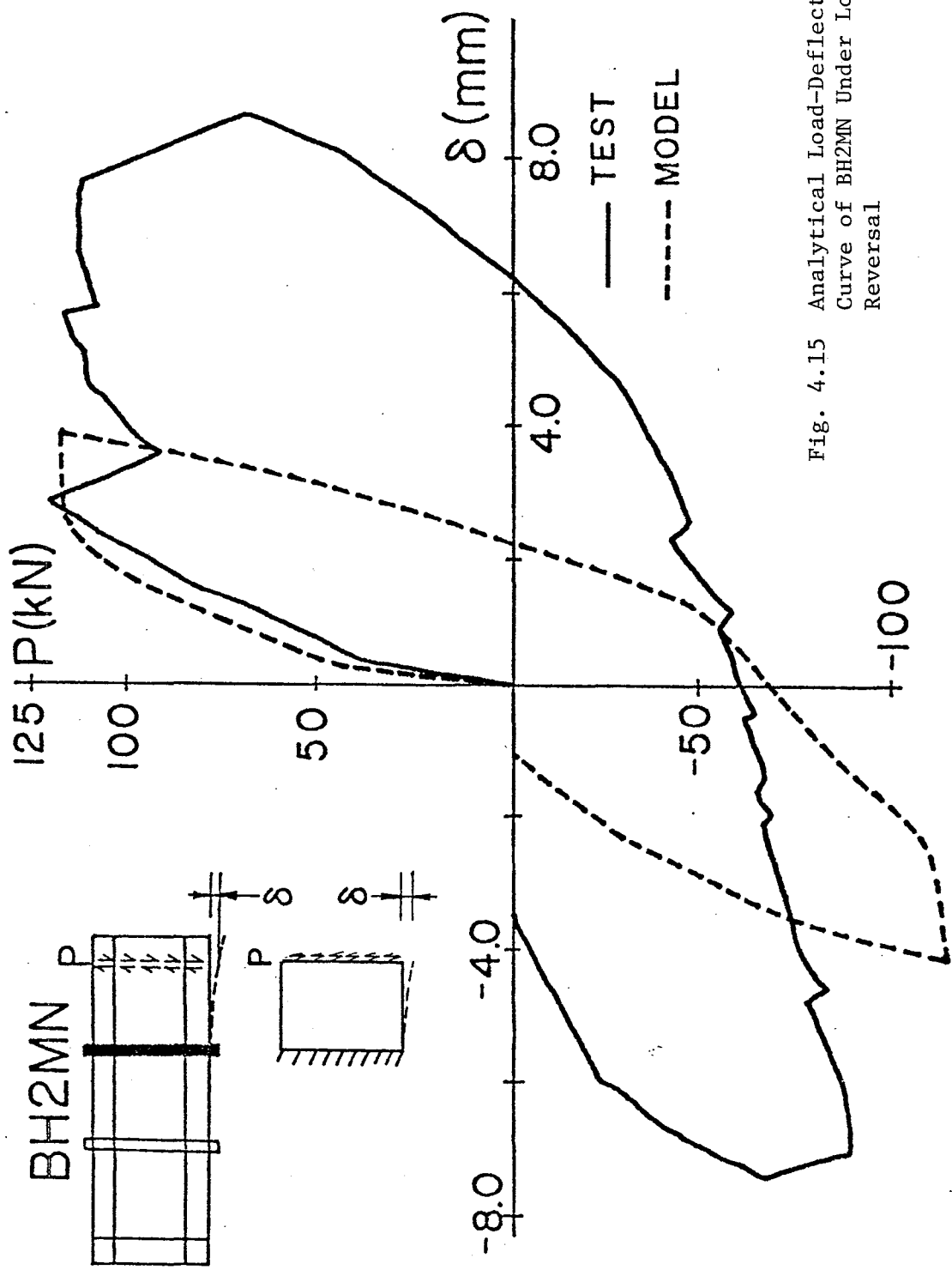
Fig. 4.15 Analytical Load-Deflection Curve of BH2MN Under Load Reversal

EXPERIMENT

—— POSITIVE LOADING
---- NEGATIVE LOADING

MODEL
BH2MN
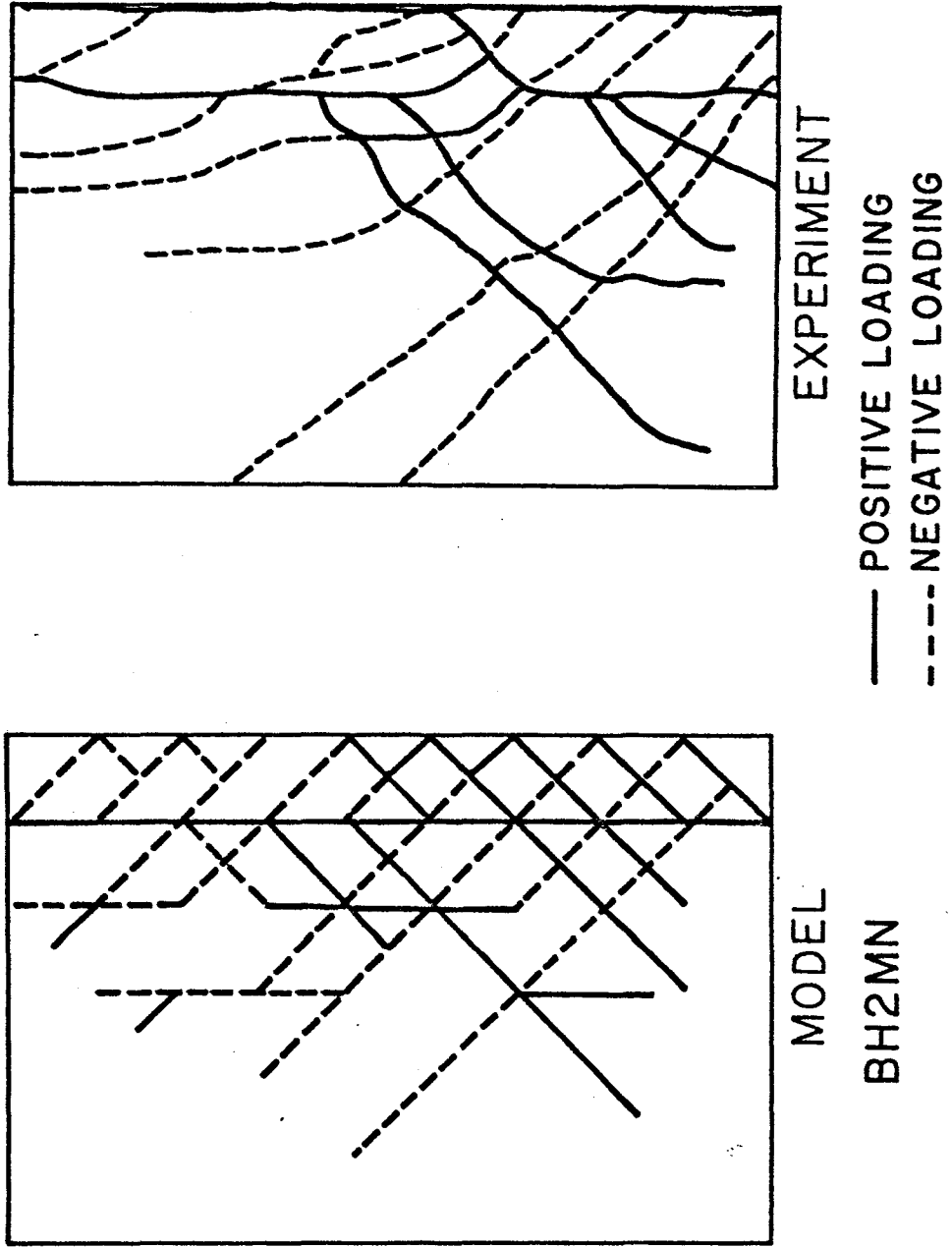
Fig. 4.16   Analytical Crack Pattern of BH2MN Under Load Reversal
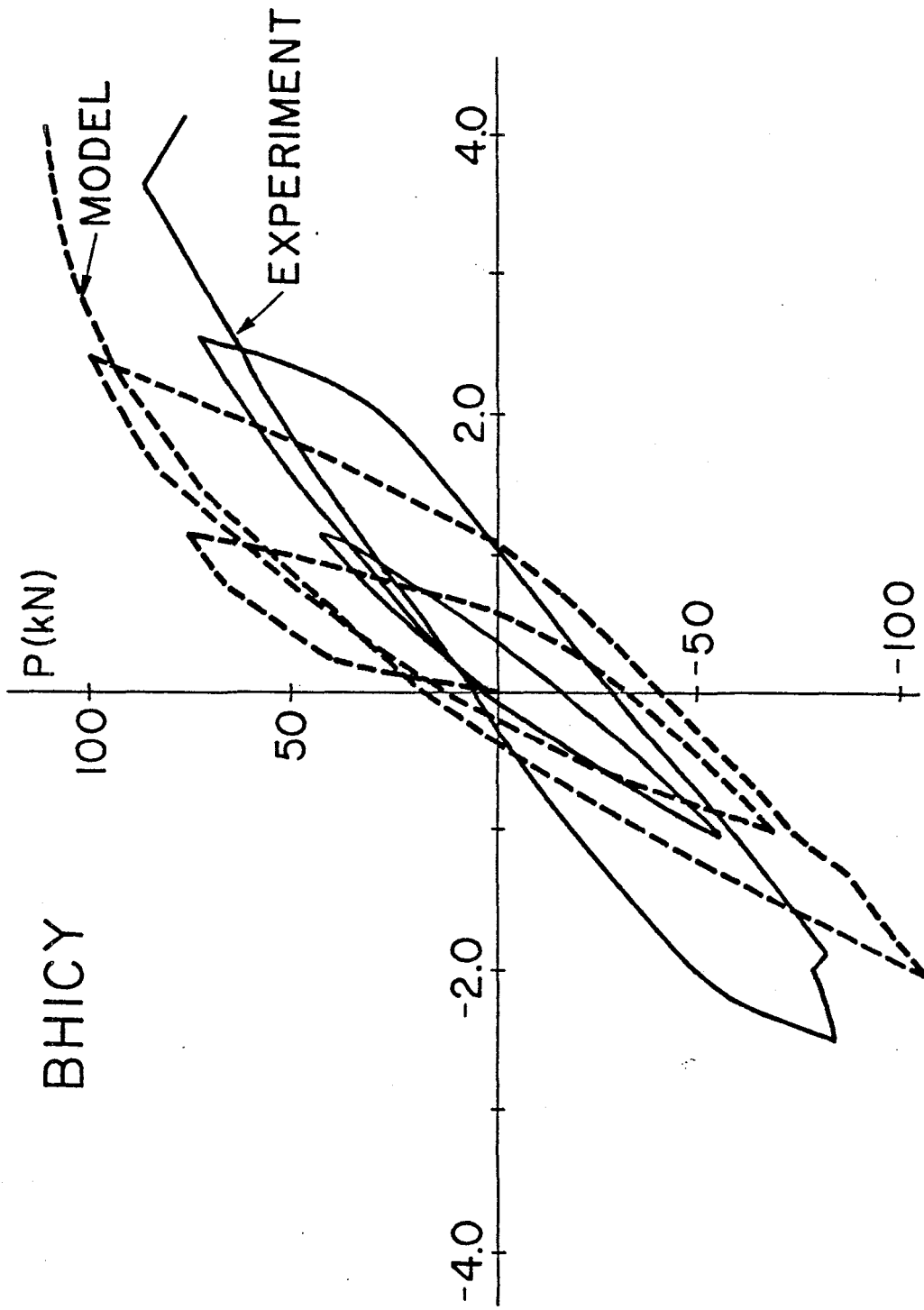
Fig. 4.17 Analytical Load-Deflection Curve of BH1CY
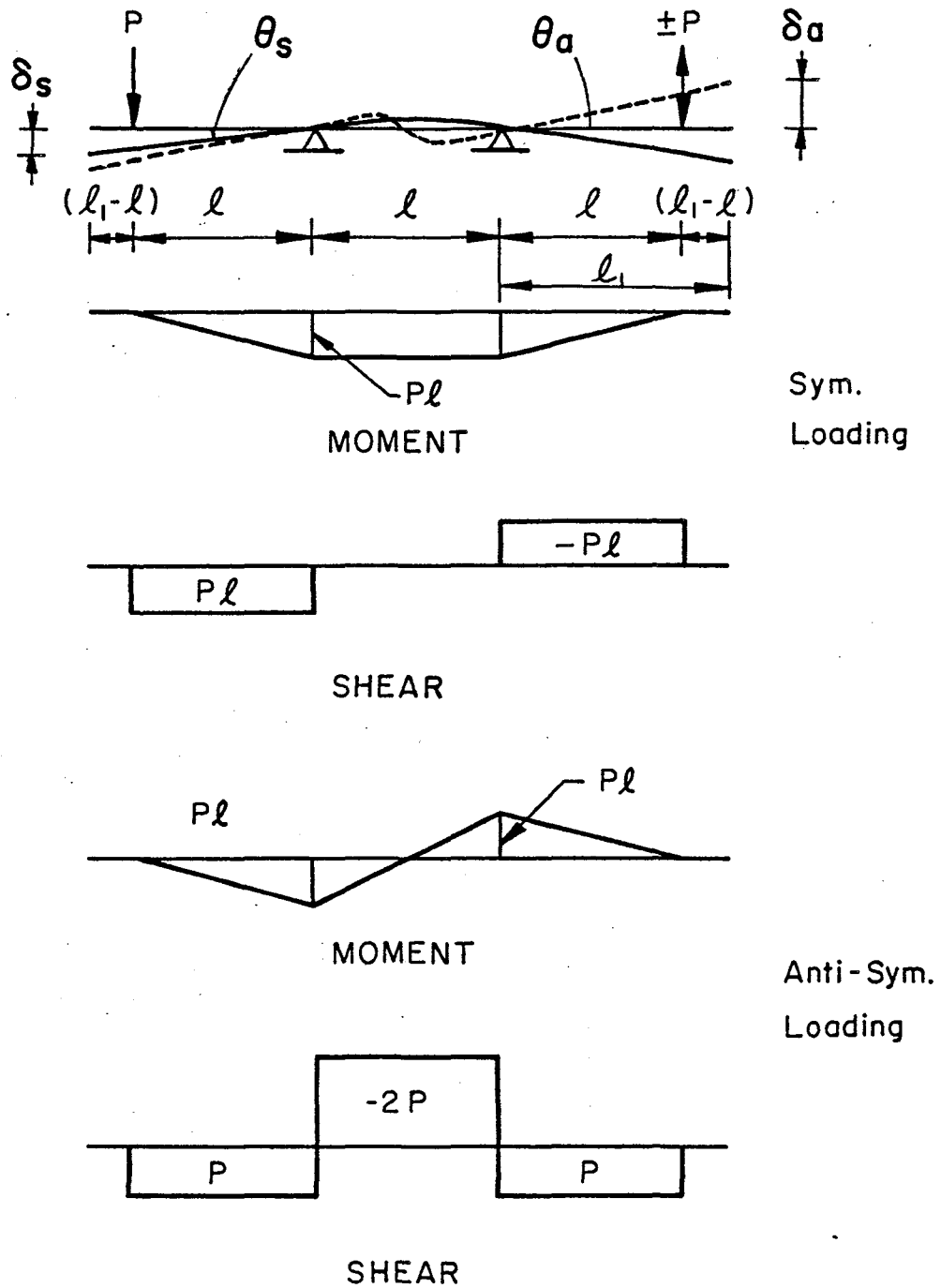
Fig. 5.1   Equivalent Beam Calculation in Stiffness Tests
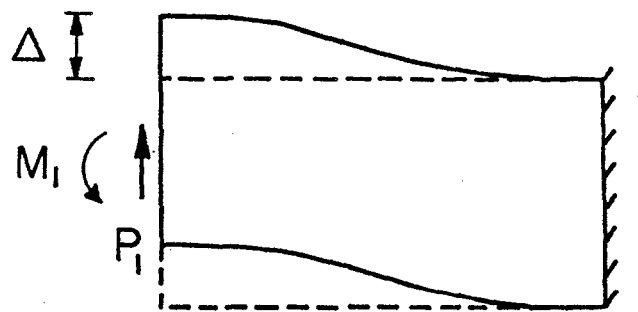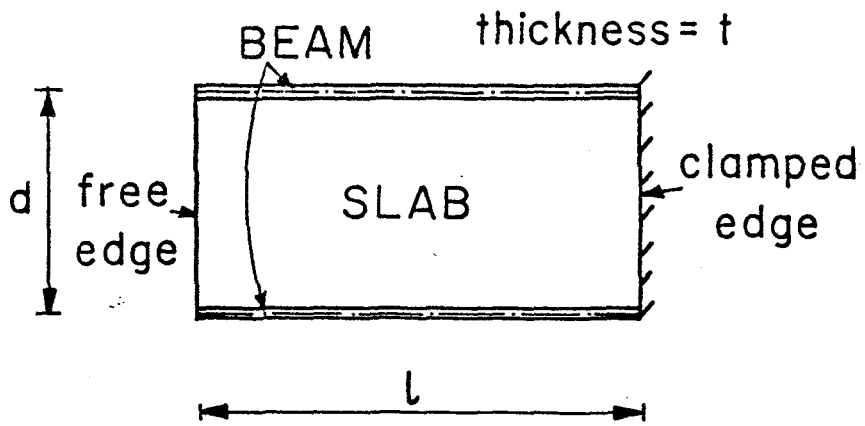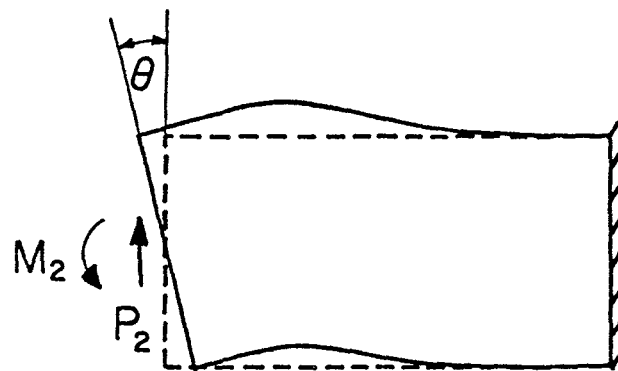
Fig. 5.2   Procedure to Compute Effective Moment of Inertia
and Shear Area
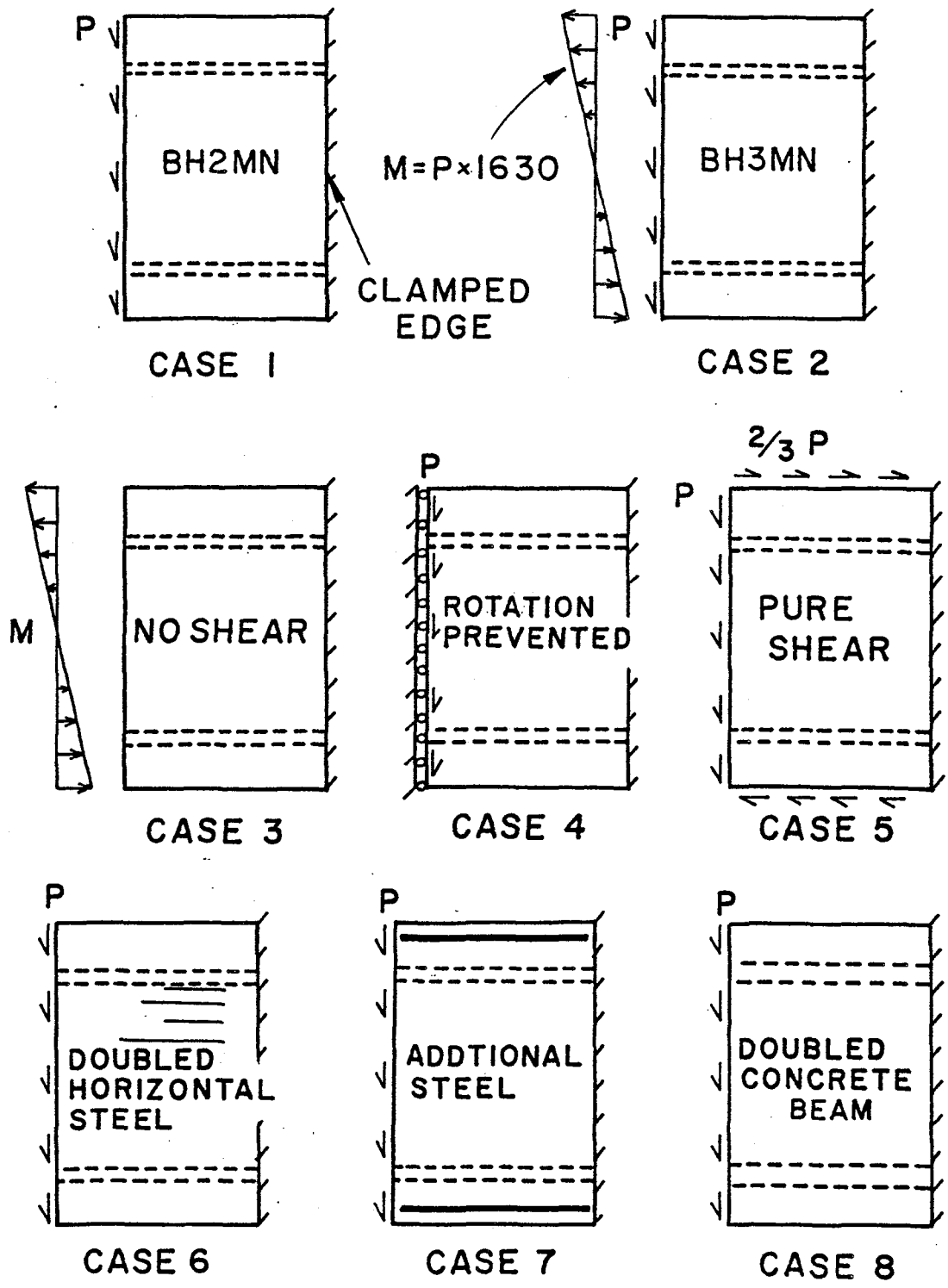
Fig. 5.3 Loading and Boundary Conditions of Analyzed Slab Panels
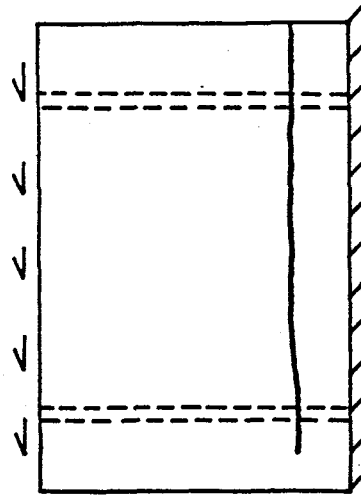
FLEXURAL FAILURE
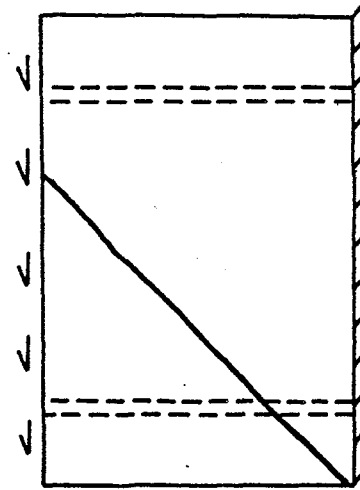
SHEAR FAILURE

$$V_s = \frac{A_v \times f_y \times d}{s}$$

STRONG BEAM

Link

Fig. 5.4   Failure Mode of Analyzed Slab Panels

CRITICAL SECTION

σ_y

ϵ

Φ (CURVATURE)

M

P

Φ

M

$M = T_t \times l_1 + T_c \times l_2 + C \times l_3$

T_t

T_c

C

l_1

l_2

l_3
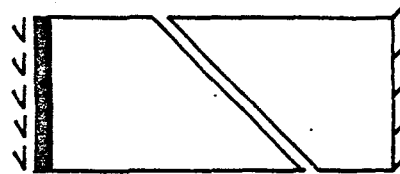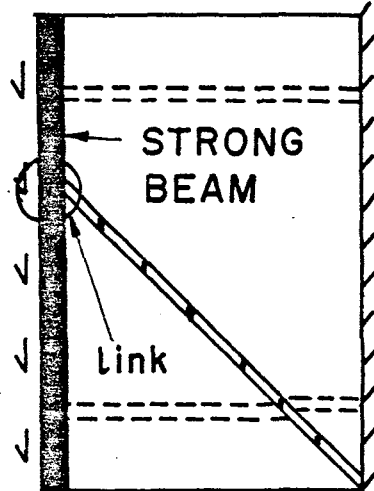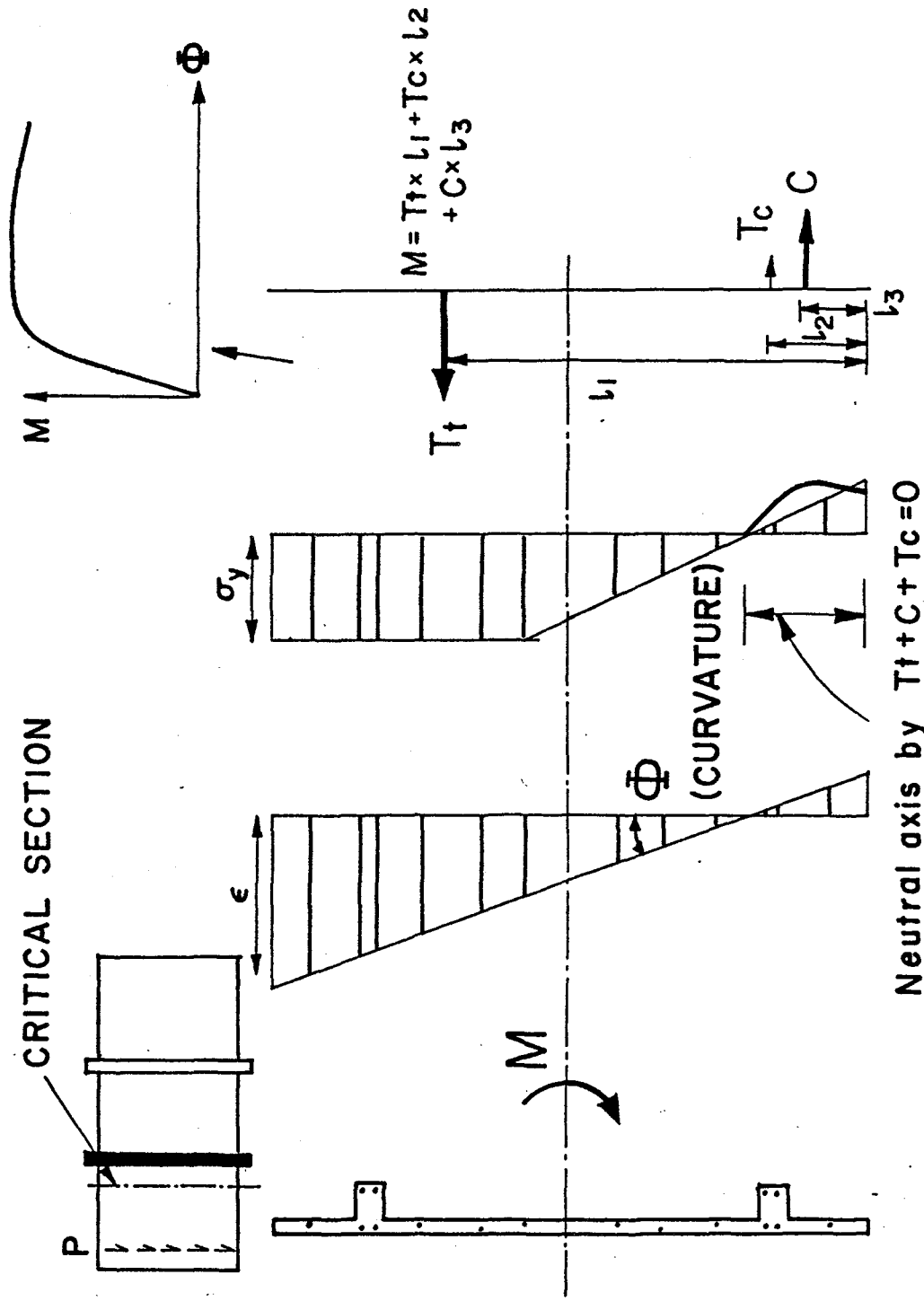
Neutral axis by $T_t + C + T_c = 0$

Fig. 5.5 Procedure to Compute Flexural Capacity of Critical Section
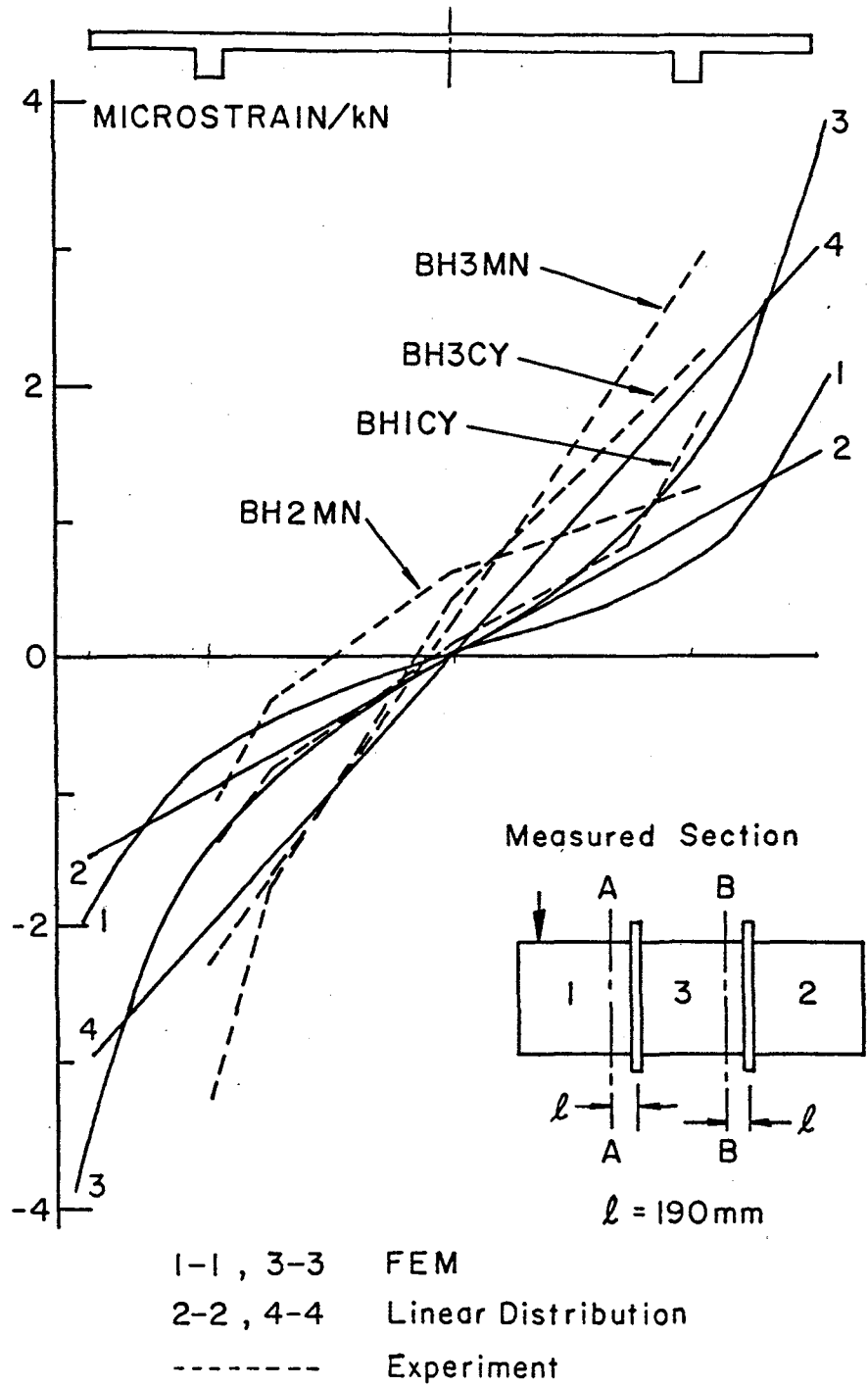
Fig. 5.6 Strain Distribution of Slab Panels in
Elastic Range

CASE 1, 2, 6

CASE 3, 4

M diagram

V diagram

CASE 5

CASE 7

M diagram

V diagram
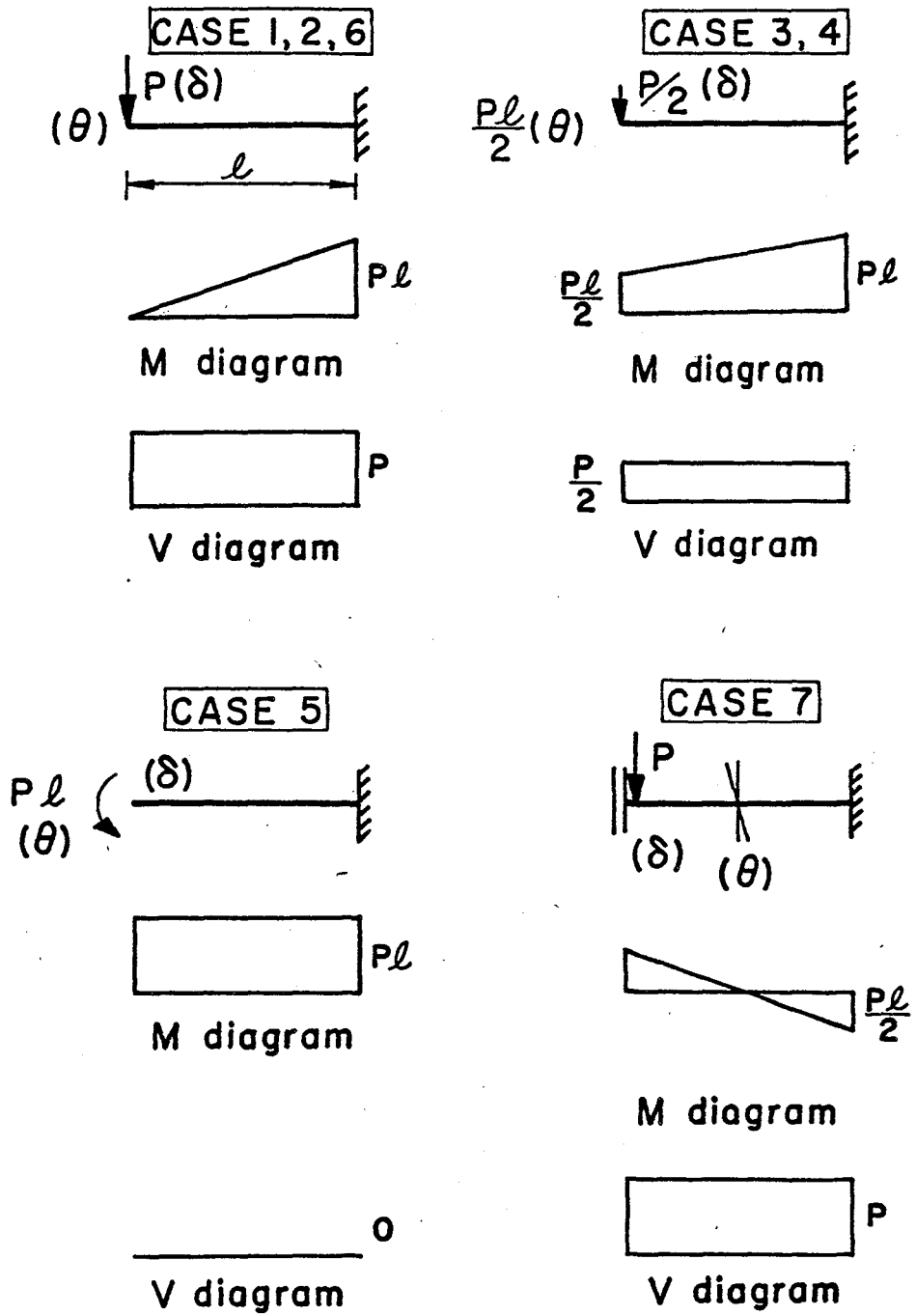
Fig. 5.7 Equivalent Beam Calculation in Strength Tests

-294-
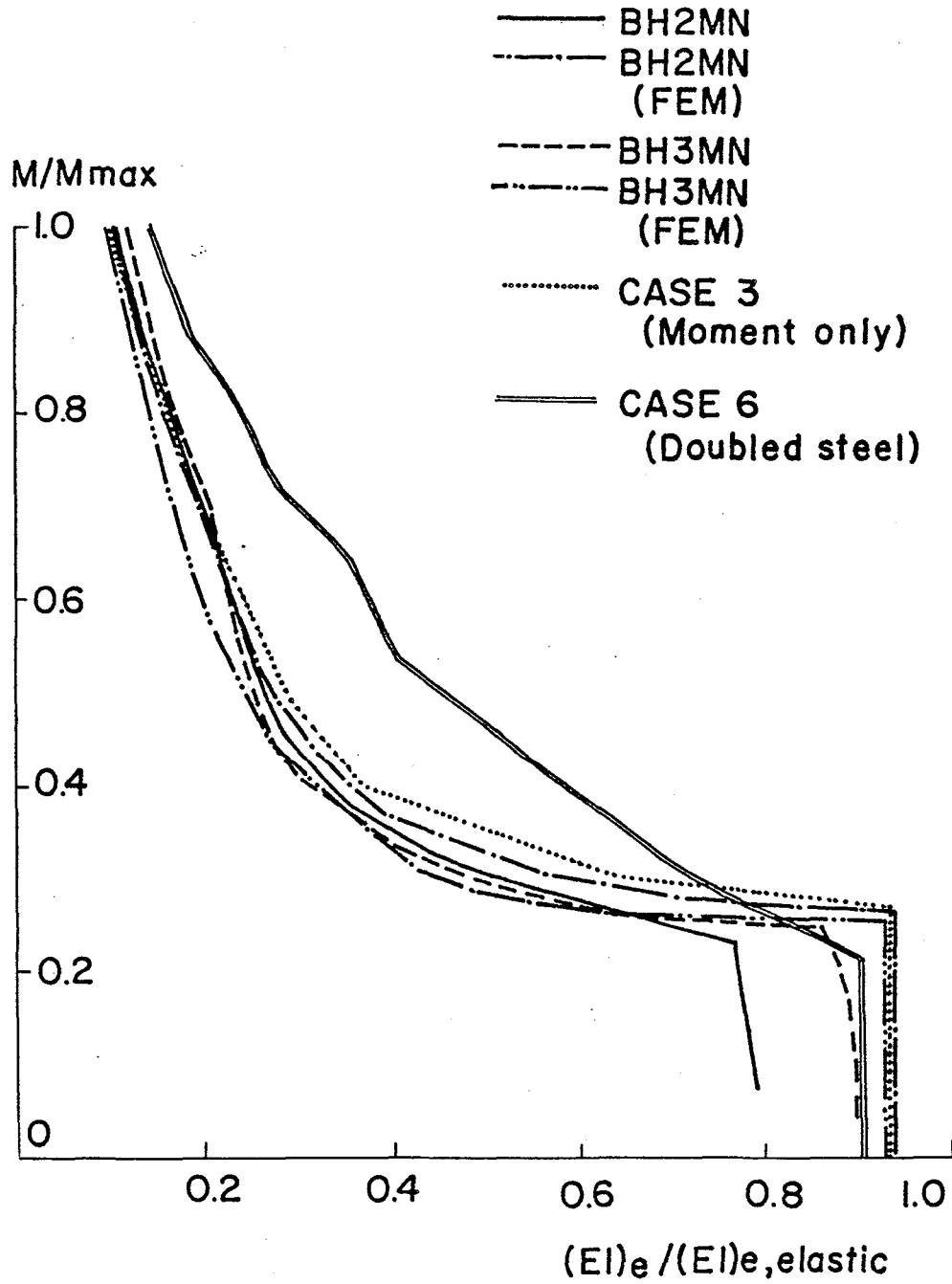
Fig. 5.8 Moment – Equivalent Moment of Inertia Relationship
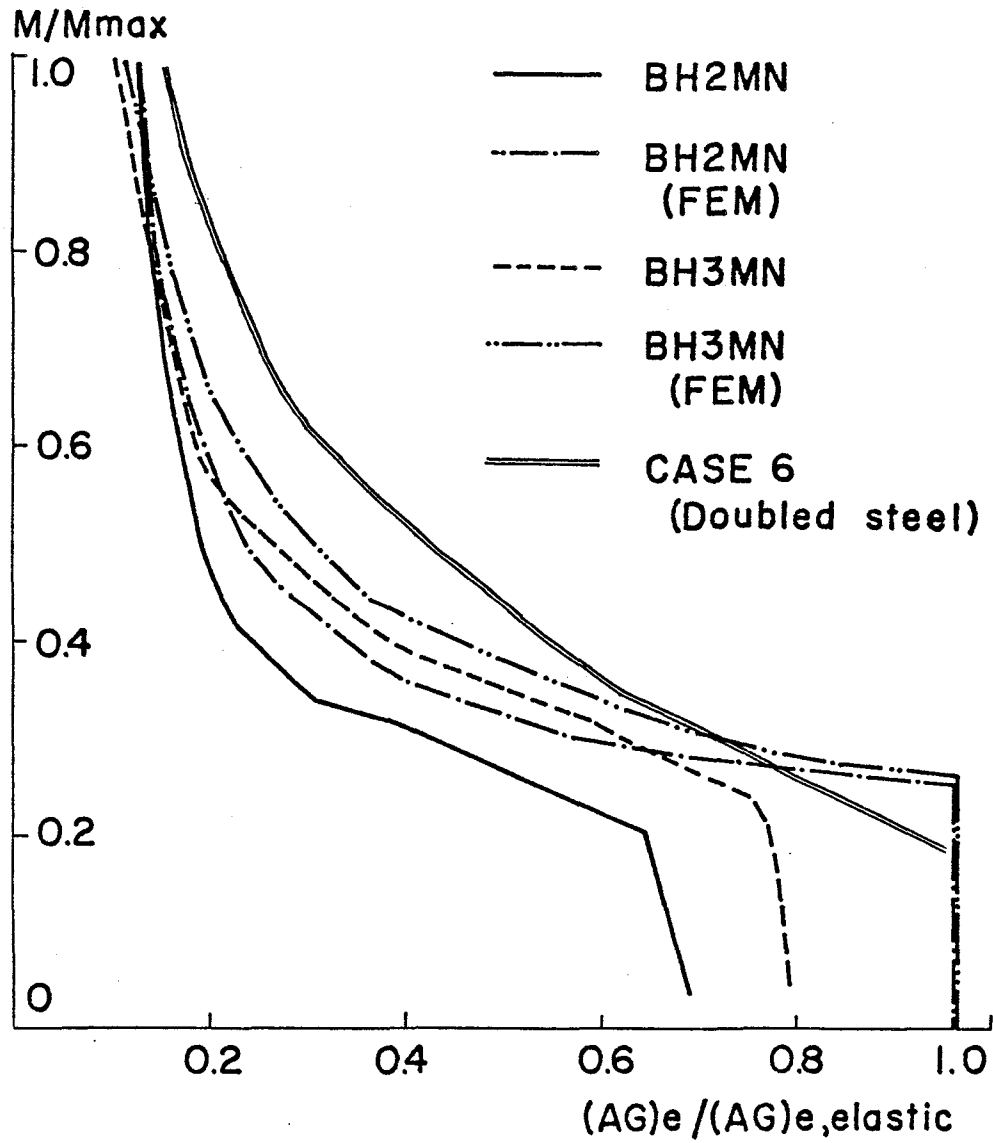
Fig. 5.9 Moment − Equivalent Shear Area Relationship
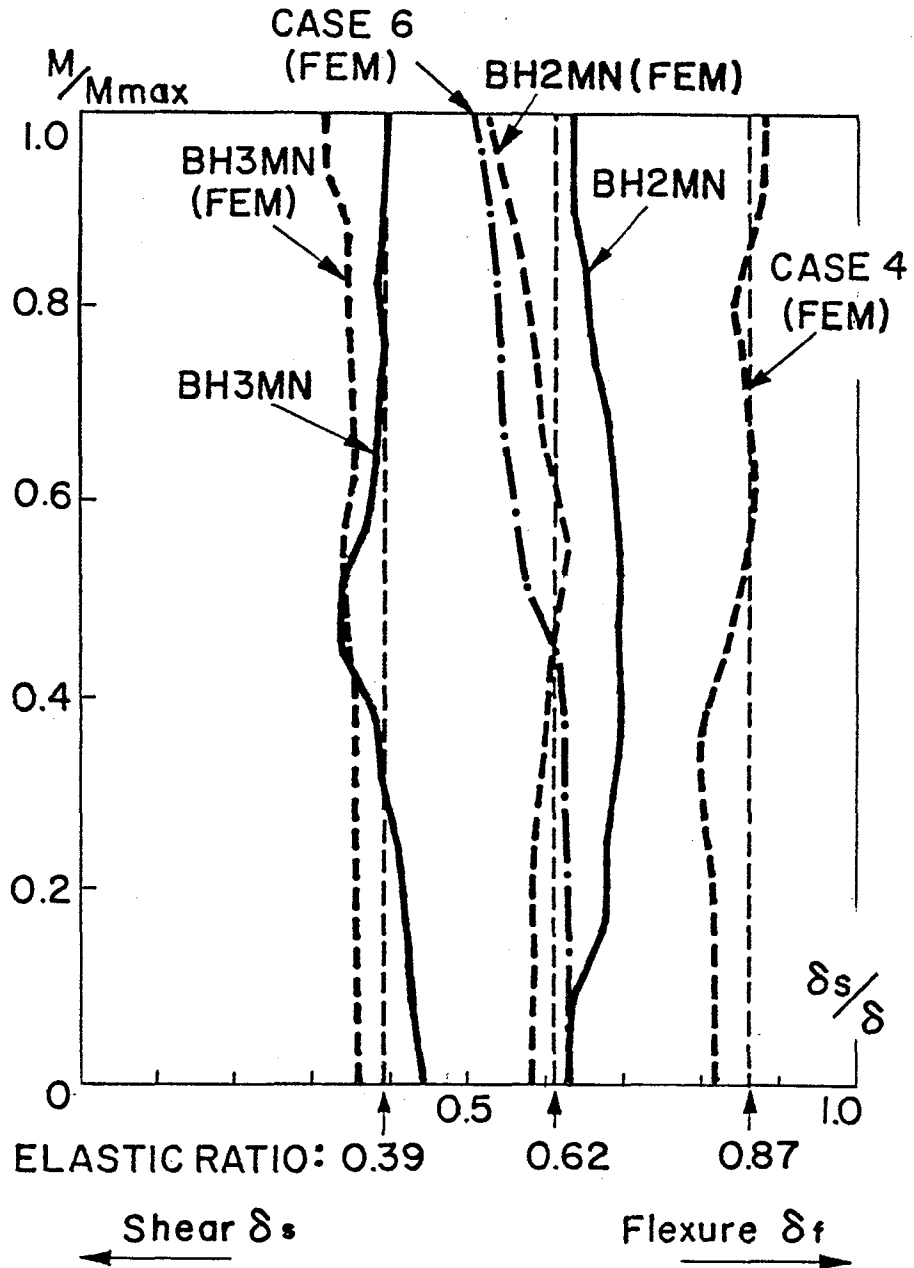
Fig. 5.10   Proportion of Flexural and Shear
Deformations in Slab Panels
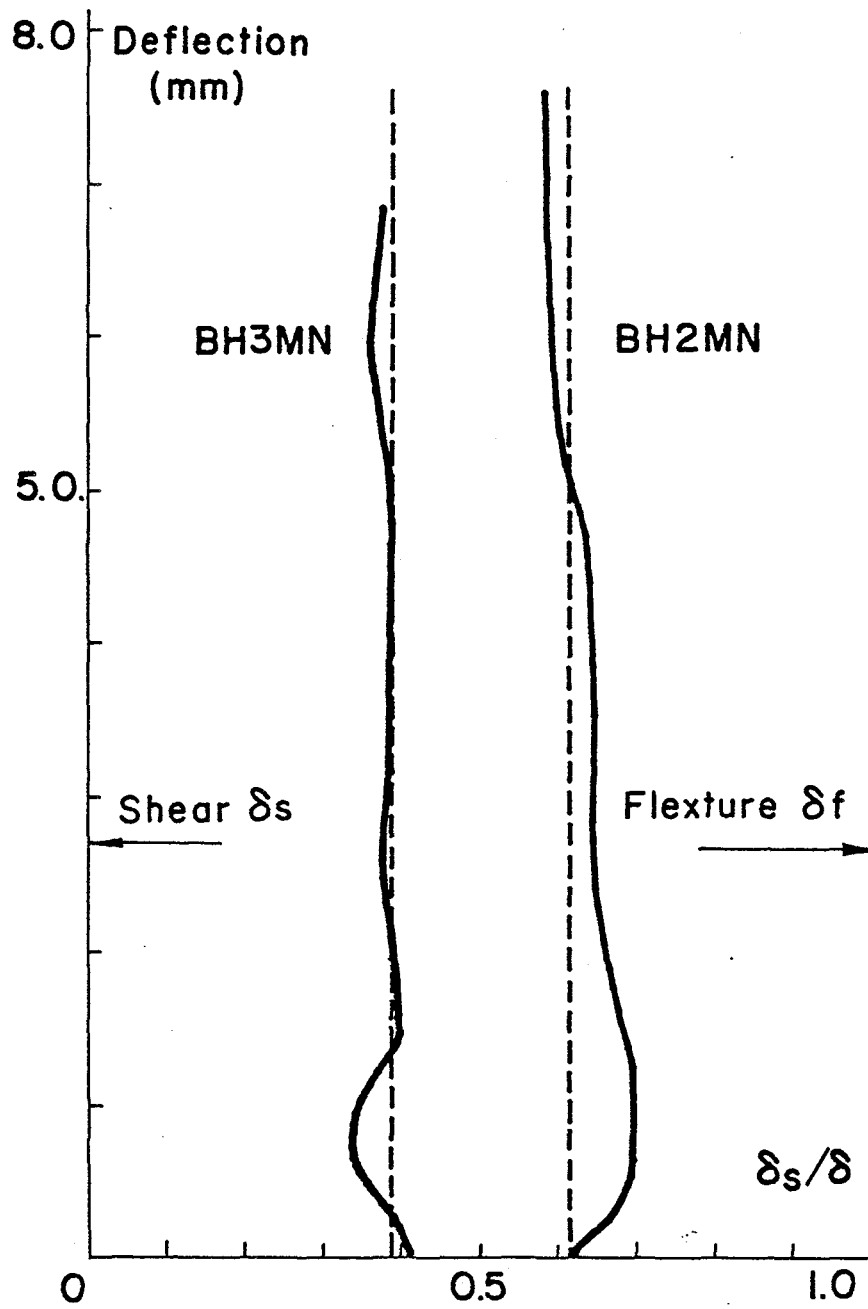
Fig. 5.11 Proportion of Flexural and Shear
Deformations in BH2MN and BH3MN (plotted
against deflection level)
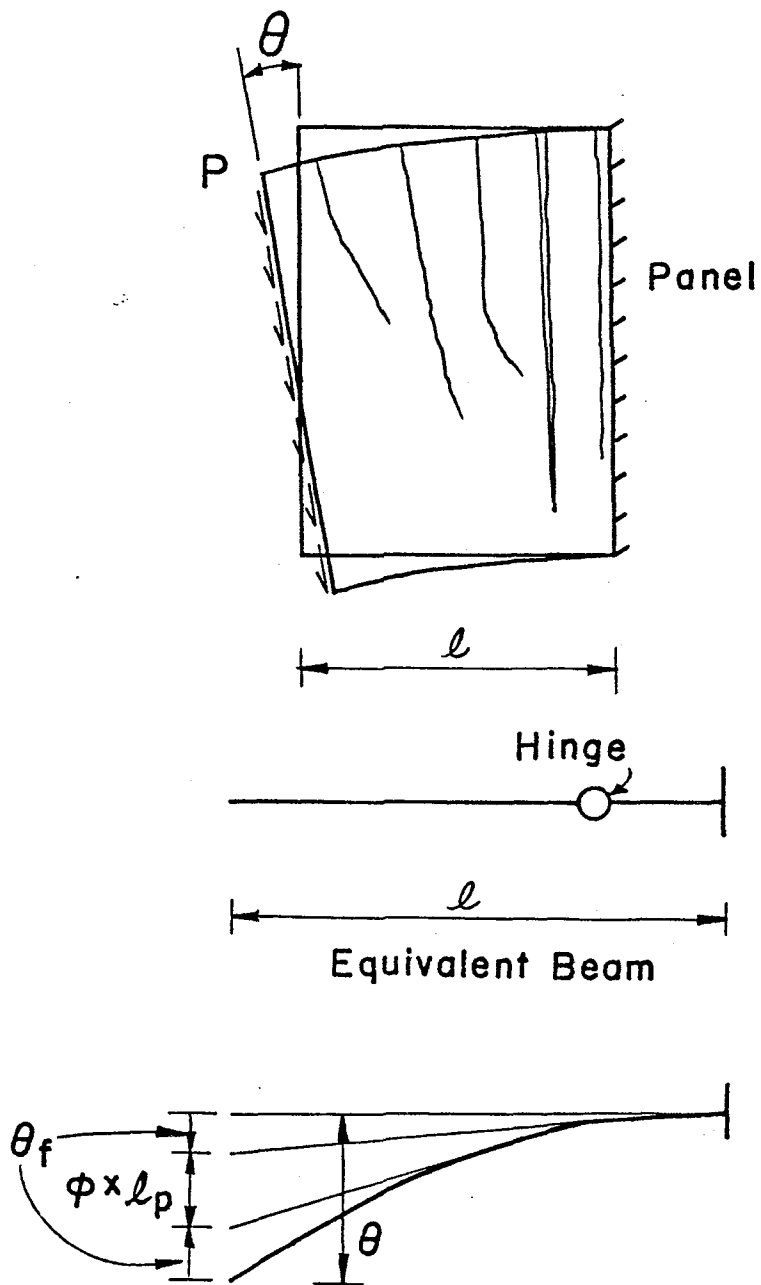
Fig. 5.12 Elastic and Hinge Rotations in Equivalent Beam
(Used for the calculation of degraded stiffness)
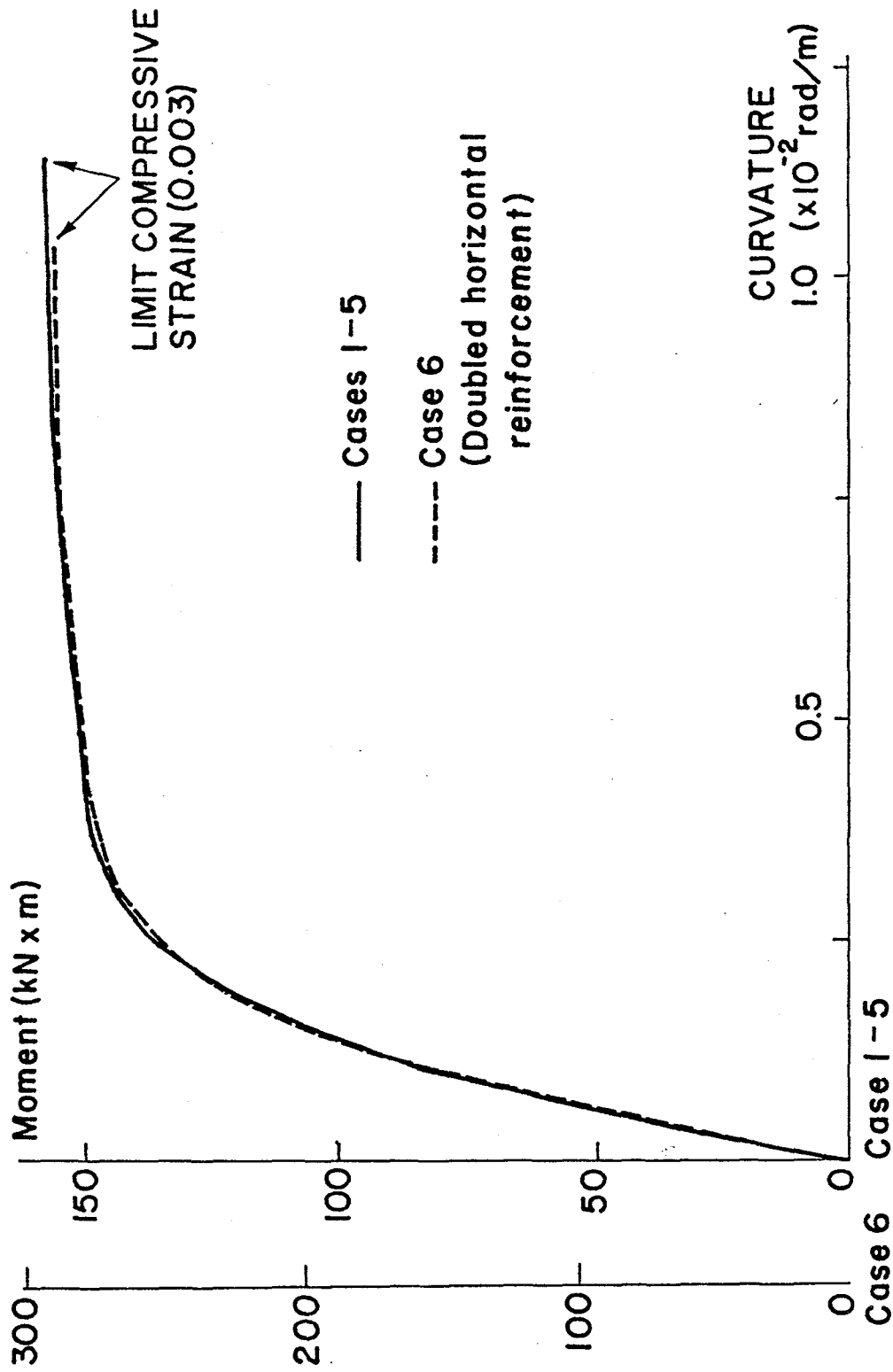
Fig. 5.13 Moment-Curvature Relationship at Critical Sections
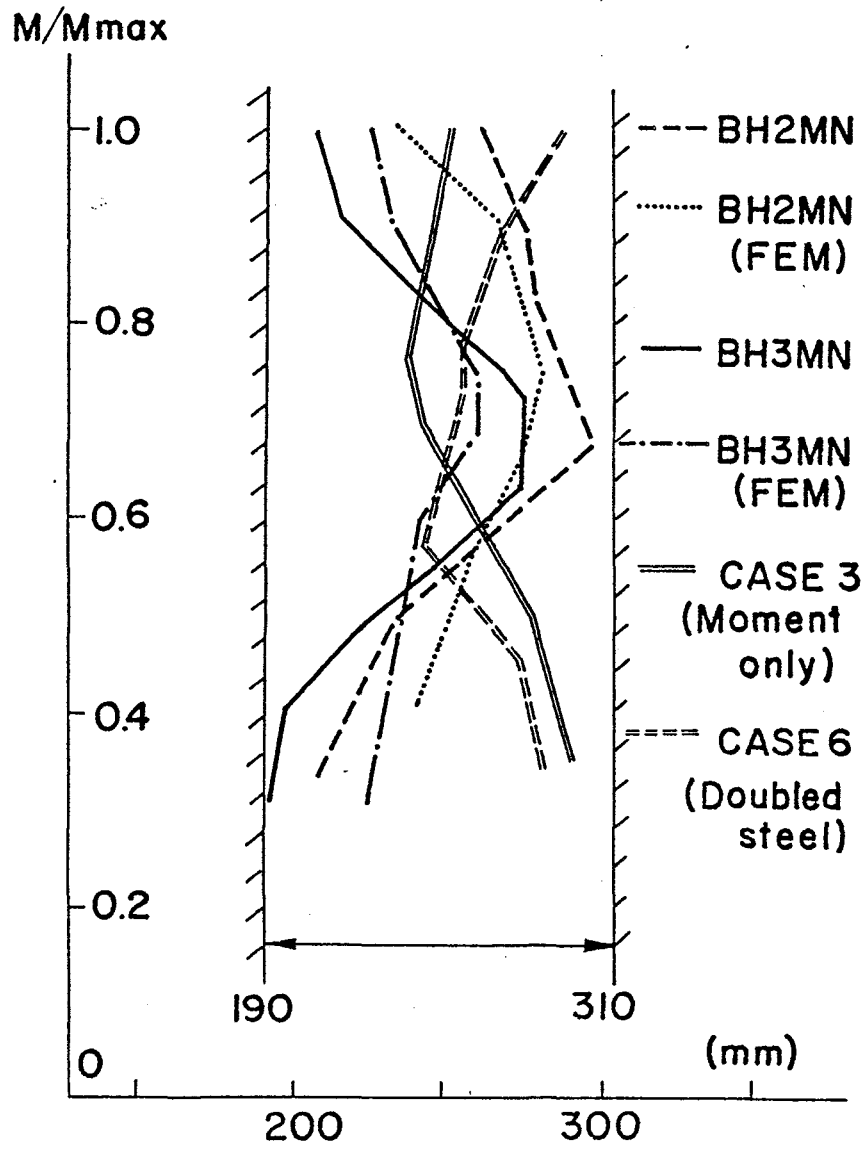
Fig. 5.14 Hinge Length in Slab Panels
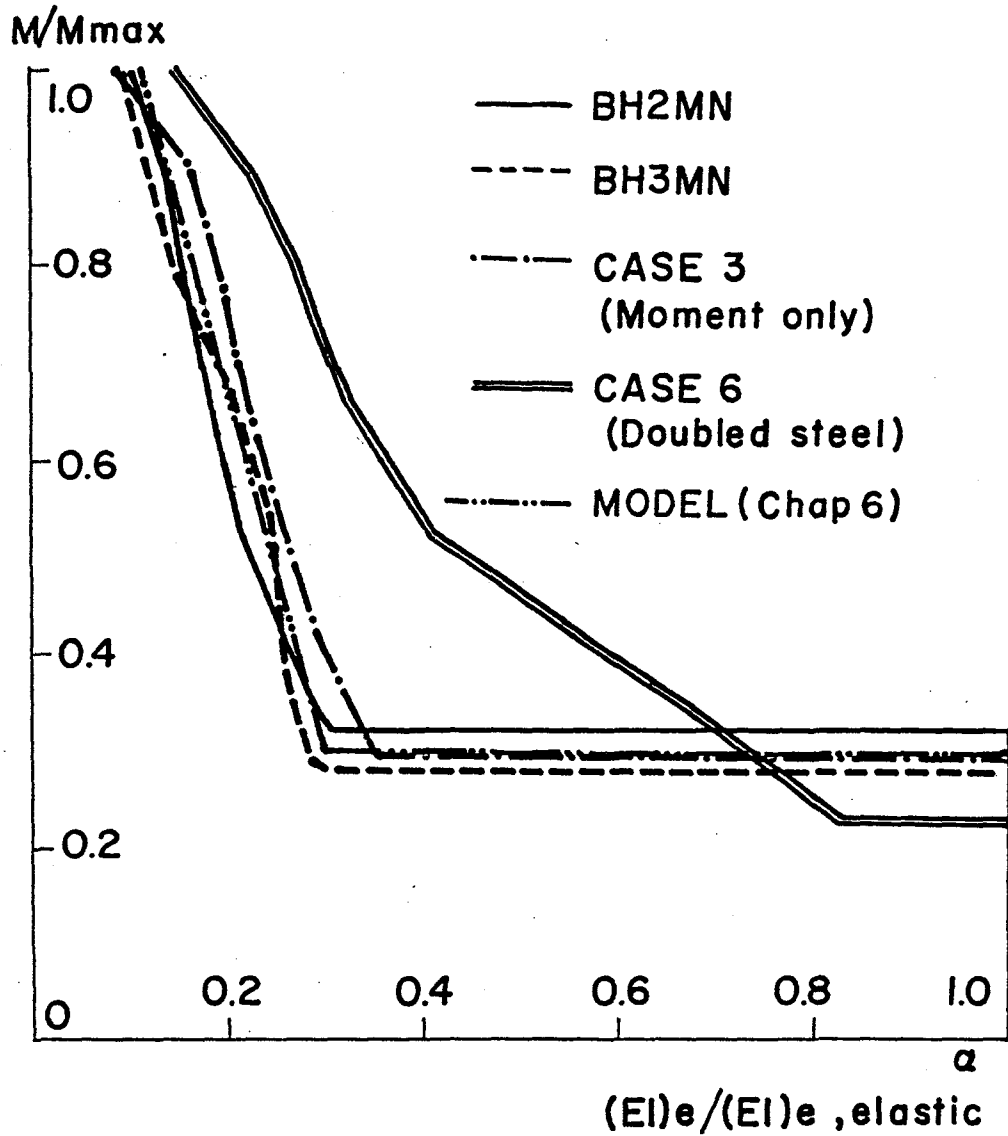
Fig. 5.15 Analytical Moment - Equivalent Moment of Inertia Relationships
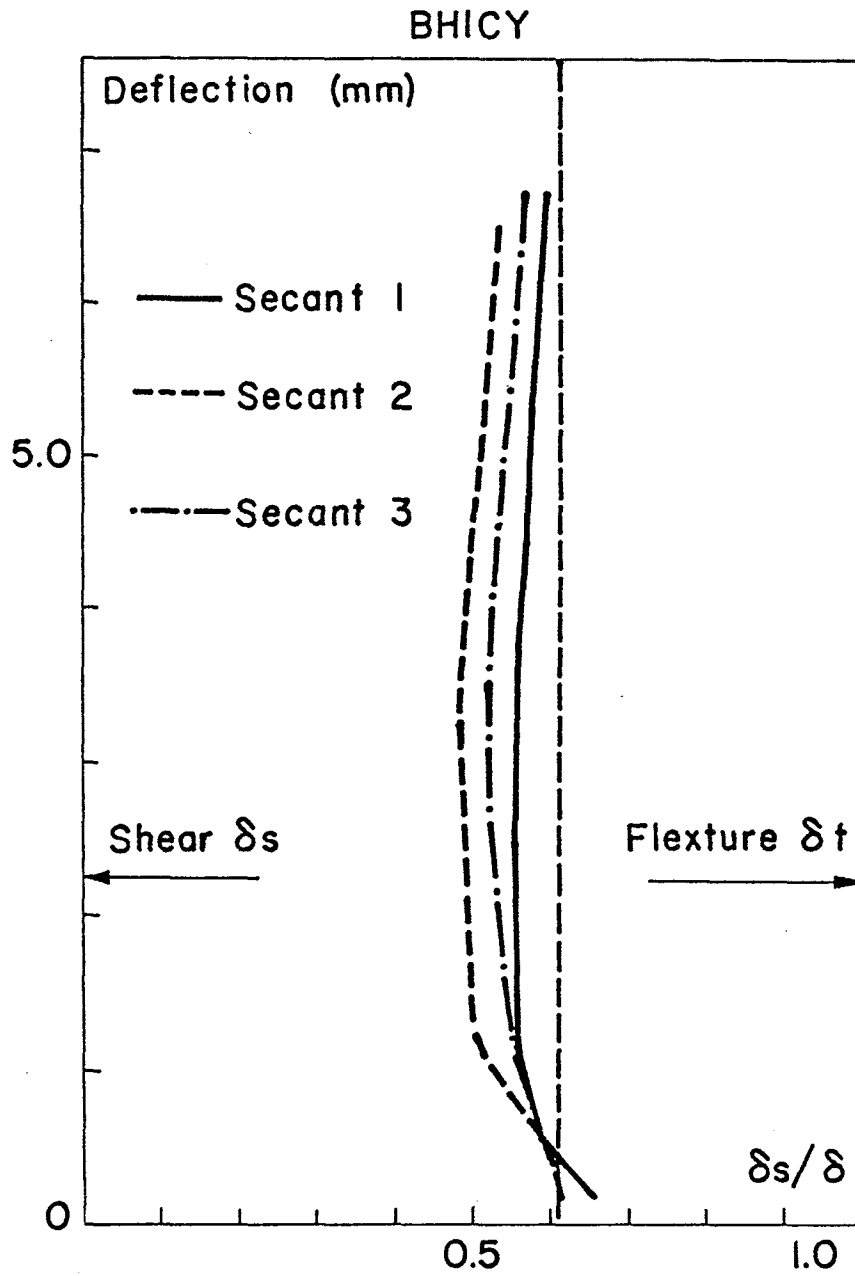
BHICY

Fig. 5.16 Proportion of Flexural and Shear
Deformations in BH1CY
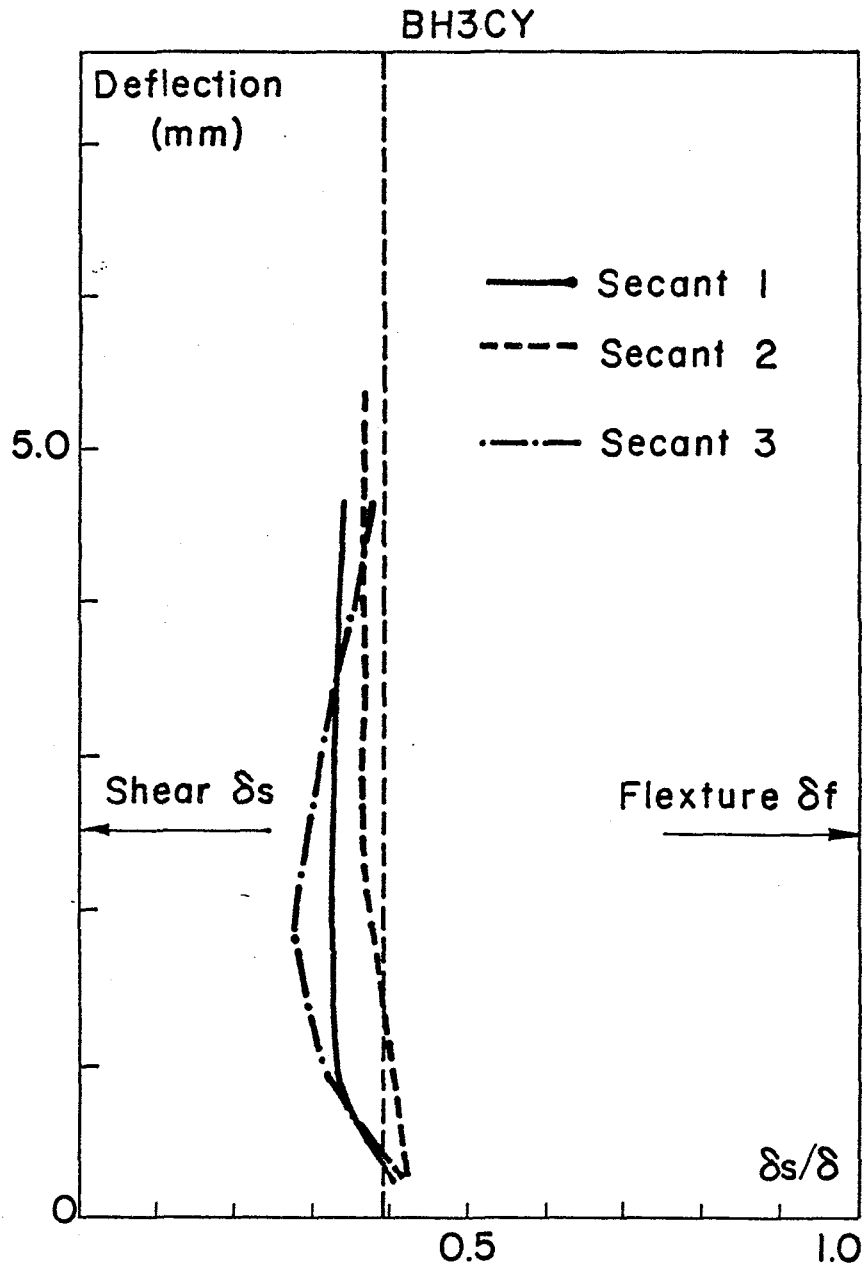
Fig. 5.17 Proportion of Flexural and Shear
Deformations in BH3CY
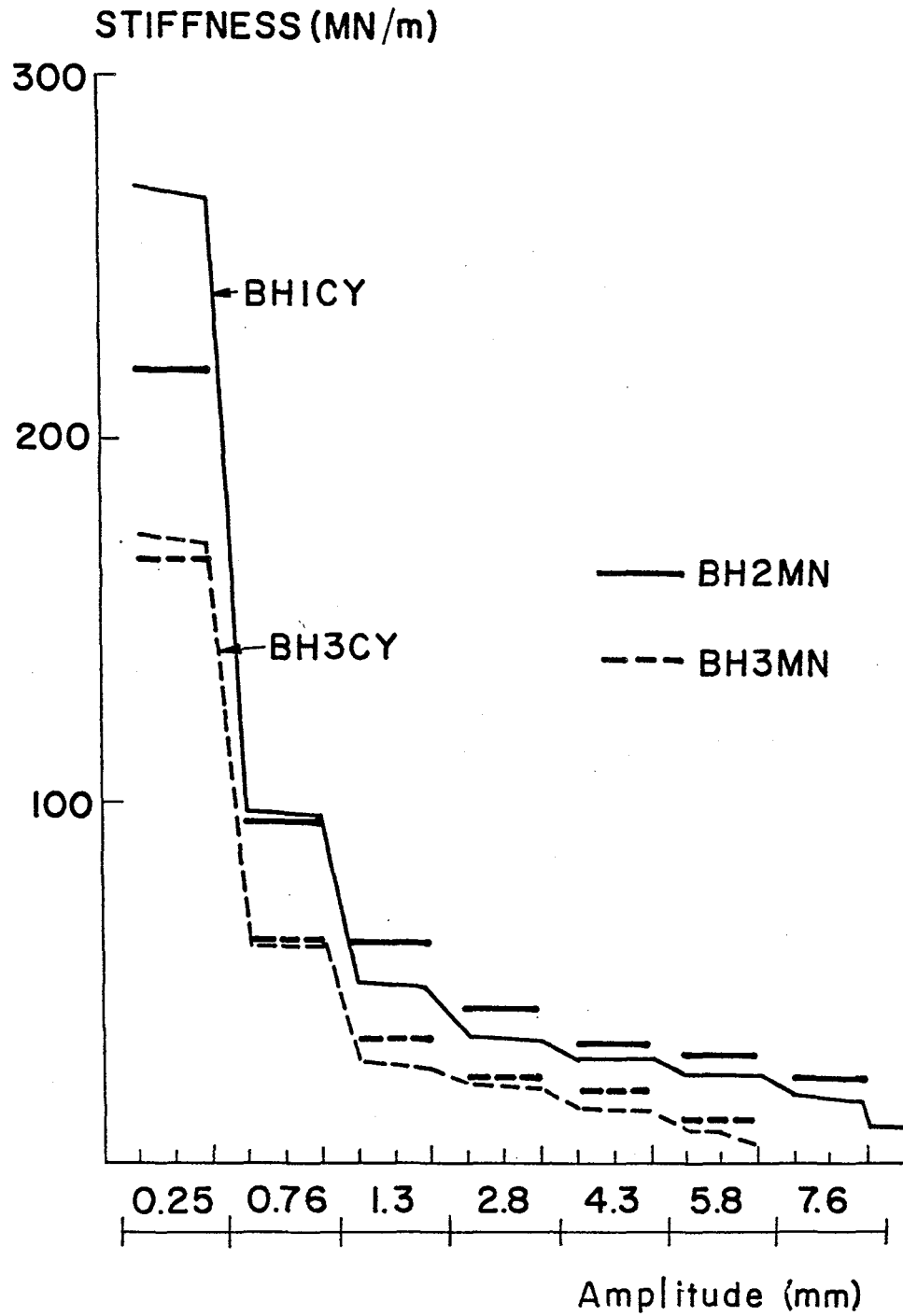
Fig. 5.18 Comparison of Stiffness Degradation
Between Monotonic and Cyclic Loading Tests
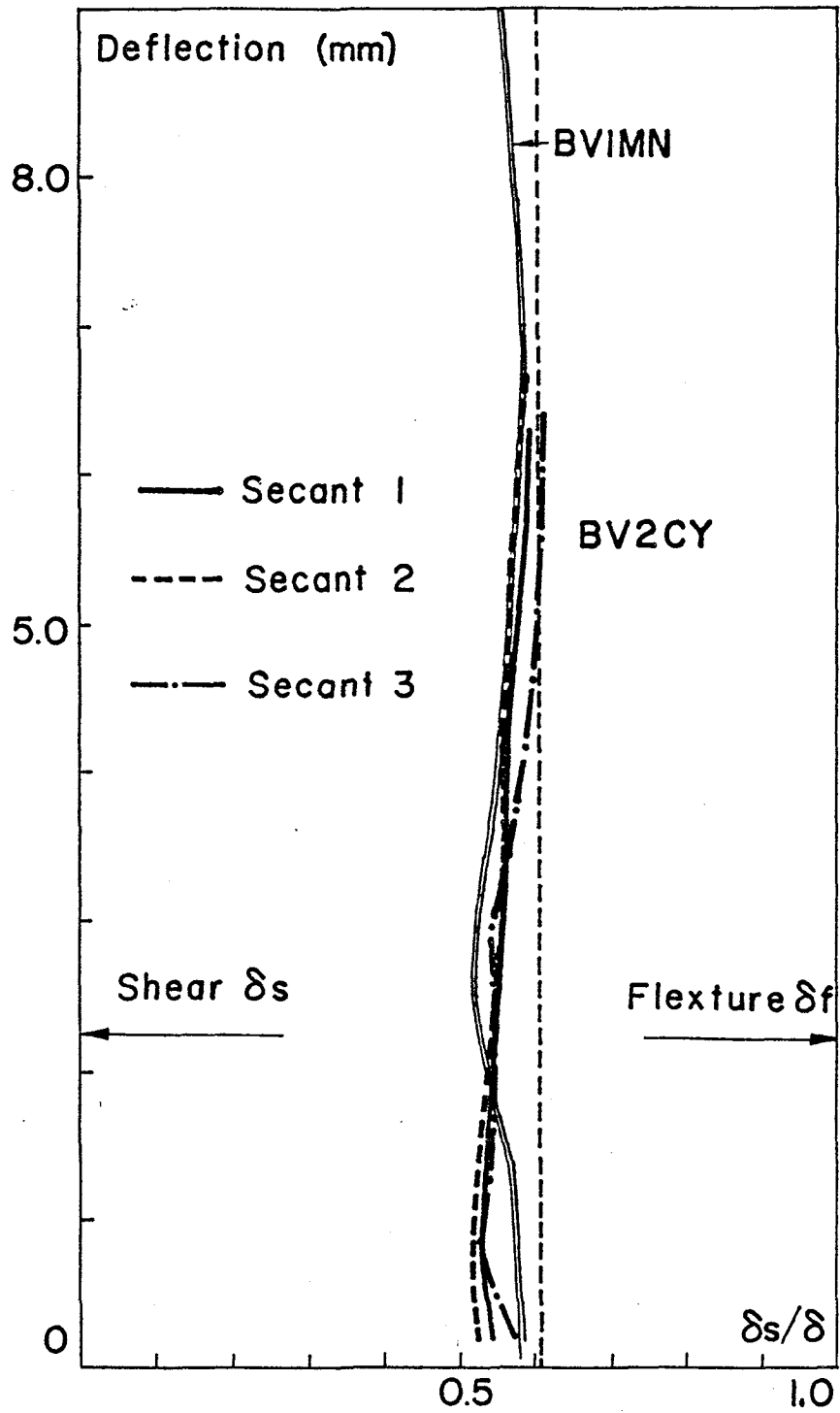
Fig. 5.19 Proportion of Flexural and Shear
Deformations in Slab Panels with
Vertical Load
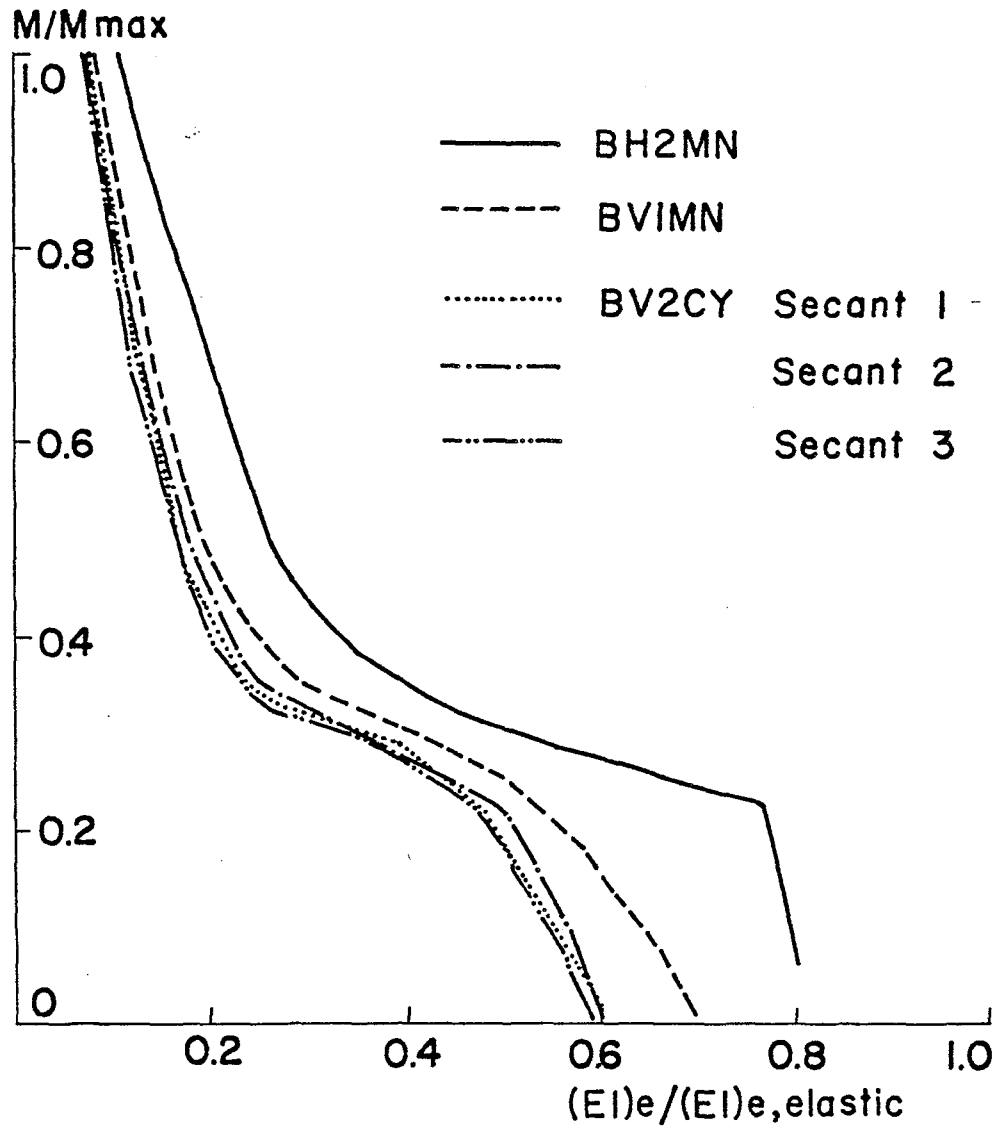
Fig. 5.20 Degradation of Equivalent Moment of Inertia in
Slab Panels with Vertical Load

WALL   FRAME 2   FRAME 3

FRAME 1

6 m x 6 = 36 m

SLAB (200mm thick)

BEAM (300mm x 500mm)

WALL (320mm thick)

COLUMN (600mm x 600mm)
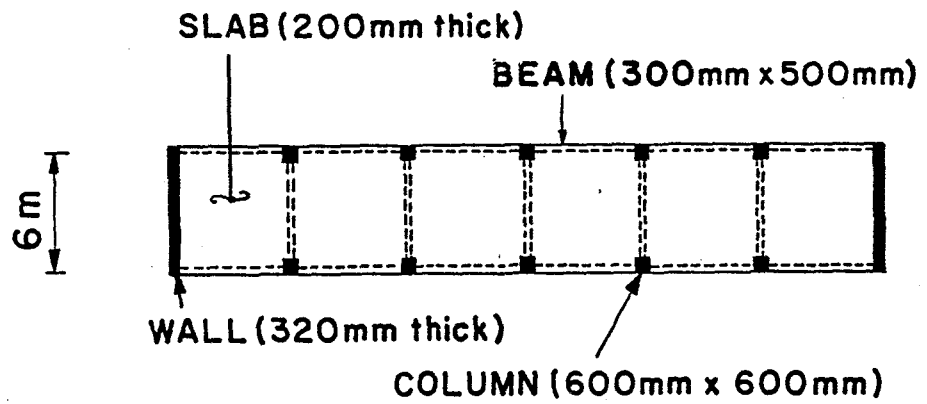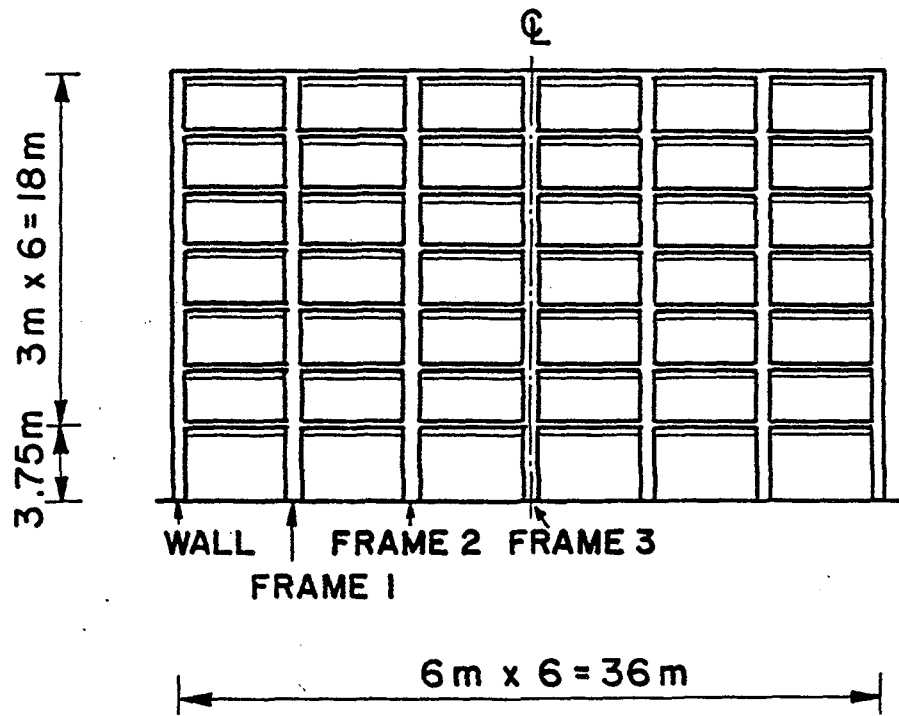
Fig. 6.1   Dimensions of Model Structure

FLOOR SLAB

WALL

FRAME

ELEMENT

FLOOR SLAB

WALL

FRAME

SUBSTRUCTURE

Axis of symmetry

STRUCTURE

GROUND MOTION
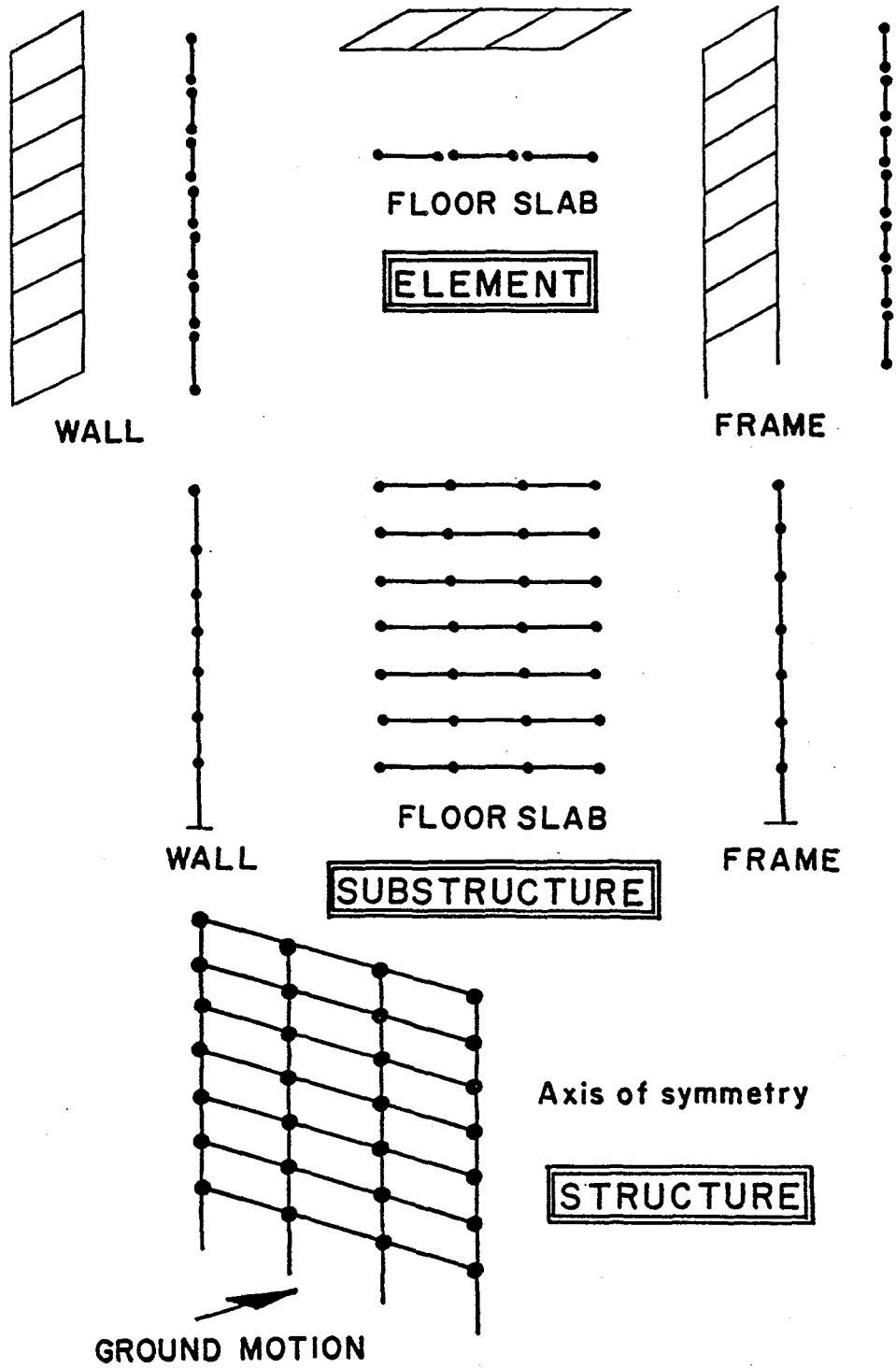
Fig. 6.2 Formulation of Stiffness Matrix
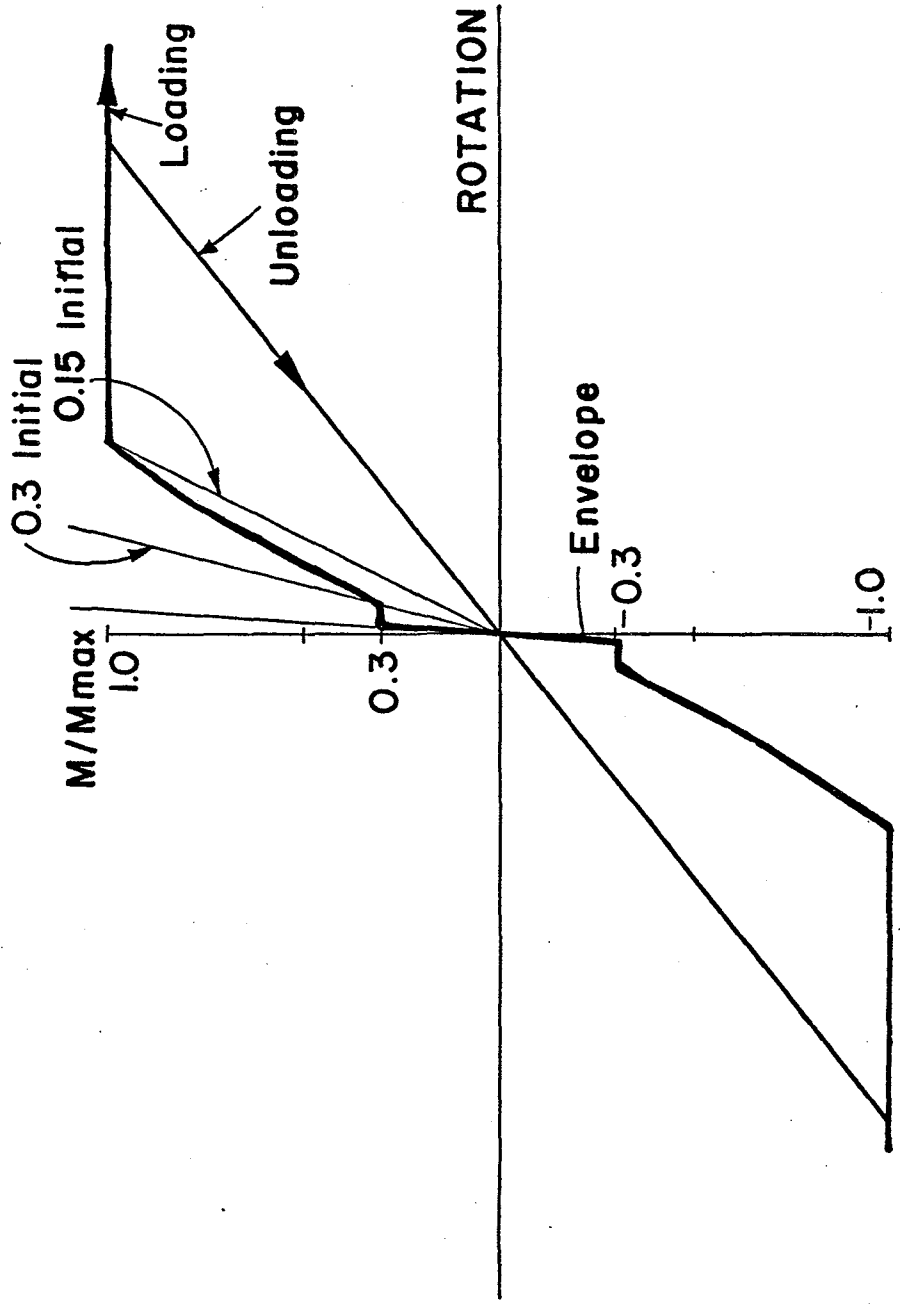
Fig. 6.3 Hysteretic Moment-Rotation Model for Floor Slabs and Walls
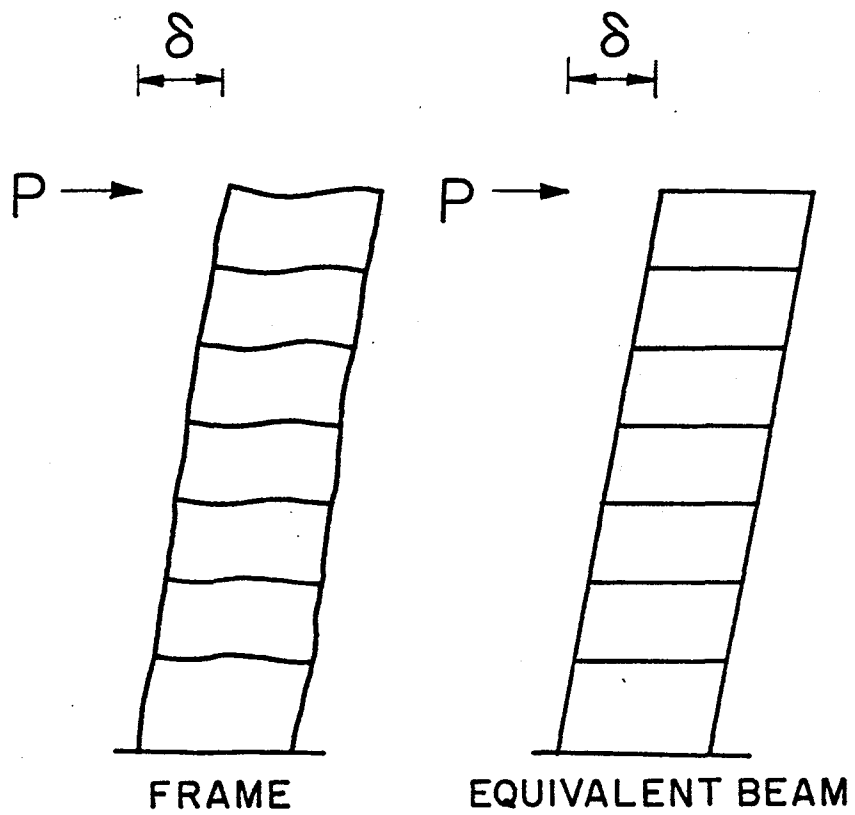
Fig. 6.4 Computation of Shear Area of Equivalent Beam
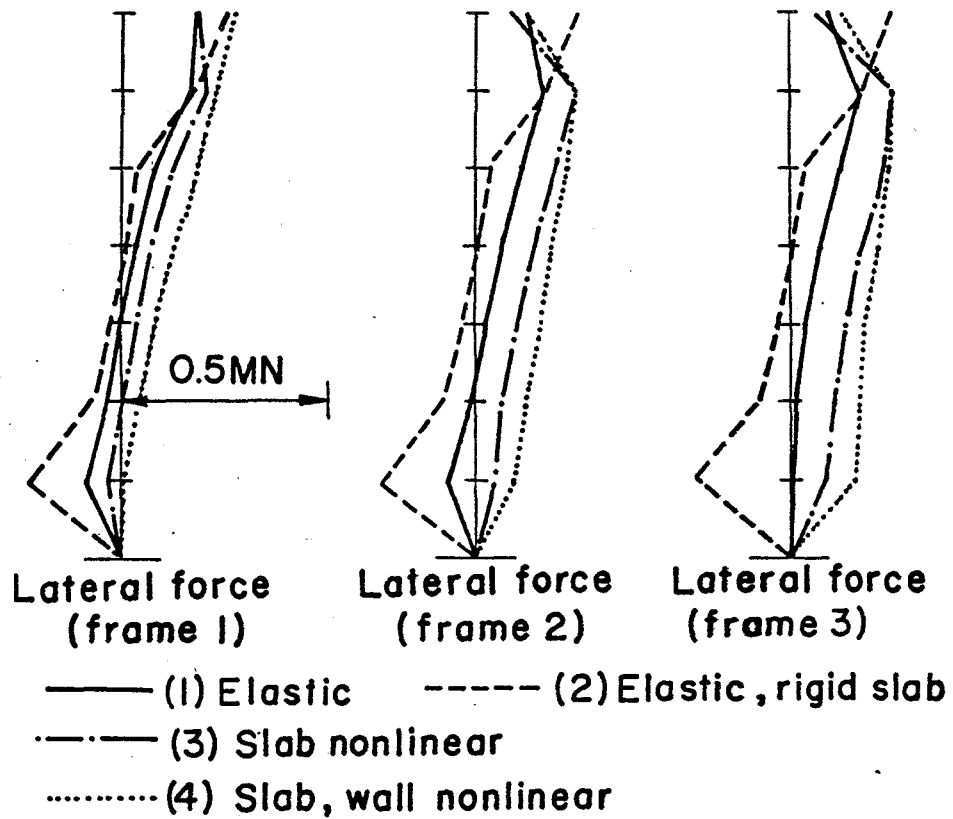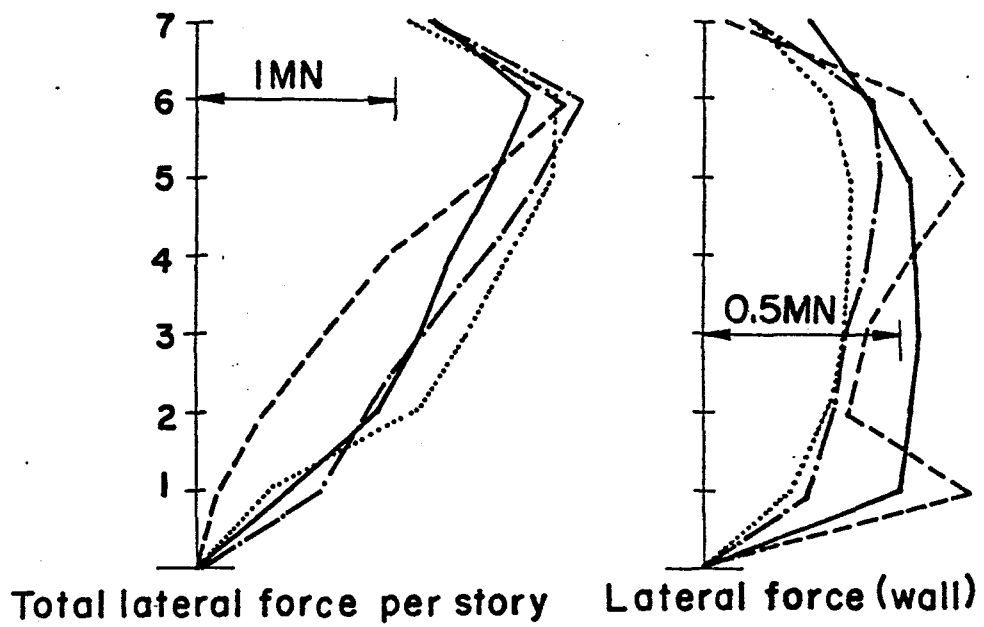
Fig. 6.5 Lateral Force Distribution in Vertical Elements

(1) Elastic   (3) Slab nonlinear   (4)Slab,wall nonlinear
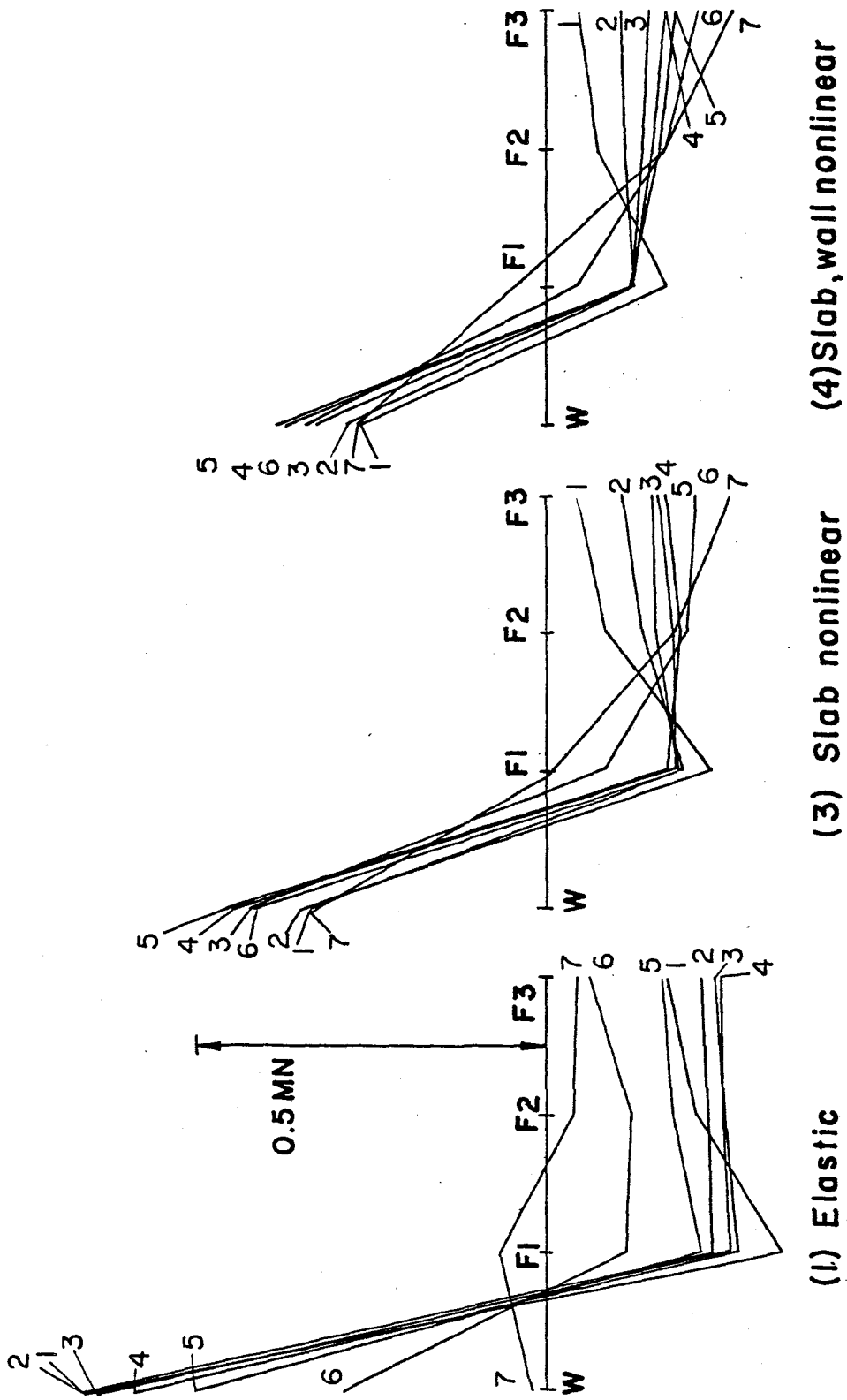
Fig. 6.6   Lateral Force Distribution in Floor Slabs

50 mm

7th floor Displacement, middle

4   8 time (sec)
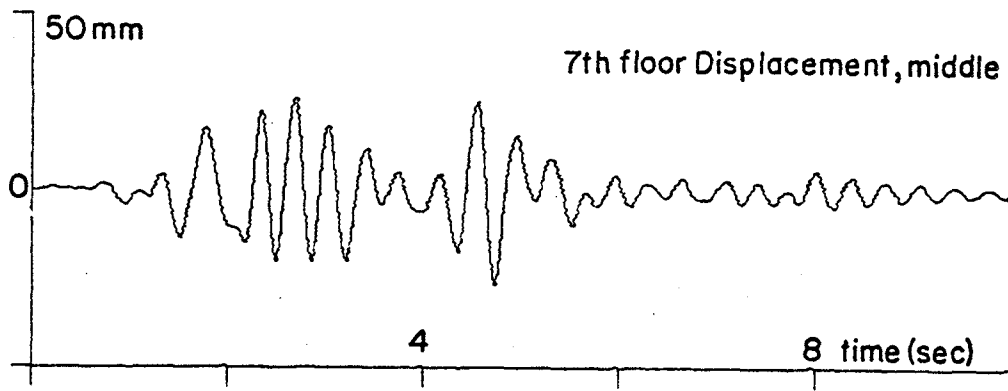
Fig. 6.7(a)   Time-Displacement (7th floor middle) Relationship
              in Elastic Analysis

3.0 MN

Wall Base shear

4   8 time (sec)
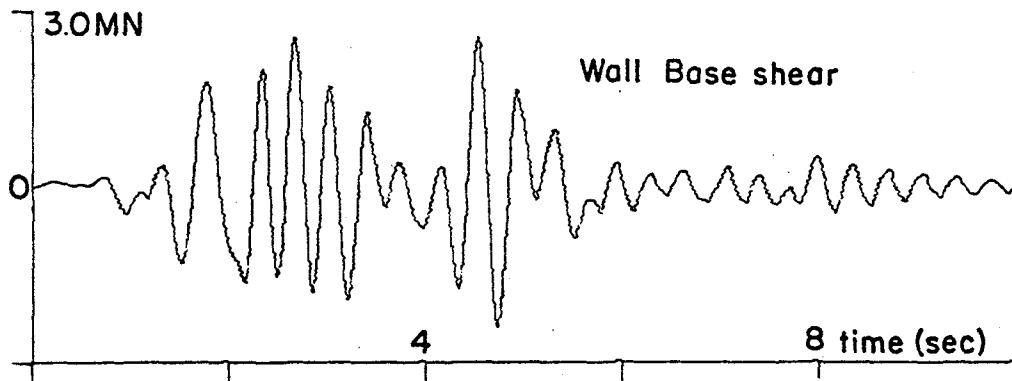
Fig. 6.7(b)   Time-Base Shear (wall) Relationship in Elastic
              Analysis

0.5MN

Frame 3 Base shear

4   8 time (sec)
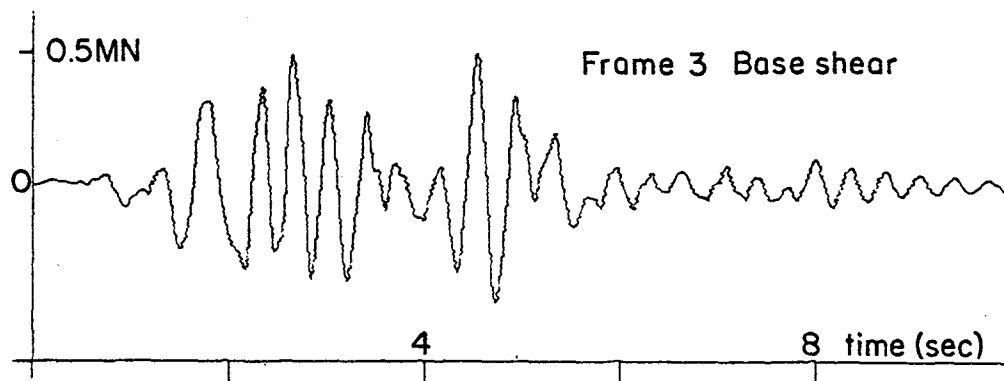
Fig. 6.7(c)   Time-Base Shear (frame 3) Relationship in
              Elastic Analysis

5.0MN x m

7th floor Moment

0

4   8   time(sec)
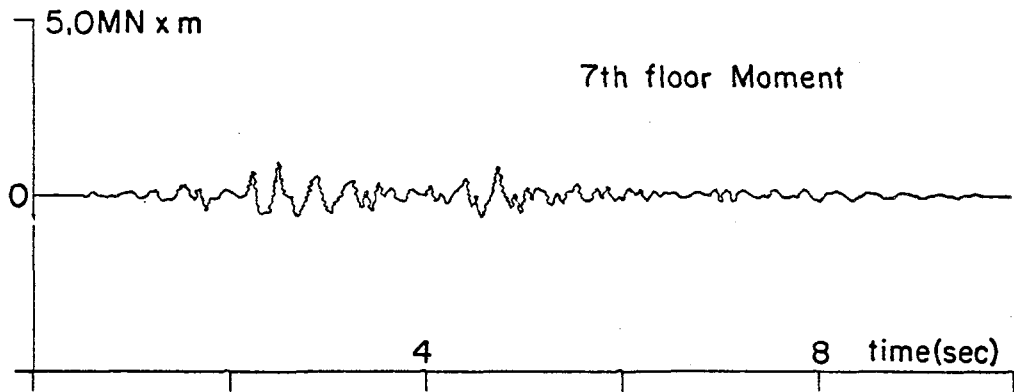
Fig. 6.7(d)   Time—Maximum Moment (7th floor) Relationship
in Elastic Analysis

5.0MN x m

4th floor Moment

0

4   8   time(sec)
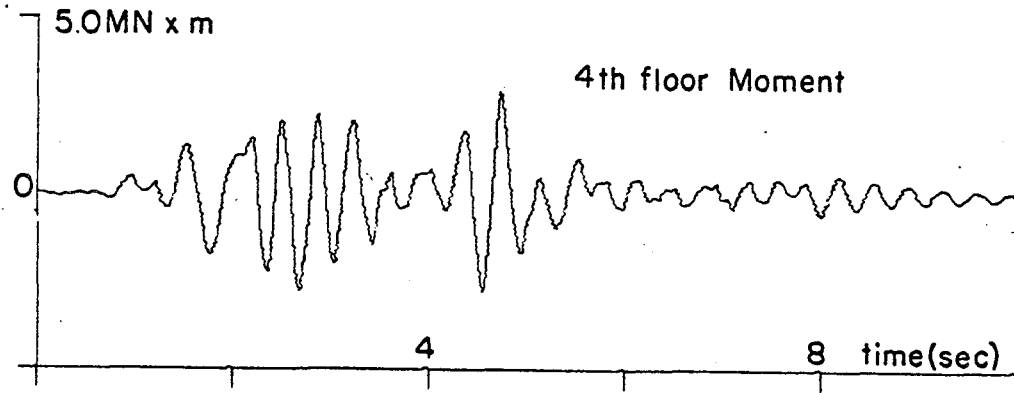
Fig. 6.7(e)   Time—Maximum Moment (4th floor) Relationship
in Elastic Analysis

5.0MN x m

lst floor Moment

0

4   8   time(sec)
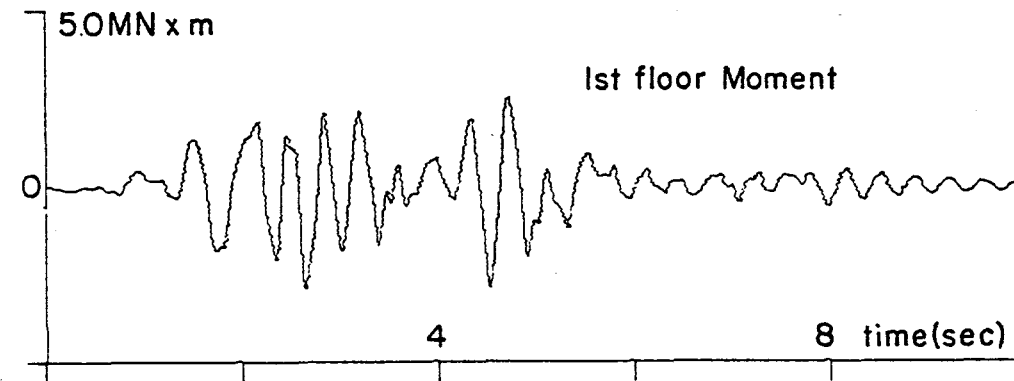
Fig. 6.7(f)   Time—Maximum Moment (1st floor) Relationship
in Elastic Analysis

REFERENCES

1.1   American Concrete Institute
       BUILDING CODE REQUIREMENTS FOR REINFORCED CONCRETE
       AND COMMENTARY, ACI Standard 318-77, 318-77C,
       Detroit, 1977

1.2   Arnold, V. E., Greimann, L. F. and Porter, M. L.
       PILOT TESTS OF COMPOSITE FLOOR DIAPHRAGMS, Progress
       Report, ERI-ISU-AMES-79011 Project 1270, Engineering
       Research Institute, Iowa State University, September,
       1978.

1.3   Black, M. S.
       ULTIMATE STRENGTH STUDY OF TWO-WAY CONCRETE SLABS,
       Journal of the Structural Division, Proceedings of
       ASCE, Vol. 101, No. ST7, January, 1975

1.4   Cardenas, A. E. and Sozen, M. A.
       FLEXURAL YIELD CAPACITY OF SLABS, Journal of the
       American Concrete Institute, Proceedings, Vol. 70,
       No. 2, February, 1973, pp. 124-126

1.5   Carpenter, J. E., Kaar, P. H., and Corley, W. G.
       DESIGN OF DUCTILE FLAT PLATE STRUCTURES TO RESIST
       EARTHQUAKES, Proceedings, Fifth World Conference on
       Earthquake Engineerings, Rome, January, 1973

1.6   Cervenka, V., and Gerstle, K. H.
       INELASTIC ANALYSIS OF REINFORCED CONCRETE PANELS,
       EXPERIMENTAL VERIFICATION AND APPLICATION, IABSE
       Publication, Vol. 32-1, 1971, pp. 21-39

1.7   Corley, W. G., and Jirsa, J. O.
       EQUIVALENT FRAME ANALYSIS FOR SLAB DESIGN, Journal
       of the American Concrete Institute, Proceedings,
       Vol. 67, No. 11, November, 1970, pp. 875-884

1.8   Coull, A.
       INTERACTION OF COUPLED SHEAR WALLS WITH ELASTIC
       FOUNDATIONS, Journal of the American Concrete Institute,
       Proceedings, Vol. 68, No. 6, June, 1971, pp. 456-461

1.9   Coull, A., and Hag, A. A.
       EFFECTIVE COUPLING OF SHEARWALLS BY FLOOR SLABS,
       Journal of the American Concrete Institute, Proceedings,
       Vol. 72, No. 8, August, 1975, pp. 429-431

1.10   Dilger, V., Elmasri, M. Z., and Ghali, A.
       FLAT PLATES WITH SPECIAL SHEAR REINFORCEMENT SUBJECTED
       TO STATIC DYNAMIC MOMENT TRANSFER, Journal of the
       American Concrete Institute, Proceedings, Vol. 75, ·
       No. 10, October, 1978, pp. 543-549

1.11   Edger, L., and Bertero, V. V.
       EVALUATION OF CONTRIBUTION OF FLOOR SYSTEM TO DYNAMIC
       CHARACTERISTICS OF MOMENT-RESISTING SPACE FRAMES,
       Proceedings, Sixth World Conference on Earthquake
       Engineerings, New Delhi, January, 1977

1.12   Fintel, M., Banard, P. R. and Derecho, A. T.
       STAGGERED TRANSVERSE WALL BEAMS FOR MULTISTORY CON-
       CRETE BUILDINGS - A DETAILED STUDY, Portland Cement
       Association, Skokie, Illinois, 1968

1.13   Foutch, D. A. and Jennings, P. C.
       DYNAMIC TESTS OF FULL SCALE STRUCTURES, Proceedings,
       Sixth World Conference on Earthquake Engineerings,
       New Delhi, January, 1977

1.14   Gluck, J.
       ELASTO-PLASTIC ANALYSIS OF COUPLED SHEAR WALLS,
       Journal of the Structural Division, Proceedings of
       ASCE, Vol. 99, No. ST8, August, 1973, pp. 1743-1761

1.15   Goldberg, J. E. and Herness, E. D.
       VIBRATION OF MULTISTORY BUILDINGS CONSIDERING FLOOR
       AND WALL DEFORMATION, Bulletin of the Seismological
       Society of America, Vol. 55, No. 1, February, 1965,
       pp. 181-200

1.16   Gupta, M. M.
       DESIGN AIDS FOR SINGLY-REFINFORCED BEAMS AND ONE-WAY
       SLABS, Journal of the American Concrete Institute,
       Proceedings, Vol. 72, No. 12, December, 1974,
       pp. 723-726

1.17   Harnden, C. T.
          TESTS OF ONE AND TWO STORY FLAT PLATE MODELS,
          Journal of the Structural Division, Proceedings of
          ASCE, Vol. 100, No. ST3, March, 1974, pp. 513-531

1.18   Hawkins, N. M., Mitchell, D. and Symmonds, D. W.
          HYSTERETIC GEHAVIOR OF CONCRETE SLAB-TO-COLUMN
          CONNECTIONS, Proceedings, Sixth World Conference on
          Earthquake Engineerings, New Delhi, January, 1977

1.19   Hawkins, N. M.
          SEISMIC RESPONSE CONSTRAINTS FOR SLAB SYSTEMS,
          Proceedings, Workshop on Earthquake Resistant Rein-
          forced Concrete Building Construction, University
          of California at Berkeley, July, 1977

1.20   Hawkins, N. M. and Lu, Le-Wu
          TESTING OF REINFORCED CONCRETE BUILDING ELEMENTS,
          Proceedings of Advisory Meeting on Earthquake
          Engineering and Landslides, Taipei, Republic of China,
          August, 1977

1.21   Islam, S. and Park, R.
          TEST ON SLAB-COLUMN CONNECTIONS WITH SHEAR AND
          UNBALANCED FLEXURE, Journal of the Structural Division,
          Proceedings of ASCE, Vol. 102, No. ST3, March, 1976,
          pp. 549-568

1.22   Jain, S. C. and Kennedy, J. B.
          YIELD CRITERION FOR REINFORCED CONCRETE SLABS,
          Journal of the Structural Division, Proceedings of
          ASCE, Vol. 100, No. ST3, March, 1974, pp. 631-644

1.23   Joh, O. and Ohno, K.
          SEISMIC PROPERTIES OF TWO DIMENSIONAL MDOF SYSTEMS,
          Annual Transactions of the Architectural Institute
          of Japan, 1969-1972. (In Japanese)

1.24   Joh, O. and Ohno, K.
          VIBRATION ANALYSIS OF BUILDINGS WITH CONSIDERATION FOR
          THE IN-PLANE DEFORMATION OF FLOOR SLABS, Proceedings,
          Sixth World Conference on Earthquake Engineerings,
          New Delhi, January, 1977

1.25   Long, A. E.
        A TWO-PHASE APPROACH TO THE PREDICTION OF THE PUNCHING
        FAILURES OF SLABS, Journal of the American Concrete
        Institute, Proceedings, Vol. 72, No. 2, February, 1975,
        pp. 37-45

1.26   Lynn, P. P. and Kumbasar, N.
        FREE TRANSVERSE VIBRATION OF FLAT SLABS, Journal of the
        Engineering Mechanics Division, Proceedings of ASCE,
        Vol. 95, No. EM1, February, 1969, pp. 255-269

1.27   Mahaidi, R. S. and Nilson, A. H.
        COUPLED SHEAR WALL ANALYSIS BY LAGLANGE MULTIPLIERS,
        Journal of the Structural Division, Proceedings of ASCE,
        Vol. 101, No. ST11, November, 1975, pp. 2359-2366

1.28   Mehrain, M. and Aalami, B.
        ROTATIONAL STIFFNESS OF CONCRETE SLABS, Journal of the
        American Concrete Institute, Proceedings, Vol. 103,
        No.9, September, 1974, pp. 429-435

1.29   Muto, K.
        ASEISMIC DESIGN ANALYSIS OF BUILDINGS, Maruzen Co.,
        Tokyo, Japan, 1974

1.30   Nilson, A. H. and Walters, D. B.
        DEFLECTION OF TWO-WAY FLOOR SYSTEMS BY THE EQUIVALENT
        FRAME METHOD, Journal of the American Concrete Institute,
        Proceedings, Vol. 72, No. 5, May, 1975, pp. 210-218

1.31   Paulay, T.
        ELASTO-PLASTIC ANALYSIS OF COUPLED SHEAR WALLS, Journal
        of the American Concrete Institute, Proceedings, Vol. 67,
        No. 11, November, 1970, pp. 915-922

1.32   Pfaffinger, D. D.
        COLUMN-PLATE INTERACTION IN FLAT SLAB STRUCTURES, Journal
        of the Structural Division, Proceedings of ASCE, Vol. 98,
        No. ST1, January, 1972, pp. 307-326

1.33   Qudeer, A. and Stafford-Smith, B.
        THE BENDING STIFFNESS OF SLABS CONCERNING SHEAR WALLS,
        Journal of the American Concrete Institute, Proceedings,
        Vol. 66, No. 6, June, 1969, pp. 464-473

1.34   Ramakrishnan, V.
            COMPARISON OF THREE DIMENSIONAL ANALYSIS OF CONCRETE
            SHEAR WALL BUILDINGS AND THEIR ACTUAL BEHAVIOR, Methods
            of Structural Analysis, Vol.1, ASCE, 1976, pp. 95-114

1.35   Rice, P. F.
            PRACTICAL APPROACH TO TWO-WAY SLAB DESIGN, Journal of
            the Structural Division, Proceedings of ASCE, Vol. 99,
            No. ST1, January, 1973, pp. 131-143

1.36   Sen, B., Sengupta, S. and Nath, T. K.
            ITERATIVE METHOD FOR SOLVING RECTANGULAR PLATES, Journal
            of the Structural Division, Proceedings of ASCE, Vol. 98,
            No. ST1, January, 1972, pp. 135-151

1.37   Stephen, R. M. and Bouwkamp, J. G.
            DYNAMIC BEHAVIOR OF AN ELEVEN STORY BUILDING,
            Proceedings, Sixth World Conference on Earthquake
            Engineerings, New Delhi, January, 1977

1.38   Taranath, B. S.
            THE EFFECT OF WARPING ON INTER-CONNECTED SHEARWALL-FLAT
            PLATE STRUCTURES, Proceedings of Institution of Civil
            Engineers, Vol. 61, Part 2, December, 1975, pp. 711-724

1.39   Tso, W. K. and Chan, P. C. K.
            FLEXIBLE FOUNDATION EFFECT ON COUPLED SHEAR WALLS,
            Journal of the American Concrete Institute, Proceedings,
            Vol. 69, No. 11, November, 1972, pp. 678-683

1.40   Tso, W. K. and Mahmoud, A. A.
            EFFECTIVE WIDTH OF COUPLING SLABS IN SHEAR WALL
            BUILDINGS, Journal of the Structural Division, Pro-
            ceedings of ASCE, Vol. 103, No. ST3, March, 1977,
            pp. 573-586

1.41   Vanderbilt, M. D., Sozen, M. A. and Siess, C. P.
            TESTS OF A MODIFIED REINFORCED CONCRETE TWO-WAY SLAB,
            Journal of the Structural Division, Proceedings of ASCE,
            Vol. 95, No. ST6, June, 1969, pp. 1073-1093

1.42   Vanderbilt, M. D.
            SHEAR STRENGTH OF CONTINUOUS PLATES, Journal of the
            Structural Division, Proceedings of ASCE, Vol. 98,
            No. ST5, May, 1972, pp. 961-973

1.43   Zaghlool, E. R. F. and Rawdon de Paiva, H. A.
        STRENGTH ANALYSIS OF CORNER COLUMN-SLAB CONNECTIONS,
        Journal of the Structural Division, Proceedings of
        ASCE, Vol. 99, No. ST1, January, 1973

2.1   ACI-ASCE Committee 426, THE SHEAR STRENGTH OF REINFORCED
        CONCRETE MEMBERS, Journal of the Structural Division,
        Proceedings of ASCE, Vol. 99, No. ST6, June, 1973,
        pp. 1148-1157

2.2   Adham, S. A. and Ewing, R. D.
        INTERACTION BETWEEN UNREINFORCED MASONRY STRUCTURES
        AND THEIR ROOF DIAPHRAGMS DURING EARTHQUAKES, North
        American Masonry Conference, 1978, University of
        Colorado, Proceedings, pp. 57-1 - 57-5

2.3   Alexander, C. M., Heidebrecht, A. C. and Tso, W. K.
        CYCLIC LOAD TESTS ON SHEAR WALL PANELS, Proceedings,
        Fifth World Conference on Earthquake Engineerings,
        Rome, 1973

2.4   Applied Technology Council
        TENTATIVE PROVISIONS FOR THE DEVELOPMENT OF SEISMIC
        REGULATIONS FOR BUILDING - A COOPERATIVE EFFORT WITH
        THE DESIGN PROFESSIONS, BUILDING CODE INTERESTS AND THE
        RESEARCH COMMUNITY, National Science Foundation, June,
        1978

2.5   Backmann, H.
        INFLUENCE OF SHEAR AND BOND ON ROTATIONAL CAPACITY OF
        REINFORCED CONCRETE BEAMS, IABSE Publication, Vol. 30,
        Part II, Zurich, 1970, pp. 11-28

2.6   Barda, F.
        SHEAR STRENGTH OF LOW-RISE WALLS WITH BOUNDARY ELEMENTS,
        Ph.D. Dissertation, Lehigh University, Bethlehem,
        Pennsylvania, 1972

2.7   Benjamin, F. R. and Williams, H. A.
        BEHAVIOR OF REINFORCED CONCRETE SHEAR WALLS, Transactions
        of ASCE, Vol. 124, 1959, pp. 669-702

2.8   Cardenas, A. E. and Magura, D. D.
         STRENGTH OF HIGH-RISE SHEAR WALLS-RECTANGULAR CROSS
         SECTIONS, Response of Multistory Concrete Structures
         to Lateral Forces, SP 36-7, American Concrete Institute,
         Detroit, 1972

2.9   Cardenas, A. E., Hanson, J. M., Covley, W. G. and
         Hognestad, E.
         DESIGN PROVISION FOR SHEAR WALLS, Journal of the
         American Concrete Institute, Proceedings, Vol. 70,
         No. 3, March, 1973, pp. 221-227

2.10   Cervenka, V.
         INELASTIC FINITE ELEMENT ANALYSIS OF REINFORCED CONCRETE
         PANELS UNDER IN-PLANE LOADS, Ph.D. Dissertation, Univer-
         sity of Colorado, Boulder, 1970

2.11   Cheng, F. Y. and Kitipitayangkul, P.
         INRESB-3D, A COMPUTER PROGRAM FOR INELASTIC ANALYSIS OF
         REINFORCED-CONCRETE STEEL BUILDINGS SUBJECTED TO
         3-DIMENSIONAL GROUND MOTIONS, Department of Civil
         Engineering, University of Missouri-Rolla, Rolla,
         Missouri, Civil Engineering Study Structural Series
         79-11, August, 1979

2.12   Clough, R. W., King, I. P. and Wilson, E. L.
         STRUCTURAL ANALYSIS OF MULTI-STORY BUILDINGS, Journal
         of the Structural Division, Proceedings of ASCE,
         Vol. 90, No. ST3, June, 1964, pp. 19-34

2.13   Corley, W. G.
         ROTATIONAL CAPACITY OF REINFORCED CONCRETE BEAMS,
         Journal of the Structural Division, Proceedings of ASCE,
         Vol. 92, No. ST5, October, 1966, pp. 121-146

2.14   Darwin, D.
         INELASTIC MODEL FOR CYCLIC BIAXIAL LOADING OF REINFORCED
         CONCRETE, Ph.D. Dissertation, Civil Engineering Depart-
         ment, University of Illinois, Urbana-Champaign, 1974

2.15   Douglas, B. M. and Trabert, T. E.
         COUPLED TORSIONAL DYNAMIC ANALYSIS OF A MULTISTORY
         BUILDING, Bulletin of the Seismological Society of
         America, Vol. 63, No. 3, June, 1973, pp. 1025-1039

2.16   Fintel, M.
        STAGGERED TRANSVERSE WALL-BEAMS FOR MULTISTORY CON-
        CRETE BUILDINGS, Journal of the American Concrete
        Institute, Proceedings, Vol. 65, No. 5, May, 1968,
        pp. 366-378

2.17   Fintel, M.
        DUCTILE SHEAR WALLS IN EARTHQUAKE RESISTANT MULTI-
        STORY BUILDINGS, Journal of the American Concrete
        Institute, Proceedings, Vol. 71, No. 6, June, 1974
        pp. 296-304

2.18   Fintel, M.
        DUCTILE SHEAR WALLS IN EARTHQUAKE RESISTANT MULTISTORY
        BUILDINGS, Reinforced Concrete Structures in Seismic
        Zones, SP-53, American Concrete Institute, Detroit,
        1977

2.19   Fiorato, A. E., Oesterle, R. G. and Corley, W. G.
        IMPORTANCE OF REINFORCEMENT DETAILS IN EARTHQUAKE-
        RESISTANT STRUCTURAL WALLS, Proceedings of a Workshop
        on Earthquake-Resistant Reinforced Concrete Building
        Construction, July, 1977, pp. 1430-1451

2.20   Gibson, R. E., Moody, M. L. and Ayre, R. S.
        FREE VIBRATION OF AN UNSYSMMETRICAL MULTISTORIED
        BUILDING MODELED AS A SHEAR-FLEXIBLE CANTILEVER
        BEAM, Bulletin of the Seismological Society of America,
        Vol. 62, No. 1, February, 1972, pp. 195-213

2.21   Gluck, J.
        LATERAL-LOAD ANALYSIS OF ASYMMETRIC MULTI-STORY
        STRUCTURES, Journal of the Structural Division,
        Proceedings of ASCE, Vol. 96, No. ST2, February, 1970,
        pp. 317-333

2.22   Guendelman-Israel, R. and Powell, G. H.
        DRAIN-TABS, A COMPUTER PROGRAM FOR INELASTIC EARTHQUAKE
        RESPONSE OF THREE-DIMENSIONAL BUILDINGS, Earthquake
        Engineering Research Center, Report No. UCB/EERC-77/08,
        University of California, Berkeley, March, 1977

2.23   Heidebrecht, A. C. and Swift, R. D.
        ANALYSIS OF ASYMMETRICAL COUPLED SHEAR WALLS, Journal
        of the Structural Division, Proceedings of ASCE,
        Vol. 97, No. ST5, May, 1971, pp. 1407-1422

2.24   International Conference of Building Officials
        UNIFORM BUILDING CODE, Whittier, California, 1976

2.25   Kanaan, A. E. and Powell, G. H.
        GENERAL PURPOSE COMPUTER PROGRAM FOR INELASTIC DYNAMIC
        RESPONSE OF PLANE STRUCTURES, Earthquake Engineering
        Research Center, Report No. EERC-73-6, University of
        California, Berkeley, April, 1973

2.26   Macleod, L. A., Wilson, W., Bhatt, P. and Green, D.
        TWO DIMENSIONAL TREATMENT OF COMPLEX STRUCTURES,
        Proceedings, The Institution of Civil Engineers, Vol. 53,
        Part 2, December, 1972, pp. 589-593

2.27   Majid, K. I. and Onen, Y. H.
        THE ELASTO-PLASTIC FAILURE LOAD ANALYSIS OF COMPLETE
        BUILDING STRUCTURES, Proceedings, The Institution of
        Civil Engineers, Vol. 55, Part 2, September, 1973,
        pp. 619-634

2.28   Mattock, A. H.
        ROTATION CAPACITY OF HINGING REGIONS IN REINFORCED
        CONCRETE BEAMS, Flexural Mechanics of Reinforced
        Concrete, Proceedings of the International Symposium,
        Miami, Florida, November, 1964, pp. 143-181

2.29   Mee, A. L., Jordaan, I. J. and Word, M. A.
        WALL-BEAM FRAMES UNDER STATIC LATERAL LOAD, Journal
        of the Structural Division, Proceedings of ASCE,
        Vol. 101, No. ST2, February, 1975, pp. 377-395

2.30   Nair, R. S.
        OVERALL ELASTIC STABILITY OF MULTISTORY BUILDINGS,
        Journal of the Structural Division, Proceedings of
        ASCE, Vol. 101, No. ST12, December, 1975, pp. 2487-2503

2.31   Neville, A. M.
        THREE-DIMENSIONAL ANALYSIS OF SHEAR WALLS, Proceedings,
        The Institution of Civil Engineers, Vol. 51, February,
        1972, pp. 347-357

2.32   Oesterle, R. G., Fiorato, A. E., Johal, L. S., Carpen-
        ter, J. E., Russell, H. G. and Corley, W. G.
        EARTHQUAKE RESISTANT STRUCTURAL WALLS - TESTS OF ISOLATED
        WALLS -", A Report to National Science Foundation,
        No. GI-43880, November, 1976

2.33   Paulay, T. and Santhakumar, A. R.
        DUCTILE BEHAVIOR OF COUPLED SHEAR WALLS, Journal of
        the Structural Division, Proceedings of ASCE, Vol. 102,
        No. ST1, January, 1976, pp. 93-108

2.34   Richter, P. J., Reddy, D. P. and Agbabian, M. S.
        THREE-DIMENSIONAL DYNAMIC ANALYSIS OF MULTISTORY CON-
        CRETE OFFICE BUILDING, Response of Multistory Concrete
        Structures to Lateral Forces, SP-36, American Concrete
        Institute, Detroit, 1973, pp. 151-186

2.35   Rutenberg, A., Jennings, P. C. and Housner, G. W.
        THE RESPONSE OF VETERANS HOSPITAL BUILDING 41 IN THE
        SAN FERNANDO EARTHQUAKE, Earthquake Engineering
        Research Laboratory, California Institute of Techno-
        logy, Report No. EERL 80-03, 1980

2.36   Shepherd, R. and Donald, R. A. H.
        THE INFLUENCE OF FLOOR FLEXIBILITY ON THE NORMAL MODE
        PROPERTIES OF BUILDINGS, Journal of Sound and Vibration,
        Vol. 5(1), 1967, pp. 29-36

2.37   Shepherd, R. and Donald, R. A. H.
        SEISMIC RESPONSE OF TORSIONALLY UNBALANCED BUILDINGS,
        Journal of Sound and Vibrations, Vol. 6(1), 1967,
        pp. 20-37

2.38   Shiga, T., Shibata, A. and Takahashi, J.
        HYSTERETIC BEHAVIOR OF REINFORCED CONCRETE SHEAR WALLS,
        Proceedings of the Review Meeting, U.S.-Japan Cooperative
        Research Program in Earthquake Engineering with Emphasis
        on the Safety of School Buildings, Tokyo, 1976,
        pp. 107-117

2.39   Stamato, M. C. and Stafford-Smith, B.
        AN APPROXIMATE METHOD FOR THE THREE DIMENSIONAL ANALYSIS
        OF TALL BUILDINGS, Proceedings, The Institution of Civil
        Engineers, Vol. 43, 1969, pp. 361-379

2.40   Taranath, B. S. and Stafford-Smith, B.
        TORSION ANALYSIS OF SHEAR CORE STRUCTURES, Analysis of
        Structural Systems for Torsion, SP 35-7, American
        Concrete Institute, Detroit, 1972

2.41   Tomii, M. and Osaki, Y.
        EXPERIMENTAL STUDIES ON SHEARING RESISTANCE OF FRAMED
        REINFORCED CONCRETE SHEARWALLS WITHOUT OPINING, PART 1,
        AND PART 2, Transactions of the Architectural Institute
        of Japan, No. 51, September, 1955, No. 52, March, 1956

2.42   Tomii, M. and Tokuhiro, I.
        ELASTIC ANALYSIS OF SHEAR WALLS LOADED ANTISYMMETRICALLY
        WITH REGARD TO THEIR LONGITUDINAL AND TRANSVERSAL CENTER
        LINES, PART 1 AND PART 2, Transactions of the Archi-
        tectural Institute of Japan, No. 160, June, 1969,
        No. 161, July, 1969, No. 162, August, 1969, No. 163,
        September, 1969

2.43   Tomii, M.
        SHEAR WALLS, State-of-the-Art Report 21-4, Proceedings,
        ASCE-IABSE International Conference on Tall Buildings,
        1973

2.44   Tsuboi, Y., Suenaga, Y. and Shigenobu, T.
        FUNDAMENTAL STUDY ON REINFORCED CONCRETE SHEARWALL
        STRUCTURES - EXPERIMENTAL AND THEORETICAL STUDY OF
        STRENGTH AND RIGIDITY OF TWO-DIMENSIONAL STRUCTURAL
        WALLS SUBJECTED COMBINED STRESSES, M,N,Q, Transactions
        of the Architectural Institute of Japan, No. 131,
        January, 1967

2.45   Uzumeri, S. M. and Paulay, T.
        A CRITICAL REVIEW OF THE SEISMIC DESIGN PROVISIONS FOR
        DUCTILE SHEAR WALLS OF THE CANADIAN CODE AND COMMENTARY,
        Canadian Journal of Civil Engineers, Vol. 2, No. 4,
        1975, pp. 592-601

2.46   Wilson, E. L. and Dovey, H. H.
        THREE DIMENSIONAL ANALYSIS OF BUILDING SYSTEMS - TABS,
        Earthquake Engineering Research Center, Report No.
        EERC 72-8, University of California, Berkeley, December,
        1972

2.47   Wynhoven, J. H. and Adams, P. F.
        ANALYSIS OF THREE DIMENSIONAL STRUCTURES, Journal of
        the Structural Division, Proceedings of ASCE, Vol. 98,
        No. ST1, January, 1972, pp. 233-248

2.48   Yuzugullu, O. and Schnobrich, W. C.
        A NUMERICAL PROCEDURE FOR THE DETERMINATION OF THE
        BEHAVIOR OF A SHEAR WALL FRAME SYSTEM, Journal of the
        American Concrete Institute, Proceedings, Vol. 70,
        No. 7, July, 1973, pp. 474-479

2.49   Kostem, C. N. and Heckman, D. T.
        LATERAL INTERACTION OF THREE DIMENSIONAL STEEL FRAMES
        AND OPEN TUBULAR REINFORCED CONCRETE SHEAR WALLS,
        Proceedings of the World Congress on Spatial and Shell
        Structures, Madrid, Spain, 1979, pp. 4.107-4.121.

2.50   Kostem, C. N. and Heckman, D. T.
        EARTHQUAKE RESPONSE OF THREE DIMENSIONAL STEEL FRAMES
        STIFFENED BY OPEN TUBULAR CONCRETE SHEAR WALLS,
        Proceedings of the Second U. S. National Conference
        on Earthquake Engineering, Stanford University,
        California, August 22-24, 1979, pp. 969-977.

3.1   Bathe, K. J., Wilson, E. L. and Peterson, F. E.
        SAP IV - A STRUCTURAL ANALYSIS PROGRAM FOR STATIC AND
        DYNAMIC RESPONSE OF LINEAR SYSTEMS, Earthquake
        Engineering Research Center Report No. EERC 73-11,
        University of California, Berkeley, June, 1973
        (revised April, 1974)

3.2   Nakashima, M., Huang, T. and Lu, L. W.
        BEHAVIOR OF SLAB-ON-BEAM FLOOR SYSTEMS UNDER IN-PLANE
        SEISMIC LOADING, Fritz Engineering Laboratory Report
        No. 422-7, Lehigh University, Bethlehem, Pennsylvania
        (to be published)

4.1   Adham, S., et al.
        REINFORCED CONCRETE CONSTITUTIVE RELATIONS, Agbabian
        Associates, Prepared for Air Force Weapons Laboratory
        Defence Nuclear Agency, February, 1975

4.2   Aktan, A. E., Karlsson, B. I. and Sozen, M. A.
        STRESS-STRAIN RELATIONSHIPS OF REINFORCING BARS
        SUBJECTED TO LARGE STRAIN REVERSALS, SRS. No. 397,
        Civil Engineering Studies, University of Illinois,
        Urbana-Champaign, June, 1973

4.3   Aktan, H. M.
        A METHOD TO ANALYSE THE CYCLIC BEHAVIOR OF THE SLENDER
        REINFORCED CONCRETE SHEAR WALLS, Report No. UMEE72R2,
        University of Michigan, Ann Arbor, June, 1977

4.4   Bashur, F. K. and Darwin, D.
        NONLINEAR MODEL FOR REINFORCED CONCRETE SLABS, Journal
        of the Structural Division, Proceedings of ASCE,
        Vol. 104, No. ST1, January, 1978, pp. 157-170

4.5   Beeby, A. W.
        SHORT-TERM DEFORMATIONS OF REINFORCED CONCRETE MEMBERS,
        Cement and Concrete Association, Technical Report
        No. TRA408, London, March, 1968

4.6   Branson, D. E.
        INSTANTANEOUS AND TIME-DEPENDENT DEFLECTIONS OF SIMPLE
        AND CONTINUOUS REINFORCED CONCRETE BEAMS, Alabama
        Highway Research Report No. 7, Bureau of Public Roads,
        August, 1963

4.7   Cervenka, V. and Gerstle, K. H.
        INELASTIC ANALYSIS OF REINFORCED CONCRETE PANELS THEORY,
        IABSE Publication, Vol. 32-2, 1972, pp. 31-45

4.8   Darwin, D. and Pecknold, D. A.
        ANALYSIS OF SHEAR PANELS UNDER CYCLIC LOADINGS, Journal
        of the Structural Division, Proceedings of ASCE,
        Vol. 102, No. ST2, February, 1976, pp. 355-369

4.9   Darwin, D. and Pecknold, D. A.
        NONLINEAR BIAXIAL STRESS-STRAIN LAW FOR CONCRETE,
        Journal of the Engineering Mechanics Division,
        Proceedings of ASCE, Vol. 103, No. EM2, April, 1977
        pp. 229-241

4.10   Hand, F. R., Pecknold, D. A. and Schnobrich, W. C.
        NONLINEAR ANALYSIS OF R.C. PLATES AND SHELLS, Journal
        of the Structural Division, Proceedings of ASCE,
        Vol. 99, No. ST7, July, 1973, pp. 1491-1505

4.11   Jofriet, J. C. and McNeice, G. M.
        FINITE ELEMENT ANALYSIS OF REINFORCED CONCRETE SLABS,
        Journal of the Structural Division, Proceedings of ASCE,
        Vol. 97, No. ST3, March, 1971, pp. 785-806

4.12   Kawai, T.
        A NEW DISCRETE MODEL FOR ANALYSIS OF SOLID MECHANICS
        PROBLEMS, Journal of the Seisan Kenkyu, Institute of
        Industrial Science, University of Tokyo, Vol. 29,
        No. 4, 1977, pp. 208-210

4.13   Kawai, T.
        NEW ELEMENT MODELS IN DISCRETE STRUCTURAL ANALYSIS,
        Journal of the Society of Naval Architects of Japan,
        Vol. 141, May, 1977, pp. 187-193

4.14   Kawai, T.
        A NEW DISCRETE ANALYSIS OF NONLINEAR SOLID MECHANICS
        PROBLEMS INVOLVING STABILITY, PLASTICITY, AND CRACK,
        Symposium on Applications of Computer Methods in
        Engineering, August 23-26, Los Angeles, California, 1977

4.15   Kawai, T.
        A NEW APPROACH TO SOIL MECHANICS AND GEOTECHNICAL
        ENGINEERING, Proceedings of the Third International
        Conference in Australia on Finite Element Methods,
        1979

4.16   Kawai, T. (editor)
        ANALYSIS OF SOLID MECHANICS PROBLEMS WITH NEW DISCRETE
        MODELS, A Text for Special Seminars held at Institute
        of Industrial Science, Tokyo University, Course No. 48,
        October 1-3, 1979. (In Japanese)

4.17   Kupfer, H. B. and Gerstle, K. H.
        BEHAVIOR OF CONCRETE UNDER BIAXIAL STRESSES, Journal
        of the Engineering Mechanics Division, Proceedings of
        ASCE, Vol. 99, No. EM4, August, 1973, pp. 853-866

4.18   Liu, T.C.Y., Nilson, A. H. and Slate, F. O.
        STRESS-STRAIN AND FRACTURE OF CONCRETE IN UNIAXIAL AND
        BIAXIAL COMPRESSION, Journal of the American Concrete
        Institute, Proceedings, Vol. 69, May, 1972, pp. 291-295

4.19   Nilson, A. H.
        NONLINEAR ANALYSIS OF REINFORCED CONCRETE BY THE FINITE
        ELEMENT METHOD, Journal of the American Concrete
        Institute, Proceedings, Vol. 65, September, 1968,
        pp. 757-766

4.20   Ngo, D., and Scordelis, A. C.
        FINITE ELEMENT ANALYSIS OF REINFORCED CONCRETE BEAMS,
        Journal of the American Concrete Institute, Proceedings,
        Vol. 64, March, 1967, pp. 152-163

4.21   Ngo, D.
        A NETWORK-TOPOLOGICAL APPROACH TO THE FINITE ELEMENT
        ANALYSIS OF PROGRESSIVE CRACK GROWTH IN CONCRETE MEMBERS,
        Ph.D. Dissertation, Civil Engineering Department,
        University of California, Berkeley, 1975

4.22   Peterson, W. S., Kulicki, J. M. and Kostem, C. N.
        THE INELASTIC ANALYSIS OF REINFORCED CONCRETE SLABS,
        Fritz Engineering Laboratory Report No. 378B.3,
        Lehigh University, Bethlehem, Pennsylvania, 1973

4.23   Salem, M.
          NONLINEAR ANALYSIS OF PLANAR REINFORCED CONCRETE
          STRUCTURES, Ph.D. Dissertation, Civil Engineering
          Department, University of Illinois, Urbana-Champaign,
          1974

4.24   Scordelis, A. C.
          FINITE ELEMENT ANALYSIS OF REINFORCED CONCRETE
          STRUCTURES, Proceedings of the Specialty Conference
          on Finite Element Method in Civil Engineering,
          June 1 and 2, 1972, Montreal, Quebec, Canada,
          pp. 71-114

4.25   Suidan, M. and Schnobrich, W. C.
          FINITE ELEMENT ANALYSIS OF REINFORCED CONCRETE,
          Journal of the Structural Division, Proceedings of
          ASCE, Vol. 99, No. ST10, October, 1973, pp. 2109-2122

4.26   Valliappan, S. and Doolan, T. F.
          NONLINEAR STRESS ANALYSIS OF REINFORCED CONCRETE,
          Journal of the Structural Division, Proceedings of
          ASCE, Vol. 98, No. ST4, April, 1972, pp. 885-898

4.27   Wilson, E. L., Bathe, K. J. and Doherty, W. P.
          DIRECT SOLUTION OF LARGE SYSTEMS OF LINEAR EQUATIONS,
          Computers & Structures, Vol. 4, 1974, pp. 363-372

4.28   Ziegler, H.
          MODIFICATION OF PRAGER'S HARDENING RULE, Quarterly
          of Applied Mathematics, Vol. 17, No. 1, 1957
          pp. 120-134.

4.29   Zienkiewicz, O. C., Valliappan, S. and King, I. P.
          ELASTO-PLASTIC SOLUTIONS OF ENGINEERING PROBLEMS
          'INITIAL STRESS' FINITE ELEMENT APPROACH, International
          Journal for Numerical Methods in Engineering, Vol. 1,
          1969, pp. 75-100

5.1   Kriz, L. B., and Lee, S. L.
          ULTIMATE STRENGTH OF OVER-REINFORCED BEAMS, Journal
          of the Engineering Mechanics Division, Proceedings
          of ASCE, Vol. 86, No. EM3, June, 1960, pp. 3-13.

5.2   Popovics, S.
          REVIEW OF STRESS-STRAIN RELATIONSHIP FOR CONCRETE,
          Journal of the American Concrete Institute,
          Proceedings, Vol. 67, No. 3, March 1970, pp. 243-248.

5.3   Rao, N. M. M.
          EVALUATION OF RECTANGULAR STRESS DISTRIBUTION FOR
          NON-RECTANGULAR STRUCTURAL CONCRETE MEMBERS IN ULTIMATE
          STRENGTH DESIGN, Master's Thesis, New Mexico State
          University, University Park, New Mexico, July, 1966.

6.1   Adeli, H., Gere, J. M. and Weaver, W.
          ALGORITHMS FOR NONLINEAR STRUCTURAL DYNAMICS,
          Journal of the Structural Division, Proceedings of
          ASCE, Vol. 104, No. ST2, February, 1978, pp. 263-280.

6.2   Bathe, K. J.
          ADINA - A FINITE ELEMENT PROGRAM FOR AUTOMATIC
          DYNAMIC INCREMENTAL NONLINEAR ANALYSIS, Acoustics
          and Vibration Laboratory, Mechanical Engineering
          Department, Report No. 82448-1, Massachusetts
          Institute of Technology, Cambridge, Massachusetts,
          1975. (Revised December, 1978).

6.3   Bathe, K. J. and Wilson, E. L.
          NUMERICAL METHODS IN FINITE ELEMENT ANALYSIS,
          Prentice-Hall, New Jersey, 1976.

6.4   Clough, R. W. and Johnston, S. B.
          EFFECT OF STIFFNESS DEGRADATION ON EARHTQUAKE
          DUCTILITY REQUIREMENTS, Proceedings of Japan Earth-
          quake Engineering Symposium, Tokyo, October, 1966,
          pp. 227-232.

6.5   Mondkar, D. P. and Powell, G. H.
          STATIC AND DYNAMIC ANALYSIS OF NONLINEAR STRUCTURES,
          Earthquake Engineering Research Center, Report
          No. EERC 75-10, University of California, Berkeley,
          March, 1975.

6.6   Newmark, N. M.
          A METHOD OF COMPUTATION FOR STRUCTURAL DYNAMICS,
          Journal of the Engineering Mechanics Division,
          Proceedings of ASCE, Vol. 85, No. EM3, June 1959,
          pp. 67-94.

6.7   Nickell, R. E.
       DIRECT INTEGRATION METHODS IN STRUCTURAL DYNAMICS,
       Journal of the Engineering Mechanics Division,
       Proceedings of ASCE, Vol. 99, No. EM2, April, 1973,
       pp. 303-317.

6.8   Riddell, R. and Newmark, N. M.
       FORCE DEFORMATION MODELS FOR NONLINEAR ANALYSES,
       Journal of the Structural Division, Proceedings of
       ASCE, Vol. 105, No. ST12, December, 1979, pp. 2773-
       2778.

6.9   Takeda, T., Sozen, M. A. and Nielsen, N. N.
       REINFORCED CONCRETE RESPONSE TO SIMULATED EARTHQUAKES,
       Journal of the Structural Division, Proceedings of
       ASCE, Vol. 96, No. ST12, December, 1970, pp. 2557-2573.